YIELD STRESS OF AN OIL WELL CEMENT SLURRY USING A CONTROLLED STRESS RHEOMETER

BY

D.R. KITCHING, M.Sc.

A thesis submitted for the degree of Doctor of Philosophy

School of Architecture and Building Engineering

University of Liverpool

October 1989

To my wife, Anne, and our sons

Benjamin, Jonathan, Matthew and Toby,

without whose love

and self-sacrifice this work would not exist.

SUMMARY

Yield Stress is an important rheological property of an oil well cement slurry system not only in the prediction of flow behaviour but also in assessing the pumping pressures required to restart a flow which has stopped. The yield stress also has significance in terms of mud removal and settling stability. It is a transient property dependent on previous shear history, time and shear rate.

The oil industry test methods use smooth coaxial cylinders in a controlled speed viscometer and are unrepresentative of field procedures. Additionally, theoretical approaches are too complex to predict the yield stress of an oil well cement slurry. Therefore, the effects of mixing and standing time on yield stress were examined experimentally, using a Carri-Med controlled stress rheometer.

Yield stress behaviour and the effects of hydration of the cement are considered as are various technqiues and equipment which have been used to study the yield stress. The measuring systems, which were parallel plates, vane-in-cup and annular plate and cone, were analysed and calibrated. Errors associated with the measuring system are evaluated and experimental problems, such as sample size, slippage and edge effects, are investigated.

Yield stress measurements using different measuring systems with different surface treatments were found to vary when testing a similar slurry, especially when using different rates of applied stress. This was not fully explained, but the difference in yield value due to rate of applied stress became insignificant with increased standing times.

The annular plate and cone (APC) measuring system was selected, as it enabled mixing of the slurry sample to be followed by a standing time and testing, to obtain the yield stress, without the uncertainty of sample transfer. It was necessary to modify the Carri-Med flow run software to do this. The results of yield stress for a specific oil well cement slurry, having undergone a certain mixing shear energy per unit mass in a mixing time and having stood for a nominated standing time were evaluated into a model. This model is of the form

$$\tau_y = \rho \; E_T/M \; e^{a(t_{stand})^{\frac{1}{2}}-b} \; t_{mix} \; -c-d(\ln t_{stand})$$

where a, b, c and d are constants determined by experiment and E_T/M is the total shear energy per unit mass.

ACKNOWLEDGEMENTS

I am most grateful to my supervisor Dr. P.F.G. Banfill whose knowledge, concern and assistance have been very helpful throughout the research period and during the completion of this thesis. His discussion provoked thought to solve problems and his comments assisted with the clarity of the manuscript.

I am indebted to B.P. Research Centre who provided financial support, together with the Science and Engineering Research Council, for this CASE award.

The cheerful assistance of technical staff Les Smith, Bill Baker and Sid Robinson and that of departmental secretary Anne Kennerley is acknowledged.

The fellowship of cement researchers Sue Gill and Nina Baker was most appreciated.

Finally thanks are given to Pat Baker who painstakingly typed the thesis.

CONTENTS

CONTENTS (cont'd.) Page No.

CONTENTS (cont'd.) Page No.

CONTENTS (cont'd.) Page No.

CONTENTS (cont'd.) Page No.

Conversion Factors

1	Pa	=	2.089 lb.f/100ft^2
1	Pa	=	10 dynes/cm^2
1	Pa	=	0.000145 p.s.i.
1	N/m^2	=	1 Pa
1	Nm	=	10^7 dyne cm
1	mPas	=	1 cP
1	g/cm^3	=	8.345 lb/gall

The oil industry uses 1bf.100ft^2 or 1bf./ft^2 for yield stress and centipoise (cP) for plastic viscosity. Slurry density is given in lb/gall., which is in U.S. units, otherwise most units used in the industry are imperial for convenience. S.I. units are becoming universally accepted, hence, they are given prominence in the above table.

The particular Carri-Med C.S. Rheometer, which was used in this thesis and its software operated in c.g.s. units. These units were retained, so these conversions are given together with the p.s.i conversion to indicate the magnitude of the stress.

Glossary

aggregate	a group of particules held together in clumps.
angle of response	rotation of measuring system prior to yield.
arctic cementing	cementing at temperatures below 20°F.
Bearden unit	empirical unit used to measure thickening of a cement slurry in a consistometer by the deflection of a spring in the measuring head.
blow out preventor	equipment to shut down escaping fluids when drilling strikes high pressure formation.
casing	steel pipe that lines the drilled oil well.
consistometer	device which simulates changes in temperature and pressure a slurry undergoes being pumped down the hole and measures the thickening of the slurry.
deviated well	gradual bending away from vertical whilst drilling.
dilatant	increase in volume caused by shear
dispersants	additives which keep particles separated or break down flocculation
drilling fluid	fluid circulated during drilling to remove cuttings and assist drilling operation.

elastoplastic	a plastic material showing some elasticity.
equilibration time	time allowed to reach an equilibrium or steady state.
flocculated dispersion	particules are dispersed throughout the medium in flocs or aggregates.
fluid loss additive	additive which prevents water being extracted from the cement slurry.
free water	water that separates from the cement slurry after mixing.
fracture gradient	pressure at which rock formation fractures divided by the depth the fracture occurs.
gas channelling	high pressure rock formation gas undermining cement structure as pore pressure in cement is reduced during hydration.
hesitation squeeze	technique of intermittent application of pressure separated by periods of pressure loss to facilitate cementing perforations by overcoming excessive pumping rates.
hydration	chemical reaction which occurs when water is added.
intrinsic viscosity	limiting value of reduced viscosity as the volume fraction approaches zero.
laitance	skin formed on surface of free water from cement slurry mainly composed of free lime and fine cement.

liner	length of casing which hangs inside a casing but does not reach the surface.
lost circulation zone	location where circulating fluids are lost to rock formation.
mud	drilling fluid contaminated with cuttings.
OPC	ordinary portland cement.
open hole log	record of well diameter with depth.
perforations	holes through the primary cementing and/or the casing.
plastic viscosity	slope of the flow curve of a Bingham plastic.
polydispersity	many different particle sizes in a suspension.
primary cementing	original cementing job on any section of the well.
retarder	cement additive which delays setting time.
rheopexy	negative thixotropy.
rigid close packing	cement particles in a slurry jam so that no flow occurs.
salt dome	geological feature formed by salt flowing into strata under pressure.
shear thickening	increase in viscosity with increasing shear rate in steady flow.
shear thinning	decrease in viscosity with increasing shear rate in steady flow.

shoe	fitting on entry end of casing or tubing to guide casing or exiting fluids.
silanised	surface treatment with a silicon compound to increase adhesion of suspending medium to particles.
slippage	sliding effects during the transfer of stress to particulate suspensions which occur at surface boundaries.
slurry	a water based mixture which is pumpable.
SME	specific mixing energy
sol gel	solid particles held in a suspending medium which is also held in position.
spacer	fluid forming a buffer between drilling fluid and cement.
squeeze cementing	cement slurry forced into formation through perforations at fixed depth.
SSMP	small sample mixing procedure.
stab-in cementing	large casing cementing by inserting small tube through which cement flows and locating tube in collar at the bottom of the casing.
thixotropic	decrease of apparent viscosity under shear stress followed by gradual recovery when stress is removed.
wash	fluid designed to clean mud from hole.
yield stress	stress at which material begins to flow.

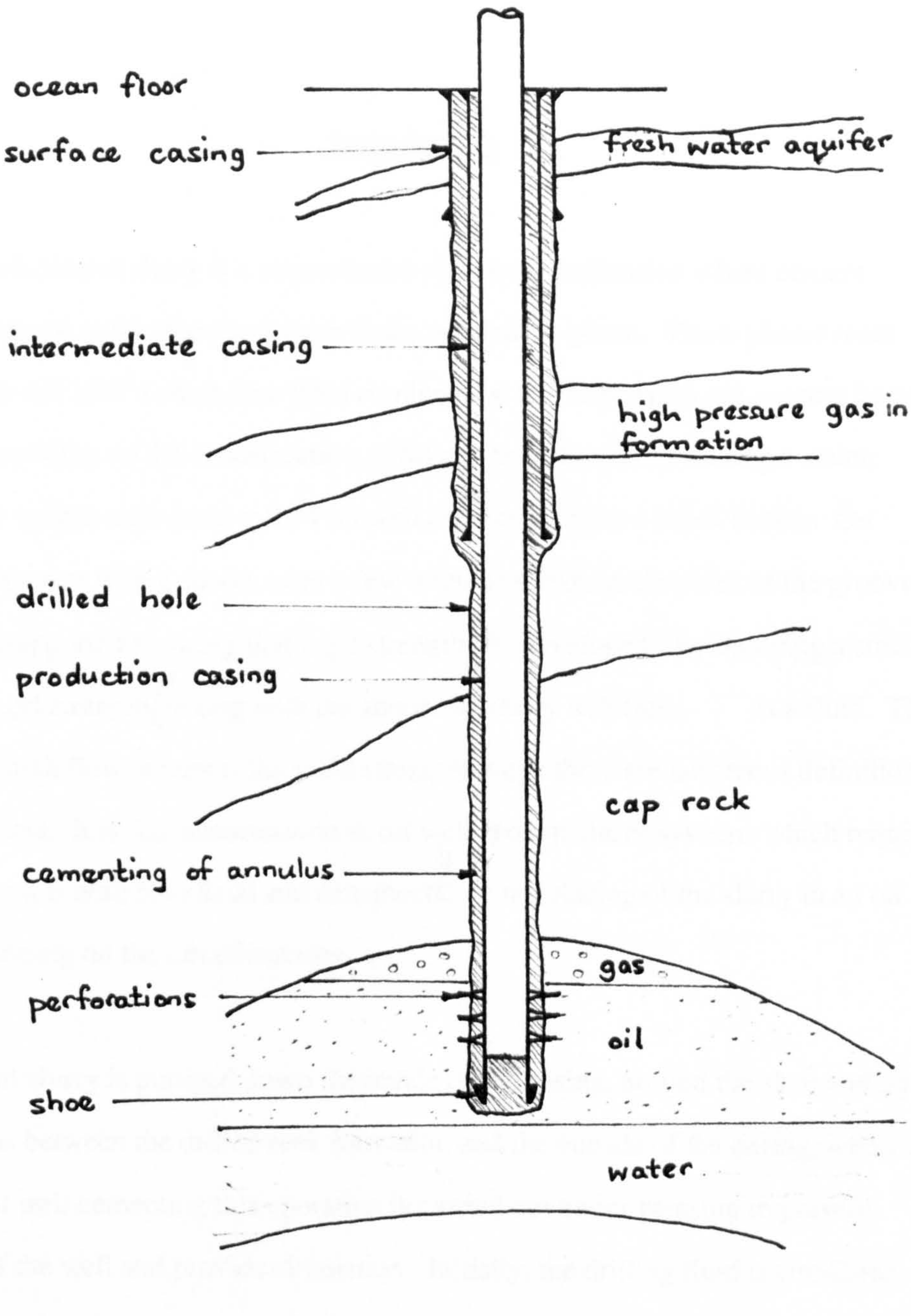

Diagram of Oil Well Cementing Features

CHAPTER 1

Introduction

Oil well cement slurry is a concentrated two phase suspension where cement particles are the solid phase and water is the continuous phase. These phases react chemically and after a short time from combination the suspension can support its own weight depending on the concentration. This can be observed by mixing a water: cement by weight ratio (w/c) = 0.44 oil well cement slurry in a small beaker. On making a groove with a spoon, after a few minutes standing, the sides of the groove remain unsupported showing that a gel strength has developed. By applying a stress above the gel strength by mixing with the spoon the slurry will flow as a fluid. The stress at which flow occurs is the yield stress,although there are numerous definitions of yield stress. It is this phenomenon in oil well cement slurry systems which requires study since it is both beneficial and detrimental to the placing of the slurry in an oil well depending on the circumstances.

Cement slurry is pumped down the inside of the casing, around the shoe and up the annulus between the drilled rock formation and the outside of the casing, where it sets. In oil well cementing this operation is carried out under pressure to prevent collapse of the well and provide circulation. Initially, the drilling fluid is circulated followed by the washes, or spacers, then the cement slurry and finally the displacement fluid. All of which ensure the removal of the drilling mud and that the cement slurry is placed in the correct position. Basically , the function of the cement slurry is to seal the annulus, thereby preventing ingress or egress of fluids. These

fluids, either oil, water or gas, may be the cause of leakage, contamination or corrosion of the casing. The cement slurry when set supports the casing and strengthens weak rock formations. The cement slurry is also put to many other uses in oil well cementing such as stab-in cementing with large casings and anchoring of the blow-out preventor, liner cementing, squeeze cementing, which repair primary jobs, leaks and lost circulation; also to plug perforations enhancing oil recovery in zones becoming depleted and finally abandonment, by the use of cement plugs at various depths.

To achieve all these objectives it is essential that the rheological properties of the cement slurry are known and can be controlled at all stages of the cementing operation. This is made more difficult not only with increased temperature and pressure at greater depths, but with the use of deviated wells , where a number of oil wells are drilled in some cases almost horizontally, from one location to exploit the field.

Some other problems that require knowledge of rheological properties of the slurry during cementing include:-

a) stoppage of cement flow because of a faulty valve which allows development of the gel strength resulting in start up pressures sufficient to fracture weak rock formation;

b) settlement of cement particles in horizontal flow resulting in poor bond or lack of sealing-off migratory fluids;

c) displacement of drilling mud in an annulus with an offset casing, where removal by the cement slurry from the inside of the casing causes contamination of the cement and lack of removal of the drilling mud from the outside of the casing gives rise to poor cementing.

During displacement the flow properties of the cement slurry become important. A more efficient displacement is produced with a turbulent flow velocity profile, but a turbulent flow inside the casing may have a laminar flow in the annulus. However with a cement slurry a plug flow might be a more likely flow condition. Plug flow exists when the central portion is an unsheared mass and the cylindrical outer portion is flowing at a stress above the yield stress of the cement slurry.

The design of the slurry, or slurries, since according to well conditions multistage cementing may be necessary especially when downhole formations are unable to support the hydrostatic pressures of a long cement slurry column, depends on the type of cement job. For a primary cementing job some of the factors which affect the cement slurry design include:-

a) the open hole log and casing size so as to obtain the volume of the annulus;
b) well conditions including fracture gradients, lost circulation zones, abnormal pressure formations, such as high gas pressure, or unusual geological feature, such as salt domes, temperature profiles and
c) the mud system

This is because a certain cement slurry density exerts a pressure on the rock

formation at depth or the slurry can dissolve the salt from the salt dome or the high pressure gas migrates, by channelling through the cement, undergoing enormous expansion from depth. Having assessed the method and equipment to place the cement slurry in the well, laboratory tests can be performed to obtain the most suitable slurry using various additives such as extenders, which decrease the slurry density, fluid loss additives, retarders or dispersants, which are self explanatory. These laboratory tests include slurry density, free water, thickening time, compressive strength and rheological measurements performed on both the slurry and slurry/drilling mud combinations, to ensure compatibility. The pump rate and placement pressure calculations can then be made giving displacement volumes and times. Implementation records and post job evaluation is performed as a final exercise to ensure better future performance.

The rheological properties appear buried under the weight of this design data, especially the yield stress upon which so much is dependent. It is obtained in the laboratory from the cement slurry having been mixed with a high speed domestic food blender, which bears little relation to field mixing using jet mixers or recirculating mixers employing centrifugal pumps. The cement slurry sample is transferred to a FANN viscometer, which is a basic constant speed concentric cylinder shearing device with a torsion spring. This viscometer using conversion factors provides the stress response of the cement slurry to five or six different shear rates from which the yield stress is extrapolated. The gel strength is determined using this apparatus by direct measurement at a slow speed after allowing the slurry to stand for a short time. (10 secs., 1 min. and 10 mins.)

This laboratory test procedure and apparatus are unsuitable to simulate the mixing shear history and assess the development of the yield stress of an oil well cement

slurry which is allowed to stand for any short time after shearing. The oil industry puts the emphasis of prime concern on the ability of a slurry to remain pumpable until it is in position and then develop strength quickly so as to shorten time and costs. The thickening time is measured simulating downhole temperatures and pressures as they change with depth using an elaborate and expensive apparatus known as a pressurised consistometer. This consists of a rotating cylindrical slurry container with an inbuilt paddle stirrer enclosed in a pressure chamber, which is oil filled, and has a heating element to provide the necessary temperature range. To simulate a depth of 20000 ft., temperature and pressure up to 222°C and 22000 psi can be achieved. The slurry consistency is measured, using a coil spring attached to the stirrer, in Bearden units which are empirical. The thickening time is the time to reach 100 units from the initial application of temperature and pressure. The thickening time of the slurry is designed to exceed the pumping time of the slurry with a margin for error. Slurry contaminated with various amounts of spacer fluid and drilling mud are also tested in this apparatus to show compatibility. The various types of cementing such as hesitation, squeeze and liner are given different simulation schedules to be used in testing with the pressure consistometer.

This discussion shows that the prediction of the yield stress at various stages of slurry development under downhole conditions is most important. The starting point of the work described in this thesis is the instrumentation used to measure the yield phenomenon and the inadequacy of the existing industrial test methods. The theoretical analysis of time dependent cement slurries is impossibly complex and the theory relating dynamic properties to yield stress is still sought. Attention is directed at improved experimental methods to measure the yield stress and investigate related behaviour such as rigid close packing. The recent development of controlled stress

rheometers makes it possible to measure the yield stress more reliably. The experimental work described here is concerned with the use of this type of instrument.

CHAPTER 2

Rheology of Oil Well Cement Slurry

NOTATION

a_e	=	effective radius of particle contact
a,b,c,d	=	rate constants
C_D, C_F	=	coefficients of destruction, formation
C_0	=	constant of link destruction
C_1	=	initial link length ratio
C_S	=	ratio of length shear plane to length of link
D	=	relative diffusion constant. vane and tube diameter
D_C	=	diameter of cylindrical shear surface
D_e	=	effective diameter
E	=	energy . rate of energy dissipation
E_A	=	activation energy of link formation
E_T	=	total energy input in mixing
e'_{ik}	=	rate of strain tensor
F	=	torque of the vane . conversion factor
f_s	=	torque/unit length
G	=	shear rate
h	=	gap separating the plates
I	=	strain rate invariant . maximum value of i
i + 1	=	number of particles in a chain
i,j,k	=	subscripts denoting number of plane, direction or item
K	=	equilibrium constant for destruction Kitching number
k	=	reaction rate constant in the Arrhenius equation. Einstein's viscosity coefficient. Boltzmann's constant.
L	=	length . gap thickness
M	=	torque on parallel plate
m, n, p	=	power indices

N	=	number of particles per unit volume, rotational speed
p'_{ik}	=	deviatoric stress tensor
q	=	half the average number of links to a particle
R	=	radius of the plate
R_c	=	Reynolds number
r_a r_c	=	average sand particle radius on the annulus, cone
r_i	=	radius of engraved indentation
T	=	torque . absolute temperature
$T(t)$	=	time dependent yield criterion
t, t'	=	current time, non-current time
t_D, Λ	=	relaxation time
t_s, t_T	=	shear induced rate constant for link destruction, formation
V	=	volume . velocity
v	=	yield value of the material
v_{ik}	=	yield stress tensor component
w	=	water cement ratio
α	=	cone angle
β	=	rate of change of stress
γ	=	shear strain
$\dot{\gamma}$	=	shear rate
ε'_{ik}	=	strain tensor component
$\eta, \eta_0, \eta_\infty$	=	viscosity, zero shear , infinite shear rate viscosity
η_1	=	constant reciprocal mobility in plastic region
η_a, η_e, η_r	=	apparent , equilibrium , relative viscosity
η_ω	=	viscosity of suspending medium
Θ	=	angular displacement
μ_e, μ_p	=	effective , plastic viscosity
μ	=	rigidity modulus. viscosity
ρ	=	density
σ	=	shear stress
λ	=	structural level parameter, second order structure rate constant
τ, τ_y, τ_c	=	stress, yield stress, critical stress
Λ	=	crowding factor
Φ, ϕ	=	particle volume fraction
Φ_L	=	volume fraction of aggregates
Ω, ω	=	angular velocity. rotational speed

Rheometry is the measurement of rheological properties and consists of two parts. The first characterises the non-Newtonian behaviour in a rheological flow configuration, then it correlates that behaviour to a real situation; the second, formulates rheological equations of state enabling solutions to practical flow problems (Walters, 1975). This chapter briefly looks at the second part. Since, even with the wealth of literature on non-Newtonian flow, solution to the yield stress of a cement slurry in any flow situation was not available from the rheological equations.

Emphasis in this chapter is then given to the first part where the terms and behaviour of yield stress are discussed. This is followed by a description of the methods and techniques for measuring the yield stress of a cement slurry from which the non-Newtonian behaviour has been characterised. Finally, the application of measurement techniques in the oil industry in order to correlate to the behaviour in the field is covered.

2.1 Theoretical Approaches to Structure in Fluids

The object of theoretical approaches is to describe, using equations, the behaviour of fluids in terms of stress and strain variables. These rheological equations of state are solved by employing equations of motion and continuity with due regard to certain boundary conditions. A solution, however, is only possible when the fluid is a rheologically simple one and the flow situation is also simple (e.g. steady simple shear of a Newtonian fluid). When the flow situation is not slow or of small deformation and the fluid is complicated rheologically (e.g. cement slurry) then theoretical modelling from first principles is not only very complex but most probably impossible.

The following approaches have been used to describe the structure in fluids:

1) continuum mechanics
2) structural kinetics
3) microstructural
4) thermodynamic.

Before applying a theory the mechanism has to be understood so that the relevant factors may be taken into account. It is because the mechanism of yield in concentrated suspensions is not well understood that theoretical modelling is difficult.

2.1.1 Continuum Mechanics

Oldroyd (1974) uses the Mises-Hencky criterion for yield, which assumes that yield occurs when the potential energy per unit volume due to deviatoric stresses reaches a certain critical value of

and

$$2\mu \dot{\varepsilon}_{ik} = v_{ik}$$

From which the yield criterion is expressed in tensor from as

$$v^2 = \frac{1}{2} \dot{P}_{ik} \dot{P}_{ik} \qquad 2.1$$

meaning that only deviatoric components of the stess and strain tensors are involved in the yield criterion.

Harris (1967) developed the yield criterion for an incompressible isotropic thixotropic material using continuum mechanics and assuming that in laminar shearing motion there would be an undisturbed yield and a current yield which is a function of past flow history. The simplest form of integral equation for the current yield comprises a time dependent function of strain rate invariants and a memory function which is an integral function of the relaxation spectrum. Simple forms of relaxation time were considered but the theory has not been verified experimentally since the approach is not clear and the yielding process is insufficiently understood. The yield criterion,

$$T(t) = \tau^2(y)$$

in simple shearing is given as

$$T_1 - \int_{-\infty} f(I[t']) N (t-t')dt' \qquad 2.2$$

_where f(I[t']) is the strain rate invariaint function at non-current time and

where T_1 is the initial undisturbed yield criterion and the yield criterion memory function N(t-t') is defined by

$$\int_0^{\infty} \frac{S(\Lambda)}{\Lambda} \exp\ (- [t-t'] / \Lambda)d\Lambda$$ where $S(\Lambda)d\Lambda$ is the relaxation spectrum

and Λ is the relaxation time.

2.1.2 Structural Kinetics

In the structural kinetic approach the parameters are lumped together and changes of the rheological properties with time caused by changes in internal structure are described by an equation of state and a rate equation in terms of a certain level of structure, λ. These equations describe thixotropy and assume a Newtonian response for each degree of structure and so cannot describe yield stress which is merely added in to the equation of state in models such as those of Worrall and Tuliani (1964) and Cheng (1979). The number of thixotropic links is assumed to be an adequate measure of the degree of structure, but as not all structural units are identical the structural parameter is used to give an equation of state, which from the Cheng model is:

$$\tau = (\tau_{y\infty} + d\lambda) + (\eta_{\infty} + c\lambda)\,\dot{\gamma} \qquad 2.3$$

and a rate equation from the Cross (1965) model of:

$$\frac{d\lambda}{dt} = a\,(1-\lambda) - b\,\dot{\gamma}^{m}\,\lambda \qquad 2.4$$

where the first term is the rate of build-up of structure and the second, is the breakdown rate. The structural parameter, λ, is a linear scale of structure with $\lambda = 0$ being the fully broken down state and $\lambda = 1$ the fully built-up state.

Combining these equations on the equilibrium flow curve where

$\frac{d\lambda}{dt} = 0$ gives:

$$\tau_e = \left(\tau_{y\infty} + \frac{d}{1 + \frac{b}{a}\dot{\gamma}^{m}}\right) + \left(\eta_{\infty} + \frac{c}{1 + \frac{b}{a}\dot{\gamma}^{m}}\right)\dot{\gamma} \qquad 2.5$$

Mewis (1979) concludes that the adequacy of a single scalar structural parameter to describe structure is suspect since even dilute dispersions require a second order tensor for their material characterisation. Also some data show more gradual changes than a single rate constant. Mewis suggests that it is more probable to have a distribution of

rate constants with first order reactions in the same way as the memory functions of continuum mechanics models with more than one relaxation time. However this adds to the complexity and does not enable us to further understand the mechanism of yield.

The structural kinetics approach is useful in practical applications and its parameters can be directly measured by experiment. This is discussed later in the section on the measurement of yield stress.

2.1.3 Microstructural

In this approach there are two forms of development, either the phenomenological or the structural. The former adopts a derived mathematical model without many arbitrary assumptions and then obtains the value of its parameters from experiments. These parameters do not have any simple microstructural interpretation. The latter development obtains a microscopically detailed picture of the system using physics, chemistry and fluid mechanics to depict the behaviour, but as it is difficult to establish results in this way arbitrary assumptions have to be made.

By studying their development in three stages, the description of the structure, the relating of the rheology to the structure and the evaluation of the parameters in those relations, Chaffey (1976) carried out a detailed comparison of the following microstructural theories:

1) Impulse
2) Modified impulse
3) Kinetic

4) Thermodynamic

Apart from thermodynamic theory, in dispersions the fall in viscosity with increasing shear rate is attributed to the breaking of inter-particle links. If N is the number of particles per unit volume and q is half the average number of links to a particle then in a continuous chain with no branches the number of links is Nq. In the impulse theory the links are multiple networks (ie. q is unlimited). From chemical kinetics the general rate law is given by:-

$$\frac{dq}{dt} = \frac{1}{2} C_F \lambda N - C_D t_D^{-1} q \qquad 2.6$$

where λ is a second order structure rate constant and t_D^{-1} is a reciprocal relaxation time which is a rate constant dependent on the shear rate and

$$K = 2/\lambda\, t_D^{-1}$$

is taken as the equilibrium constant for destruction.

C_F and C_D equal N in the impulse theory but in the modified impulse theory, since the average number of links per chain is $\frac{1}{1-q}$,

$$C_F = (1-q^2) \quad \text{and} \quad C_D = (1-q).$$

In the kinetic theory N_i is the number of chains of (i + 1) particles and

$$\frac{dN_i}{dt} = \lambda\left(\frac{1}{2}\sum_{j=0}^{j=i-1} N_j\, N_{i-j-1} - N_i \sum_{j=0}^{\infty} N_j\right) - t_D^{-1}\left(iN_i - 2\sum_{j=1}^{\infty} N_{i+j}\right) \qquad 2.7$$

where the first term on the right hand side is the union of shorter chains, the second term is the loss of chains by further reaction, the third term is the direct breaking of chains and the fourth term is the chain increase from breakdown of longer chains. This eventually gives a rate equation of the form:

$$\frac{dq}{dt} = \frac{1}{2}\lambda N(1-q)^2 - t_D^{-1} q \qquad 2.8$$

For a steady state

$$\frac{dq}{dt} = 0$$

and the three theories give the following relationships

impulse $\qquad q = \dfrac{N}{K}$

modified impulse $\qquad q = \dfrac{1}{(1+\frac{K}{N})}$

kinetic $\qquad q = 1 + \dfrac{K}{2N} - \left(\dfrac{K}{N} + \dfrac{K^2}{4N^2}\right)^{\frac{1}{2}}$

showing that the impulse theory produces an indefinite increase in link formation at low shear rate. The modified impulse and the kinetic are restricted to long chains but all produce the same small structure at high shear rate, with the impulse producing the denser structure.

2.1.4 Thermodynamic

According to Mewis (1979) the thermodynamic argument has not been developed and only similarities with structural parameters have been discussed. A thermodynamic approach to the microstructural argument is only briefly mentioned here since generally, it refers to dilute flocculated dispersions.

In thermodynamic structural theories Chaffey (1976) points out that the volume of the aggregate chain is taken as:

$$V_i = V_0 \left(1 + \frac{3}{2} i\right)$$ where V_0 = volume of a spherical

particle. The ratio of the volume of particles to fluid is taken as being the same inside and outside of the aggregates

$$\text{i.e. } V_i = \frac{(i+1)}{N} \quad \text{but} \quad V_i = (i+1)^{\frac{3}{2}} V_0 / 8\phi, \text{and as } V_i \geq (i+1) V_0$$

the concentration, ϕ, must be small when the V_i is only valid for $i < 20$ or 30. The distribution of aggregate sizes is based on the Helmholtz free energy being a minimum

and is given by:

$$N_i = N/(i+1)(I + e^{-E/kT}) \qquad 2.9$$

where I is the maximum value of i, E is the binding energy per particle, and N_i is the number of chains of i + 1 particles.

2.1.5 Application of Theories to Practical Fluid Behaviour

The development of these theories as previously outlined finally yields equations for viscosity in terms of shear rate from which it is possible to predict the type of flow behaviour that can be represented. Chaffey 1976 does this very clearly and only the pertinent points from his analysis will be summarised here. From impulse theory the final equation is:

$$\eta = \eta_\infty + \frac{4 E a_e [\pi C_1 D + (4/3) a_e^2 G] \phi^2}{V_0^2 (1/C_s t_B + G)^2} \qquad 2.10$$

where a_e is the effective radius of particle contact and where as G, the shear rate, approaches zero, η_0 becomes > η_∞ predicting shear thinning and as G rises, η rises to a maximum then falls to η_∞. Although this equation cannot predict shear thinning followed by shear thickening this behaviour has been achieved by assuming a distribution of time constants, t_B.

$$\frac{\eta}{\eta_\infty} = 1 + \frac{(1 + t_T^P G^P)}{(C_0 + t_s^n G^n)} \qquad 2.11$$

where p relates to link formation and n to link destruction. Hence when $p > n$ shear thickening is predicted and shear thinning when $p < n$.

In the kinetic theory:

$$\frac{\eta}{\eta_\infty} = \left(\frac{K}{N}\right) \sum_{i=1}^{\infty} i^c q^i \qquad 2.12$$

which is developed using expressions for λ and t_D which in the absence of shear stress are reduced by a factor following from Arrhenius law of chemical kinetics namely:-

$$\lambda = \lambda_m \exp\left(-\frac{E_A}{kT} - \frac{\tau V_k}{kT}\right) \qquad 2.13$$

$$t_D = t_m \exp\left(\frac{E + E_A}{kT} - \frac{\tau V_k}{kT}\right) \qquad 2.14$$

where E is the energy of a link, E_A the activation energy of link formation and $E + E_A$ the energy of link destruction and V_k the characteristic molecular volume. No simple equation for η can be obtained since τ is an independent variable but with $c = 3$

$$\frac{\eta}{\eta_\infty} = 1 + 3!\,(\frac{N}{K}) \qquad 2.15$$

and $$G = \frac{1}{\eta}\,(\frac{E}{2V_k} - \frac{kT}{2V_k}\log_e \frac{(\eta/\eta_\infty - 1)}{3N\lambda_m t_m}) \qquad 2.16$$

Whereby for any τ the values of λ and t_D are finite and $K \neq 0$ so that η is finite. As τ approaches zero so does G giving a definite value of η_0 at $G = 0$. Also, K increases as τ increases implying η decreasing with increase in G.

Thermodynamic theory is developed using Mooney's equation for the viscosity of spheres and an analog of it for flattened particles which produces

$$\eta = \eta_\omega \;(\exp \frac{2.5\,\Phi_L}{1 - \Lambda_L\Phi_L}) \;\; (\exp \frac{0.52\,r\Phi}{1 - \Lambda\Phi}) \qquad 2.17$$

where r = aspect ratio of particles, Λ is a crowding factor and

$$\Phi_L = \sum_{i=1}^{I} (i+1)^{1/2}/8\,(I + e^{-E/kT})$$

is the volume fraction of aggregates. The calculation of I is very complicated involving viscous traction of a particle in the surface of the largest aggregate and the hydrodynamics of flow around the aggregate. As G approaches infinity Φ_L approaches zero and η approaches η_∞. This is inapplicable at low G since low hydrodynamic forces allow formation of large aggregates. Extrapolating to G =0 gives indefinitely increasing η which is consistent with a yield stress.

For kinetic theories to give a yield stress, constants in the relaxation time would have to be zero meaning no link destruction at rest. Destruction would be due to shear only inferring no Brownian motion which is explicitly stated in these theories. In general the theories refer to dilute flocculated dispersions, especially the thermodynamic theory. The structural theories mainly predict shear thinning with structure which builds up at rest and is destroyed by shear.

Even with all the work done in kinetic theory there is no simple explanation of shear thinning since a number of analogies and mechanisms give rise to the phenomenon. According to Bird (1979), the subject requires more careful experimentation and realistic molecular models. The theoretical approaches to the formation and breakdown of structures in concentrated dispersions are a long way from explaining some of the experimentally observed behaviour of those fluids. Since as will be shown later cement slurries are concentrated suspensions of chemically reacting particles in water the situation is even more complex and it is unlikely that a theoretical approach will give useful results at this juncture. Rather the experimental, phenomenological approach will

be more fruitful.

2.2 Terms Associated with Yield Stress Behaviour

Since yield stress is so important and there is a certain amount of confusion in the literature, the terms will be defined here.

2.2.1 Thixotropy

The original definition by Peterfi (1972) was an isothermal reversible sol-gel transformation due to mechanical disturbance,according to Cheng (1987). The BS glossary (1975) goes further by defining thixotropy as the decrease in viscosity under stress followed by gradual recovery when the stress is removed; the effect is time dependent. Mewis (1979) gave a generally accepted definition similar to the B.S. one but replacing stress with shear then flow, respectively, and stated in his conclusion on reviewing thixotropy that the presence of a reversible variable structure was required.

2.2.2 Static Yield Stress

This is the value of yield stress obtained in a thixotropic material after prolonged storage. The time for storage depends on achieving a fully built-up structure. In some cases, such as waxy crude oil, the static yield stress is unstable due to the fragile crystalline structure developed by processes other than ageing and when disturbed cannot be reformed by storage (Cheng 1985). This illustrates that there can be other types of structure in thixotropic material and in order to investigate the yield stress probing by shear stress rather than shear rate is essential.

2.2.3 Dynamic Yield Stress

This is the yield stress obtained by extrapolating the equilibrium flow curve of a thixotropic material to zero shear rate. It is postulated by Cheng (1985) that if the material were examined at sufficiently low shear rates the dynamic yield stress would increase to the static value as shown in Figure 2.1. The dynamic yield stress is the value obtained when using various models, such as the Bingham model, shown in Fig. 2.2, and applying curve fitting techniques.

Since extrapolation is the key feature of dynamic yield values the flow curve is measured by varying the shear rate. Some materials when examined at extremely low shear rates, below 10^{-6} sec^{-1}, indicate a tendency towards zero yield stress according to Walters and Barnes, (1985), whilst other materials have shown an upturn as in Fig. 2.1 (Cheng, 1985).

2.2.4 Equilibrium Flow Curve

This is the flow curve obtained from a thixotropic material when the rate of breakdown of structure due to shear is in equilibrium with the rate of recovery of that structure. It is where the structure is in equilibrium with shear rate (i.e. the shear stress will not vary with time).

2.2.5 Static Gel Strength

This term is used for the development of yield stress in a fluid, not necessarily

thixotropic, which is due to a chemical reaction producing a change in structure, (i.e. a gelation). It is therefore irreversible by ageing. Gelation is time dependent and can also be slowed down by the application of a shear rate so strictly speaking it is also a function of shear rate. Therefore a more precise definition would be that it is the stress required to initiate flow in a fluid at a particular shear rate after the fluid had been static for a specified period of time. It is commonly used, in practical terms, in the oil well cementing industry.

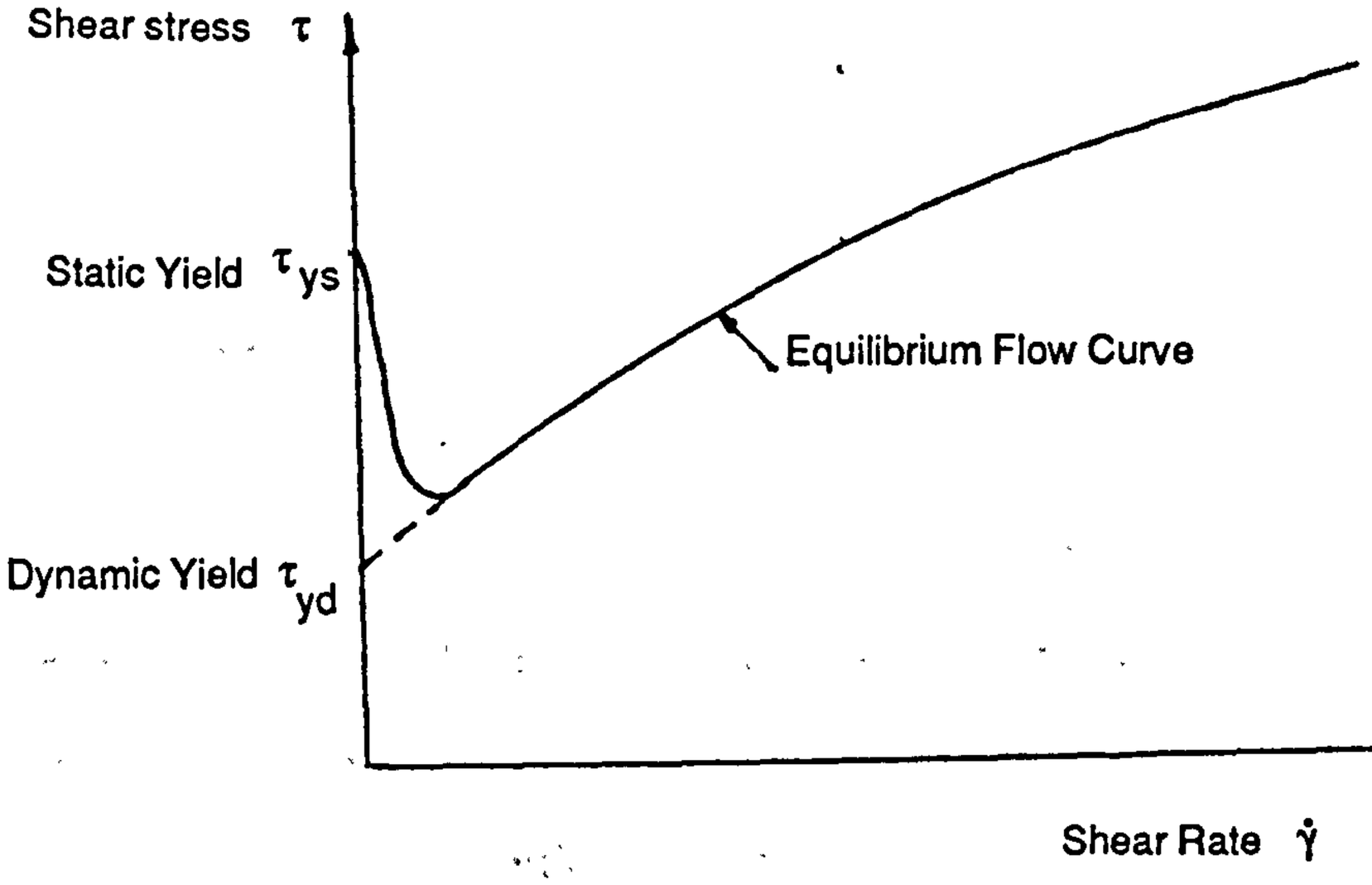

Fig. 2.1 Dynamic and Static Yield Stresses (Cheng,1985)

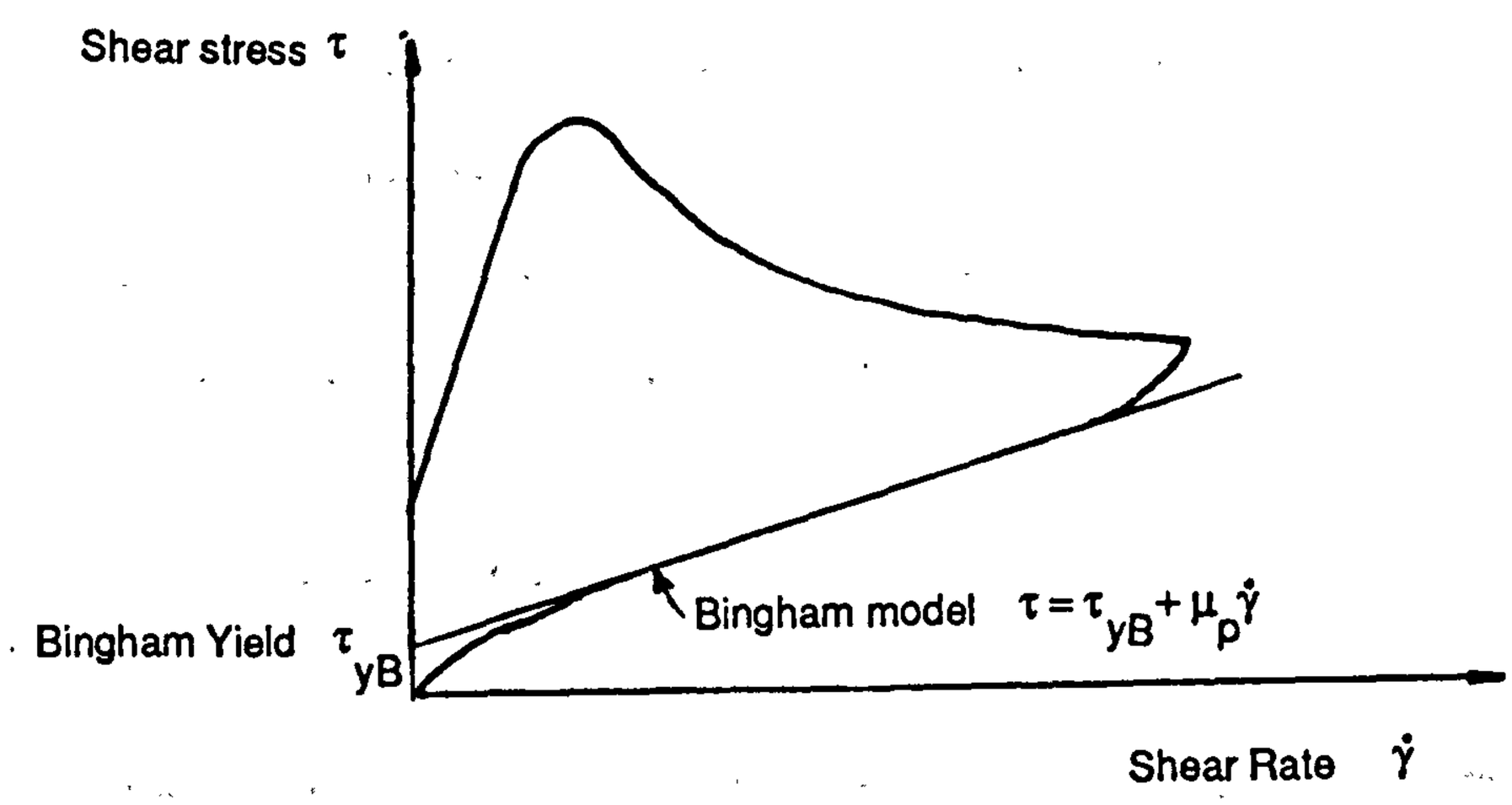

Fig. 2.2 Dynamic Yield Stress from a Bingham Model

2.2.6 Initial Yield Stress

When determining the flow curve of a sample using the Carri-Med controlled stress rheometer the stress at which flow is first detectable is termed the initial yield stress. It depends on the geometry of the measuring system being used and on the rate of increase of stress, as well as the properties of the sample.

2.2.7 Yield Stress

When used in general terms in this thesis is taken to mean that stress which will cause the start of continuous flow in the material at a certain point in time whatever the amount of , though dependent on, previous shear history. It is measured at a shear rate and hence exists on the flow curve. It may be said to be the level of stress of the remaining structure in the material at any point in time.

2.3 Measurement of Yield Stress

Before describing techniques in detail it is necessary to note the general behaviour of a fluid with a yield stress.

2.3.1. Development of Yield Stress Behaviour with respect to Constant Shear Rate and Applied Stress

The development of a yield stress can be distinguished between the behaviour under an applied stress and that under an applied shear rate as follows:-

Under shear stress below the yield value, a non-Newtonian fluid will give a constant shear strain; whereas, above the yield value, shear rate increases with stress. The stress at which the shear rate is no longer zero is the yield stress. This is best shown by the curves in Fig. 2.3. Determination of

$$\frac{d\gamma}{dt} \neq 0$$

is difficult since it requires the constant strain, γ, to be distinguished from the near zero shear rate and this depends not only on the length of time of observation but also the time between application of stress and start of the observation period, Cheng (1985).

Under an applied shear rate the behaviour of an elasto-plastic material would be for the stress to increase to the yield value and remain there regardless of increase in shear rate. In a non-Newtonian fluid with a yield stress, under applied shear rate an equilibrium stress would be reached depending on the shear rate and because of this dependency this equilibrium stress would not be the yield stress. However if the shear rate were reduced to zero a residual value is found on the stress axis which is the yield value for that particular fluid. In a thixotropic fluid, depending upon the previous shear history, stress decay or recovery can precede equilibrium and a constant structure flow curve is obtained with an intercept on the stress axis. This constant structure curve will vary according to the state of the structure of the fluid. Each intercept is a yield stress which is a function of structure. When the structure is in equilibrium with the shear rate (i.e. neither decaying nor recovering at that shear rate) the stress remains constant with time at that shear rate and the equilibrium flow curve can be obtained. Since the yield

stress increases with recovery of structure the maximum yield stress at fully built-up structure is the same as the yield stress from the equilibrium flow curve as shown in Figure 2.4.

2.3.2 Alternative Methods of Measurement of the Yield Stress of a Concentrated Suspension

Numerous methods have been used to measure the yield stress of suspensions since the Bingham formulation by Oldroyd (1947). Many of these use existing pieces of equipment originally used for other materials, such as the shear box and the U tube viscometer, then modified for suspensions. Tattersall and Banfill (1983) mention the wide range of results for cement pastes obtained using such an assortment of methods and techniques. However, the main methods used to measure the yield stress of concentrated suspensions are:-

1. translatory penetrometers
2. tube or gun rheometers
3. oscillatory rheometry
4. rotational rheometers/viscometers.

These have all been used for cement pastes but repeatability, even when using the same type of apparatus and techniques, can be a problem. Banfill (1987) suggested that the main reasons for the different results were:-

1. geometric suitability of apparatus;

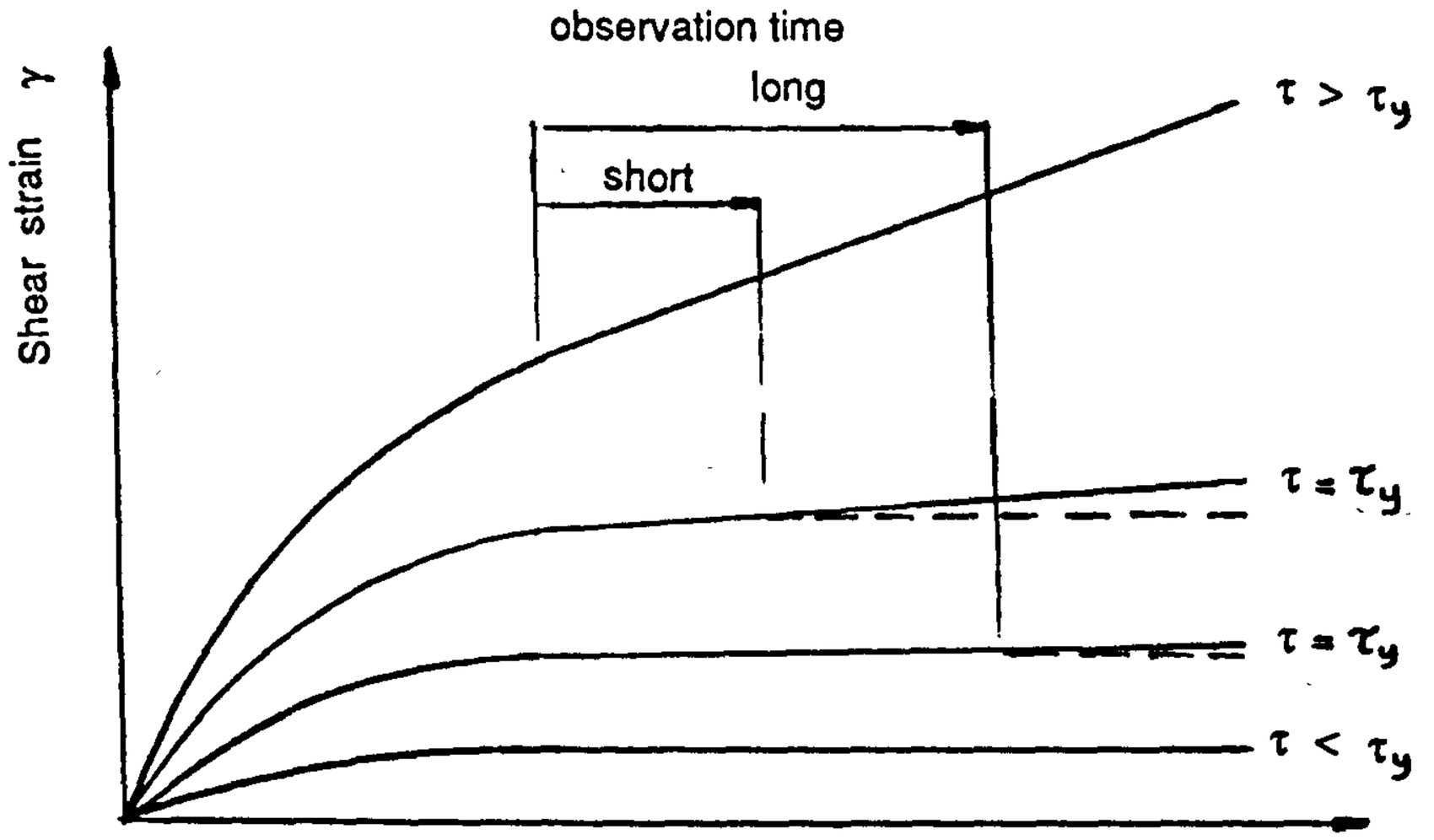

Fig. 2.3 Yield where $\frac{d\gamma}{dt} \neq 0$ (Cheng,1985)

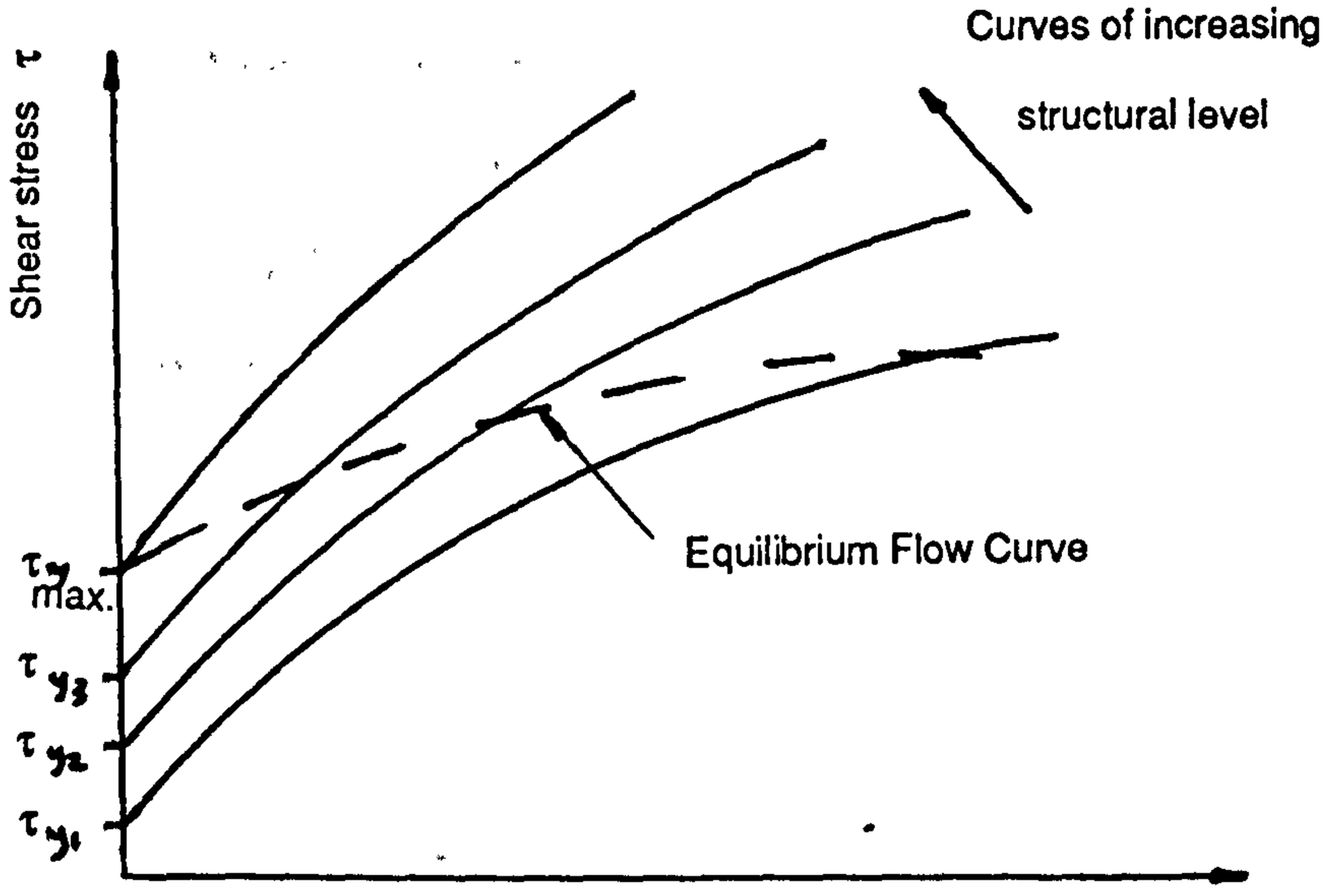

Fig. 2.4 Yield Stresses in a Thixotropic Fluid (Cheng,1985)

2. structural breakdown - mixing, loading and testing the sample;
3. wall slip and plug flow;
4. variation in cement composition during manufacture.

2.3.2.1 Translatory penetrometers

These devices consist of driving, in translation rather than oscillatory or rotary motion, a particular shaped element into a sample of the material, using either gravity or some external force. Yield stress has been derived in relation to the depth of penetration. The apparatus is in common use for empirical comparison of materials. However, the rheological properties of the type of material, for which penetrometers seem suitable, are not fully understood (i.e. pastes and semi-solids). Hence, the interpretation of the results is difficult. Tattersall and Banfill (1983) highlight the discrepancies when comparing yield stress determination by penetrometers with those by coaxial cylinder viscometry.

2.3.2.2 Tube or Gun Rheometer

Basically these devices comprise a cylindrical tube which is filled with the material to be tested. The tube is attached to a pressure vessel so that the pressure on the material can be steadily increased until flow occurs. Measurements are taken to extrapolate the minimum pressure which causes yield and the yield stress is determined from:

$$\tau_y = \frac{D}{4}\frac{P_{min}}{L} \qquad 2.18$$

As pointed out by Cheng (1985) this device overcomes the problem of disturbance of the structure of the sample when transferring from a mixing container to a viscometer or when inserting a measuring device into the sample. However, the actual loading of the tube must cause considerable disturbance, unless the loading closely follows high speed mixing. The detachable tube enables ageing tests, since disturbance and evaporation are controlled.

Haimoni (1985) performed a number of tests on cement paste using a gun rheometer and found the gel strength to be a function of the tube diameter. He attributed this relation to the effect of a slip layer of lower particle concentration, near the wall of the tube. The thickness of this layer varied with tube surface roughness, tube diameter and cement paste stiffness. He concluded that the true gel strength would only be measured if the suspension was sheared within itself, such as with a vane, rather than along the inside of a tube.

2.3.2.3 Oscillatory Rheometry

Rheometers are used to measure the dynamic properties of viscoelastic fluids. This is done by subjecting the sample to sinusoidal stress waveforms at a set frequency. The response of the sample is a strain wave form whose amplitude and phase difference is measured. The dynamic properties are calculated from this data. On modern rotational rheometers controlled by computer the motion is a torsional oscillation. Jones et al (1987) have derived mathematical formulae for a number of measuring systems,

including the effects of inertia, to evaluate both the dynamic viscosity, η', and the dynamic rigidity, G', for this type of instrument. There is no simple relation between

these dynamic properties and the properties derived from steady simple shear flow (i.e. yield stress, etc.). Cheng (1985) gives a method of measuring yield stress using oscillatory testing by observing when the response waveform gets a flat top thereby indicating yield has been exceeded. This method requires extrapolation, which is not likely to be precise. As Walters (1975) remarks, the dynamic properties probably describe the material behaviour under given operating conditions better than other properties, and the experimental determination of complex dynamic viscosity is pursued in the investigation of the molecular structure of viscoelastic material, where there is a strong correlation between structure and elasticity. The orthogonal rheometer, parallel plates both rotating at the same angular velocity but on eccentric axes, is another means of obtaining oscillatory stresses. Jones (1987) notes that oscillatory testing can be non destructive and using combined steady shear with oscillatory stresses found qualitative agreement with pulsatile pipe flow results.

Mewis (1979) warns that with thixotropic materials oscillatory testing could interfere with structure build up, especially in particulate systems, except where there is sufficient deformation caused by molecular aggregation in the structure build up. He also comments that when measuring a transient yield stress it is essential to obtain a constant shear rate throughout the sample since yield stress changes with time and shear rate, in thixotropic materials. Where transient structure exists it remains to be established under which conditions a given material deforms homogeneously during the particular experiments.

2.3.2.4 Rotational Viscometers

Rotational viscometers generally measure the viscosity of a sample of fluid by the

fluid being held in one element, such as a cup or plate, whilst a second element (e.g. a cone) immersed in the fluid is rotated,usually at set speeds. The torque generated is measured and the viscosity calculated. With non-Newtonian fluids it is the rheological properties which require measurement to model their behaviour. These properties, such as yield and power law index, are measured with a rheometer and in the special case of normal stress with a rheogoniometer. Although torque is applied and angular movement measured, or visa versa, the rheological properties are calculated in similar fashion to viscometry. The controlled stress rheometer enables deformation of the sample to be studied in the non-destructive region around yield, which was not possible with constant shear rate instruments.

2.3.3 Techniques using Controlled Shear Rate Instruments

The yield value can be inferred from the results obtained in experiments using controlled shear rate instruments by:

1. direct extrapolation
2. shear stress relaxation
3. step change in shear rate
4. extrapolation using models
5. direct measurement with a vane.

2.3.3.1 Direct Extrapolation

Direct extrapolation of the flow curve in the low shear rate region has in the past been carried out on the downcurve to obtain the Bingham yield value and viscosity to

characterise the Bingham model which applied over a limited range of shear rates and as is emphasised by Tattersall and Banfill (1983) caution is necessary if extrapolation is made outside this range.

2.3.3.2 Shear Stress Relaxation

In this technique which is described by Nguyen (1983) the shear rate is stopped at various times and for various periods of time. The residual shear stress is measured which is the yield stress, as shown in Fig. 2.5. This technique may be used on a fully broken down suspension with no chemical reaction but is unsuitable where the yield stress is dependent on previous shear history and subject to chemical reaction, such as is the case with cement slurry. The technique is also used with constant shear rate apparatus and has poor reproducibility.

2.3.3.3 Step Change in Shear Rate

A sample is sheared at a reference shear rate $\dot{\gamma}_e$ and on obtaining equilibrium stress, a step is made to a higher, or lower, shear rate at which the initial stress, τ_0, is noted. This is repeated for a number of different steps in shear rate. The curve τ_0 v $\dot{\gamma}_0$ is plotted giving a constant structure curve with intercept τy, for that particular reference $\dot{\gamma}_e$ structure. The reference shear rate is changed and the series repeated to give a plot of τ_y

v $\dot{\gamma}_e$. This enables τ_y to be expressed for a range of structures. A diagrammatic form of the experiment is shown in Fig. 2.6. The yield stress may be expressed in terms of its equilibrium viscosity $\eta_e = \tau_e/\dot{\gamma}_e$ which is a structural parameter.

In order to obtain yield stress as a function of time Cheng (1985) devised a variation to the above method by measuring the rate of change of stress at the initial stress, τ_0, at each step. Plotting β_0 against $\dot{\gamma}$ for each $\dot{\gamma}_e$ and extrapolating the intercept β_y, which when plotted against τ_y and integrating the curve gives τ_y as a function of time; this has been done for a 10% bentonite paste using a gun rheometer the results being as shown in Figure 2.7.

Mewis (1979) comments that with the complex effect of the measuring conditions on the results the step method is not suitable for fast screening. The time of rest between steps is prohibitive with cement slurry, where fast screening is essential, since the time of rest must be sufficient to reach equilibrium conditions.

The use of stress instead of shear rate as the step function is problematic with values above yield, when using a controlled stress rheometer, since, instead of reaching a shear rate equilibrium the shear rate tends to infinity and a technique for this apparatus has not been developed to obtain τ_y as a function of time, using the step change method.

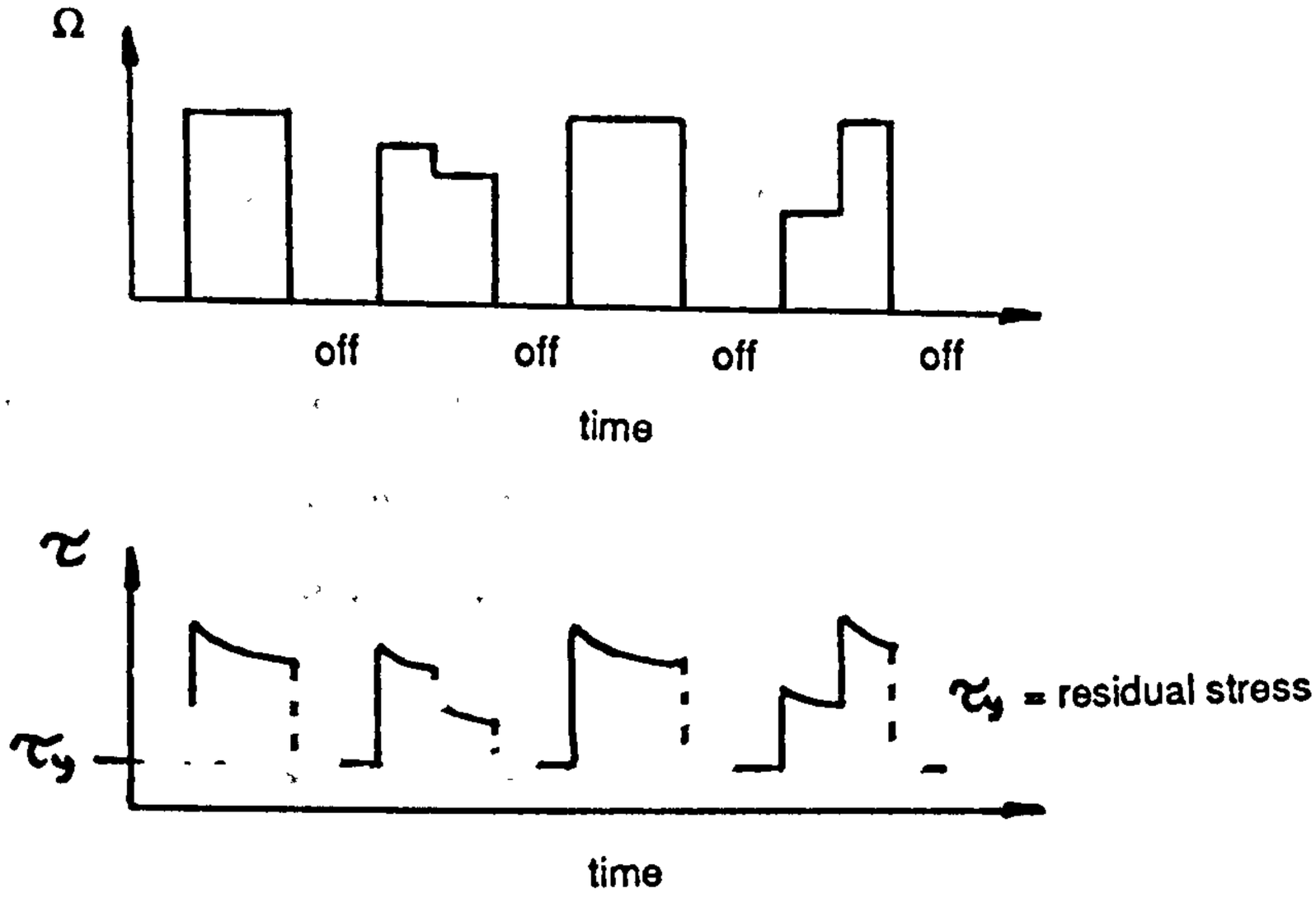

Fig. 2.5 Yield Stress by Relaxation Method

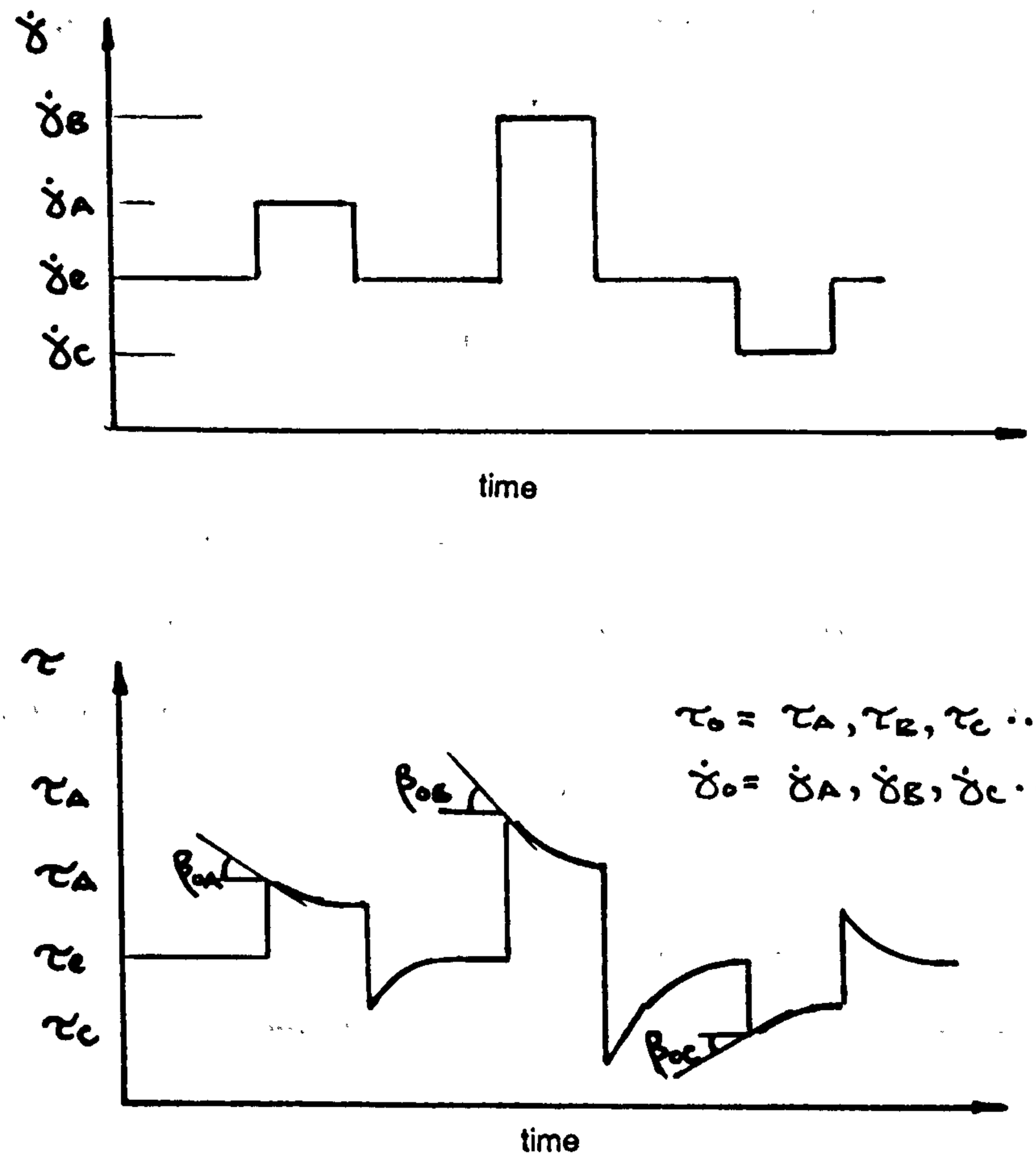

Fig. 2.6 Step Change in Shear Rate (Cheng,1987)

2.3.3.4 Extrapolation using Model Fits

Extrapolation using model fits has according to Ngugen (1983) been used by Bukham et al. (1982) who on using the Casson model found good correlation for bentonite and cements with s = 4 in the Casson equation:

$$\tau^{1/s} = (\tau y)^{1/s} + (\eta_{\infty}\dot{\gamma})^{1/s}$$

where τ_y is the Casson yield stress and η_{∞} the infinite shear viscosity. For the investigation of yield stress the model fit method is hampered by the model being representative over a certain range and extrapolation being a doubtful exercise outside that range.

2.3.3.5 Direct Measurement with Vane

In the past, researchers have studied τ_y using constant shear rates at very low value, O.1 r.p.m. and O.1 degree /sec., so as not to disturb the development of structure. Though how this is achieved is not made clear nor, as is pointed out by Nguyen (1983), that these experiments are constant speed rather than constant shear rate.

In this method a vane, as shown in Fig. 2.8, replaces the cylindrical bob in the concentric cylinder arrangement. Nguyen and Boger (1985) provide geometrical constraints to minimise errors when using the vane in a cup. The main advantage of a vane is that it measures shear within the material thereby overcoming the problem of

slippage encountered with cylindrical bobs.

2.3.4 Controlled Stress Rheometers to Measure Yield Stress

The fundamental objection to the use of controlled shear rate instruments for the evaluation of yield value is that yield is defined as the behaviour at zero shear rate and these instruments cannot measure at a zero speed. Extrapolation of a flow curve is always necessary. Controlled stress instruments do not have this disadvantage and stresses may be applied which cover the range around the yield stress and permit it to be defined reliably. It is merely necessary to calculate the stresses from the applied torque and the geometry of the measuring system.

limitations_of the

This section describes the various measuring systems which may be used in controlled stress rheometers.

The measuring system in this context refers to the geometry of the elements in contact with the sample and inducing a particular flow behaviour to that sample. The configurations that have been used include:-

1. coaxial cylinders
2. rotating disc
3. cone and plate
4. annular cone and plate
5. parallel plate
6. vane

The first three configurations, shown in Fig. 2.9, have been the subject of much research, including Krieger et al. (1953), Bird et al. (1962), Walters (1975) (1987), Mannheimer (1983) Tattersall and Banfill (1983) Nguyen (1983) and Cheng (1987), to overcome the following sources of error which tend to be common to all rotational measuring systems:-

1. edge and end effects
2. slippage
3. secondary flow
4. viscous heating

2.3.4.1 Cone and Plate

With the exception of the cone and plate, quite involved correction calculations are required to obtain stress and shear rate from measurements of torque and angular velocity for non-Newtonian fluids with these systems. The cone and plate is unsuitable for use with particulate suspensions because the particles jam near the zero gap at the cone apex or cause error in the gap setting. This disadvantage was overcome to some extent with the annular cone and plate as suggested by Cross and Kaye (1986) and discussed in more detail in the next chapter. The reason the cone and plate does not require correction for analysis of non-Newtonian fluids is because in torsional flow the configuration imposes a constant shear rate throughout the sample. This means that the shear stress is not dependent on the radius of the cone, assuming that shear stress is a function of shear rate which is the case (Oldroyd, 1956).

2.3.4.2 Rotating Disc

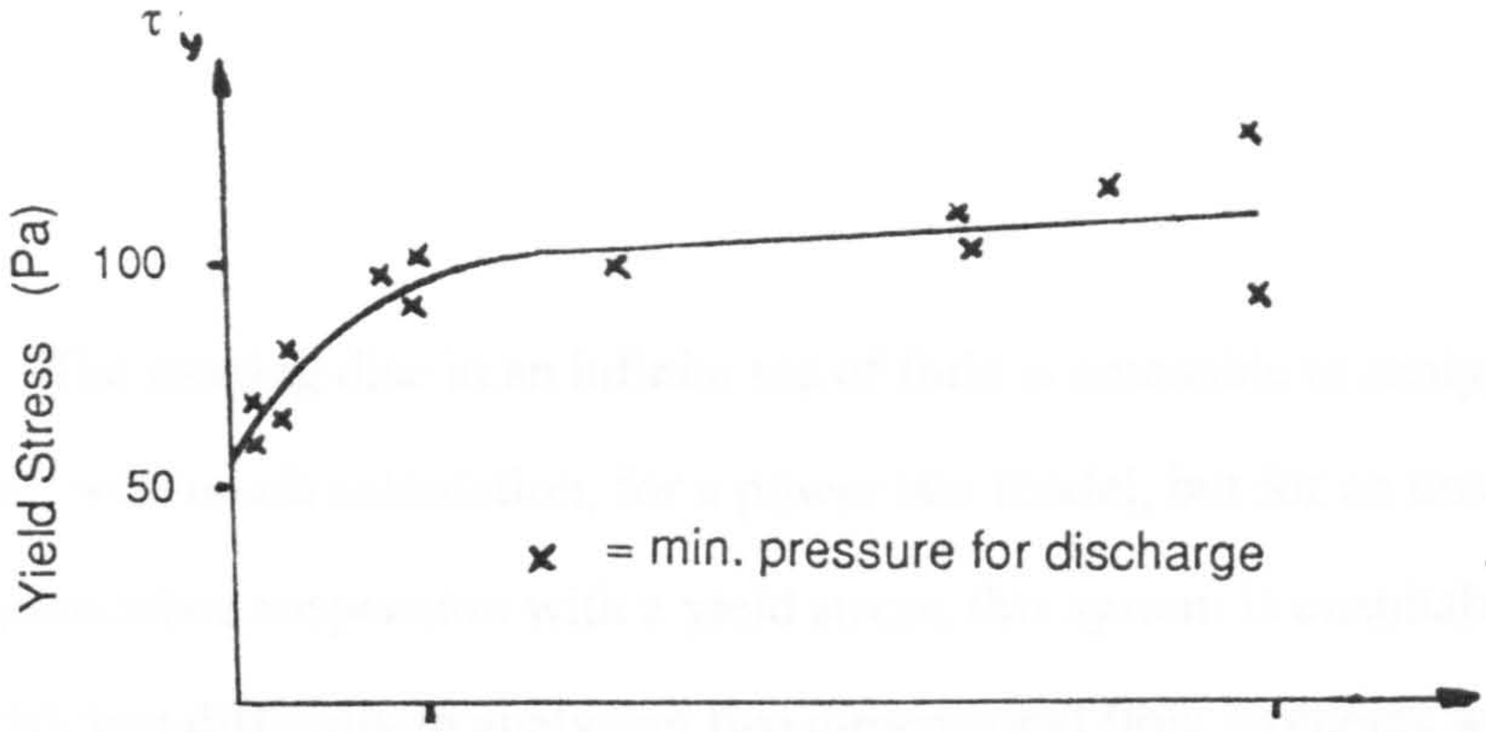

Fig. 2.7 Development of τ_y with Time for 10% bentonite paste (Cheng,1985)

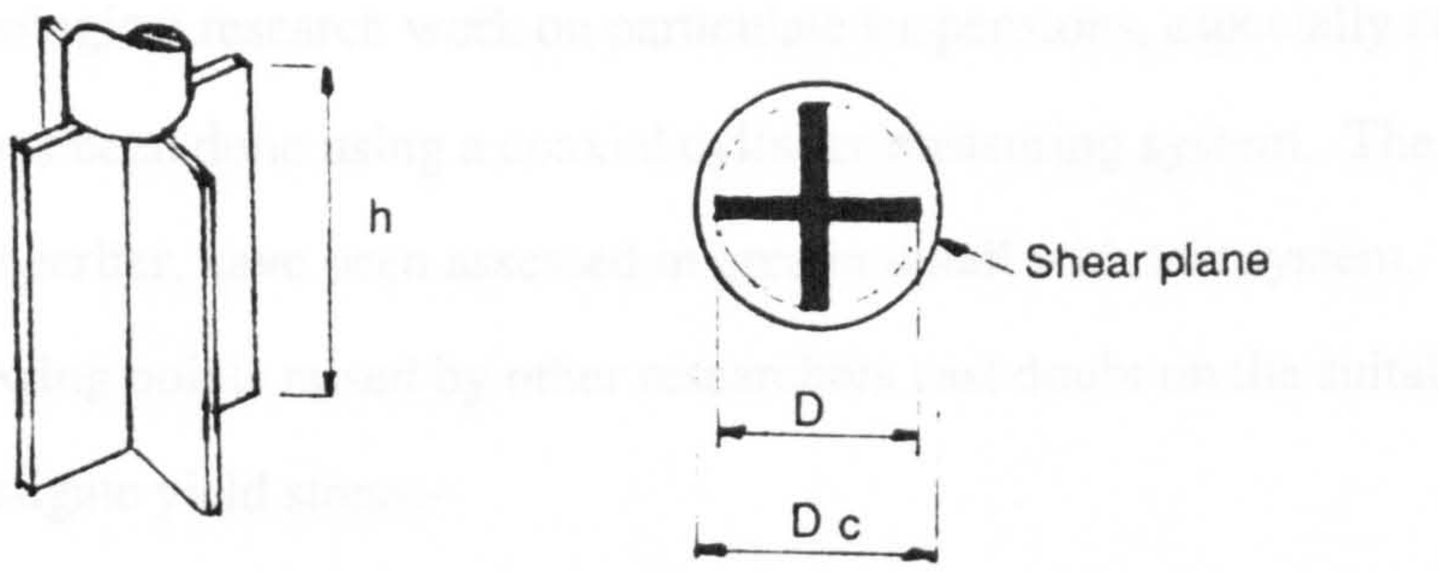

Fig. 2.8 Four Blade Cylindrical Vane

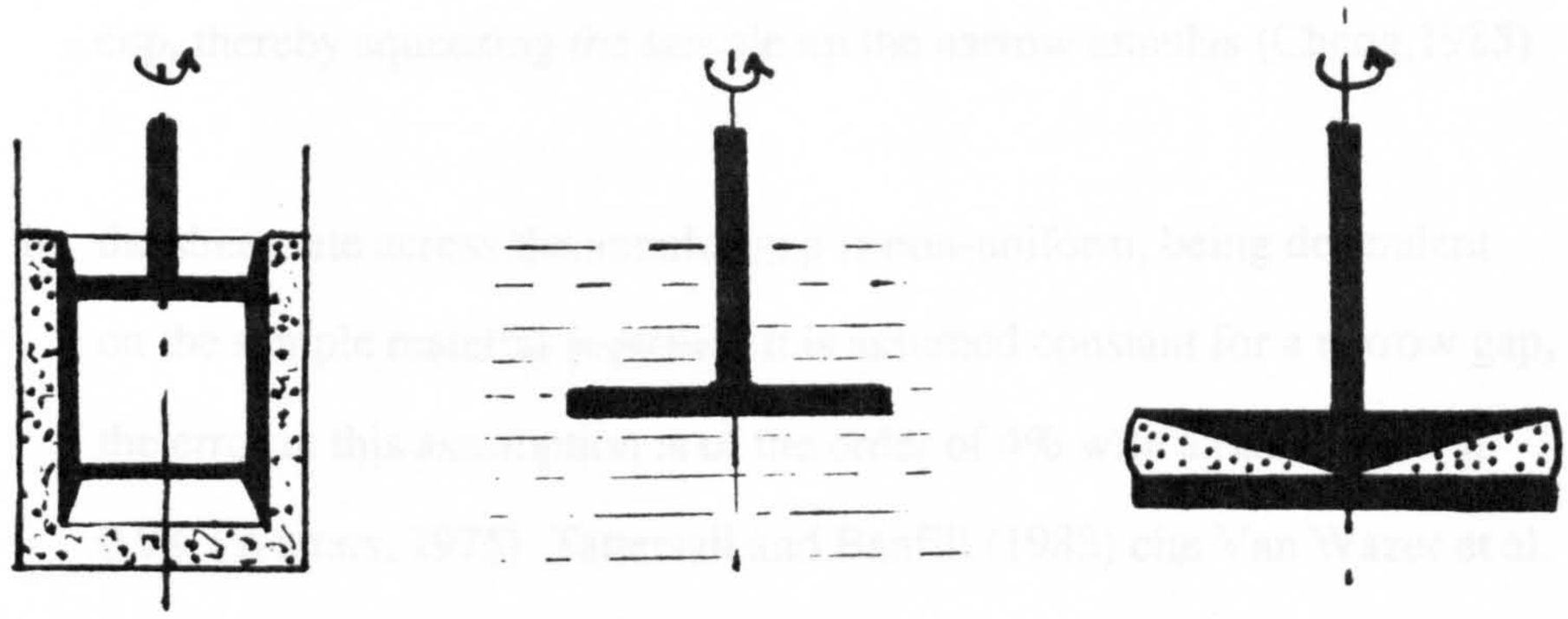

Fig. 2.9 Measuring Systems

The rotating disc in an infinite sea of fluid is amenable to analysis for a Newtonian and, with much calculation, for a power law model, but for an unknown model, such as a particulate suspension with a yield stress, this system is unsuitable. Also, there is sufficient difficulty in analysing two dimensional flow problems without venturing into three dimensions with fluids such as cement slurry.

2.3.4.3 Coaxial Cylinder

Most of the rheological research work on particulate suspensions, especially cement pastes or slurries, has been done using a coaxial cylinder measuring system. The sources of error, mentioned earlier, have been assessed in greater detail with this system. However, the following points raised by other researchers cast doubt on the suitability of this system to investigate yield stress:-

a) structure is destroyed when immersing the bob into the sample filled cup, thereby squeezing the sample up the narrow annulus (Cheng,1985)

b) the shear rate across the annulus gap is non-uniform, being dependent on the sample material properties; it is assumed constant for a narrow gap, the error in this assumption is of the order of 4% with a radius ratio at 0.98. (Watters, 1975). Tattersall and Banfill (1983) cite Van Wazer et al. (1963) and McGreary (1961) for suggesting a gap size of at least 10 times the largest particle size which is supported by the latter's work on packing fraction being independent of container size when the container was greater than 10 times the particle size.

c) anomalous plug flow with cement paste on the stationary cylinder observed by Tattersall and Dimond (1976) occuring above the minimum shear rate at which normal plug flow takes place. This anomalous plug flow occurs with cement pastes that have not been broken down in the mixing procedure and is related to the hydration of the sample at the time of testing.

2.3.4.4 Parallel Plate

(See Fig.3.2 on page 77)

The sources of error, other than experimental error which is covered well by Tatterall and Banfill (1983) and Richards (1967), have been thoroughly investigated by numerous authors, including Bird et al (1973), Walters (1975), Keentok and Tanner (1982), Kulicke et al (1977). These errors include:-

1. inertial effect of plate and sample
2. edge effects
3. surface tension
4. air bubbles in sample
5. deflection of plate
6. temperature from viscous heating
7. secondary flow effects

The general consensus is that inertial effects, surface tension and deflection of the plate give insignificant error with the parallel plate system and can be neglected. The air bubbles in a sample can significantly lower both normal and shear stresses, hence degeneration, or as recommended in the API specification (1986), the addition of liquid

defoamers, should be carried out. Temperature variation of the order of $\pm 0.5^{o}C$ affects normal stress readings but is barely perceptible in shear. This leaves edge effects and secondary flow as the major error contributors.

The presence of an edge causes secondary flow effects which become significant at higher shear rates since they are normally associated with turbulence. The error due to edge effects manifests itself in terms of an error in torque which varies as a function of the ratio of the gap to the radius of the plate. This error is of the order of 1% for a gap to plate ratio less than 0.05. In tests on parallel plates investigating the error from having a peripheral sample as opposed to a sea of liquid it was found that the total force was unaffected by a change in the gap, (Walters, 1975).

2.3.4.5 Vane in Cup

This measuring system is well suited to measure yield stress since it shears the material within the material. It does have a number of complications, such as the determination of shear rate and the disturbance of structure on loading, which are discussed in the next chapter. The vane has been used for particulate slurries and is developed for measuring yield stress by the investigations of Nguyen (1983), Haimoni (1985) and Keentok et al (1985).

2.4 Rheology of Cement Pastes

The rheological behaviour of cement pastes is complicated. The results of many researchers in the past have failed to agree either quantitatively, or even qualitatively, largely because of the variety of apparatus and experimental technique, as was noted in

the previous section. In order to better understand the rheology of cement pastes, rather than account for all the differences, it is necessary to know the chemical and physical proceesses that are taking place and the various factors that affect them. The chemical process of hydration that takes place on combining cement and water will be described first.

2.4.1 Mechanism of Hydration of Cement

As most oil well cements are based on Portland cement , including class G which is used throughout this thesis and is both sulphate resisting and coarsely ground, discussion of the hydration of Portland cement is therefore relevant. Portland cement clinker is made by burning in a kiln a mix of limestone or chalk and clay or shale, at a sufficiently high temperature (~1500°C) to theoretically obtain zero free lime, since this lime causes expansion by delayed hydration, which is increased by increased C_3A and high sulphate levels, (Bye, 1983), and to obtain phase equilibrium on cooling so that the oxides from the raw materials form the required combination of the 4 major compounds, C_3S, C_2S, C_3A and C_4AF. These compounds are given in cement chemist's shorthand which assigns each oxide unit a symbol as follows:-

Oxide	CaO	SiO_2	Al_2O_3	Fe_2O_3	H_2O	Na_2O	K_2O	SO_3
Symbol	C	S	A	F	H	N	K	$\bar{S}$

Polymorphism, the different crystalline forms of the same chemical composition, and the low levels of solid solution, which involve a distribution of the solute ions, affect the

silicates causing impure forms of alite and belite, which form ,at various cooling temperatures, with foreign ions of Mg, Al, Fe, K and Na. These points illustrate that cement clinker is a highly complex material made from very variable raw materials in a process where even the combustion products, such as ash in coal fired or sulphur in oil fired kilns, can affect the composition. The clinker is ground with gypsum to increase the sulphate content of the cement to the required composition. The gypsum which controls the setting of the cement is dehydrated in the cement mill depending on the temperature and relative humidity and can have the range $CaSO_4$ 0.0l-0.63 H_20 (Bye, 1983). A typical chemical analysis for a class G oil well cement is given in Appendix 3 together with the compound composition, calculated from the Bogue equation. The O P C and sulphate-resisting cement comparisons are from Tattersall and Banfill (1983) and the typical size distrubtion of a class G is from Haimoni (1987). From the foregoing it can be appreciated that to maintain the same composition for a class of cement is difficult even for a particular works which is why cements are often blended. The class G cement used in the North Sea has stricter control on the free lime (< 1.8%) and sulphates must be less reactive than OPC (Bensted, personal communication 1986).

Immediately cement comes in contact with water both lime and silica appear in solution. Ca^{2+} ion concentration rises rapidly as hydration proceeds at high pH and C-S-H gel, so-called since it is a poorly crystaline and ill-defined calcium silicate hydrate and calcium hydroxide (portlandite) are formed on the tricalcium silicate, C_3S, surface. At the same time the other phases tricalcium aluminate, C_3A, and tetra calcium alumino-ferrite, C_4AF, are hydrating ettringite ,$C_3A.\ 3CaSO_4.\ 31\text{-}32H_20.$, an alumino-sulphate, less rapidly in the presence of lime and gypsum. The C_4AF hydration is similar to C_3A but with Al^{+3} ions partly substituted by Fe^{3+} ions. The hydration of

the C_2S is very slow. The extent of reaction of the four phases is approximately

C_4AF		hydrates 90% in 1 day
C_3A	"	80% in 1 day
C_3S	"	40% in 1 day (60% in 20 days)
C_2S	"	20% in 10 days (40% in 100 days)

(Tattersall and Banfill, 1983)

Calorimetric studies of the rate of heat evolution during hydration of both cement and C_3S shows that an initial rapid reaction is complete within a few minutes and is followed by a dormant period with a low reaction rate, for about 3 hours. The reaction rate then rises as setting takes place.

The C_3A hydrate crystals are weak relative to the C_3S so the C_3A hydration is controlled using sulphates which act as a catalyst for C_3S hydration. Depending on time, temperature and C/S ratio which can vary from 1.5 to 3.0, the morphology of C-S-H can occur as fibres, reticules, grains or 'inner product', after several days. Only α-C_3S and $\beta-C_2S$ form strong hydrate structure, however it is the early hydration which is of concern for the rheology.

The basic early hydration of silicate components is

a) gelatinous hydration products form around cement grains

b) C-S-H gelation subsides and grows fibrous crystals after a few hours

c) $Ca(OH)_2$ at the same time forms large tubular crystals.

whereas for aluminate components it is

a) ettringite forms on the surface

b) as C_3A reacts sulphate is relased through the ettringite layer until the sulphate is depleted

c) the C_3A hydrates and turns the ettringite into needle shaped crystals of monosulphate.

Various theories are used to explain the dormant period. The protective layer theory suggests that a 'first' hydrate layer starts the dormant period and a second C-S-H layer, more permeable to water and ions, terminates it. The delayed nucleation theory considers the $Ca(OH)_2$ concentration to rise to the level of supersaturation, where it nucleates slowly at low degrees of supersaturation but rapidly on high critical supersaturation. Seeding of the portlandite crystals to encourage nucleation would shorten the dormant period but the nuclei are poisoned by silica. Finally, there is the membrane osmosis model, where the first hydrant of C_3S is a semi-permeable membrane into which water diffuses. Ca^{2+} ions pass out of this membrane but not $Si\ 0_4$. Water drawn into the membrane eventually ruptures it and fresh hydration products, which inhibit hydration less than the first hydrates, are produced. Foils and solid fibres are the new forms with the C_3S hydration and tubules are the forms of the C_3A and C_4AF hydration products. (Bye

1983). Electron microscopy can observe some of these facts but the process initiating the end of the dormant period is still controversial.

The physical interaction between particles which occur during early hydration are discussed in Chapter 8 in relation to the results of the experiments of this thesis.

2.4.2 Flow Curves

Flow curves are the means by which the rheological properties of a material are displayed. The flow curve is a plot of the relationship between a non-isotropic stress component, such as shear stress, and the corresponding deformation rate which, in the case of shear, is shear rate. Shear rate is the accepted term for rate of shear strain.

Some fluids, termed Newtonian, obey Newton's viscous law which states that the non-iso tropic stress is proportional to the corresponding deformation rate providing that the flow is isothermal and incompressible. This type of fluid, such as water and most oils, displays a straight line flow curve which passes through the origin as shown in Fig. 2.10. The slope of this flow curve is the shear viscosity which is independent of time.

It is represented by the equation $\tau = \eta\dot{\gamma}$ (2.20).Other fluids, including cement slurry, display deviations to this straight line relationship, and are termed non-Newtonian. Pseudoplastic, which is shear thinning,and dilatant, which is shear thickening, are fluids whose flow curves obey the Ostwalde de Waele or power law relationship

$$\tau = k\dot{\gamma}^n \qquad 2.21$$

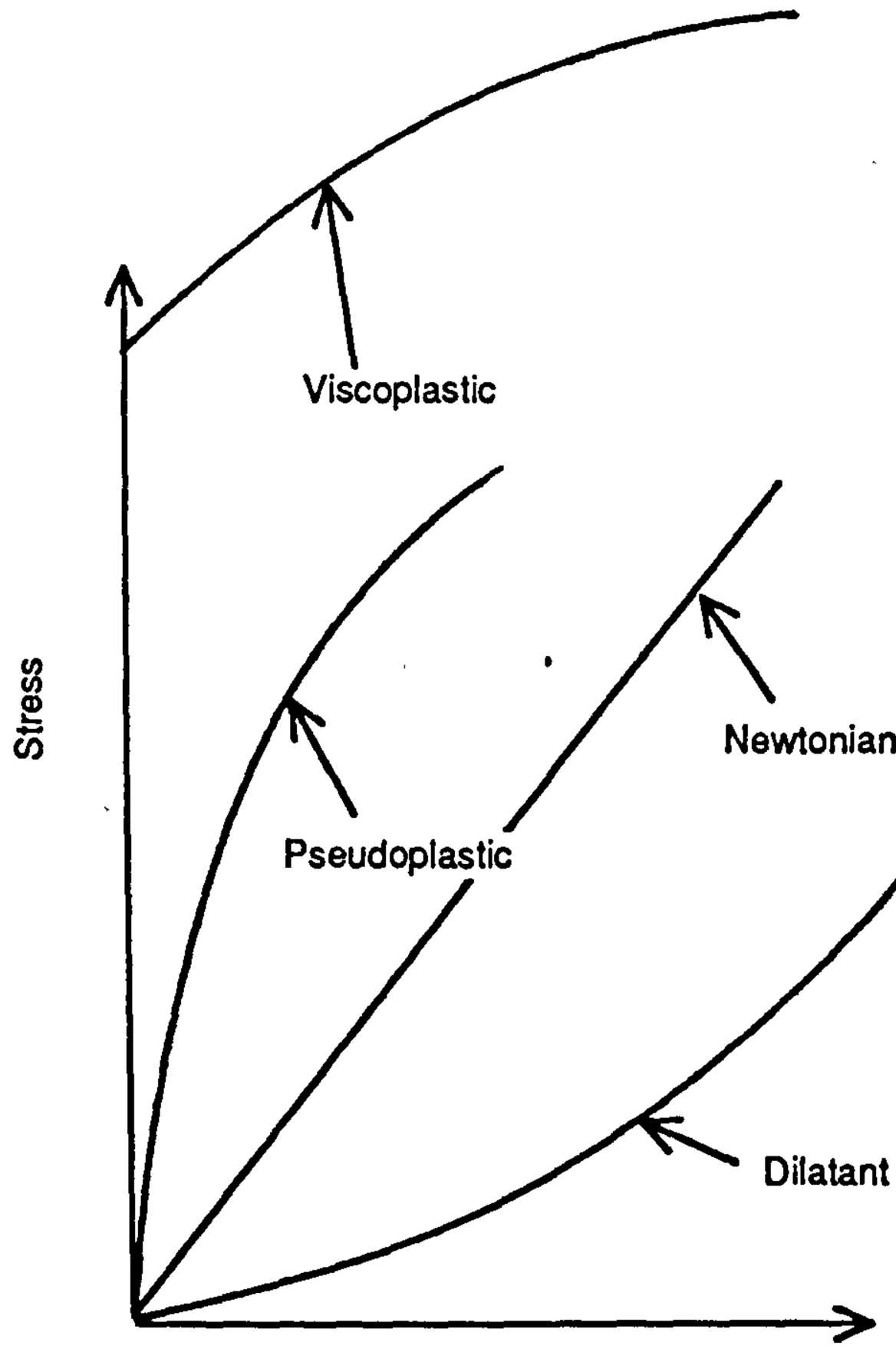

Fig. 2.10 Flow Curves of Various Fluids

where k is a constant whose dimensions depend on n.

The viscoplastic is the generalised Bingham model and is represented by the Herschel Bulkley equation

$$\tau - \tau_y = k\dot{\gamma}^n \qquad 2.22$$

which becomes the simple Bingham model when n=1. The introduction of the yield stress; τ_y, which occurs when $\dot{\gamma} = 0$ means that this flow curve can more closely reflect the behaviour of a fluid such as cement slurry. Again k depends on n as regards dimensions, which means it cannot be a material property. As Harris (1977) points out, mathematical manipulation is difficult since the derivative

$$\frac{d\dot{\gamma}}{dt}$$

depends on the sign of $\dot{\gamma}$ and the formula can only be applied to simple steady shearing.

There are many other models of time independent fluids which either better describe the fluid behaviour or perform a closer curve fitting to the flow curve, such as a power series. Examples of these models are the Kreiger-Dougherty,

$$\frac{\eta - \eta_\infty}{\eta_0 - \eta_\infty} = \frac{\tau_c}{\tau_c + \tau} \qquad 2.23$$

the Oldroyd, $$\eta = \eta_0 \left(\frac{1 + a_1 \dot{\gamma}^2}{1 + a_2 \dot{\gamma}^2}\right) \qquad 2.24$$

and the Cross model $$\eta = \eta_\infty + \frac{\eta_0 - \eta_\infty}{1 + a\dot{\gamma}^m} \qquad 2.25$$

Time dependence of the fluid behaviour further complicates flow curve description. This occurs with thixotropic fluids whose internal structure changes with time as opposed to shear rate. This point is not made clear in the literature but it is the build up of structure with time on cessation of shear, or under steady shear as with rheopexy, that shows time dependency.

The simplest example of time dependence of a viscoelastic fluid is the Maxwell model

$$\tau + \lambda \dot{\tau} = \eta \dot{\gamma} \qquad 2.26$$

where λ is a relaxation time. This model describes the decay in stress with time as the motion ceases. By multiplying this equation by the integrating factor

$$e^{\int (1/\lambda)\, dt'}$$

rearranging and integrating, the equation is expressed in the following generalised form

$$\tau = \frac{\eta}{\lambda} \int_{-\infty}^{t} \dot{\gamma} \exp\left(-\frac{[t - t']}{\lambda}\right) dt' \qquad 2.27$$

(Harris, 1977). If the fluid has many relaxation times then the viscosity interval described by the relaxation spectrum $N(\lambda)$ is $d\eta = N(\lambda) d\lambda$ which combines with the differential with respect to $d\eta$ of equation (2.27) and integrating gives on defining the memory function as

$$N(t-t') = \int_{0}^{\infty} \frac{N(\lambda)}{\lambda} \exp\left(-\frac{[t-t']}{\lambda}\right) d\lambda$$

the time dependent relationship of stress and shear rate of

$$\tau = \int_{-\infty}^{t} N(t-t')\, \dot{\gamma}(t')\, dt' \qquad 2.28$$

Using a two-component distribution function of $N(\lambda)$ Thomas and Walters (1964) showed

that equation (2.28) can reduce to the differential form

$$\tau + \lambda_1 \dot{\tau} = \eta (\dot{\gamma} + \lambda_2 \ddot{\gamma}) \qquad 2.29$$

where, in steady shearing $\ddot{\gamma} = 0$ and with no time dependency $\lambda_1 = 0$, both the Maxwell and Newton models can be obtained.

As described in section 2.1, various kinds of model describe fluid behaviour which are complicated by time dependence and show asymptotic flow curves at high shear rate with extrapolation back to a dynamic yield stress intercept. Some models do not predict this intercept and none predict a true yield stress. The state of knowledge of cement paste rheology suggests that an empirical approach is justified.

2.4.3 Breakdown of Structure during Shear

Previously accepted practice in flow curve construction was to increase the shear rate from zero to some arbitrary maximum and record the stress at each increment either manually or automatically using some arbitrary rate of increase in shear rate. The process would then be reversed immediately to zero shear rate. Tattersall (1954) whilst working with 0.28-0.32 w/c ratio O P C pastes which were tested at 4 1/2 minutes using a concentric cylinder viscometer, found at high shear rates the pastes showed shear thinning and hysteresis loops. Hysteresis loops characterise the breakdown of structure in the cement paste. The Bingham model parameters were then calculated from the down curve which displayed the broken down material. Some workers, such as Ish-Shalom

and Greenberg (1960) and Roy et al (1980), reported hysteresis loops for cement pastes similar to type 3 in Fig. 2.11 whereas most workers found type 1. Banfill and Saunders (1981) investigated the reason for this difference and found by increasing the complete cycle time of the test from 2 to 36 minutes that hysteresis loops progressed from type 1 to 2 to 3 and that different cements produced changes in hysteresis loops at different times. They concluded that shear dependent breakdown of the structure in the cement paste and time dependent build up of structure, occurring simultaneously, may be the explanation. Jones and Taylor (1977) using a fully broken down, by high vibration ,OPC cement paste , which had been sieved to accommodate their truncated cone and plate measuring device, obtained reversible flow curves. With shear rates up to 150 sec^{-1} giving shear stresses up to 100 Pa they found the model of Robertson and Stiff (1976)

$$\tau = A\ (\dot{\gamma} + C)^{B} \qquad 2.30$$

predicted the data for the range of w/c ratios considered. This range was from 0.3 to 0.6. The tests were carried out at a room temperature of 21°C, shear thickening occurred at w/c ratio > 0.4 and shear thinning at w/c ratios < 0.4, with the Bingham model fitting at 0.4. The reason given for shear thickening were viscometer characteristics at low shear rates, which is supported by Haimoni (1987), and possibly plug flow, although this was not observed. Mixing which appears to be an obvious contender was only mentioned as being of longer duration for the low w/c in order to achieve reversible flow curves. Tattersall and Banfill (1983) report this incorrectly concluding more concentrated pastes broke down more rapidly when, in fact, the reverse is the case. Knowing that A and C vary linearly with w, the w/c ratio, and obtaining a best fit of their data for B, the model obtained is

$$\tau = (kw + l)\{\dot{\gamma} + (mw + p)\}^{(r/_w + Se^{-w})} \qquad 2.31$$

where k,l,m,p,r and s are constants to be experimentally determined.

Roy and Asaga (1979) and Banfill (1981) found mixing methods and time of mixing to affect the yield stress and plastic viscosity of a cement paste by reducing both values with increased mixing.

Flow curves are dependent on the experimental conditions, such as mixing methods, and Worrall and Tuliani (1964), found that two different materials can give similar hysteresis loops. They are therefore unable to characterise fluids which break down. Tattersall (1955) using the coaxial cylinder viscometer at constant speeds of rotation found that torque decreased with time,for an O P C w/c = 0.3 , to the relation

$$T - T_E = (T_0 - T_E)\exp^{(-Bt)} \qquad 2.32$$

which is diagrammatically displayed in Fig. 2.12. B was theoretically derived by Tattersall, based on simple linkage theory, to be

$$B = \frac{2\pi K}{n_o \psi}\omega(\omega - \omega_1) \qquad 2.33$$

where ψ is the work done in breaking one link, n_o is the number of links at the start of testing and K and ω_1 are constants. Plots of $\ln (T-T_E)$ against time which should be straight lines were subsequently found by Dimond (1975) and Tattersall and Dimond (1976) to progress from type 1 to type 2 to type 3 lines, shown on Fig. 2.13, by the reduction in the amount of hydration at the time of testing or the increase in water cement ratio. The time of intersection of these lines, t_{int}, was found to increase linearly with the decrease in free water measured by centrifuging the paste. The time of break up of plug flow observed in a smooth coaxial cylinder was found to correlate with the t_{int} and working with effective gap widths, revised shear rates gave reasonable linear correlation with B, as opposed to $\dot{\gamma}^2$ correlation.

Lapasin et al (1980) using serrated coaxial cylinders confirmed the breakdown curves of Tattersal (1955) and that the amount of structure breakdown decreases exponentially as the water cement ratio increases or the coarseness of the cement increases. They derived from Tattersall's linkage theory a linear relationship between their breakdown constant, B, and testing rotational speed, ω. Lapasin et al. did not experience the anomalous plug flow of Tattersall and Dimond having used a partly broken down paste, which according to Tattersall and Banfill (1983) might indicate that if the initial yield value is reduced by the mixing procedure anomalous plug flow is overcome.

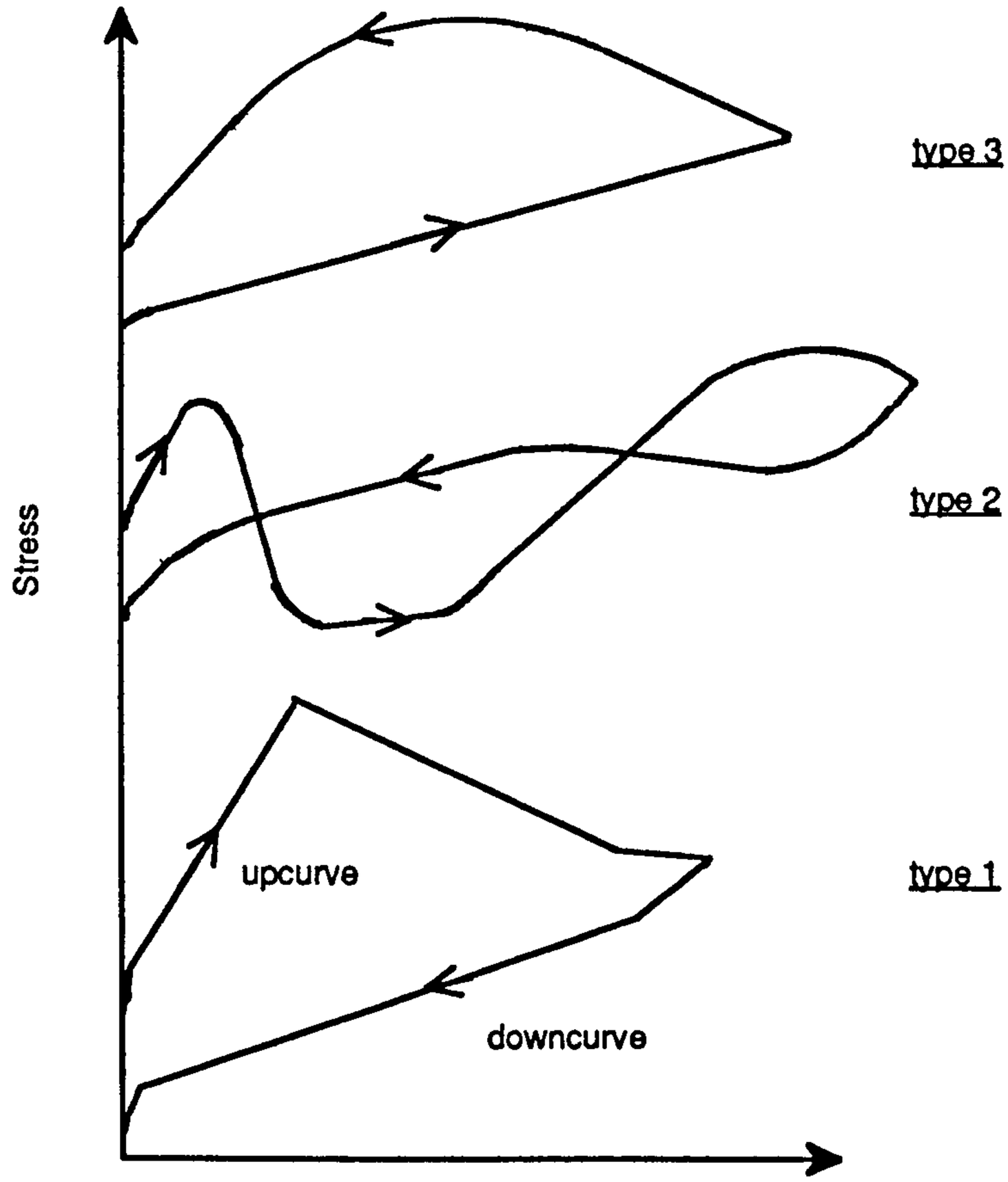

Fig. 2.11 Hysteresis Loops reported for Cement Paste Flow Curves

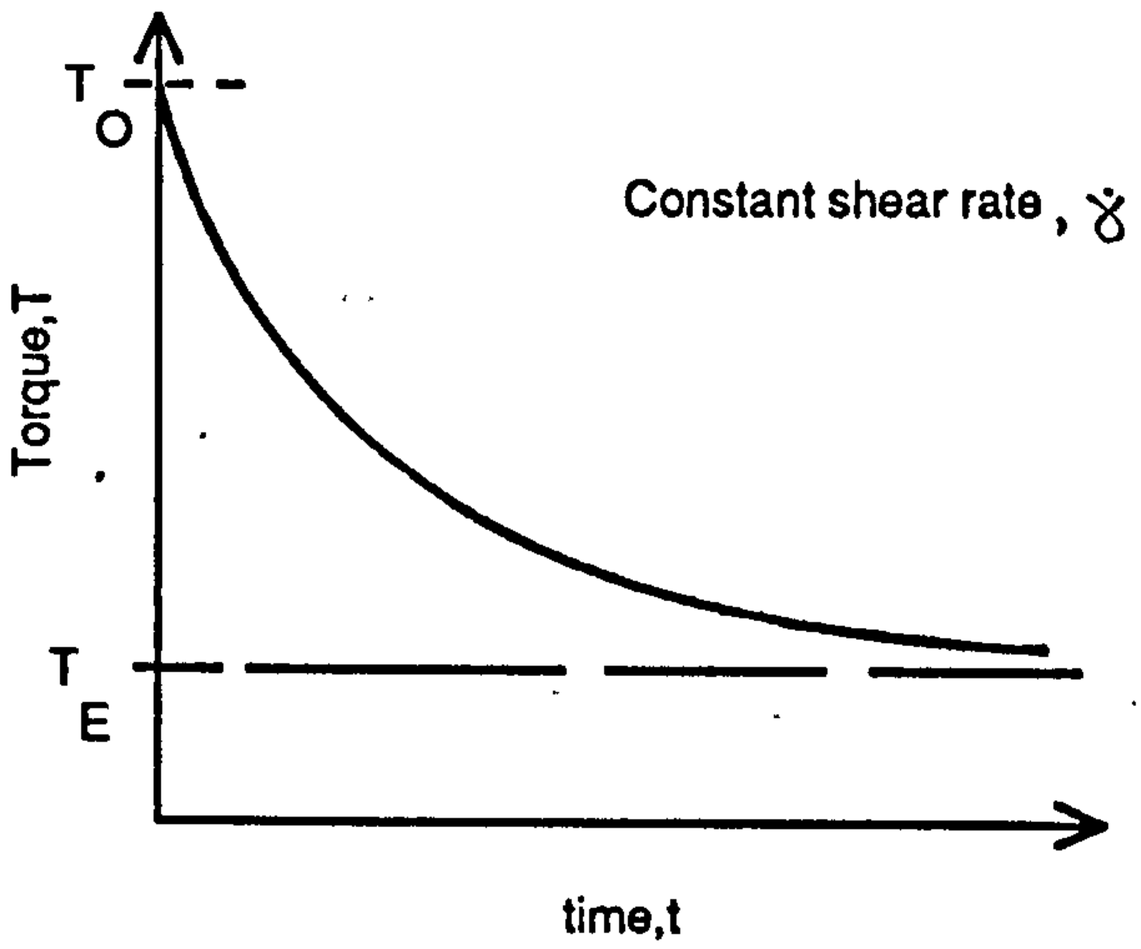

Fig. 2.12 Breakdown Curve

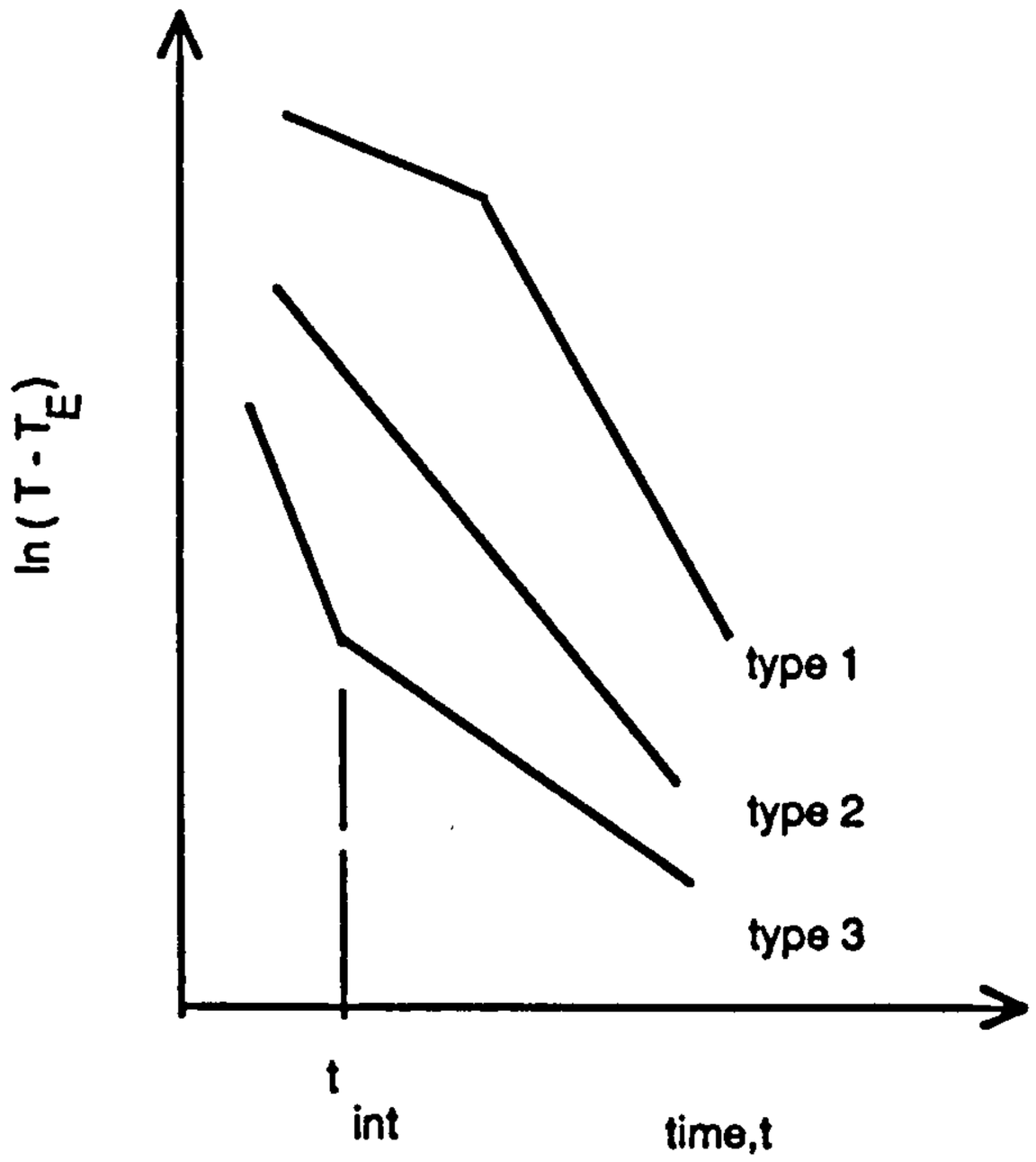

Fig. 2.13 Semi-logarithmic Breakdown Curves

2.4.4 Build-up of Structure

As already noted, as a cement paste hydrates it thickens and eventually sets. Researchers whilst investigating the flow curves of early hydrating cement pastes found the down curve was at higher stress level than the up curve at corresponding shear rates (see previous section).

This infers that the build up of structure occurs from the start of hydration and continues whilst undergoing shear. Banfill (1980) using a helical impeller, to overcome the anomalous plug mentioned in the previous section, found on continuously shearing a w/c ratio = O.35 OPC at constant speed that the torque on the impeller decreased to a minimum as the structure broke down then increased as hydration rebuilt the structure. The hydration section was found to fit the equation:

$$T - T_{min} = At^{b} \qquad 2.34$$

On using a high energy mixer to obtain a fully broken down paste Banfill (1980) found that the rate of hydration was dependent on the shear rate during mixing. Further discussion of this model and the additional work on this subject by Bhatty and Banfill (1984) is made in Chapter 8 when discussing the results of this thesis.

2.5 Oil Well Cement Technology

Portland cement was first used to shut off water in an oil well cement in 1903. By 1940 there were only 2 types of cement with 3 additives to overcome the problems of

short thickening time and late strength development of the then deep wells (2000-3000 ft). Now to cope with depths 10 times those of 1940 and the range of conditions in the field including problems such as weak formation, lost cirulation, gas channelling and arctic cementing, there are 8 cementing systems with over 50 additives. These systems comprise accelerators, retarders, fluid loss additives, dispersants, extenders, weighting agents, lost circulatioin and foaming or defoaming agents and account for the majority of types used and marketed by Dowell Schlumberger (1984).

Although the oil industry continues to develop additives for its specific requirements the testing of cement in the laboratory was standardised in 1948 with the API code 32. This code has been revised over the years and the current standard is API Spec.10 (1986). There are however tests which the industry performs which are not covered by API Spec. 10 and these include, particle size distribution, pipe viscometry, and ultrasonic testing.

Also, there is no specific test in the API specifications (1986) for the gel strength of a cement slurry. There is however in Appendix P of that document a tentative empirical investigation procedure to compare the early static gel strength development of a spacer/base cement slurry mixture with the measured consistency of the slurry over its thickening time. This is done by letting the mixture stand for 3 ten minute periods at the start, half way and three quarters the way through the thickening time and measuring the consistency at the beginning and the end of each ten minute cessation of mixing period.

There are no guidelines for the use of the results and the test merely serves as a standard comparative procedure.

In addition to their use for mud removal and as spacers, which separate the drilling mud and cement slurry, high gel strength slurries are required for lost circulation plugs where they develop their gel strength quickly, when stationary in voids and fractures.

2.5.1 Gel Strength in the Oil Industry

Gel strength is defined in cement technology by Dowell Schlumberger (1984) as a measure of the attractive forces between the particles of a fluid when under static (non-flowing) conditions. To attain gel structure the fluid is required to be left to stand for a period. The reference also defines a yield point (presumably that where a yield stress acts) as the measurement of attractive forces between particles when fluid is in motion, under flow conditions, and states that it is a dynamic property of the fluid.

The method given to measure gel strength is as follows:-

A slurry is mixed and poured into the cup of a FANN V.G. viscometer and stirred at 600 r.p.m for 10 secs. The viscometer is stopped and the slurry is left standing for 10 secs, 1 min or 10 min after which the viscometer is restarted at 3 r.pm. and the maximum dial reading recorded. This is called the initial gel strength, the 1 minute or the 10 minute gel strength, depending on the standing time.

The difference in gel strength measurements of drilling mud, spacer fluid and cement slurry is used to predict the efficiency of mud removal prior to cementing when the method of removal is by viscous displacement. This mud removal method is used when

plug or turbulent flow is unsuitable usually due to high pressure on weak formations. To prevent the cement slurry from pushing its way through the spacer both density and gel strength should be lower in the slurry, thereby ensuring efficient removal.

Any temporary halt to the cement slurry when flowing into place during cementing can be detrimental to the cement job since gel strength development can with a cement of 6-hour thickening time cause several hundred p.s.i to be added to the pressure required to move the slurry after a 15 minute stoppage. (Sabins and Sutton, 1986).

2.5.2 Oil Well Flow Calculations

Having designed the cement slurry to the requirements of the applicable oil well and assessed the volume of slurry and the other fluids involved in the placement, calculations for flow rate and pressure drop can be made, depending on the chosen flow regime. As with classical hydrodynamics, Reynolds number, Re, is used to determine the flow regime, where

$$R_e = \frac{\rho V D}{\mu}$$

and μ is the viscosity. This works for a Newtonian fluid but an effective viscosity, μ_e, is required when the fluid is a Bingham and the flow is in the laminar flow regime. However when flow is turbulent with the Bingham fluid, the

$$R_e = \frac{\rho VD}{\mu_p}$$, may be used

where μ_p is the plastic viscosity. When dealing with Newtonian fluids flowing in the pipe annulus an effective diameter $D_e = 0.8165(D_2 - D_1)$ is used with the Fanning friction factor (which is defined as the ratio of the shear force on the inside wall of the pipe to the kinetic energy of the fluid) to determine the pressure drop along a length of well, using the modified Poiseuille equation

$$\Delta p = \frac{32 \mu_p L v}{D_e^2} \qquad 2.35$$

The Fanning friction factor is

$$\frac{16}{R_e}$$

approximates to , of a Newtonian fluid
for laminar flow, and $0.057(R_e)^{-0.2}$ for turbulent flow. To account for Bingham in turbulent flow, modification is required to the pipe flow formula, by using the Hedstrom number to obtain the critical R_e number which represents laminar flow so that laminar pipe flow formula may be used. Metzner and Reed, according to Dowell Schumberger (1984), have modified the R_e, similarly, to accommodate the pseudoplastic fluids. The Hedstrom number is

$$H_e = \frac{3.7 \times 10^6 \rho}{\mu_p^2} \frac{\tau y}{100} D_e^2 \qquad 2.36$$

in oil industry units, and the critical R_e is obtained from a graph of H_e against R_e for the Bingham fluid.

Plug flow is a flow regime where a solid plug of material at or lower than the yield stress flows in the central portion of the pipe or annulus as shown in Fig. 2.14. Plug flow occurs with a Bingham fluid. Assuming a linear stress distribution with no wall slip then

$$\frac{\tau_y}{\tau_w} = \frac{d}{D}$$

and in the laminar flow equation for a Bingham fluid the flow equation becomes

$$\frac{8V}{D} = \frac{\tau_w}{\mu_p} \left[1 - \frac{4}{3}\left(\frac{\tau_y}{\tau_w}\right) + \frac{1}{3}\left(\frac{\tau_y}{\tau_w}\right)^4\right] \qquad 2.37$$

Dowell Schlumberger (1984) assume $d/D = 0.8$ for successful mud removal and the plug flow equation gives

$$V_{plug} = 0.4354 \frac{\tau_y}{\mu_p} D$$

which is used in the modified R_e equation of

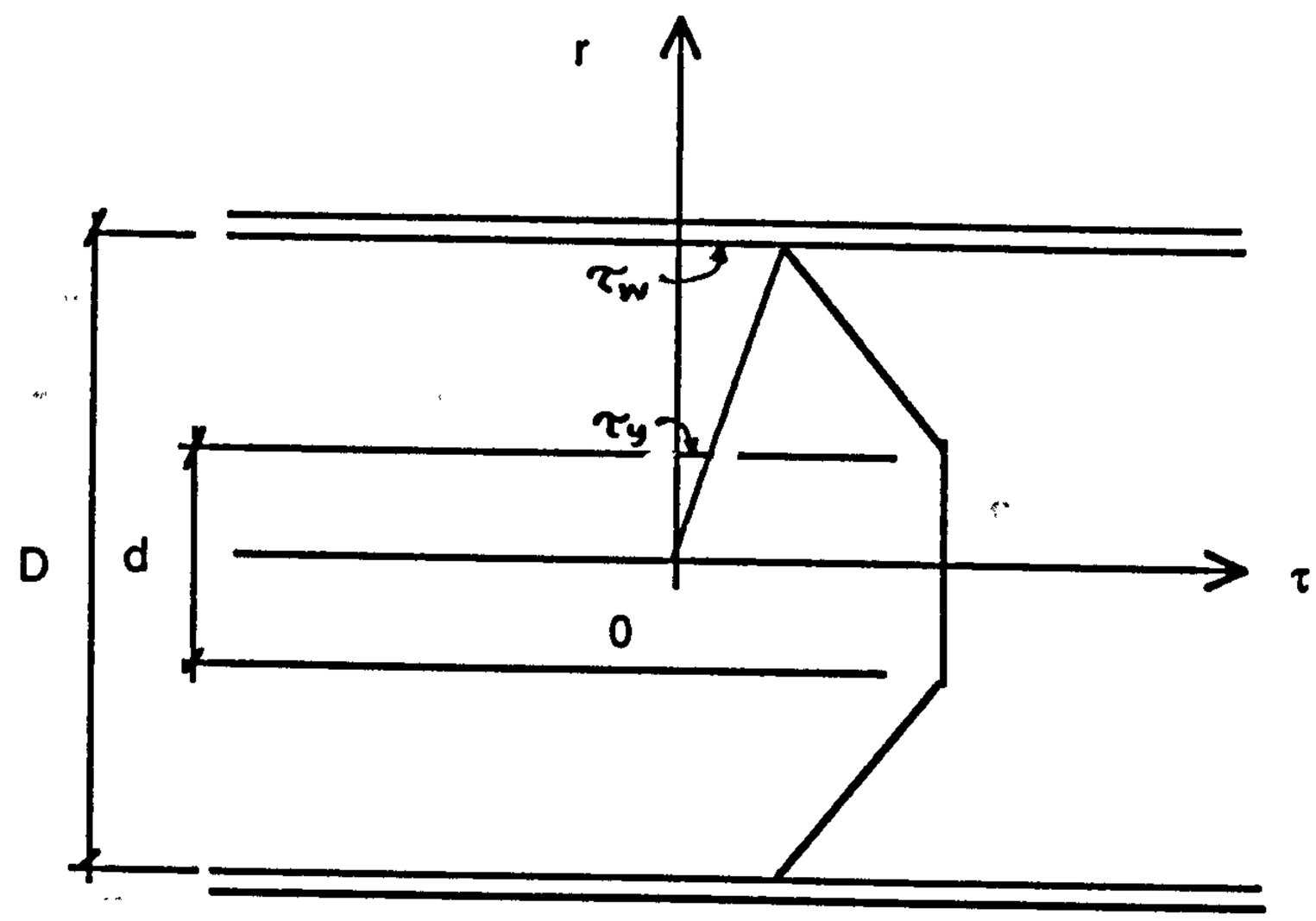

Fig. 2.14 Plug Flow

$$R_e = \frac{928\,\rho\,V\,D_e}{\mu_p + 6.65\,\frac{\tau_y}{V}D_e} \qquad 2.39$$

From which the Fanning friction factor can be obtained and used to calculate the pressure drop.

2.6 Conclusion

Oil well cement slurry is an extremely complex fluid. Theoretical approaches to determine their structure or predict their flow behaviour even in simple flow configurations is not available. The complications added by cement slurry being a time dependent fluid make the possibility of a mathematical solution to the yield stress and flow behaviour highly unlikely.

Yield stress in cement slurry is a transient quantity which depends, apart from material composition and thermal condition, on the previous shear history, the level of structure attained and the rate of application of stress at the point of yield.

The mechanism of yield is not well enough understood to enable theoretical modelling. The use of a level of structure which is a single scalar parameter, to describe structure of cement is untenable and the microstructural approach is more applicable to dilute flocculated dispersions.

Although dynamic properties may well best describe material behaviour under given operating conditions they have not, as yet, been mathematically related back to yield stress and with transient structure the conditions under which the material deforms homogeneously have not been established. Therefore, the measurement of yield stress, especially of a cement slurry, is best performed at the present time using a rotational measuring system under controlled stress rheometry.

The value of yield stress of a cement slurry is required to solve practical problems in the cementing of an oil well. Previous methods and techniques to measure yield stress have been examined and assessed. The main criticism with constant shear rheometers is that the structure to be measured is first destroyed.

In the following chapters the techniques and measuring systems used in conjunction with the constant stress rheometer are described, to facilitate the measurement of the transient yield stress of an oil well cement slurry.

The measuring systems most suitable for investigating the yield stress of cement slurry are:

a) annular plate and cone

b) vane

The former because the shear rate and shear stress do not vary across the measuring system and the latter because it gives direct measurement without the problems of slippage and anomalous plug flow.

CHAPTER 3

The Controlled Stress Rheometer and Ancillary Equipment

This chapter describes the rheometer used in the experimental work and the different measuring geometries employed in the measurement of the rheological properties of cement slurry. Formulae used for computation of the results are explained and various preliminary checks and calibrations are described. Details of the experimental methods used for cement slurry follow in Chapter 4.

3.1 Detailed Description of the Carri-Med C.S. Rheometer

The Carri-Med controlled stress rheometer used in this project was a model no CS 500 which has a maximum applied torque of 500000 dyne cm. The layout of this rheometer is shown in Fig. 3.1 It has a rigid cast metal base and air bearing support pillar mounted on adjustable levelling feet to ensure both a vertical rotational axis and horizontal measuring plates. The base houses the pneumatic ram and micrometer assembly which adjusts the height of the fixed bottom plate of the measuring system. The ram rises automatically when the instrument has completed a biasing routine after programming or switching the ram up toggle switch. The ram rises to the preset level, which is adjusted . by using the micrometer. With the sample to be tested placed on the bottom plate the ram squeezes the sample into the correct measuring configuration.

The micrometer scale enables direct reading of height to 5μm and, by interpolation, an estimate to ± 1μm of vertical movement. One revol ution of the knurled micrometer wheel moves the ram vertically lmm.

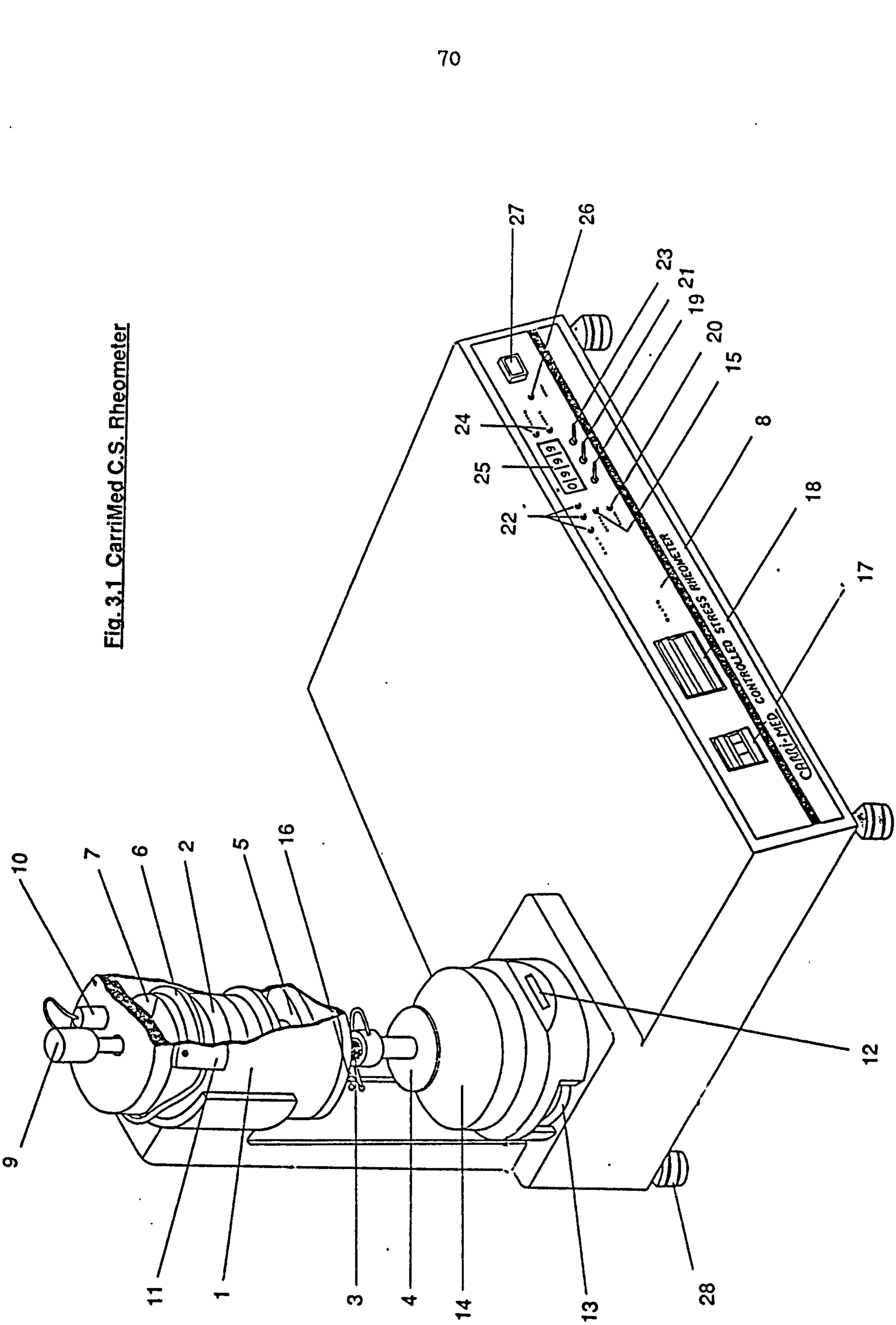

Fig. 3.1 CarriMed C.S. Rheometer

Part Nos. Fig. 3.1

1. Air bearing housing
2. Air bearing
3. Motor drive spindle
4. Detachable upper member of measuring system
5. Drive motor stator
6. High resolution tachometer disc
7. Angular displacement measuring ramp
8. Electronic console front panel
9. Draw rod
10. Non-contact angular displacement transducer
11. Holder for photo-electronic tachometer transducer
12. Micrometer scale
13 Gap-setting micrometer wheel
14. Bottom plate of cone and plate assembly
15. Temperature indicator light (for bottom plate temperature control)
    - indicates temperature correct
16. Gap setting indicator light and lead
17. Temperature setting thumbwheel switch (for bottom plate)
18. Torque setting thumbwheel switch
19. Torque 'on/off' switch
20. 'Bias' indicating light
21. Ram operating switch
22. Bias 'offset' indicator lights
23. Radians/second - Radian selector switch
24. Indicator lights for 23

25. Digital indicator for 23

26. Air pressure warning light

27. Main switch/indicator

28. Adjustable levelling feet.

The bottom plate is made of copper, which is chrome plated. The temperature of the bottom plate is controlled with a Pt 100 Peltier system. The internal microprocessor of the rheometer, which is also housed in the base, also controls the thermo-electric effects of the heat pump which forms the basis of the Peltier system. It has quick temperature response to small samples, but for the large ones needed for the vane in cup, a water jacket with a temperature controlled water bath had to be employed. Since a heat source is required for the Peltier, it is housed in a heat exchanger jacket which is connected to a sufficiently continuous flow of water (> 0.5 litre/minute). This system can control temperature in the range -5^{o}C to 60^{o}C using an ambient continuous flow of water. Higher temperatures can be obtained by using heated water supplies.

The basis of the Carri-Med controlled stress rheometer is the air bearing which is incorporated in the electronically controlled induction motor. The drive motor houses a hollow spindle through which a rod is inserted to allow various rheological measuring devices to be attached to the lower end. The top cover of the drive motor housing is free fitting and can be rotated to adjust the position of the angular displacement measuring system, without disturbing the sample. Care has to be taken with the transducer cable when making adjustments and precious seconds can be lost when adjustment has to be made during a computer controlled run, since the LEDs only indicate that adjustment is required when the ram is raised. Torque cannot be turned on unless the displacement measuring ramp is in the correct position and provided that the torque switch is on and the indicators are off. Air is supplied to the bearing from two Compton type P3081 compressors feeding a small air receiver type 2P/3077 (approximately 35 litres capacity)

manufactured by Dawson, McDonald and Dawson Ltd. The air passes through a filter assembly via a 5mm bore nylon supply line at a pressure of about 0.26 Pa (38 p.s.i). The filter assembly comprises two Norgren filters housed in removeable glass pots, arranged in series, followed by Norgren pressure reducing valve (No. 11-818-100 operating on 10 bar down to 0-4 bar pressure) and a pressure gauge 0-4 bar. The first filter is a 50 micron manual drain filter and the second a type F 42-201-MO, which retains particles above 0.01μm, the standard of cleanliness required for the air bearing. Condensation was a problem and the glass pots had to be dried daily when the rheometer was in use.

The rheometer can be operated manually by thumbwheels and toggleswitches on the front panel or, as in this case, automatically via an IEEE 488 interface to an Apple 11^e microcomputer, which was linked to an Epson FS 80 printer.

A red warning light on the front panel indicates low air pressure and is linked to cut out the torque motor drive. The digital display can, by using a selector switch, either show radians/second from the angular velocity tachometer system or radians from the angular displacement system.

Angular displacement is measured by transducer, which electronically senses the difference in distance of a movement of a ramp on a disc mounted on the motor drive spindle. There are two linear ramps on the disc and with a sensitivity of 5V/radian movements from 0.001 to 1 radian can be measured. When switched on the rheometer electronics automatically sense the movement of the ramp caused by the windmilling effect of the air bearing and computes this torque and applies the required balancing torque to stabilize the spindle so that the transducer is positioned at the lower end of the ramp. If this position is altered by squeezing the sample on ram up then adjustment of the top

cover to the drive motor mentioned earlier is required. The balancing of the windmill effect is called biasing and on completion a green bias indicator light switches on and then the pneumatic ram can be activated. If the ram up toggle switch is operated twice the bias can be overridden to facilitate gap setting or air bearing checks.

Angular velocity is measured by another disc, which is attached to the spindle and has slots finely spaced around the periphery. These slots are examined by a photo-electric transducer which produces an output signal (0.2 volts/radian/sec) proportional to the angular velocity. Low velocities less than 0.001 radians/sec. cannot be measured with this system, hence the need for angular displacement measurement.

Carri-Med have designed computer software compatible with Apple computers to control the testing of a sample on the rheometer by interacting with the internal microprocessor of the rheometer. Three types of programme were available on the Apple, the flow run, the creep and the oscillation hardware package. The oscillation package deals with dynamic properties and complex viscosity, which cannot be mathematically related to yield stress so it was not used. The creep requires accurate knowledge of the yield stress in order to probe the structure prior to yielding, so with a continually varying yield with time, as is the case with cement slurry, this package was not suitable. The flow run package was used to investigate yield stress of the oil well cement slurry. This was done using various measuring systems which were attached to the drive rod and placed in direct contact with the sample. These measuring systems are described and analysed in the next section of this chapter.

The flow run package comprises two floppy discs, the Utility disc, which was used to obtain raw data printout from a data storage disc, and the Flow Run Release 3.5 disc.Release 3.5 refers to the particular update of the Flow Run programme. The Flow Run programme enables about 50 test procedures to be stored on the flow run disc.

Apart from sample reference, the information in a test procedure necessary for a flow run on a sample is the temperature, peak torque, equilibration time (the time after ram up and before stress is applied to allow the sample to obtain equilibrium, arbitrarily set at 30 seconds), ascent, peak hold, and descent times and the factors to convert angular velocity to shear rate and torque to shear stress.

The flow start menu allows cataloguing and initialising of data discs, with progression to the flow menu. This menu enables initialisation procedure, (i.e. selecting or forming a testing procedure), run rheometer, using the previous or a selected test procedure and finally, an analysis and compare facility. The compare facility allows 4 flow curves to be displayed on one graph. The peak hold curves were not able to use the compare facility, since those curves were time based.

The computer divides the peak torque, ascent and descent times by 200 and divides the peak hold time by 100 and increments the steps progressively through ascent, hold and descent; unless any of these times are zero, in which case that phase is ignored. If the material response to an increment is unchanged from the previous reading that data is not stored. Each time a stress increment is sent to the rheometer on the ascent phase the angular velocity is read simultaneously.

The angular velocity starts being filed at 0.02 rad./sec (not 0.01 since the flickering display " 0 <-> 0.01" gives odd results). The initial yield value reported is the stress at 0.02 rad/sec and the dynamic yield is the value of the extrapolation of the stress axis using the first 5% of the ascent data pairs.

The analysis programme fits mathematical models such as Herschel-Bulkley, Bingham, Casson, power law and polynomial by taking logarithms where necessary and fitting the data curve to straight lines, obtaining the regression coefficient and the

standard error of fit which is expressed as

$$\text{standard error} = \left(\frac{\Sigma(\dot{\gamma}\,\text{actual} - \dot{\gamma}\,\text{predicted})^2}{n-2}\right)^{\frac{1}{2}} \qquad 3.1$$

The predicted model is plotted and displayed for comparison on the same plot as the actual curve. Options allow part of the actual curve, a minimum of 10 points, to be analysed between selected limits. The flow curve can be displayed and analysed as viscosity/shear rate or log-log of those parameters. The partial curve between limits can be expanded to fill a full display so obtaining a better detailed picture of that portion of the curve. The peak hold curve is not analysed.

3.2 Measuring Geometries

In order to measure rheological properties using a controlled stress rheometer it is necessary to obtain simple shear flow in the sample. The rotational rheometers all allow continuous flow to be examined, at the price of curvilinear flow, which requires careful mathematical treatment, as shown in this chapter, for the analysis of the various measuring geometries. This is especially important when considering non-Newtonian fluids, such as cement slurry.

The measuring geometry induces a shear flow in the sample, which depends on the configuration for the distribution of shear across the sample. The three geometries used in this project are the parallel plate, the vane in cup, and the annular plate and cone.

3.2.1 Parallel Plate

The parallel plate is a flat disc which is mounted on a vertical drive assembly which

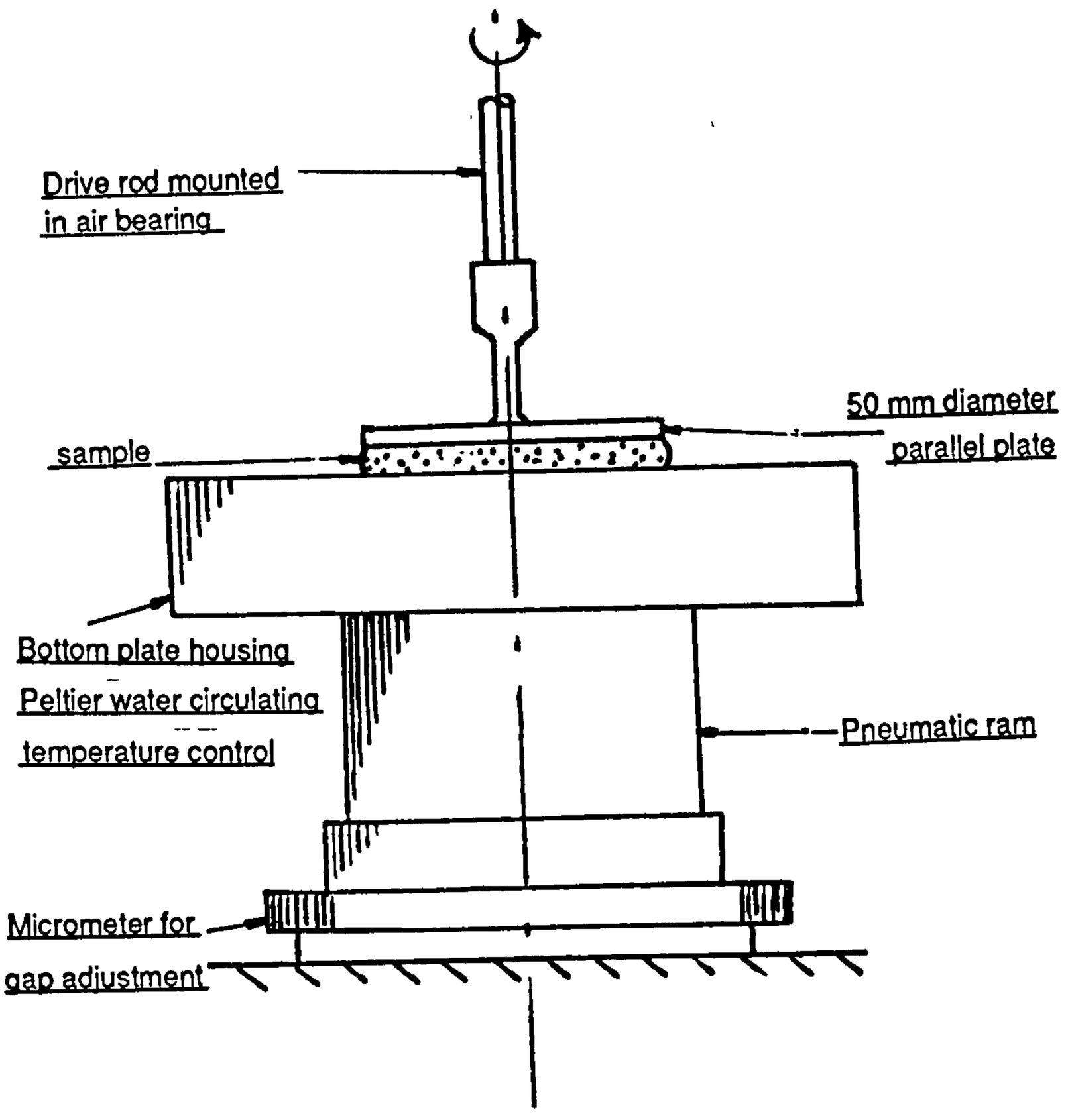

Fig. 3.2 Layout of Parallel Plate on CarriMed C.S. Rheometer

sandwiches a sample between it and another flat disc fixed to provide a known gap between the two as shown in Fig. 3.2

It is suitable for particulate suspensions because the gap can be adjusted to accommodate various particle sizes, which is not the case with either the coaxial cylinder or the cone and plate measuring system.

Analysis of the parallel plate for use with non-Newtonian fluids has been examined by Walters (1975), Krieger et al (1952) and Cross and Kaye (1986)(1987) and is dealt with shortly.

However, in order to obtain a flow curve for a Newtonian fluid, linear factors are applied to the torque and angular velocity which provide the shear stress and shear rate as follows:

$$\tau_R = \frac{2}{\pi R^3} T \quad , \quad \dot{\gamma}_R = \frac{R}{h} \Omega \qquad 3.2$$

where R = radius of the plate, h = gap separating the plates, T = torque and Ω = angular velocity. Because of the parallel plate configuration, the shear rate varies linearly with radius and the shear stress is calculated at the rim only; since, with a Newtonian sample, the shear stress must also vary linearly with the radius because the viscosity is constant. However, when considering a non-Newtonian time independent fluid corrections have to be made to these relationships.

The Carri-Med manual (1986) gives the equation

$$\tau_R = \frac{2T}{\pi R^3}\left(\frac{3}{4} + \frac{1}{4}\,\frac{d \ln\left(\frac{2T}{\pi R^3}\right)}{d \ln \dot{\gamma}_R}\right) \qquad 3.3$$

and cites Krieger and Wood (1966) who derived an expression for viscosity as a function of shear rate in terms of apparent viscosity,

$$\eta_a = \frac{2LM}{\pi R^4 \Omega} \qquad 3.4$$

for viscosity with parallel plate
from Stokes' relation. The Krieger and Wood expression is

$$\eta_{(gm)} = \eta_a \left(1 + \frac{1}{4}\left(\frac{d \ln \eta_a}{d \ln g_m}\right)\right) \qquad 3.5$$

On transferring to our notation $g_m = \dot{\gamma}_R$, $L = h$ and $M = T$ and with the work of Kaye (1987) the above can be shown to be in agreement with each other and with the results of Cross and Kaye (1986),(1987). This is explained as follows:

from $\eta_a = \frac{2hT}{\pi R^4 \Omega}$ since Ω is not constant but varies with T,

on the differentiating we get

$$\frac{d\eta_a}{dT} = \frac{2h}{\pi R^4}\left(\frac{1}{\Omega} - \frac{T}{\Omega^2}\frac{d\Omega}{dT}\right) \qquad 3.6$$

we can now substitute for all η_a and $\frac{d\eta_a}{dT}$ terms in equation 3.5

using $d\ 1n\ \eta_a = \frac{d\eta_a}{\eta_a}$ as follows:

$$\eta_{(\dot\gamma R)} = \frac{2T}{\pi R^3\dot\gamma R}\left[1 + \frac{1}{4}\frac{\pi R^4\Omega}{2hT}\frac{dT}{d1n\dot\gamma_R}\left(\frac{1}{\Omega} - \frac{T}{\Omega^2}\frac{d\Omega}{dT}\right)\frac{2h}{\pi R^4}\right] \qquad 3.7$$

$$\text{as } \eta_{(\dot\gamma R)} = \frac{\tau_{(R)}}{\dot\gamma_R},\ \tau_{(R)} = \frac{2T}{\pi R^3}\left[1 + \frac{1}{4}\frac{d\ln T}{d\ln\dot\gamma_R}\left(1 - \frac{d\ln\Omega}{d\ln T}\right)\right] \qquad 3.8$$

$$\text{now } \dot\gamma_R = \frac{\Omega R}{h}, \text{therefore } d\ 1n\dot\gamma_R = d\ 1n\Omega \text{ and}$$

$$\tau_{(R)} = \frac{2T}{\pi R^3}\left[\frac{3}{4} + \frac{1}{4}\frac{d\ 1nT}{d\ 1n\ \dot\gamma_R}\right] \qquad 3.9$$

which is the same as equation (3.3), also

$$\tau_{(R)} = \frac{3T}{2\pi R^3}\left[1 + \frac{1}{3}\frac{d\ 1n\ T}{d\ 1n\ \Omega}\right] \qquad 3.10$$

and $$\tau_{(R)} = \frac{3}{2\pi R^3}\left[T + \frac{\Omega}{3}\frac{dT}{d\Omega} \right] \qquad 3.11$$

on transposing this becomes the Cross and Kaye(1981) equation which we wish to use in the manner described by them

$$T + \frac{\Omega}{3}\frac{dT}{d\Omega} = \frac{2\pi R^3}{3}\ \tau_{(R)} \qquad 3.12$$

The above working was complicated by the different notation used and the form in which Carri-Med and Krieger and Wood presented their equation. To clarify, equation 3.12 will be derived simply from first principles.

If T = torque, Ω = angular velocity , τ_r = shear stress at radius r, $\dot{\gamma}_r$ = shear rate at radius r, then

$$\dot{\gamma}_r = \frac{\Omega r}{h} \qquad 3.13$$

$$T = \int_0^R 2\pi\, r^2 \tau_r\, dr \qquad 3.14$$

integrating by parts,

$$T = \frac{2\pi R^3 \tau_R}{3} - \int_0^R \frac{d\tau_r}{dr} \frac{2\pi r^3}{3} \quad dr \qquad 3.15$$

differentiating 3.14 $$\frac{dT}{d\Omega} = \int_0^R 2\pi r^2 \frac{d\tau_r}{d\Omega} \quad dr \qquad 3.16$$

from 3.13 $$\frac{d\dot{\gamma}_r}{d\Omega} = \frac{r}{h}$$ giving $$\frac{d\dot{\gamma}_r}{dr} = \frac{\Omega}{h}$$

now $$\frac{d\tau_r}{d\Omega} = \frac{d\tau_r}{dr} \frac{dr}{d\dot{\gamma}_r} \frac{d\dot{\gamma}_r}{d\Omega} = \frac{d\tau_r}{dr} \frac{r}{\Omega} \qquad 3.17$$

in 3.16 gives $$\frac{dT}{d\Omega} = \int_0^R \frac{2\pi r^3}{\Omega} \frac{d\tau_r}{dr} \, dr \qquad 3.18$$

hence in 3.15 we have:

$$T = \frac{2\pi R^3 \tau_R}{3} - \frac{\Omega}{3} \frac{dT}{d\Omega} \qquad 3.19$$

which is the Cross and Kaye equation, and may be expressed as:

$$T = \frac{2\pi R^3 \tau_R}{3} - \frac{h}{3}\frac{dT}{dh} \qquad 3.20$$

by differentiating 3.14 with respect to h and using:

$$\frac{d\tau_r}{dr} = \frac{d\tau_r}{d\dot{\gamma}r}\frac{d\dot{\gamma}_r}{dr} = \frac{d\tau_r}{d\dot{\gamma}r}\frac{\Omega}{h} \quad \text{and} \quad \frac{d\tau_r}{dh} = \frac{d\tau_r}{d\dot{\gamma}r}\frac{d\gamma_r}{dh} = \frac{d\tau_r}{d\dot{\gamma}r} - \frac{\Omega r}{h^2}$$

and substituting into the differentiated equation.

Cross and Kaye (1987) show how a simple correction to the shear rate enables non-Newtonian fluids to be evaluated.

$\frac{\Omega}{3}\frac{dT}{d\Omega}$ is regarded as a correction for non-uniformity of shear rate to

the value of T,(i.e $T' = T + \frac{\Omega}{3}\frac{dT}{d\Omega}$,see Fig. 3.3)

The T - Ω curve is non-linear, but they assume that it approximates to a series of straight lines from

Ω to $\frac{4\Omega}{3}$.

The τ_R is calculated from T' in equation 3.19.Nowif the τ_R is required to be calculated using the T value then the correction for shear rate is

$$\text{slope} = \frac{dT}{d\dot{\Omega}}$$

$$\therefore \quad T' = T + \frac{\Omega}{3}\frac{dT}{d\dot{\Omega}}$$

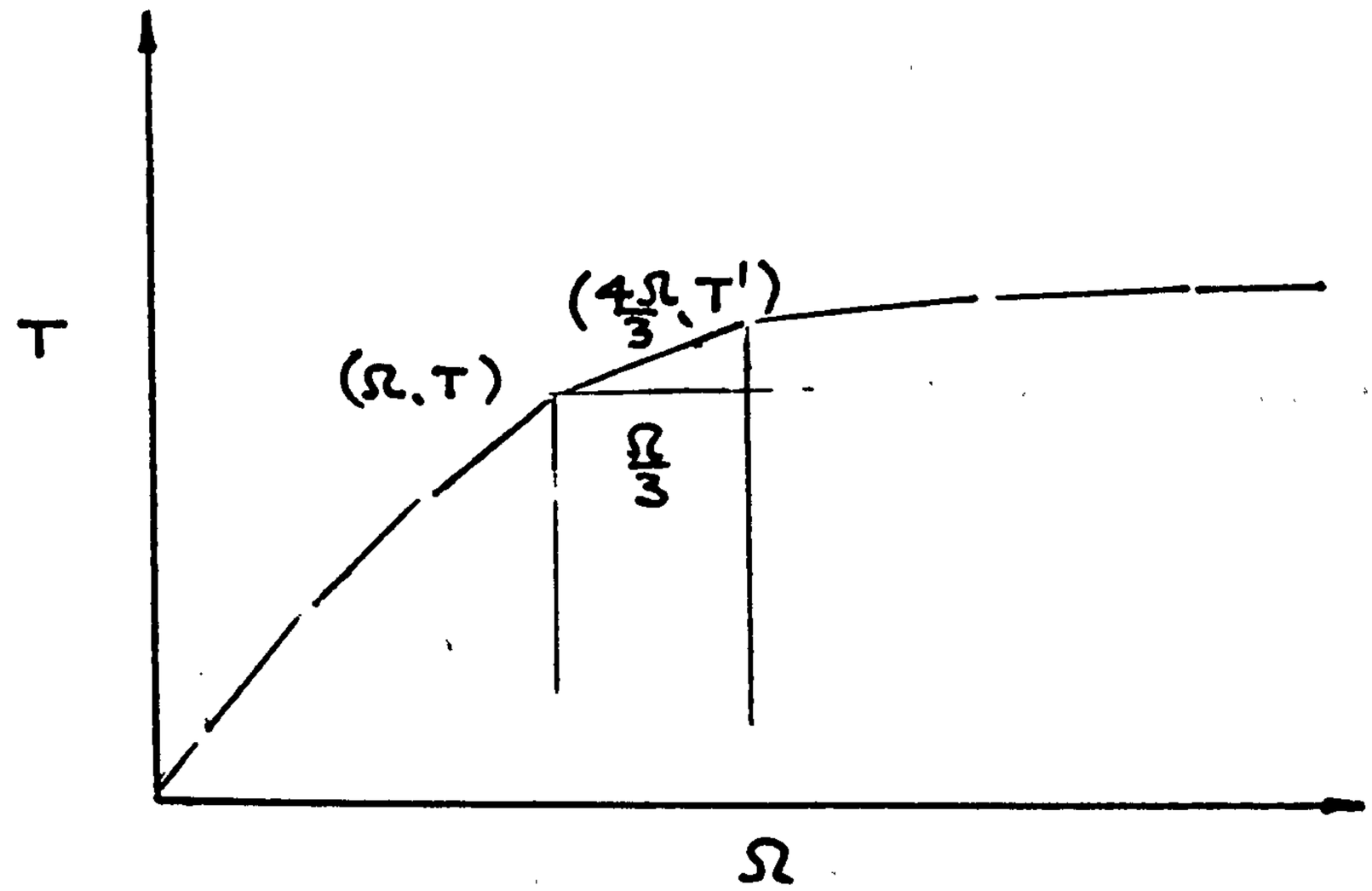

Fig. 3.3 Simple Technique for the Evaluation of a non-Newtonian Flow Curve

(Cross and Kaye,1987)

$$\frac{3}{4}\dot{\gamma}_R \text{ or } \frac{3\Omega R}{4h}$$

Hence for non-Newtonian fluids

$$\tau_R = \frac{3T}{2\pi R^3} \qquad 3.21 \qquad \text{i.e. } \frac{3}{4} \text{ x Newtonian value}$$

$$\text{and} \quad \dot{\gamma}_R = \frac{3\Omega R}{4h} \qquad 3.22 \qquad \text{i.e. } \frac{3}{4} \text{ x Newtonian value}$$

The error calculated by Cross and Kaye for a power law fluid of the shear thinning type when using this technique was just over 1%.

3.2.2 Vane in Cup

Keentok et al (1985) have shown that the shearing diameter of a four bladed vane rotating in a Bingham liquid is slightly larger than the vane diameter.

A computer simulation, which showed the ratio of diameters to be approximately 1.025, agreed with their experiments on two greases to± 0.7%. They also found this ratio to be independent of vane diameter. However, the simulation gave the ratio, D_c/D,

(see Fig 2.8 page 40)

to be decreasing exponentially with increase in τ_y/η_p whereas experiments showed D_c/D to increase linearly. The phenomenon could not be explained.

Haimoni (1985) using various constant shear rate viscometers, investigated the use

of a vane to measure the gel strength of an oil well cement slurry with particular reference to the following aspects:-

1. stress distribution and progressive failure
2. rotational speed and rate of applied stress
3. vane shape and dimensions

Progressive failures occur at the top and bottom edges of the vane because the strain is not constant and depending upon the material behaviour various stress distributions occur. For a cement paste with a vane at H/D ratio $\geq$ 2, Haimoni assessed the error whilst assuming a rectangular stress distribution to be less than 1%. This was based on Merrifield's (1980) correction factors for progressive failure on a cylindrical vane of an idealised stress-strain model.

Nguyen and Boger (1985) found the measured yield strength, using the vane, of a red mud suspension to be essentially constant over a rotational speed of 0.1 r.p.m to 8 r.p.m., whereas Haimoni found the yield strength of cement slurry to be a function of rotational speed over the same range.

Since the viscometer applied torque to the material in proportion to the rotational speed the rate of application of shear stress would have the same effect on the measured gel strength as would the rotational speed.

Haimoni investigated blade shapes other than rectangular, which gave a cylindrical shear surface, but found diamond and spherical vanes to be much worse because of a) the progressive failure problem at the edges, and b) the variation of shear rate at the edges, which has the effect similar to variation of rotational speed, mentioned

previously.

Nguyen (1983) shows that complete analysis and interpretation of the vane is difficult despite its simple geometry. The conventional analysis for the yield stress from the torque assuming a fully immersed vane and rectangular stress distribution on all edges is:

$$\tau_y = \frac{F_{max}}{\frac{\pi d^3}{2}\left[\frac{L}{d} + \frac{1}{3}\right]} \qquad 3.23$$

where F_{max} is the maximum torque, d is the vane cylindrical diameter and L the length of the vane.

However a material which is anisotropic, such as soil or cement slurry, may have different yield values in different shear planes. For example, the anisotropic ratio

$$= \frac{\tau_{e\ max}}{\tau_{S\ max}}$$

(where τ_{emax} is the end yield stress and τ_{smax} the side yield stress of the vane) may vary from 0.6 to 0.4 for similar soils, depending on soil structure formation, pore water pressure and depth. It is found that remoulded or well mixed soils have anisotropic values similar to conventional ones, hence well mixed cement slurries should not reflect

this condition especially when making single point τ_y measurements. The shear surface might not be so well defined if it were not for the slow propagation of the stress from the vane blade to the material and according to Nguyen (1983) it is doubtful whether the anisotropic approach is valid in the pre-yield state.

The mechanism at the yield due to a vane is given as:

1. material in between the vane moves with rotation and
   network bonds are stretched.
2. torque to keep motion constant rises (with controlled stress the motion would presumably slow down but for the fact that stress is increasing).
3. gradual breaking of bonds occurs
4. hydrodynamic forces are not strong enough to reform bonds and the material yields irreversibly
5. "cracks" in localised yield areas give rise to maximum torque followed by rapid fall-off with time.

Without the effect of anisotropy, the analysis reduces to one of stress distribution and Wiesel with Parker's refinement for end stress distribution, reported by Nguyen (1983), is

$$\tau_{e(r)} = \left(\frac{2r}{d}\right)^P \tau_s \qquad 3.24$$

p=0 gives rectangular end stress distribution, p=1 triangular tests show p ≠ 0

using $F = L.f_s + 2.F_e$ where f_s torque/unit length

with two vanes of same d_1, but different L, (L_1 and L_2) $2F_e = F_1 - L_1 f_s = F_2 - L_2 f_s$

therefore

$$f_s = \frac{F_1 - F_2}{L_1 - L_2}$$

$$\text{so } F_s (d_1 L_1) = L_1 \left(\frac{F_1 - F_2}{L_1 - L_2}\right) \qquad 3.25$$

$$\text{and } F_s (d_1 L_2) = L_2 \left(\frac{F_1 - F_2}{L_1 - L_2}\right) \qquad 3.26$$

and plotting the torques, F_1 and F_2 , against angle of response, a yield condition was observed at approximately 20^o angle for their red mud. On calculating F_e and plotting against angle it was unaccountably found that after yielding F_S began falling but F_e carried on rising.

However,another method, using $\tau_{e(r)} = \left(\frac{2r}{d}\right)^P \tau_s$

$$\text{which gives } F_{max} = \frac{\pi d^3}{2}\left(\frac{L}{d} + \frac{1}{(p+3)}\right)\tau_y \qquad 3.27$$

with 10 different L/d ratios, straight line plots of

$$\frac{2F_{max}}{\pi d^3}$$

against $L/_d$ show the independence of geometry. The difference between these two methods was small, showing that the assumption of simultaneous yielding on both vertical and horizontal edges is valid.

As regards geometry and boundary conditions, Nguyen reported that $L/_d > 3.0$ gave inconsistent results, Donald et al (1977) found small vanes might give a higher τ_y due to soil disturbance when the area ratio

$$\left(\frac{\text{c.s.a. blades + rod}}{\text{c.s.a. cup}}\right) > 10 \text{ to } 15\%$$

c.s.a. = cross sectional area

Nguyen reported that F_{max} increases with speed fromN = 0.017 r.p.m. to N = 0.1 r.p.m,although essentially constant for N < 10 r.p.m. A speed of N = 0.017 or (0.1 degree/s) was recommended.

Nguyen (1983) investigated distances of boundaries from the vane and found no significant effect when

$$\frac{d}{D} < 0.5 \text{ and } \frac{Z_1}{d} > 1.0 \text{ and } \frac{Z_2}{d} > 0.5,$$

for his red mud at a concentration of 65.8% by weight.

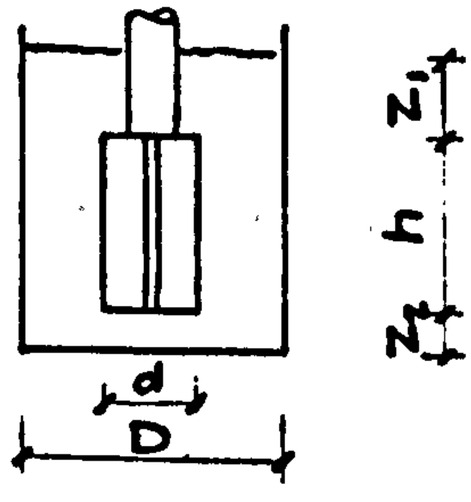

Fig. 3.4 Notation for Vane in Cup

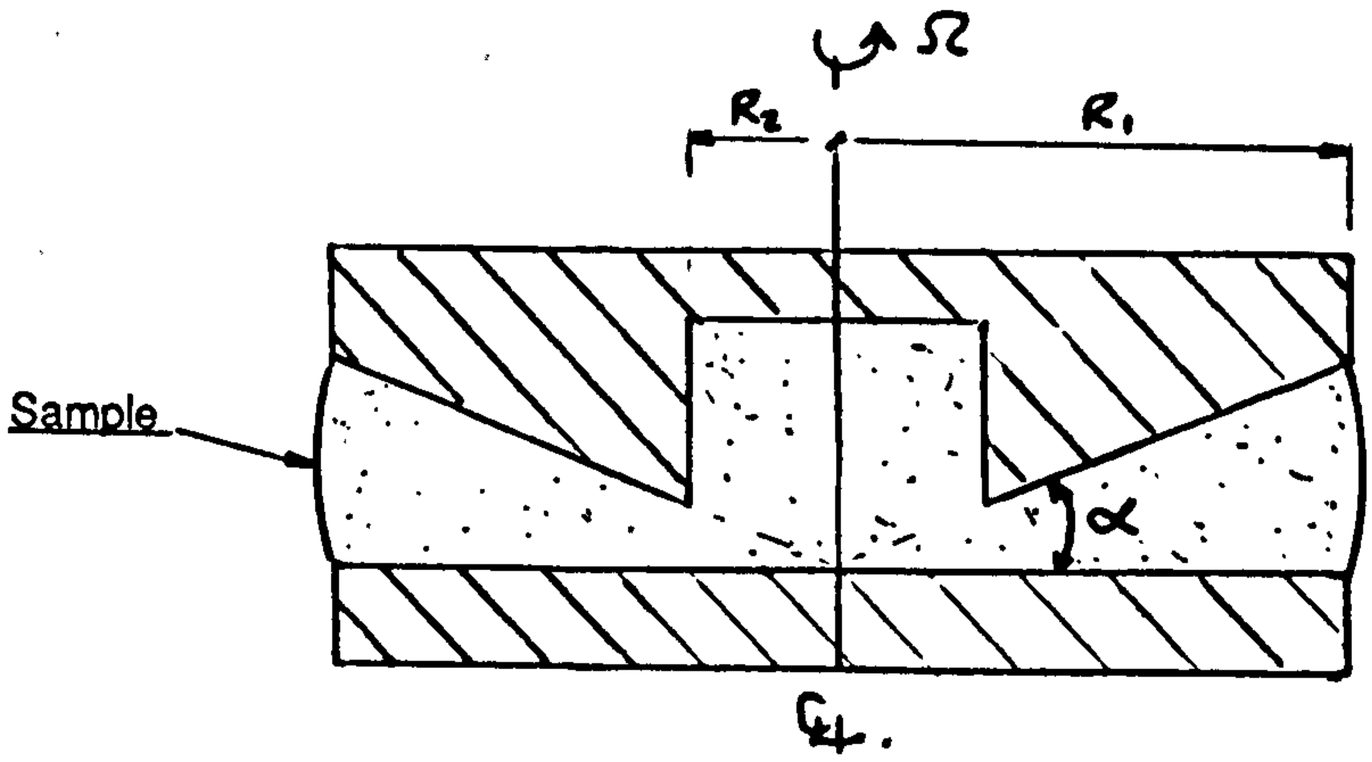

Fig. 3.5 Annular Cone and Plate

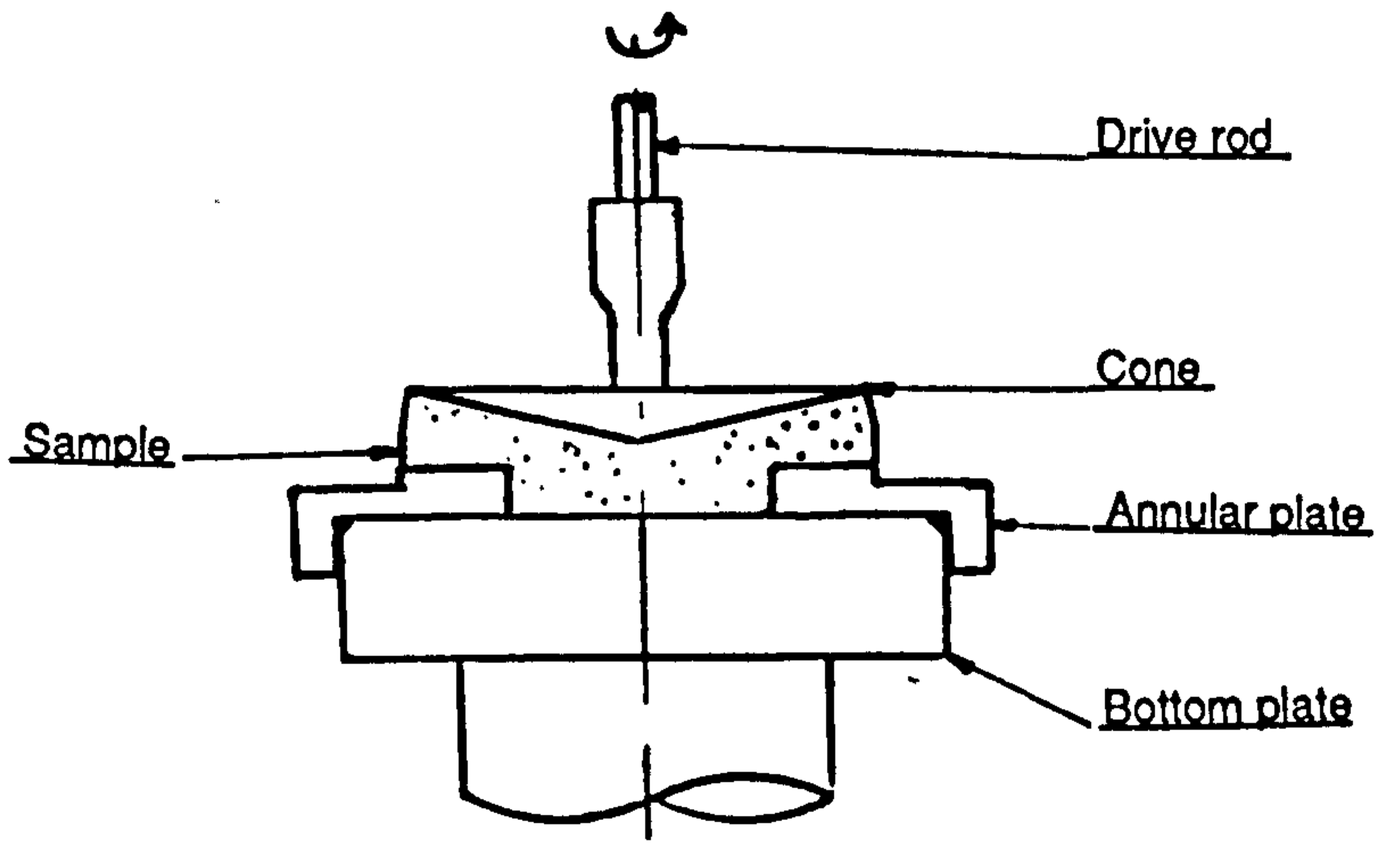

Fig. 3.6 Annular Plate and Cone Assembly on the CarriMed C.S. Rheometer

3.2.3 Annular Plate and Cone

The annular cone and plate shown in Fig. 3.5 was proposed by Cross and Kaye (1986) to overcome the truncation of the cone, in the cone and plate system, which was necessary to accommodate particulate suspensions without jamming, whilst retaining the uniform shear rate across the radius. The stress remains constant and independent of material characteristics in the cone and plate. Walters (1975) shows that these factors remain acceptable under the following conditions:

1. inertia effects are negligible
2. the gap angle is small so that $\text{cosec}^2\alpha \approx 1$ and since the geometry of the system is finite the following assumptions are also required ($\alpha \leq 4^\circ$)
3. cone and plate have the same radius
4. sample edge surface is a sphere with radius centre at cone vertex
5. steady simple shear flow continues to free surface
6. surface tension forces are negligible

Because construction of the annular cone from an existing cone is difficult, since the recess would interfere with the screw socket attachment to the drive rod, the recess was put in the plate, which was custom made to fit over the bottom plate of the Carri-Med C.S. rheometer as shown in Fig. 3.6.

The shear rate, $\dot{\gamma}$,is given by:

$\dot{\gamma} = \frac{\Omega}{\tan\alpha} \triangleq \frac{\Omega}{\alpha}$ and the stress, τ is given by

$$T = \int_{R_2}^{R_1} 2\pi r^2 \tau \, dr = \frac{2\pi\tau}{3} (R_1^3 - R_2^3)$$

which on transposing gives: $\tau = \frac{3T}{2\pi (R_1^3 - R_2^3)}$ 3.29

The analysis is straightforward and the problem is merely one of setting up zero horizontal and vertical displacement of the cone and plate, since the analysis of a displaced cone and plate is much more complicated.

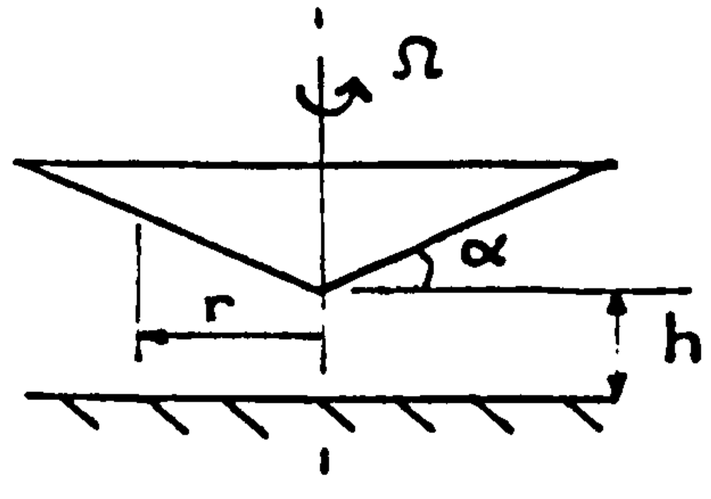

Fig. 3.7 Notation for Cone and Plate

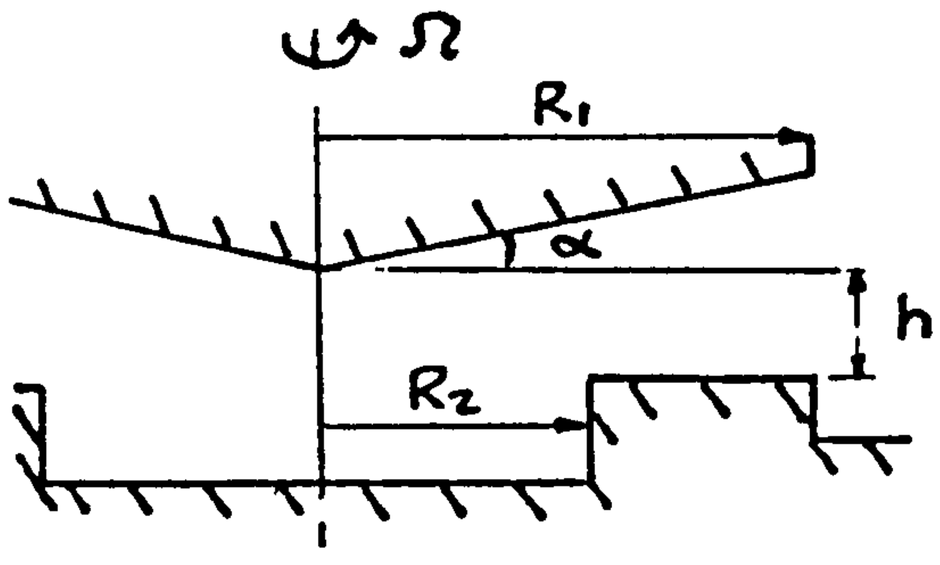

Fig. 3.8 Notation for AP&C

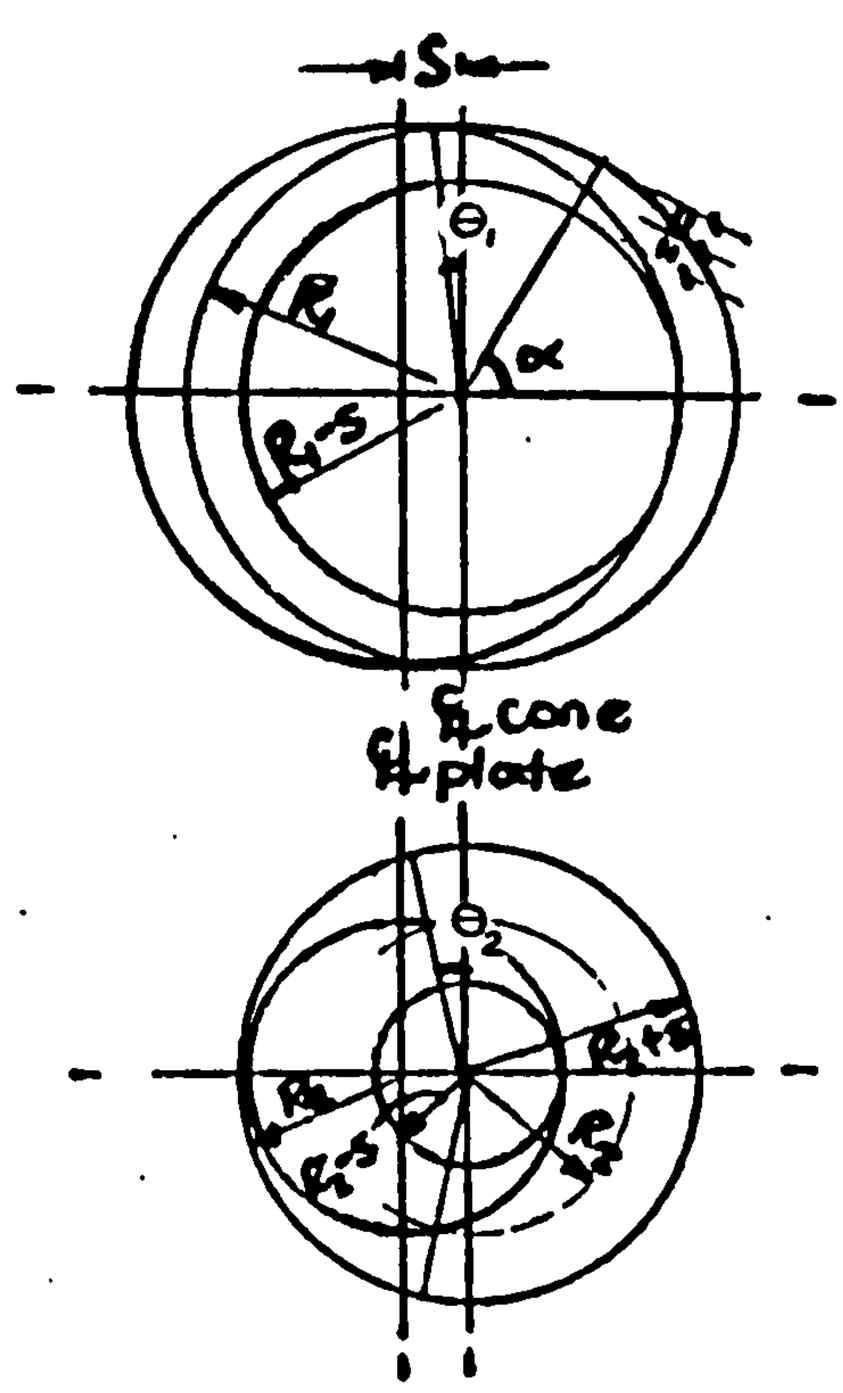

Fig. 3.9 Horizontal displacement of AP&C

3.2.4 Displacement Errors with the APC

When setting up the annular plate and cone (AP C) errors can occur in both vertical and horizontal positioning of both members in relation to each other. It is necessary to establish the effect of these errors on the measurements of shear stress and their likely magnitude. These errors are considered separately for ease of computation

3.2.4.1 Vertical Displacement Error

Using the notation shown in Fig. 3.7 and that given in section 3.2.1

$$\dot{\gamma} = \frac{r\,\Omega}{r\tan\alpha + h} = \frac{r\Omega}{r\alpha + h} \qquad 3.30$$

putting $u = r\,\alpha + h$, $\frac{du}{dr} = \alpha$

$$\text{then } \frac{d\dot{\gamma}}{dr} = \frac{\Omega h}{(h + r\alpha)^2} \qquad 3.31$$

$$T = \int_0^R 2\pi r^2 \tau\, dr \qquad 3.32$$

integrating by parts gives

$$T = \frac{2\pi R^3 \tau}{3} - \int_o^R \frac{d\tau}{d\dot{\gamma}} \cdot \frac{d\dot{\gamma}}{dr} \cdot \frac{2\pi r^3}{3}\, dr \qquad 3.33$$

differentiating equation 3.32 gives,

$$\frac{dT}{dh} = \int_0^R 2\pi r^2 \frac{d\tau}{d\dot{\gamma}} \cdot \frac{d\dot{\gamma}}{dh} dr \qquad 3.34$$

which using same substitution as above gives:

$$\frac{d\dot{\gamma}}{dh} = \frac{d\dot{\gamma}}{du} \cdot \frac{du}{dh} \text{ then } \frac{d\dot{\gamma}}{dh} = -\frac{r\Omega}{(h+r\alpha)^2} \qquad 3.35$$

from equations 3.31, 3.33, 3.34 and 3.35

$$T = \frac{2\pi R^3 \tau}{3} + \frac{h}{3}\frac{dT}{dh} \qquad 3.36$$

indicating that a displaced cone and plate requires the same correction for stress as the parallel plate regardless of cone angle. The corresponding shear rate is dependent on cone angle, however, since:

$$\dot{\gamma}_R = \frac{\Omega R}{(h + \alpha R)}$$

Equation 3.32 can be solved for a Newtonian fluid so that the displaced cone and plate

can be calibrated using such a fluid. This is done as follows using the annular plate and cone configuration, as shown in Fig. 3.8.

For a Newtonian $\tau_{fluid} = \eta\dot{\gamma}$

and we know $\dot{\gamma} = \dfrac{\Omega r}{h + r\alpha}$

$$T = \int_{R_2}^{R_1} \frac{2\pi\eta\Omega r^3 dr}{h + r\alpha} \qquad 3.37$$

let

$$u = h + r\alpha, \quad R_1 = \frac{u_1 - h}{\alpha}, \quad R_2 = \frac{u_2 - h}{\alpha} \qquad 3.38$$

$$T = 2\pi\eta\Omega \int_{u_2}^{u_1} \frac{(u-h)^3}{u\alpha 4} \, du$$

$$T = \frac{2\pi\eta\Omega}{\alpha^4} \int_{u_2}^{u_1} (u^2 - 3u + 3h^2 - \frac{h^3}{u}) \, du \qquad 3.39$$

$$T = \frac{2\pi\eta\Omega}{\alpha^4} [\frac{u^3}{3} - \frac{3}{2} hu^2 + 3h^2 u - h^3 \log_e u]_{u_2}^{u1} \qquad 3.40$$

putting $h = 0$, $u_1 = \alpha R_1$ $u_2 = \alpha R_2$ and

$$T = \frac{2\pi\eta\Omega}{\alpha} (R_1^3 - R_2^3) \qquad 3.41$$

$$T = \frac{2\pi}{3} (R_1^3 - R_2^3)\ \tau \qquad 3.42$$

For our particular geometry:

$R_1 = 3.0$ cm, $R_2 = 1.5$ cm, $\alpha = 0.0699268$ (tan 4°) on putting $h = 0.005$ (50 μm) we have from equation 3.40

$$T/\tau = 48.010449$$

and from equation 3.42, $T/\tau = 49.480084$ giving an error = - 2.97% in T/τ due to a vertical displacement error whilst setting up of + 50μm As it is anticipated that with careful setting up zeroing the vertex can be achieved to within 10μm, this error is acceptable.

Consider the effect of the deeper central section of the annular plate on the accuracy of the measurement.

Using previously derived formula the total T is:

$$T = \frac{2\pi\eta\Omega}{\alpha^4}\left\{\left[\frac{u^3}{3}\right]_{\alpha R_2}^{\alpha R_1} + \left[\frac{u^3}{3} - \frac{3}{2}hu^2 + 3h^2u - h^3\log_e u\right]_h^{(h+\alpha R_2)}\right. \qquad 3.43$$

$R_1 = 3.0,\ R_2 = 1.5,\ h = 0.7,\ \alpha = 0.0699268$

$$\text{giving } T = \frac{2\pi\eta\Omega}{\alpha 4}\ (0.0026927 + 0.0000387)$$

Hence the error in $T/_\tau$ due to ignoring the central section is

$$+\ \frac{0.0000387}{0.0026927} = +\ 1.42\%, \text{ which is also acceptable.}$$

3.2.4.2 Horizontal Displacement Error

The annular plate shown in Fig. 3.6 is a loose fit laterally on the bottom plate. It is required to centralise the annular plate with the measuring cone for accurate determination. The effect of an error in this zero horizontal displacement will be considered as follows:-

From Fig. 3.9 for small angles $S = 2R_1\theta_1 = 2R_2\theta_2, \quad \alpha = \pi/3$

$$T = \int_{R_2+s}^{R_1-s} 2\pi r^2 dr\tau + \int_{R_2-s}^{R_2+s} (\pi + 2\Theta_2)\ r^2 dr\tau$$

$$+ \int_{R_1-s}^{R_1} (\frac{4\pi}{3} - 2\Theta_1)\, r^2 dr\tau \qquad 3.44$$

$$T_{/\tau} = \frac{2\pi}{3} [R_1\text{-}s)^3 - (R_2+S)^3] + (\frac{4\pi}{9} - \frac{S}{3R_1}) [R_1^3 - (R_1\text{-}s)^3] + (\frac{\pi}{3} + \frac{S}{3R_2})$$

$$[R_2+ S)^3 - (R_2 - s)^3] \qquad 3.45$$

$$T_{/\tau} = \frac{2\pi}{3} (R_1^3 - R_2^3) - \frac{2\pi}{3} R_1^2 S + [\frac{2\pi}{3} -1) R_1 + (2-2\pi)R_2] S^2 + (1-\frac{2\pi}{9}) S^3 +$$

$$(\frac{2}{3R_2} - \frac{1}{3R_1}) S^4 \qquad 3.46$$

for small s, second order terms may be ignored since for $R_1 = 3.0$, $R_2 = 1.5$, $s = 0.05$ cm. (500μm) the s^2 term is less than 0.9% of the s term,

$-\frac{2\pi}{3} R_1^2 s = -0.9425$, whereas $\frac{2\pi}{3} (R_1^3 - R_2^3) = 49.480084$,

as before. The error in $T_{/\tau}$ = - 1.90% for an error in horizontal displacement of 0.05 cm. (500μm) on setting up.

The procedure for setting the horizontal align ment of the annular plate is to select a torque, T, which will produce, approximately, 5 radians/sec of angular rotation for a calibration fluid of constant viscosity over the particular shear rate range being tested. Calculate

$\frac{2\pi}{3}(R_1^3 - R_2^3)$, which is the stress factor, F_s, then

$$\dot{\gamma} = \frac{\tau}{\eta} = \frac{T}{F_s \eta} \qquad 3.47$$

and if a horizontal displacement s, exists then:

$$\dot{\gamma}_s = \frac{T}{(F_s - f(s))\ \eta} \qquad 3.48$$

making $\dot{\gamma}_s > \dot{\gamma}$ with $\dot{\gamma}$ known seek $\dot{\gamma}$, otherwise seek the minimum $\dot{\gamma}$ for zero s. The initial alignment can be done, by eye, to within ± 0.5 mm. (500μm)

3.3 Calibration of Measuring Systems

In order that shear stress and shear rate measurement can be achieved using the Carri-Med rheometer, conversion factors are required. Initial checks and settings are carried out prior to making a flow run and accurate measurements must be taken of the

measuring systems geometry to calculate reliable conversion factors. These points will now be discussed.

3.3.1 Conversion Factors

Since neither shear stress nor shear rate can be measured directly on the rheometer conversion factors based on the foregoing analysis are used to convert the applied torque to shear stress and the angular velocity to shear rate. The conversion factors for measuring Newtonian fluids are given in Table 3.1 for the relevant measuring systems. These factors are used in the equations

$$\tau = F_{\tau} \quad T \qquad 3.49$$

$$\dot{\gamma} = F_{\dot{\gamma}} \quad \Omega \qquad 3.50$$

allowing the viscosity to be computed from

$$\eta = \tau / \dot{\gamma} \qquad 3.51$$

These relations were used to assess the ability of the measuring systems to measure the known viscosity of a calibration oil. The calibration oil used was a mineral oil number 18 sample No. = 28286, from the Paint Research Association. The oil has the following specification in S.I. units.

η = 160Pa.s. ν = 180m^2/s ρ = 888 kg/m^3 at 20°C

η = 101Pa.s. ν = 114m^2/s ρ = 884 kg/m^3 at 25°C

Measuring System	$F_{\dot{\gamma}}$	F_{τ}
Parallel Plate	$\frac{R_p}{h}$	$\frac{2}{\pi R_p^3}$
Annular Plate and Cone	$\frac{1}{\tan\alpha}$	$\frac{3}{2\pi(R_c^3 - R_p^3)}$
Vane in Cup	$\left(\frac{1}{k} + 1 + \frac{k}{3} - \frac{k^3}{45}\right)$ $k = \ln R_c/R_v$	$\frac{3}{2\pi(R_v^3 + 3R_v^2 h)}$ (one end immersed)

Table 3.1 Newtonian Conversion Factors

Measuring System	F_{δ}	F_{τ}
Parallel Plate	$3R_p/4h$	$3/2\pi R_p^3$
Annular Plate and Cone	$1/\tan\alpha$	$3/2\pi (R_c^3 - R_n^3)$
Vane in Cup	unknown	$3/2\pi(R_v^3 + 3R_v^2 h)$ (one end immersed)

Table 3.2 non-Newtonian Conversion Factors

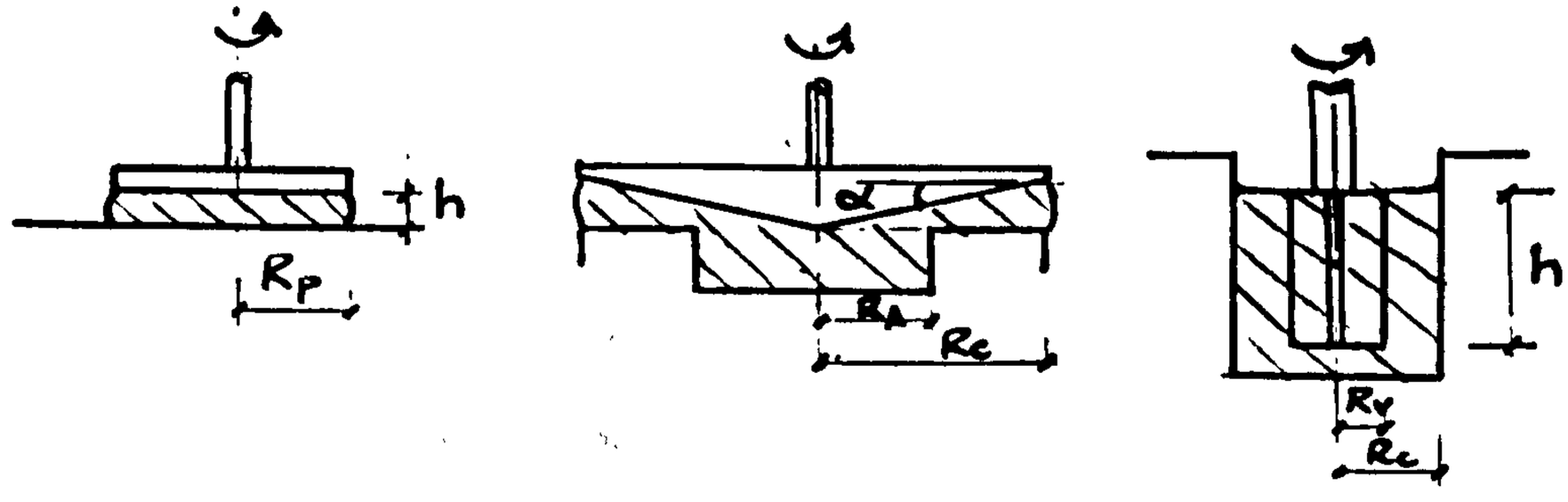

Parallel Plate Annular Plate and Cone Vane in Cup

Fig. 3.10 Notation for Conversion Factors

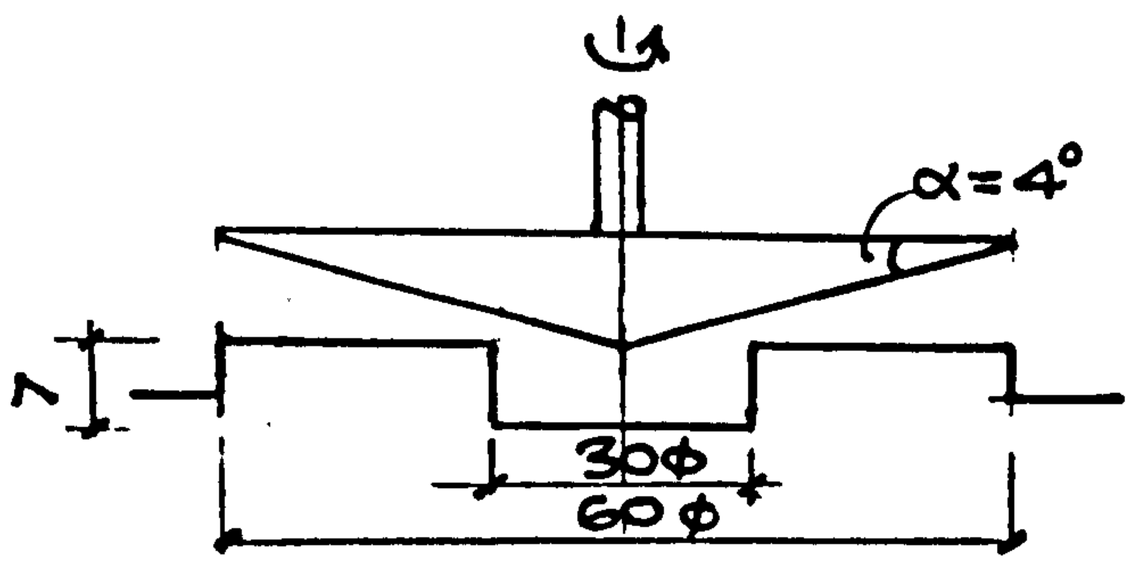

Fig. 3.11 Dimensions of the AP&C

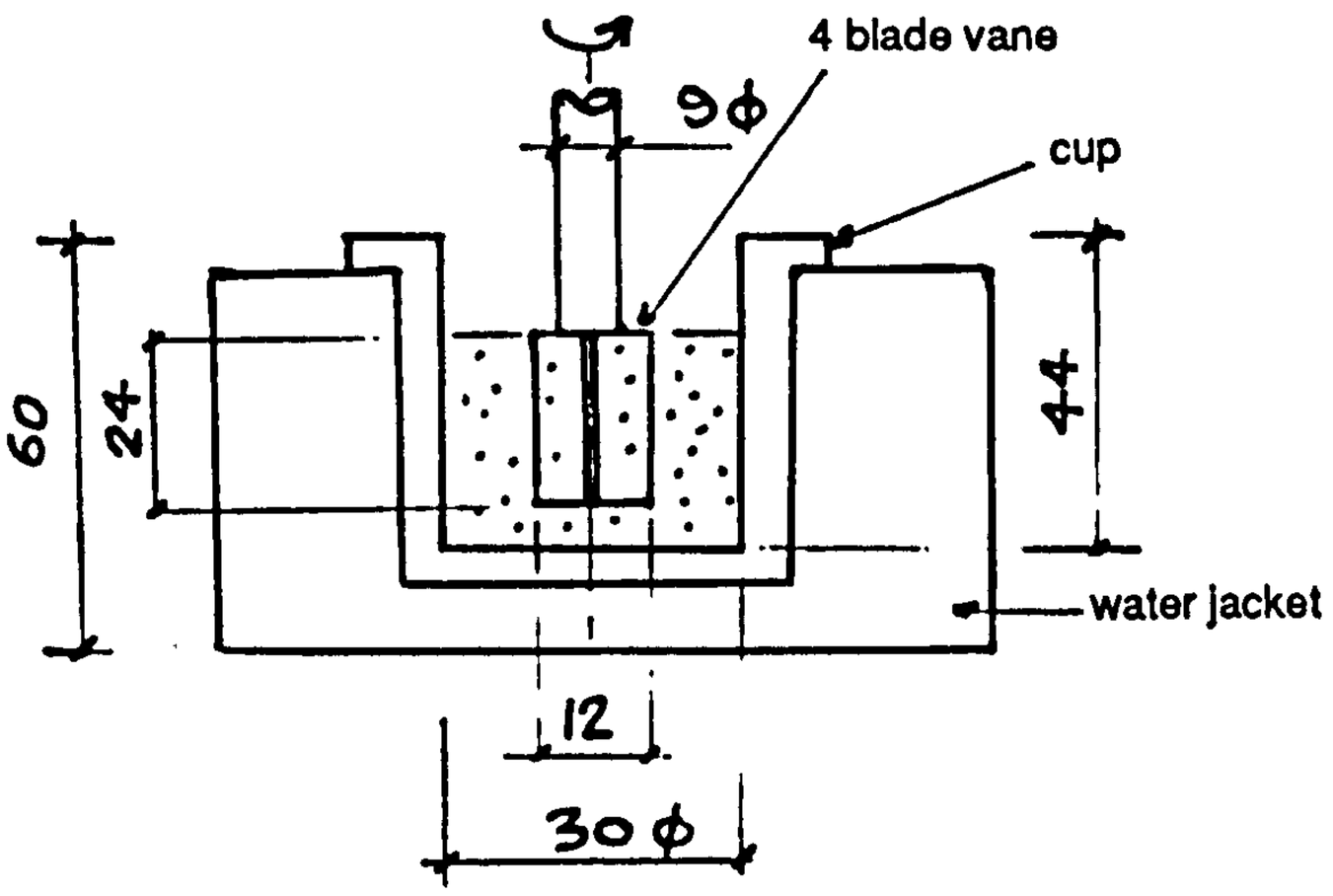

Fig. 3.12 Dimensions of the Vane in Cup

Although to infer that a measuring system can measure the stress of a non-Newtonian fluid, if it is calibrated on a known Newtonian, is not strictly correct, since the conversion factors for most measuring systems depend on the characteristics of the fluid. The exception is the cone and plate, where both factors are independent of the fluid.

The shear rate factor for the vane in cup had to be assessed in order to calibrate using the oil, since the calibration oil has no yield value.

The notation used in the Tables 3.1 and 3.2 is shown on the diagrams in Fig. 3.10. It is seen in Table 3.1 that the shear rate in the parallel plate system varies linearly with radius. Since shear stress depends on the shear rate, which is a character istic of the fluid, the shear stress will only vary linearly with radius for a Newtonian fluid because the viscosity is constant. The correction to the stress factor enabling non-Newtonian fluid measurement is made using the Cross and Kaye(1986) analysis of the previous section. The annular plate and cone (APC) is based on the theory of the cone and plate over the annulus measuring section and therefore requires no corrections to the conversion factors, provided correct vertical and horizontal positioning is achieved.

The vane in cup was originally devised to measure yield stress directly, thereby not requiring shear rate evaluation. To enable interpretation of a Newtonian flow curve the shear rate factor was obtained by considering the vane to act as a concentric cylinder. The third term of the converging series formula of Krieger and Elrod (1953) was used in order to obtain an error of less than 1% with a cup to vane radius ratio of 2.5. To obtain a shear rate factor for a cement slurry with a yield value by this approach is mathematically complex and shear rate variation across such a wide gap is indeterminable giving rise to plug flow, Dimond (1975), so this is not pursued. The

shear stress factor for a concentrated suspension with a yield value is calculated using the following derivation, which assumes that yield occurs on the peripheral edges of the vane and has a uniform stress distribution.

Using the relation between the shaft stress, τ_s, and the end stress, τ_e, of

$\tau_s = (\frac{2r}{d})^P \tau_e$ (Nguyen 1983) the torque on the vane is given by

$$T = \tau_s \frac{\pi d^2 h}{2} + \int_0^{d/2} \tau_s (\frac{2r}{d})^P 2\pi r^2 dr \qquad 3.52$$

or

$$T = \tau_s \frac{\pi d^3}{2} (\frac{h}{d} + \frac{1}{2(p+3)}) \qquad 3.53$$

for one end immersed. Putting p=0, Haimoni (1985),the shear stress factor becomes, with $d = 2R_V$ and rearranging

$$F_\tau = \frac{3}{2\pi(R_v^3 + 3R_v^2 h)} \qquad 3.54$$

for both ends immersed the shear stress factor is

$$F_\tau = \frac{3}{2\pi(2R_v^3 + 3R_v^2 h)} \qquad 3.55$$

The non-Newtonian factors are shown in Table 3.2 for each system.

3.3.2 Dimensions of The Measuring Systems

The diameter of the parallel plate measured with a micrometer was 50.03 ± 0.0013 mm, which with a gap = 1000μm, gives Newtonian $F_{\dot{\gamma}} = 25$ and $F_{\tau} = 0.0407$ and non-Newtonian $F_{\dot{\delta}} = 18.8$ and $F_{\tau} = 0.0305$.

The dimensions of the APC are shown in Fig. 3.11 and those of the vane in cup in Fig. 3.12. For the APC, the $F_{\dot{\delta}} = 14.3$ and the $F_{\tau} = 0.0202$, whereas for the vane $F_{\dot{\delta}} = 2.38$ and $F_{\tau} = 0.17$. When assessing these two geometries for edge and end effects by varying the amount of sample tested these factors required correction. Edge and end effects for these geometries are considered in the next chapter. The variations to the conversion factors were obtained by applying the reduced sample dimensions to the relevant equations (see equation Nos. 3.54 and 3.42).

In order to accurately calculate the conversion factors the measuring geometries were checked dimensionally using a micrometer, a vernier gauge and dial gauges, where appropriate. The APC overall diameter was -0.04mm in 60 mm from an average of 4 readings on both cone and plate (s.d = 0.011 mm). With the cone clamped in a lathe variation in level of the concentric surface circumferences was ± 0.03 mm and unevenness of ± 0.02 mm moving radially along the cone slope, although positioning and moving of the magnetic gauge mounting, using lathe controls, may account for a substantial amount of the error.

The diameter and alignment to the vertical was checked using a clamped dial gauge for the vane and is shown in Fig. 3.13. Other dimensions such as length, thickness and those of the conical drive rod attachment were checked, together with cup dimensions to assess volume, so that depth of immersion could be calculated from a known quantity of sample. The dimensions of the vane are shown in Fig. 3.14.

When a manual run was performed on the calibration oil at 25°C. using the vane, a flow curve such as that shown in Fig. 3.15 was obtained. The unusual phenomenon of hysteresis loop displayed for Newtonian flow curves is beyond the scope of this thesis, since only the yield stress measurement using the vane is required, and at only very low shear rates. The comments in the graph notes were made, after confirming the reason for the phenomenon, which was the sink observed, when the vane was rotated in a glass beaker filled with cement slurry.

3.3.3 Zero Gap Setting and Air Bearing Check

Prior to carrying out any determinations, and with the zero gap setting, as a daily routine, the following procedures were performed.

Zero gap setting means bringing the two parts of the measuring system together at a point of contact, such that from that datum on the micrometer the required position of the parts, whilst testing, can be set. On the Carri-Med there are two ways this setting can be achieved.

i) if both parts of the measuring system are metal an electrical connection can be installed between an indicator lamp housed in the drive motor support pillar and the rotating part of the measuring system. The ram is raised and after cancelling micrometer screw backlash, by winding downwards about 20 divisions the

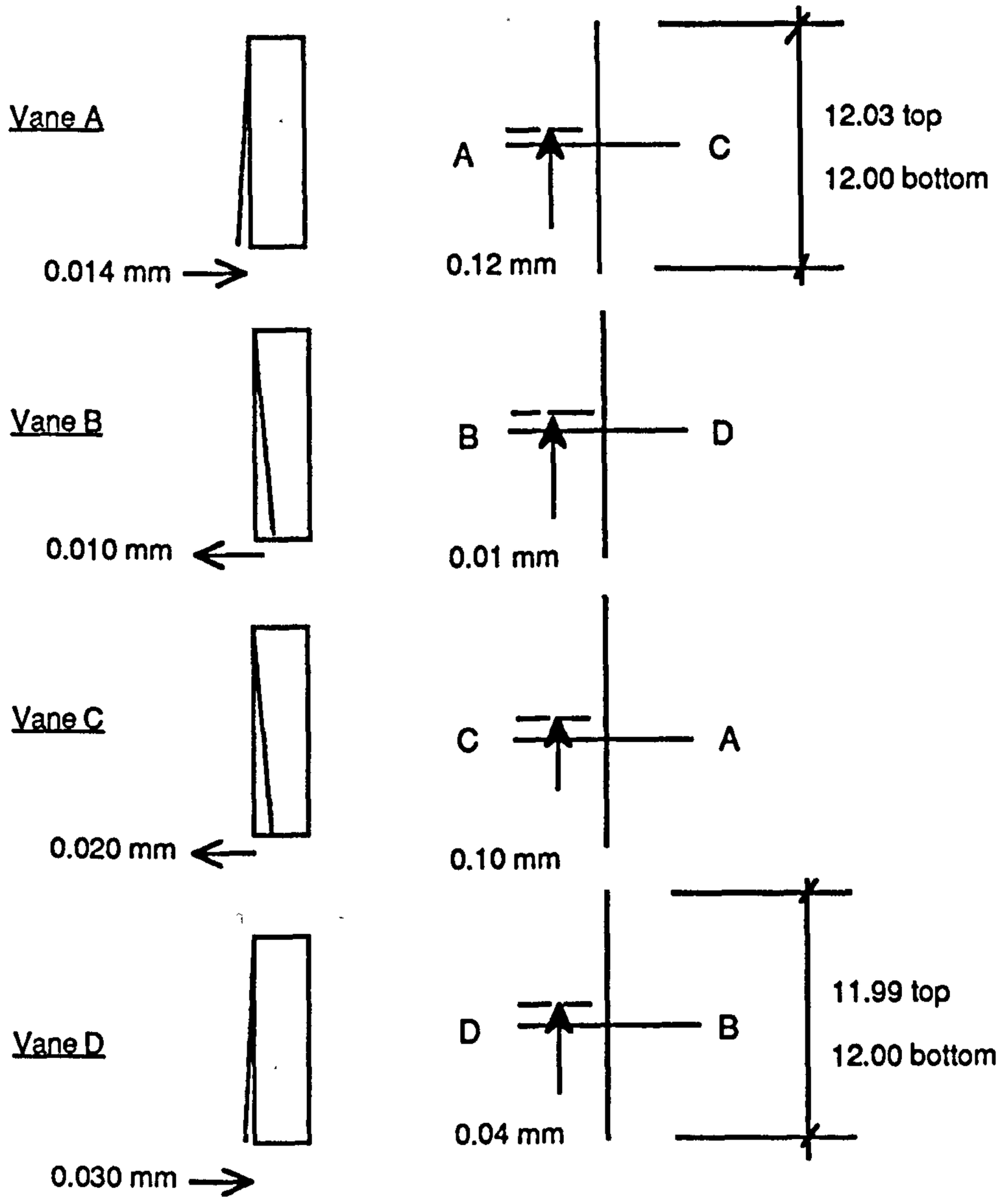

Fig. 3.13 Accuracy of Vane Construction

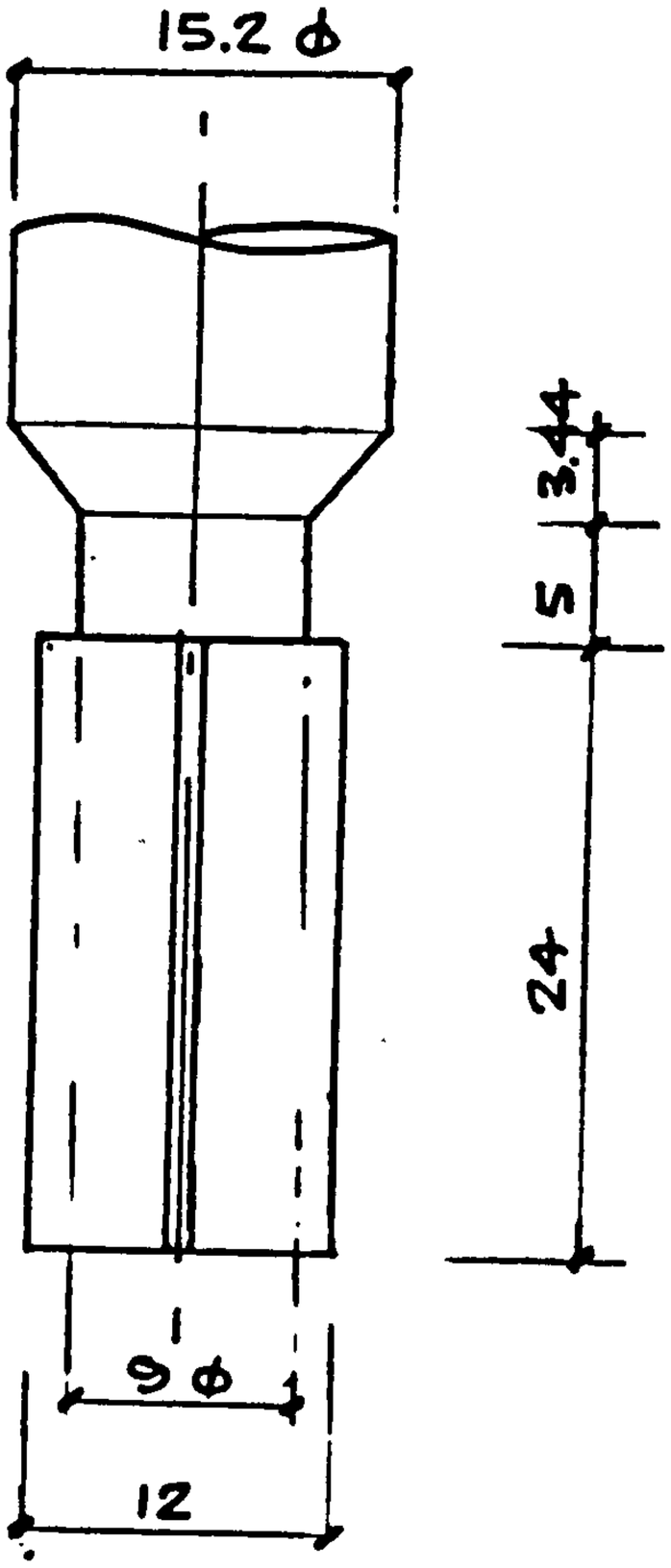

Fig. 3.14 Dimensions of the Four Blade Cylindrical Vane

Calibration oil at 25°C

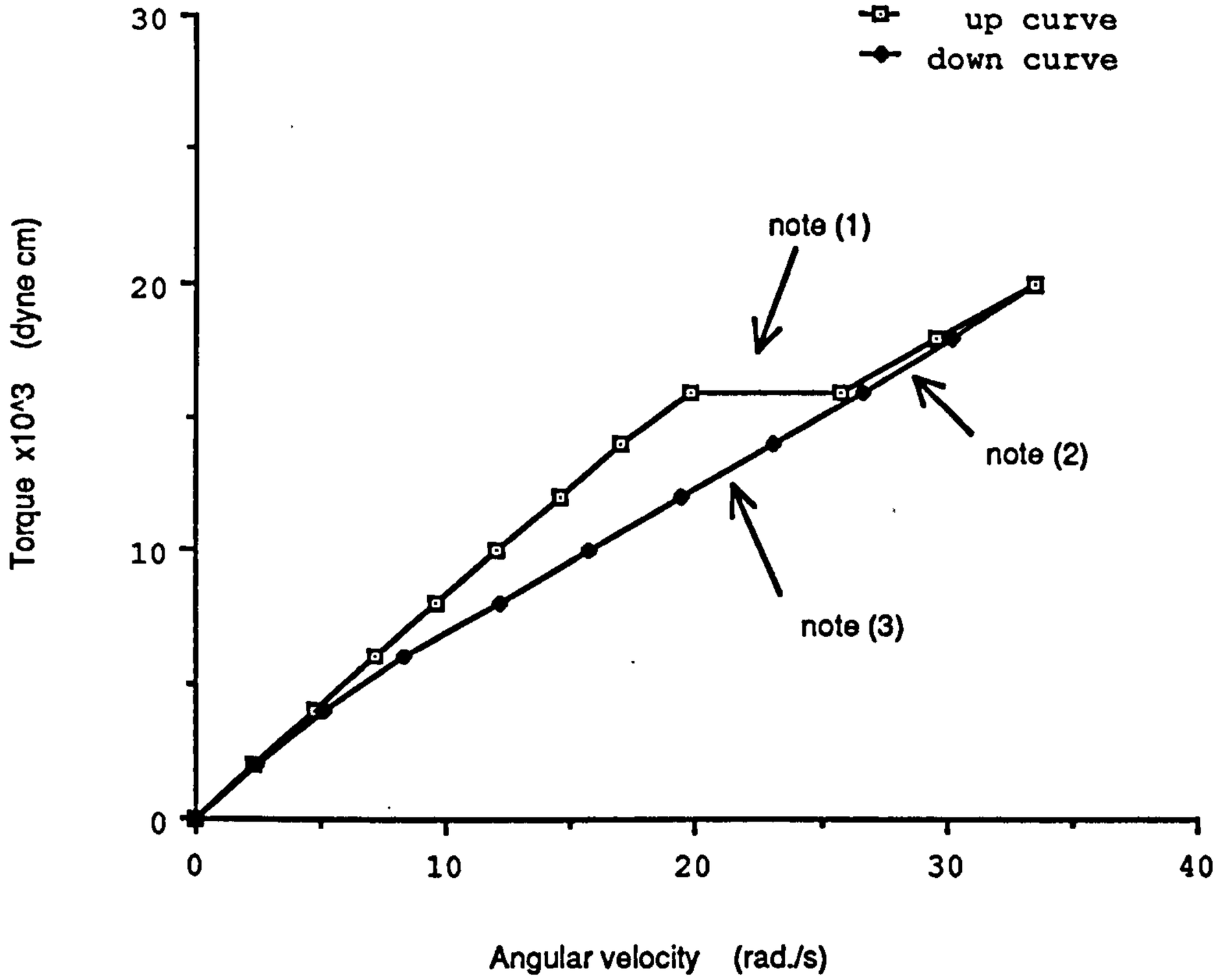

Fig. 3.15 Manual run on CarriMed using Vane in Cup

NOTES

1. Angular velocity causes vortex sink around vane which at constant stress increases depth of sink to equilibrium. Can be created at 12000 dyne cm by instantaneous loading of torque.
2. Once the sink is developed constant viscosity is maintained. However viscous heating occurs reducing viscosity which in turn affects sink depth.
3. Energy required on down curve to jump to closed sink curve but torque is being reduced. Extrapolation of downcurve does not pass through the origin indicating end effect rather than plug flow which is not associated with a Newtonian fliud.

bottom part is raised until the light glows indicating contact. The micrometer reading is noted.

ii) Without metal contact or if the surface is engraved or treated, the spindle can be made to spin slowly by giving it a short twitch. The micrometer after raising the ram and taking up the backlash is wound up until contact just stops the spinning member. The reading on the micrometer scale is noted.

This procedure is carried out a minimum of 4 times and the average reading used as the zero gap setting datum. The variation in gap setting can be due to temperature, clamping of parts to a firm base plate or erosion of surface treatment as can be seen from Table 3.3.

The air bearing check is carried out in the following manner, generally on a weekly basis.

1. Switch digital reading to angular displacement and set torque thumbwheels to zero
2. Switch torque on
3. Allow to bias for longer than 2 minutes without top measuring system in place
4. Raise ram, apply torque of 20 dyne cm. observe angular displacement rate of increase.

The digital reading of angular displacement should increase smoothly with increasing speed.

After observing slight hesitationsat 0.070 radians and at 0.150 radians, the torque

was reduced to zero and a slow angular increase was seen. After waiting about 10 minutes, with the torque switch off and the ram down, the torque was again set to zero and switched on. The angular displacement was as shown in Table 3.4, at various times after ram up. This shows that the biasing system works reasonably well as the reading is static after 5 minutes.

3.4 Conclusion

After all the checks and calibration procedures confirmed that the rheometer was set up properly and functioning normally it could be used for calibration oil and cement slurry experiments. These are described in the next chapter.

Table 3.3

Zero gap setting of some previous APC experiments.

Surface treatment	av. Division	above min µm	Date
dense coarse engraving	46.8	168	20.6.88
coarse engraving	38.3	83	15.6.88
fine engraving	32.3	23	14.6.88
sand(150-90 µm top. 90-75 µm bot.)	76.1	461	8.6.88
sand 300-150 µm top.bot.	87.8	578	3.6.88
"	89.6	596	3.6.88
smooth s.s. clamped	30.4	4	25.4.88
sand 300-150 µm, top & bot.	83.7	537	24.4.88
"	86.0	560	26.1.88
"	88.0	580	13.1.88
"	88.1	581	11.1.88
"	97.5	675	8.1 .88
smooth s.s. clamped	31.4.	14	15.12.88
sand 300 -150 µm top & bot.	82.6	526	15.12.88
"	4.9	749	10.12.88
"			
"	85.8	558	6.18.88
"	87.5	575	6.12.88
"	89.5	595	6.12.88
Smooth s.s. clamped	31.2	12	2.12.88
" unclamped	34.8	48	28.7.87
" "	35.7	46	20.7.87
" "	34.6	46	16.7.87

Table 3.4

Air Bearing Check

Time(sec) after ram up	0	10	20	30	45	60	90
Radians	0.000	-0.001	-0.002	-0.002	-0.002	-0.003	-0.003
Time (min)	2	2.50	3	4	5	6	7
Rad.	-0.003	-0.003	-0.004	-0.004	-0.005	-0.005	-0.005
Time (min)	9	10	8				
Rad.	-0.005	-0.005	-0.005				

CHAPTER 4

Experimental Technique and Phenomena in the Yield Stress Measurement of Oil Well Cement Slurry

Having set up the Carri -Med C.S. Rheometer, the yield stress measurement of cement slurry could begin. However some fundamental points, which the literature treats lightly, required consideration. These points include mixing method, sample size and manner of location, together with the surface treatment of measuring system surfaces to overcome slippage. The amount of mixing energy input was known to have an effect on the yield stress of cement slurry and one of the objectives was to study this effect. Hence suitability of the various experimental techniques to achieve this study required investigation. These techniques and the associated phenomena are discussed in the following sections.

4.1 Mixing Methods

The method of mixing a cement slurry prior to laboratory testing vary enormously. It is usual to test as early as possible to obtain the start of time related effects. This can be from 2 to 5 minutes according to the time taken for

a) hand or mechanical mixing
b) measurement of constituents
c) transfer to testing apparatus
d) setting and checking of test equipment
e) equilibration time.

An initial trial run on the C.S. rheometer to obtain a flow curve for an O.P.C cement slurry was performed using the following mix procedure:-

1. Add 4g water from pipette to 10g cement in a beaker in 30 secs.
2. Mix gently by hand with spatula for 1 min.to achieve homogeneity
3. Load sample onto bottom plate of parallel plate measuring system
4. Raise ram to bring bottom plate up to required gap setting
5. Commence manually applied torque, using toggle switches, at 2 mins. after adding water
6. Increase torque at 15 sec. intervals until yield occurs in sample.

With this procedure the sample either remained rigid or on yielding was ejected from between the plates, even when the w/c ratio was increased to 0.65 and the gap increased from 500μm to 1 mm.

4.1.1 API Mixing Using a Waring Blender

Using a Waring blender to mix a w/c = 0.46 slurry, in accordance with API Spec. 10 Section 5, but without the defoamer and without stirring for 20 mins. in the atmospheric pressure consistometer recommended in Appendix H3 of API Spec. 10, a flow curve was achieved with a 1mm gap, at a peak torque of 20,000 dyne cm., and at 41 mins. after adding the water. This compared to yielding at 165000 dyne cm peak torque after 2 mins. with a w/c = 0.35 using the previous manual mixing procedure.

The API standard mix procedure mixes 600 ml, which means approximately 800g of cement is deposited in the blender in 15 secs. This can lead to problems with homogeneity. Various funnel arrangements, including one with a vibrator, were tried to ensure an even feed of cement. Consistent control of the feed was difficult through a funnel orifice. The method resorted to was shaking by hand a cylindrical open top plastic container.

Visual examination of a slurry, w/c = 0.46, immediately after mixing in a Waring blender for 15 secs. at 4000 r.p.m, showed less than 5 ml of wet but trapped unmixed cement and a top section appearing wetter than the mid-section. This was done to see if the slurry was sufficiently mixed so that the 35 sec. high speed mixing time could be reduced and its effect on flow curves compared.

The homogeneity of a w/c = 0.46 slurry mixed in the Waring blender for the full 35 secs. of high speed mixing was found by weighing samples before, and after, drying in an oven at 110°C for 24 hours. The samples were taken from the same mix at

1, 30 and 60 mins. since adding the water, and from the top, middle and bottom of the blender on each occasion. The calculated w/c ratios are shown in Fig. 4.1. They indicate a wide variation in homogeneity for this particular mixer and that concentration of the slurry is less towards the top of the mix.

The Waring blender is controlled by adjusting the input voltage to the variable speed motor. The rotational speed of the blender is monitored by a digital transmitter from an electro-magnetic pulse sensor on the drive shaft.

API Spec 10 section 5 gives a tolerance on the 4000 r.p.m. mixing speed of ± 200 rpm and on the 12000 rpm of ± 500 rpm whilst mixing water and cement slurry, respectively. To test this an aluminium extension shaft 10 mm dia x 100 mm long was attached to the impeller inside the blender and a 20 mm dia white card disc glued to the top end. With a black mark on the disc and using a stroboscopic tachometer (model B891 by Power Instruments Inc.) the rotational speed was measured. Unfortunately the inclusion of the shaft extension appeared to impair the mixing. However, with 350 ml of water in the blender and a tachometer reading of 6000 rpm. (± 100 rpm) the digital reading varied between 6900 and 7700 r.p/m. Whilst mixing a w/c = 0.4 slurry at 13500 r.p.m. the readings varied from 13500 to 16500 rpm generally with isolated readings of 2700 and 25000 rpm. When mixing water only if the blender was lifted slightly the speed increased from 6000 to 7100 rpm. Hence setting and control of the Waring blender is inadequate for accurate mixing energy studies of cement slurry in the range of energies used in the field.

However for initial studies where other parameters were compared, such as ageing and rate of applied stress the Waring blender was used for mixing. To give the mixing

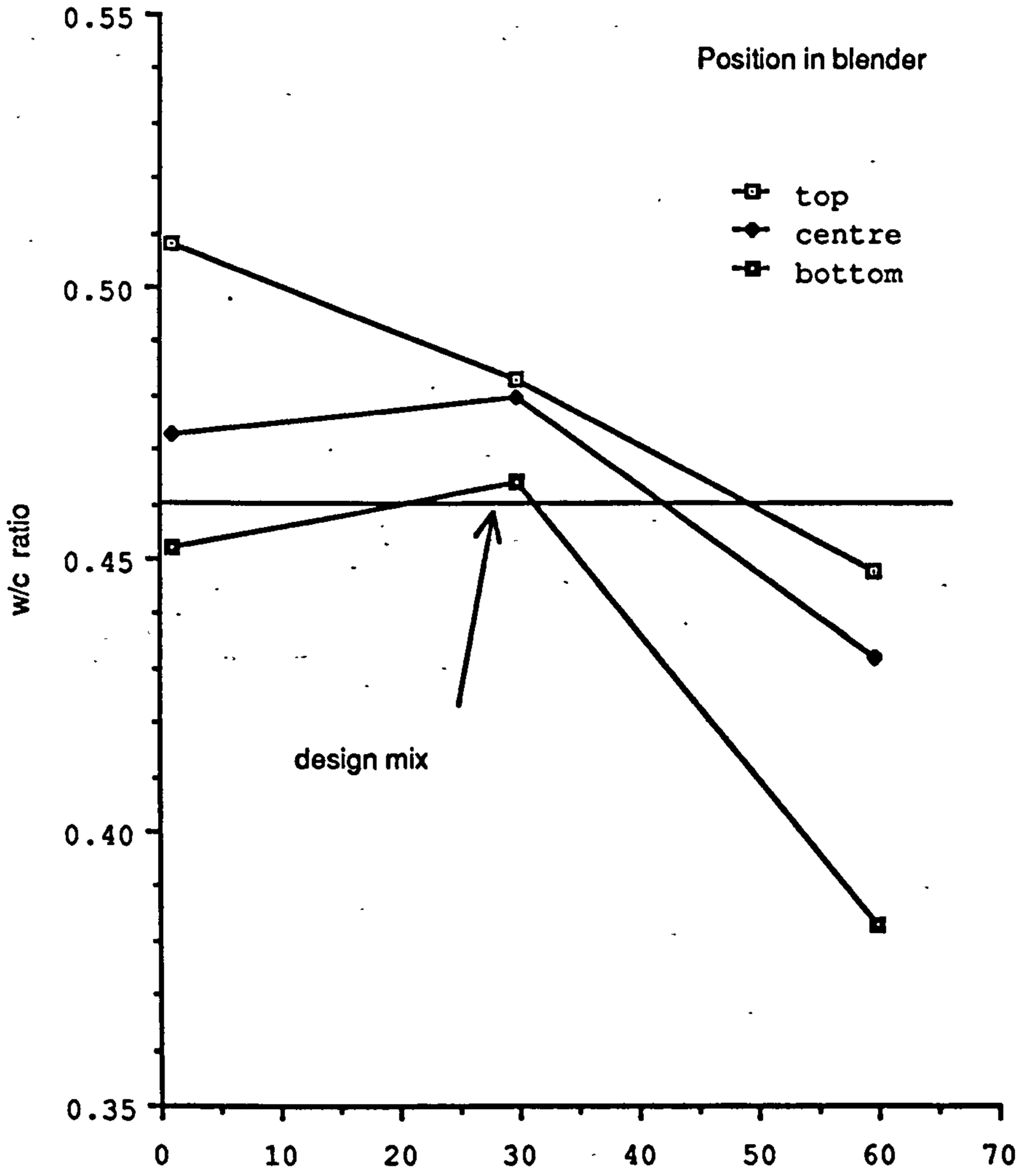

Fig. 4.1 Variation of w/c with depth in Waring blender

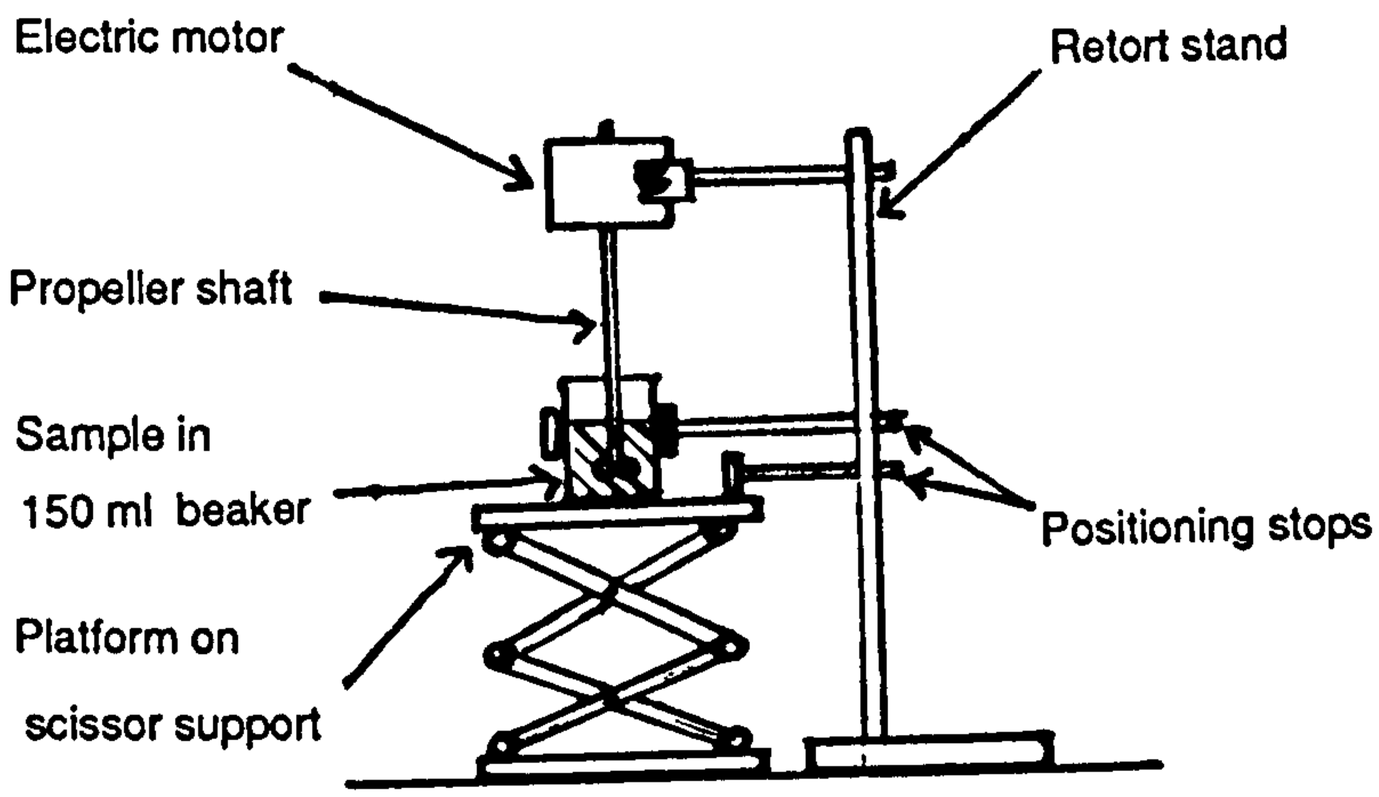

Fig. 4.2 Arrangement of Mixing Apparatus

speeds under load conditions, required by the API, two marks were scribed on the Waring unit's speed control knob corresponding to 5500 rpm and 14700 rpm on the digital readout. These figures were obtained from a calibration curve provided by BP Research with the unit.

4.1.2 A Small Sample Mixing Procedure (SSMP)

To perform numerous tests on various controlled stress measuring systems for comparative purposes, a small sample mixing procedure (SSMP) was adopted. 50 ml. of cement slurry. a convenient amount, was mixed using the apparatus shown in Fig. 4.2 in the following manner:-

1. Weigh water in 150 ml beaker and cement in another beaker
2. Start timer, transfer cement to water and blend by hand using spatula until timer reads 1 minute
3. Place beaker in position on mixing apparatus at 1:30 (min:sec.) mix at fixed speed for 1 minute
4. Transfer sample by spoon to bottom plate of measuring system.

By allowing 30 seconds for equilibration and 40 seconds for the transfer operation a comfortable start time for a test run was 5 minutes, after adding water.

The position of the propeller in the beaker and the speed of rotation were arranged to obtain optimum turbulent mixing throughout the sample without splatter.

The small quantity retained on the spatula from initial hand blending is insignificant and can be ignored as can the energy input of this hand blending in comparison with

the vigorous propeller mixing.

Transfer of the cement into the water beaker was found to be less prone to error than the converse procedure.

To enable accurate assessment of the mixing energy input, so that each proportion of the sample receives the same energy, these mechanical mixers were dispensed with and a new procedure was developed, which is outlined in Chapter 6.

4.2 Sample Size and Location

4.2.1 Parallel Plate

Preliminary manual runs to obtain the flow curve of the calibration oil (160 poise at 20°C) using the parallel plate measuring system showed that sample size and eccentricity to the vertical axis on placing the sample can have a significant effect on the measured viscosity. This can be seen in Fig. 4.3. For a number of programmed flow runs of sample size between 2 and 5 ml., tested using the parallel plate, the measured viscosity varied as shown in Fig. 4.4. A template, which provided for a 2.5 ml sample and is shown in Fig. 4.5, was used to locate the sample concentrically. Initially some oil, about 0.3 ml, adhered to the template causing undercut, as illustrated in Fig. 4.5. The error in the measured viscosity of the calibration oil,whilst using this device on the parallel plate, could be an under-estimate of approximately 20% with a 0.5 mm undercut or an over-estimate of about 7% with a 1 ml oversize sample when a 1 mm gap is used. The anti-capillary attraction rebate on the underside of the template was a later addition to overcome water being drawn out of the cement slurry samples. This location device was later found unsuitable with irregular grit and sand surfaces.

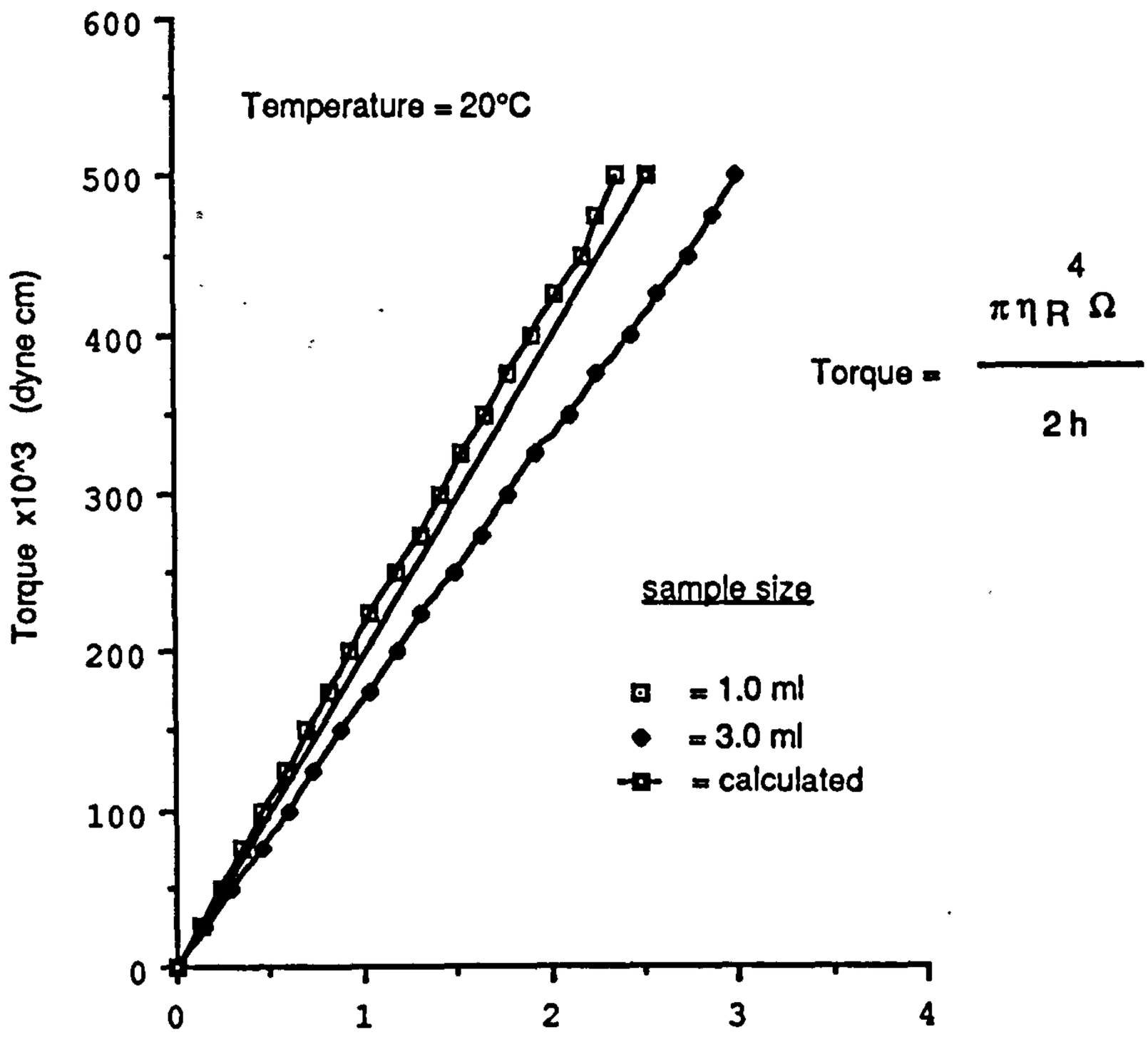

Fig. 4.3 Calibration Oil Flow Curve

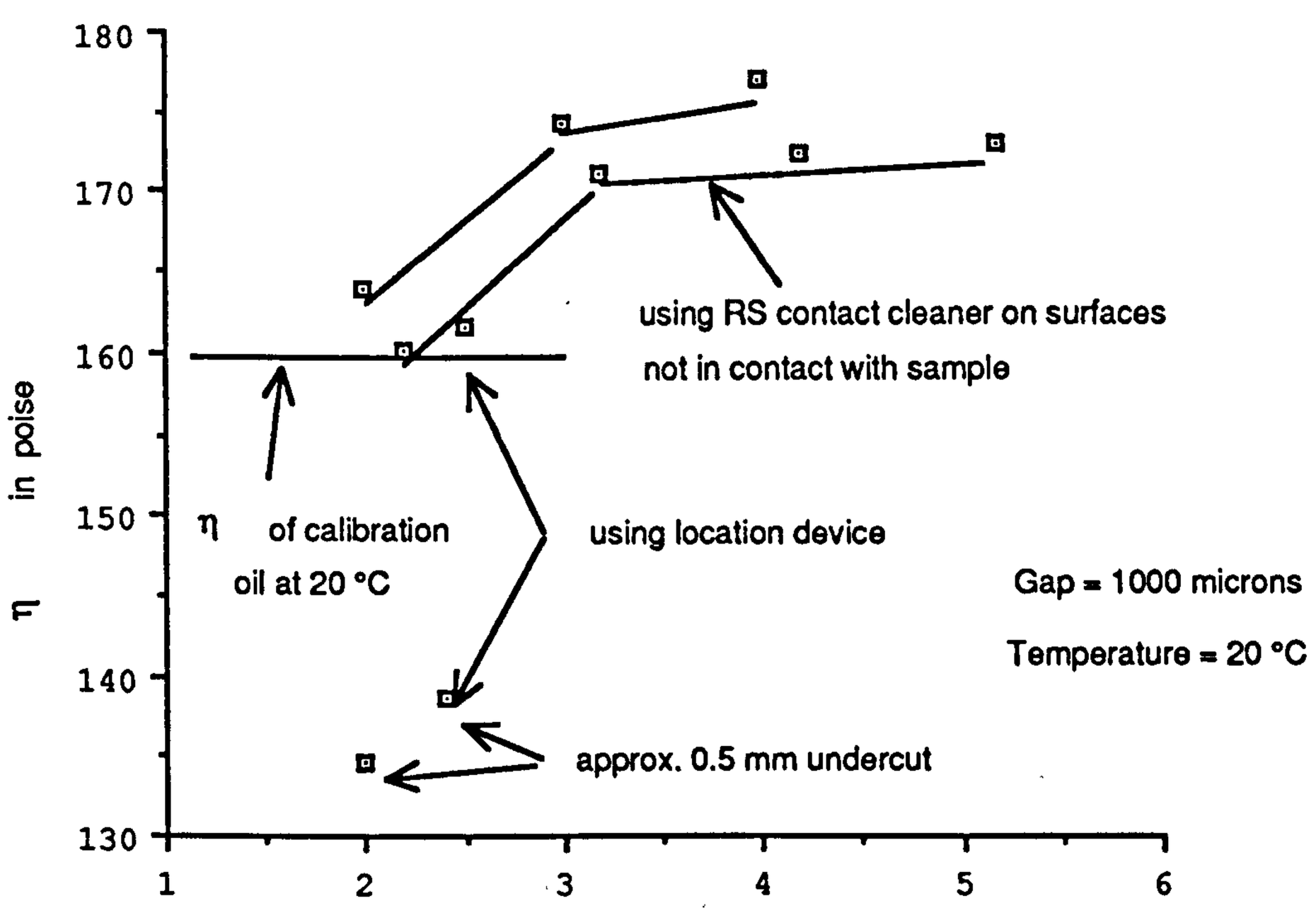

Fig. 4.4 Effect of Sample Size on Viscosity of Calibration Oil

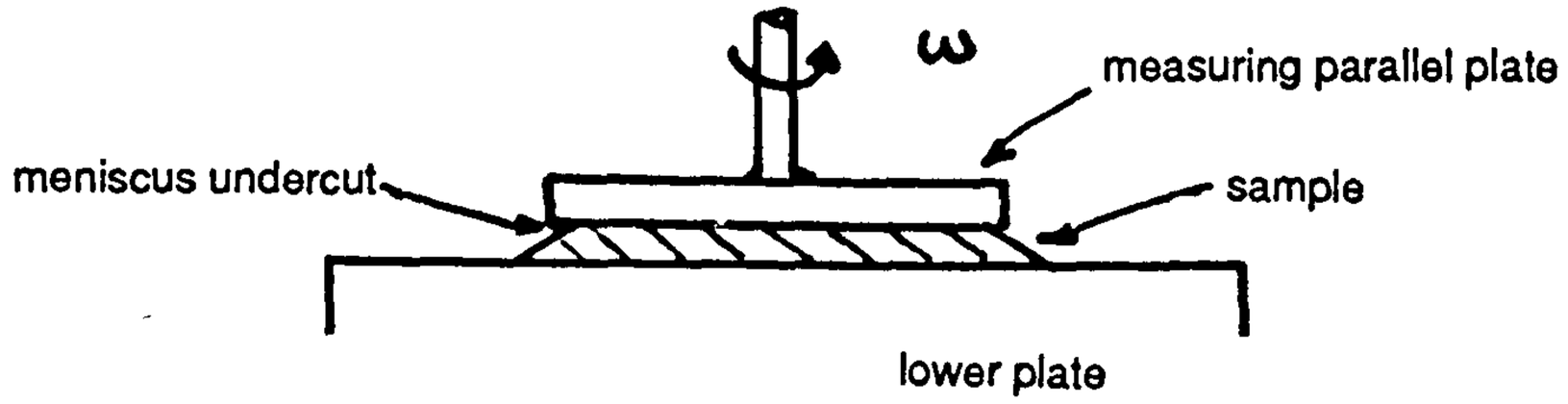

a) Sample Showing Undercut

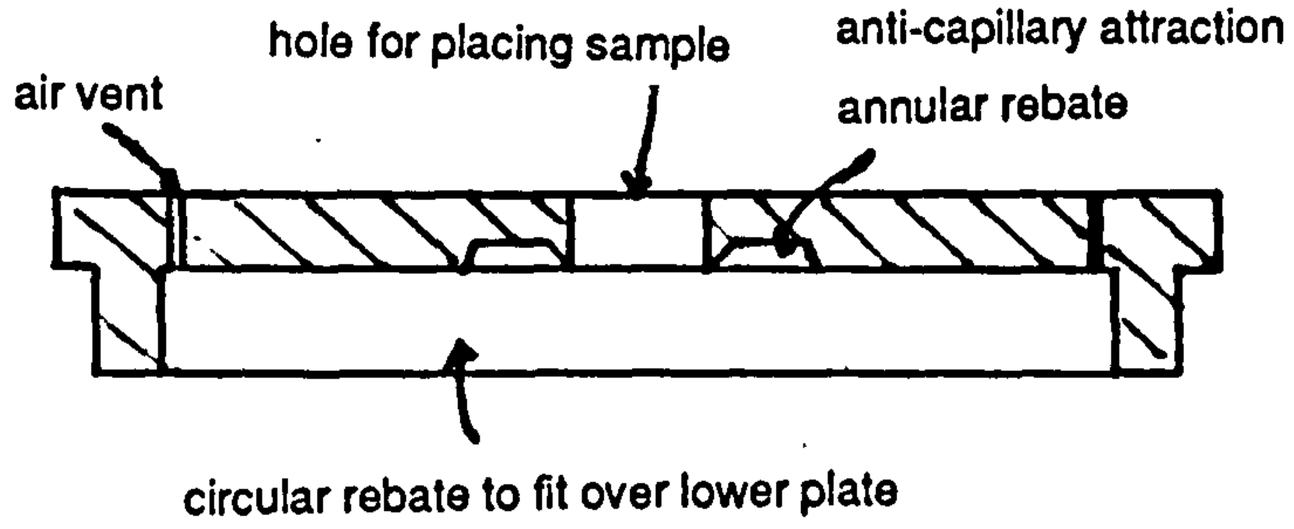

b) Cross-section of Perspex Template

Fig. 4.5 Parallel Plate sample undercut and location device

An electrical location device comprising a lamp to project the cross hairs of a microscope's eye piece onto the surface of the bottom plate was discarded because switching the lamp on and off was found to cause a bias cut out in the rheometer.

The cement slurry samples were transferred to the smooth bottom plate of the rheometer, which is fixed onto the ram of the rheometer. This transfer was by spooning from the beaker (approx. 2 1/2 spoonfuls for 2.5 c.c.). The sample could not be weighed and transferred using this sytem and careful sample selection from the beaker was required to obtain comparative results.

4.2.2 Vane in Cup

With this system the sample size could be accurately determined by weighing the sample after either pouring or spooning it into the cup. The spooning is more precise but also more time consuming than pouring. Location did not present any difficulty with the cup as this slotted into the water jacket which was firmly located on the ram.

The variation in measured sample weight to the calculated amount required was less than 0.5%, which was insignificant in affecting yield stress measurement. As was seen during calibration, a significant change in sample size effects the depth of immersion of the vane, its supporting shaft or the gap below the vane. All these factors affect the stress factor and consequently the measured yield stress. Correct determination of sample size is therefore most important when using the vane in cup.

4.2.3 Annular Plate and Cone

The weighing and location of the sample on the removable bottom annular plate

does not present a problem with this system. The sample volume, calculated at zero gap setting with smooth plates, was 8.91 c.c. This reduced to 7.49 c.c. when a plate was fixed in the centre hole enabling sample transfer. However, the volume under test between the annulus and the cone is just 3.46 c.c. This means that small changes in volume can affect the shape of the meniscus of the sample's outer boundary upon which the analysis of the system is based.

With rough surfaces an estimate was made to take account of the volume of the interstices or indentations, as the case may be. However accurately the volume of the sample was determined, difficulty was experienced in obtaining the same shape meniscus all round the A P C. This occurred because of the uneven spreading of the sample across the rough annulus when squeezing the sample to the correct gap.

Using the mixing procedure described in Chapter 6 for the A P C and a w/c = 0.44 class G cement slurry, it was found that no significant difference in flow curve could be attributed to sample size from 15.3 g to 15.9 g. Slight undercut of the meniscus at the edge of the plate and cone did not have any noticeable effect on the flow curve as it would have done with the parallel plate. Therefore, a sample size of 16.0 g was chosen as standard for this densely engraved A P C. Also, it was sufficiently in excess of the calculated amount to account for minor eccentricity on loading and not too excessive to cause overflow or excessive meniscus bulge, so that a spherical meniscus is a reasonable approximation. The flow curves for the above sample sizes are shown in Fig. 4.6. The flow curves in all the figures are only selected ones.

4.3 End and Edge Effects

The edge effects with the parallel plate are minimised, as previously mentioned, by

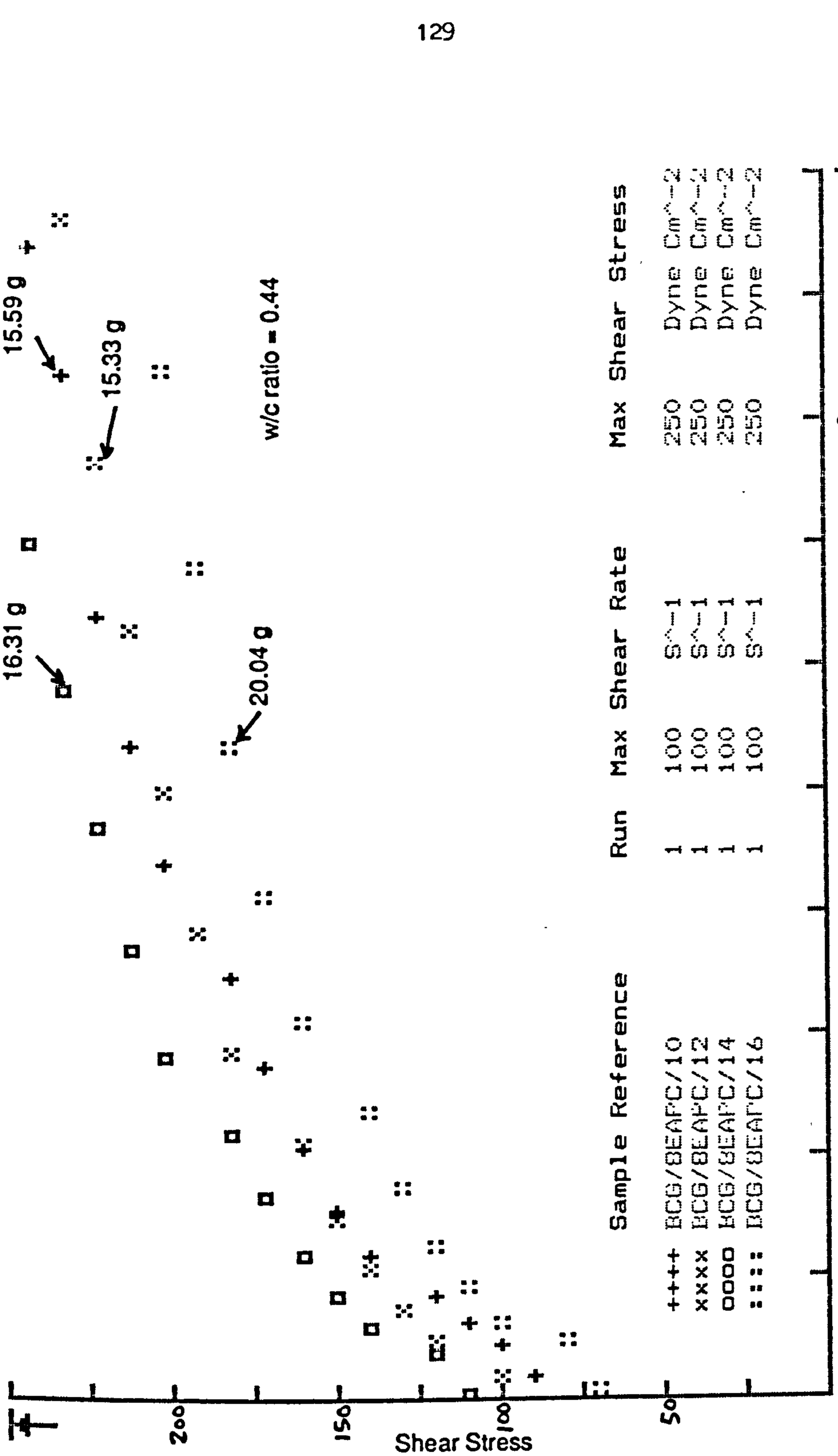

Fig. 4.6 Effect of Sample Size on Flow Curves with the Engraved AP&C

obtaining a spherical mensicus all round the plate and using the correct sample size. The end and edge effects are more obvious with the A P C and the vane in cup as can be seen from their geometry and analyses, to be described now.

4.3.1 Vane in Cup

To assess the end effect in this system the torque-stress relationship for a vane partly immersed in fluid was derived as shown in Chapter 3. Then assuming a uniform stress distribution p = 0 giving

$$\tau = \frac{2T}{\pi d^3(\frac{h}{d}+\frac{1}{6})} \qquad 4.1$$

with which d = 1.2 cm gives

$$\tau = \frac{0.442T}{(h+0.2)} \quad dyne/cm^2 \qquad 4.2$$

the shear stress factor, $F_{\tau m}$ was calculated and a series of flow curves carried out at various depths of immersion of the vane. Accurate determination of the depth of immersion using the rheometer's micrometer could not be done, since the depth below the vane had to be constant and the micrometer only had 2.88 mm of travel remaining once set up. The method employed was to add a volume of calibration oil to the oil already in the cup thereby increasing the depth of immersion, which was calculated by

weighing the oil in the cup and knowing the geometry and density of the oil. From the flow curves, some of which are shown in Fig. 4.7 the Carri Med software gave,

using a Bingham fit,the values of viscosity, η_m, and initial yield, shown in Table 4.1. The Bingham equation was used because it gave a better fit, the calculated yield value being merely a lag time, as shown shortly. Now the correct viscosity, η_T, should be 101 poise and the correct

$$F_{\tau T} = \frac{0.442}{(h+h_{end})} \text{ and since } \eta = \frac{T.F_{\tau}}{\dot{\gamma}}, \quad \frac{\eta_m}{F_{\tau m}} = \frac{\eta_T}{F_{\tau T}}.$$

where h_{end} = effective height to account for end effect

This gives on transposing

$$f(\eta) = \frac{0.442\,\eta_m}{\eta_T F_{\tau m}} = (h + h_{end}) \qquad 4.3$$

The graph of $f(\eta)$ against h, shown in Fig. 4.8, gives $h_{end} = 0.36$cm. This value indicates the end effect to be twice that which was derived earlier. For small vanes, such as can only be accommodated on the Carri-Med, the end effects, therefore, have a significant contribution to make to the stress factor, when examining flow curves with calibration oil. However it must be emphasised that this measuring system was proposed for measuring yield stress directly and so the end effect developed by high shear rates is irrelevant for our needs, plus any empirical end effect factor for oil would not necessarily apply to cement slurry. For direct yield stress of cement slurry the stress factor was based on the derived formula. It seemed logical to keep the shear

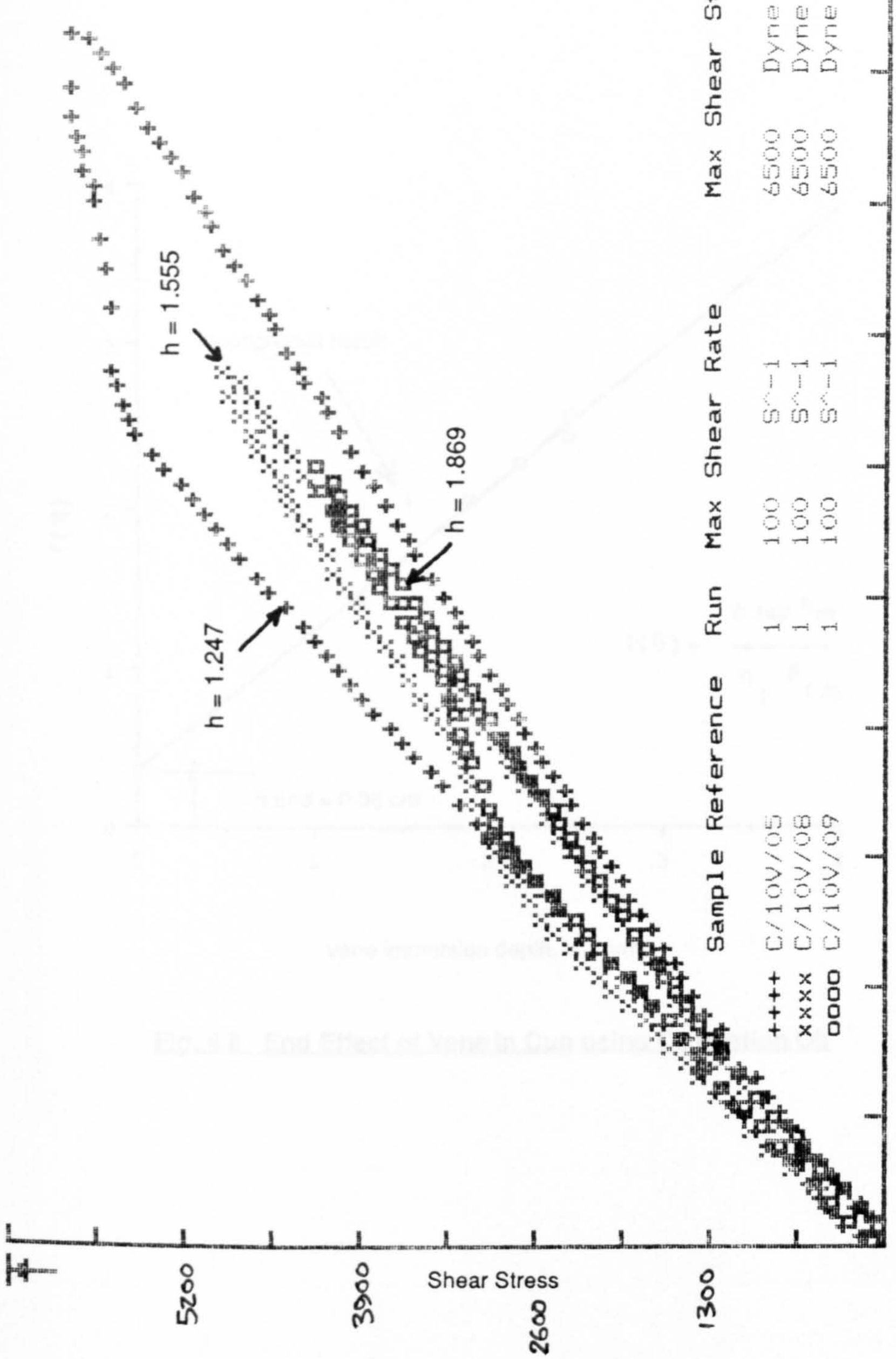

Fig. 4.7 Flow Curves on Calibration Oil using Vane in Cup at various Depths of Immersion, h cm.

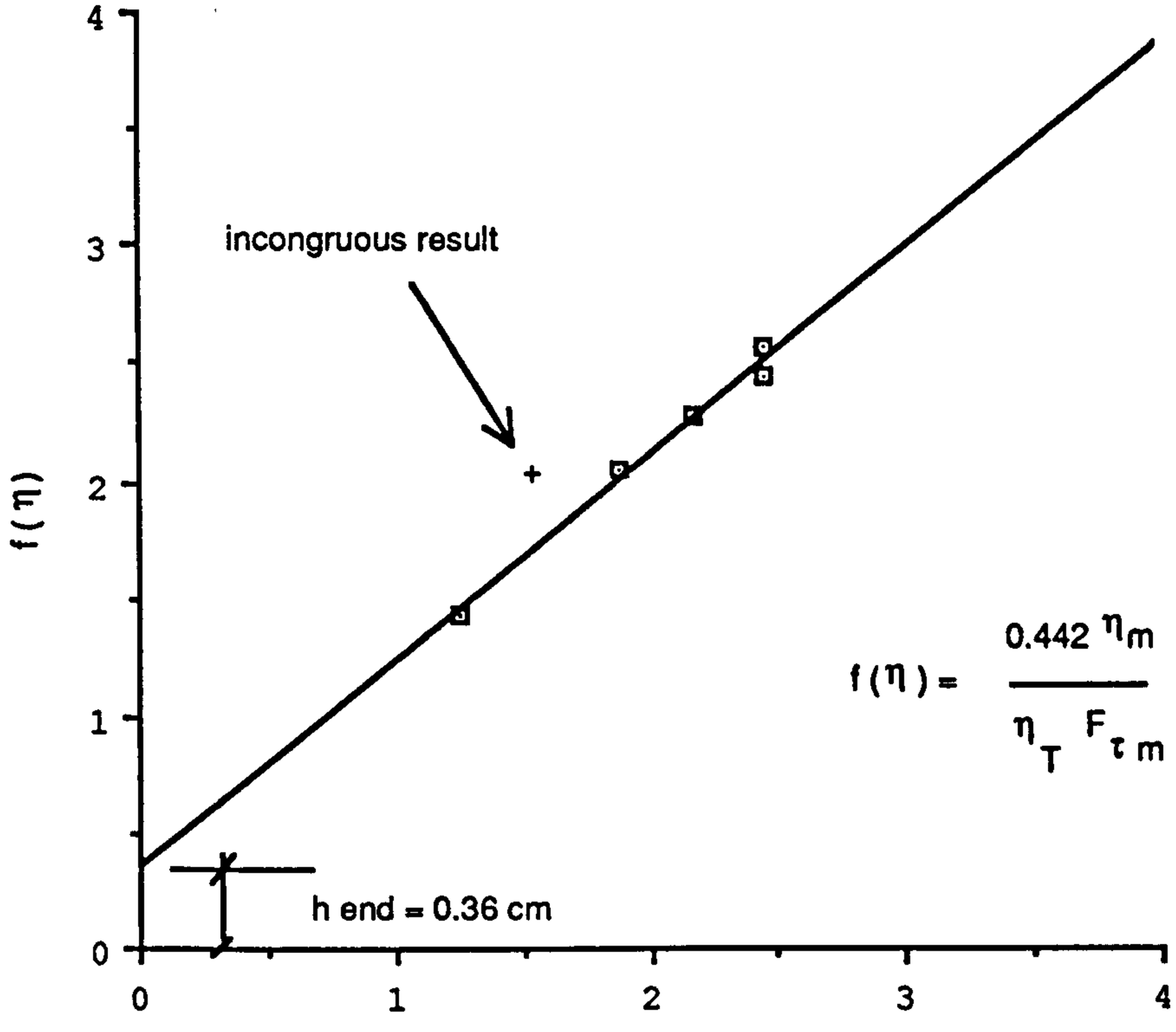

Fig. 4.8 End Effect of Vane in Cup using Calibration Oil

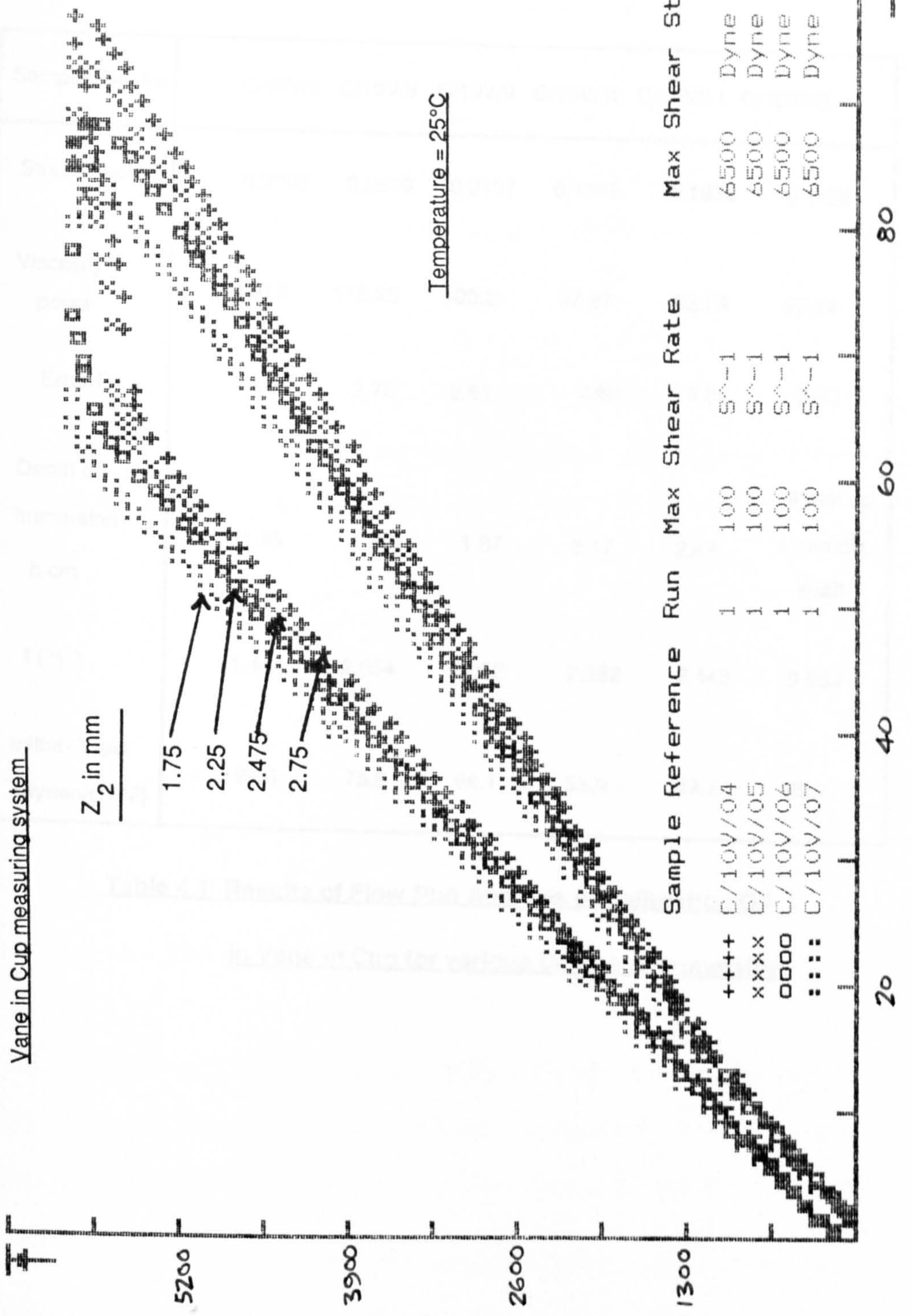

Fig. 4.9 Effect on Calibration Oil Flow Curve of Reducing Gap at bottom of Vane

Sample Ref. No	C/10V/5	C/10V/8	C/10V/9	C/10V/10	C/10V/11	C/10V/12
Stress Factor	0.3055	0.2519	0.2137	0.1865	0.1658	0.1658
Viscosity poise	100.8	118.25	100.2	97.27	92.74	97.14
Error Fit	3.07	2.75	2.81	2.82	2.82	2.70
Depth of Immersion h cm	1.25	1.56	1.87	2.17	2.47	4 mm up 9 mm dia. shaft
f (η)	1.444	2.054	2.052	2.282	2.448	2.563
Initial Yield (dynes/cm^2)	91.6	75.5	64.1	55.9	49.7	49.7

Table 4.1 Results of Flow Run Analysis of Calibration Oil in Vane in Cup for various Depths of Immersion

stress, and hence the shear rate, at the rim of an analogous parallel plate, which existed between the vane and the bottom of the cup, the same as that on the cylindrical yield surface. If this gap between the vane and the bottom of the cup was varied slightly, the effect with calibration oil is as shown in Fig. 4.9. When the gap below the vane is reduced the measured viscosity increases, which is to be expected, but as can be seen it is with marked effect. Unfortunately the geometrical boundary condition suggested by Nguyen (1983) and described in section 3.2.2. could not be achieved with the Carri-Med.

The calibration oil does not have an initial yield, hence this value must be the result of a combination of instrument lag and material inertia. The ascent time was 1 minute so the stress increments were

$$\frac{T_{peak} \times F_{\tau}}{200} \quad \text{in} \quad \frac{60}{200} \quad \text{sec.}$$

or since $T_{peak} = 20000$ dyne cm. the combination represents an overall lag time of 0.9 sec. in each case.

4.3.2 Annular Plate and Cone

Difficulty was experienced in measuring the calibration oil viscosity using this system. Values of 118 to 122 poise at 25°C were being obtained, with both sand coated and smooth surfaces, instead of 101 poise. It was felt that the cause could be

the viscous drag of the inner core of the sample on the inner gap, of 1050 μm, between the cone and the annulus. The drag results from the different shear rates in the radial plane. In the plane of rotation at the inner edge of the annulus, particles are

subject not only to the different vertical shear rates but also to the effects of the close proximity of the moving surface above the inner core. The overall effect would be to increase the torque and thereby the viscosity.

An attempt to place a sample only on the annulus was unsuccessful because of positioning difficulty which resulted in meniscus collapse on ram up. A more successful technique was placing water in the centre core with the calibration oil floated on top, which gave a measured viscosity of 106.5 poise. This confirmed that inner edge effects were significant when measuring calibration oil viscosity using the APC and would require fuller investigation of its significance when measuring cement slurry. A series of test runs to determine the yield stress of a SSMP mixed w/c = 0.44 cement slurry were carried out for each type of surface treatment. This was to ensure there were no significant edge effects in yield stress measurement even when the shear rate was almost zero. To do this each run had a different sample size so that R_1 became a variable in the relationship

$$T_y = \frac{2\pi}{3} (R_1^3 - R_2^3) \tau_y + T_{ey} \qquad 4.4$$

where T_y is the applied torque at the yield point and T_{ey} is that torque required to overcome edge effects. From the plots in Fig. 4.10 it can be seen that as expected the inner edge effect, represented by the intercept, can generally be ignored when compared to the torque which produces yield in the sample when the A P C is fully loaded (i.e. $R_1 = 3.0$ cm). The coarse engraved surface did show a significant intercept in comparison with the fully loaded torque yield but in view of the few data points, the results of the other surface, the fragile stability of cement slurry yield and

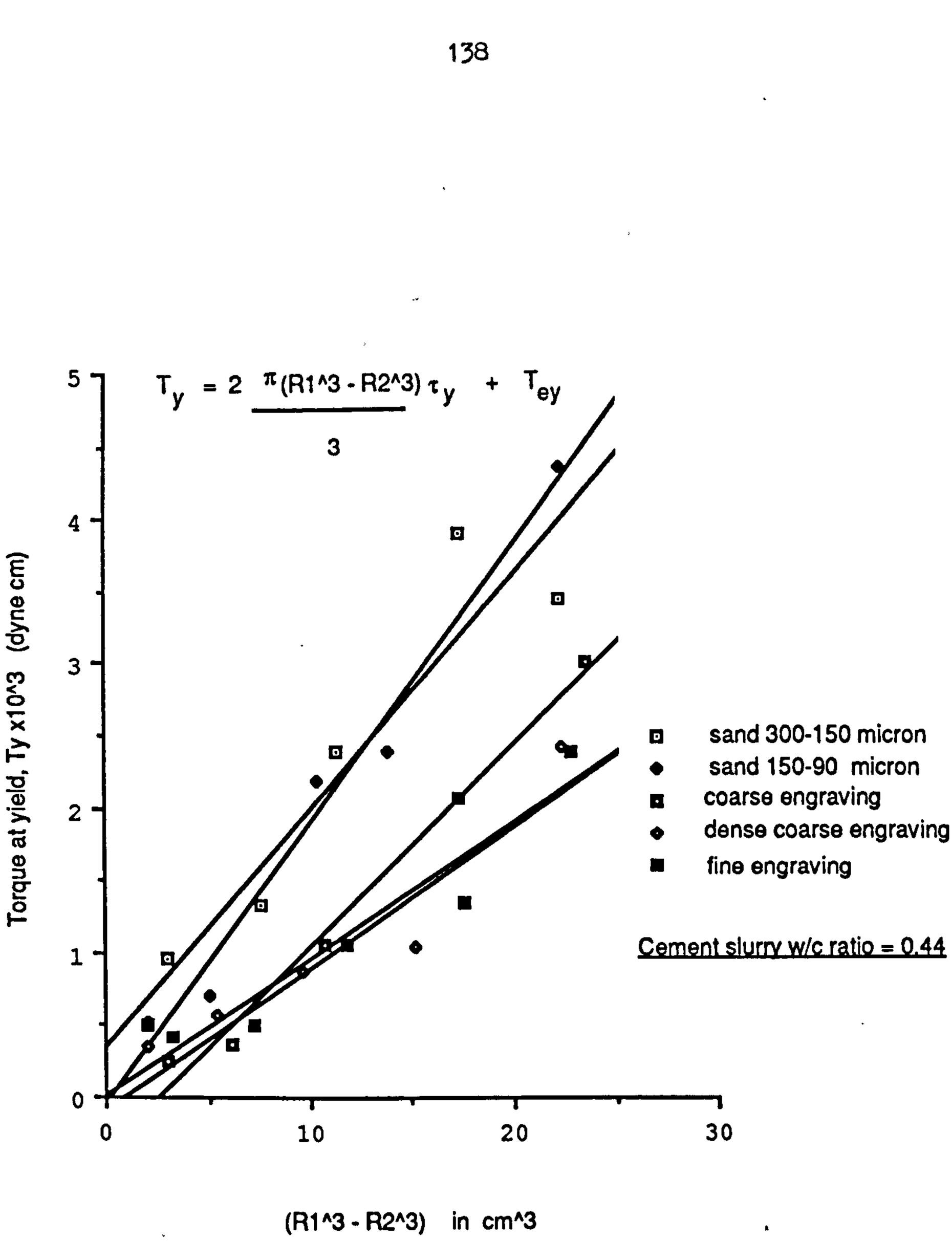

Fig.4.10 Edge Effects with the AP&C using various surface treatment

TABLE 4.2

Measurements from tests on various Surface Treatments to the APC

Sample wt(g)		R_1(cm)		$(R_1^3 - R_2^3)$	T_y	$d\tau/dt$
calc.	actual	imprint	optical	imprint R_1	dyne cm.	dyne/cm^2/min
<u>sand coated 300-150µm</u>						
8.36	8.48	1.75	1.6	1.98	515	1221
9.31	9.50	1.95	1.85	2.96	978	1199
10.58	10.79	2.225	2.13	7.64	1335	829
12.22	12.19	2.45	2.4	11.33	2396	875
14.26	14.25	2.75	2.73	17.42	3923	825
<u>sand coated 150-90µm cone / 90-75µm annular plate</u>						
8.54	8.63	1.75	1.7	1.98	515	1250
9.59	9.57	2.025	1.95	4.99	714	723
10.97	11.13	2.4	2.5	10.45	2203	612
12.73	12.35	2.575	2.5	13.80	2396	722
14.90	14.80	2.95	2.87	22.30	4376	647
<u>fine engraved</u>						
8.36	8.31	1.875	1.74	3.217	412	779
9.31	9.51	2.2	2.15	7.27	489	500
10.58	10.55	2.475	2.44	11.79	1068	545
12.22	12.26	2.75	2.73	17.42	1354	574
14.26	14.22	2.975	2.98	22.96	2414	630
<u>coarse engraved</u>						
8.40	8.52	1.86	1.87	3.06	258	858
9.42	9.58	2.125	2.12	6.22	376	604
10.78	10.74	2.415	2.43	10.71	1068	611
12.52	12.48	2.75	2.71	17.42	2084	581
14.70	14.67	3.0	2.96	23.63	3018	617
<u>dense coarse engraved</u>						
8.38	8.39	1.75	1.72	1.98	335	1239
9.38	9.47	2.065	2.015	5.43	579	636
10.69	10.67	2.35	2.28	9.60	868	663
12.37	12.67	2.65	2.65	15.23	1042	653
14.46	14.80	2.955	2.94	22.43	2414	642

TABLE 4.3

Linear Regression for various Surface Treatments to the APC

From Graphs in Fig. 4.10

T_{ey} intercept dyne cm	slope	τ_y dyne/cm^2	Linear correlation coefficient of data to equation 4.1
sand coated 300-150µm			
86.6	210.8	100.7	0.984
sand coated 150-90µm/90-75µm			
-34.5	193.9	92.6	0.990
fine engraved			
-97.2	99.3	47.4	0.964
coarse engraved			
-348.8	140.0	66.9	0.994
dense coarse engraved			
12.3	94.7	45.2	0.947

the difficulties of this particular experiment, the general conclusion that it is negligible is valid. Especially when future work in this thesis with the A P C would involve the now permanently dense coarse engraved system.

4.4 Surface Treatment of Measuring Systems

Whilst assessing edge effects of various types of surface treatment, with the series of test runs mentioned in the previous section, the ability of each surface treatment to measure the yield stress of a cement slurry, when applying the theory in the form of equation 4.4, is demonstrated by the straight lines with negligible intercept shown in the graphs of Fig. 4.10 and by the analysis figures given in Table 4.3. One of the difficulties in assessing yield from these test runs is the measurement of R_1 since any error is trebled when evaluating R_1^3. For this reason a travelling microscope was used to provide the optical readings of R_1 shown in Table 4.2. On dismantling the cone after a run a concentric slurry disc was imprinted on the cone's measuring surface. The imprint was measured to the nearest 0.5 mm in two directions, and the measurement is also shown in Table 4.2. The difference in radius between these two measurements is caused by the change in the meniscus shape of the sample, as shown in Fig. 4.11, as the radius of the sample increases On shearing the sample the meniscus shape did bulge slightly though not overmuch and, although the concave shape can be obtained by pulling the plates apart or by sample shrinkage, it was thought that these profiles were due to the shape of the sample prior to squeezing and the way surface tension negotiates edges and arrises on squeezing.The value of imprint R_1 was used in the calculation.

To obtain similar rates of applied stress the peak torque used in each run was

calculated ignoring the edge effect from equation 4.4 and putting $\tau_y = 610$ dyne/cm^2 which, when ascended to in 1 minute, was the rate used with earlier parallel plate runs and would be useful for comparison. The variation in the rates of applied stress shown in Table 4.2 are brought about by the error in weighing small samples, although the values at $R_1 = 1.8$ cm were the result of miscalculation of the peak torque. Precise calculation of the volume of the required sample was made for both sand and engraved surfaces. For the sand surface interstices the additional volume calculated for the cone was

$$\frac{2}{3}\,\pi\, r_c\, R_1^2 \quad \text{and} \quad \frac{2}{3}\,\pi\, r_a\,(R_1^2 - R_2^2)$$

for the annulus, where r_c and r_a is the average sand particle radius, on the cone and the annulus, respectively. For the engraved indentation the additional volume, assuming the same volume on both the cone and the annulus, is

$$\frac{4}{9}\,\pi\, r_i\,(R_1^2 - R_2^2).$$

This assumes the indentations to be hemi-spheres which by optical observation occupied 1/3 of the surface with fine and coarse engraving and 1/2 the surface with dense coarse engraving. The indentations averaged over 7 microscopic readings were 40μm deep for fine engraving, 70μm deep for coarse and 140μm deep for dense coarse engraving. The sand coated surface began to wear thin after 20 or so runs and, although the high gloss varnish spray could be removed and replaced, a more permanent surface treatment was sought. Sand blasting and laser welding were

rejected in favour of engraving because sand blasting had depth of erosion control difficulties and balling, an accumulation of molten metal, produces an uneven surface with the laser welding. All the engraving was carried out with a hand held jeweller's engraver with the plates fully supported and working in a radial direction around the annulus. A 15 mm wide annulus was marked on the cone and engraved as shown in Fig. 4.12.

Another problem with setting up in the rheometer either a sand coated or engraved cone and plate is the zero gap position. With sand asperities the tendency would be to get a negative vertical displacement error and with the engraved surface a positive displacement error, which can be seen from Fig. 4.13. This suggests that sand coatings would overestimate the yield value by reducing the gap and engraved surfaces underestimate it which is shown to be consistent with the results given in Table 4.3.

However, the indentation depth is 70μm and assuming the correct zero gap position to be 1/3 rd. of this the vertical error would be about 50μm. For a Newtonian fluid this produces an error in T/τ of, approximately - 3%. Now with sand coating of size 120μm on the cone and 80μm on the annulus and assuming a correct zero position at 2/3 the height of the asperi ties, say 150μm, the error in T/τ is about + 10%. So that the error caused by zero gap setting cannot solely account for the difference in yield measurements from the various surface treatments shown in Table 4.3. To confirm this, the yield value was measured for a w/c = 0.44 cement slurry over a range of gap setting errors from - 150μm to + 150μm in 50μm steps. The size of the sample was calculated to accurately account for these volume changes but unlike the runs in

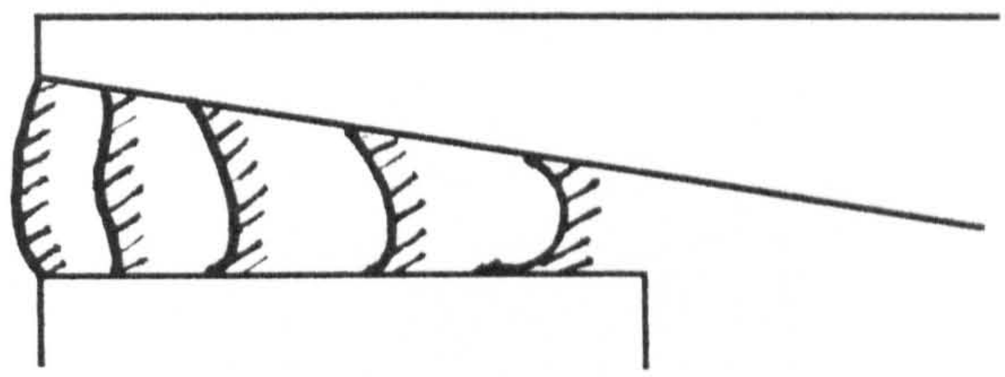

Fig. 4.11 Changing Shape of Meniscus as Sample Radius Increases across AP&C

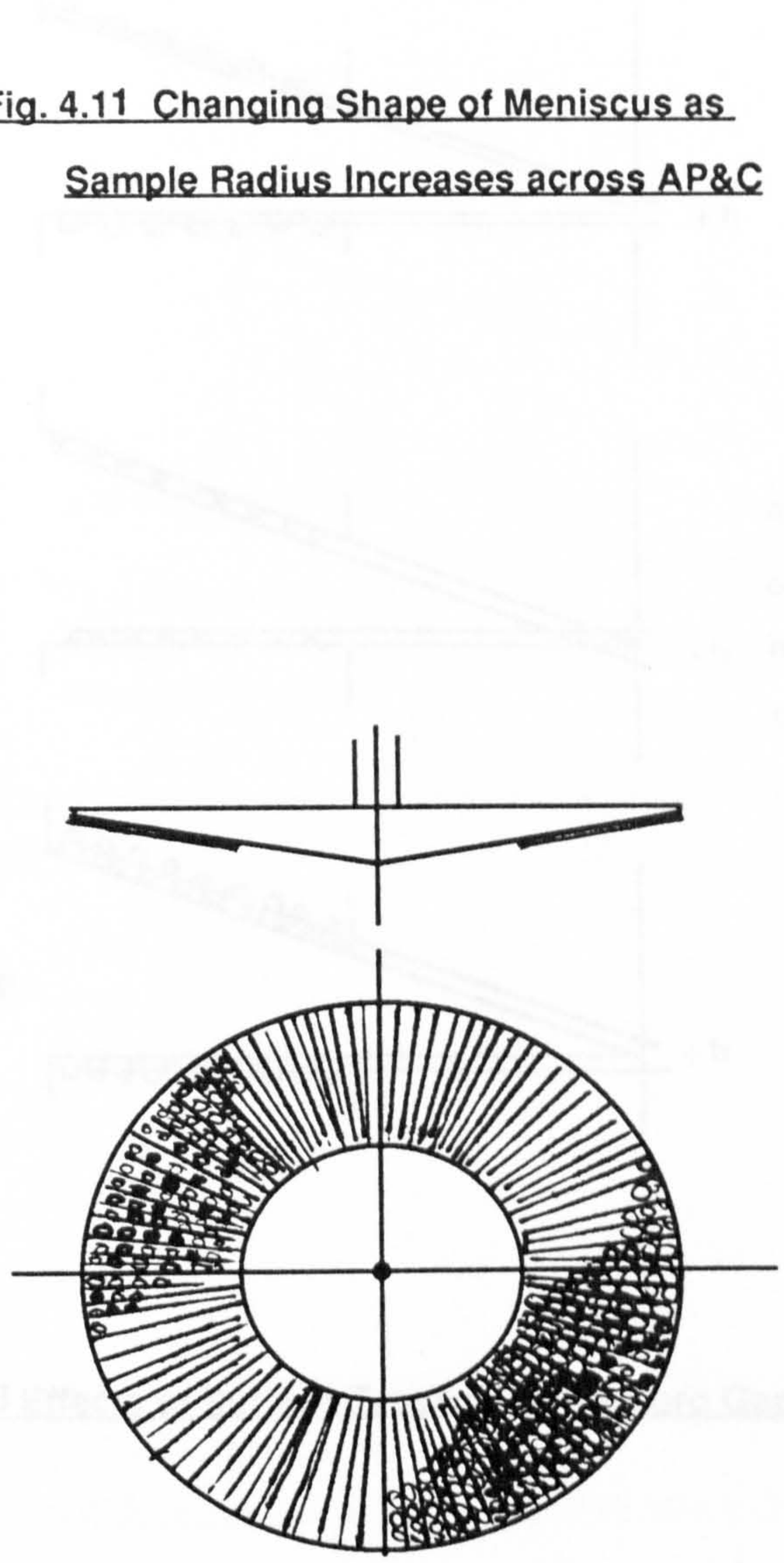

Fig. 4.12 Engraving Pattern of Stainless Steel Cone

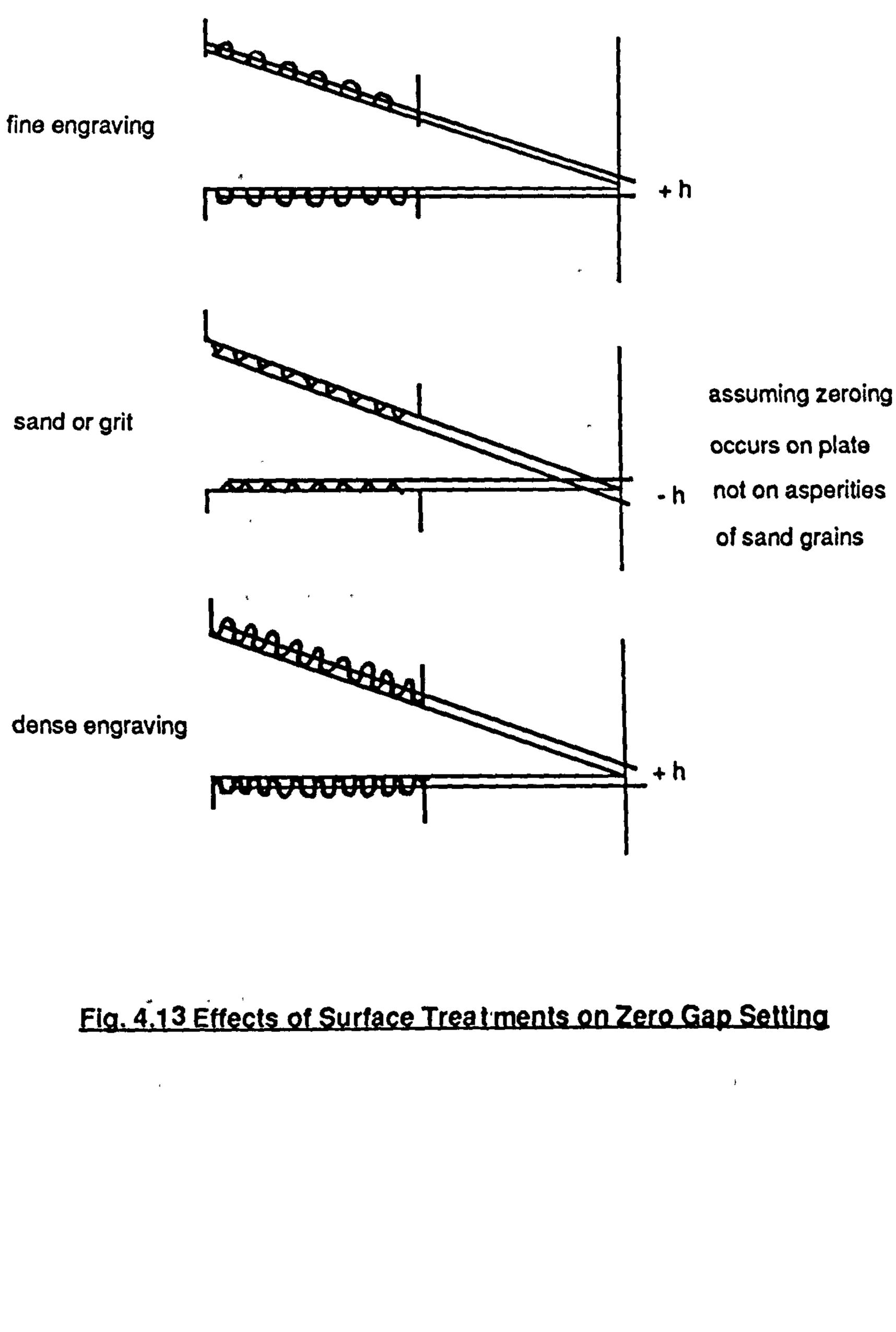

Fig. 4.13 Effects of Surface Treatments on Zero Gap Setting

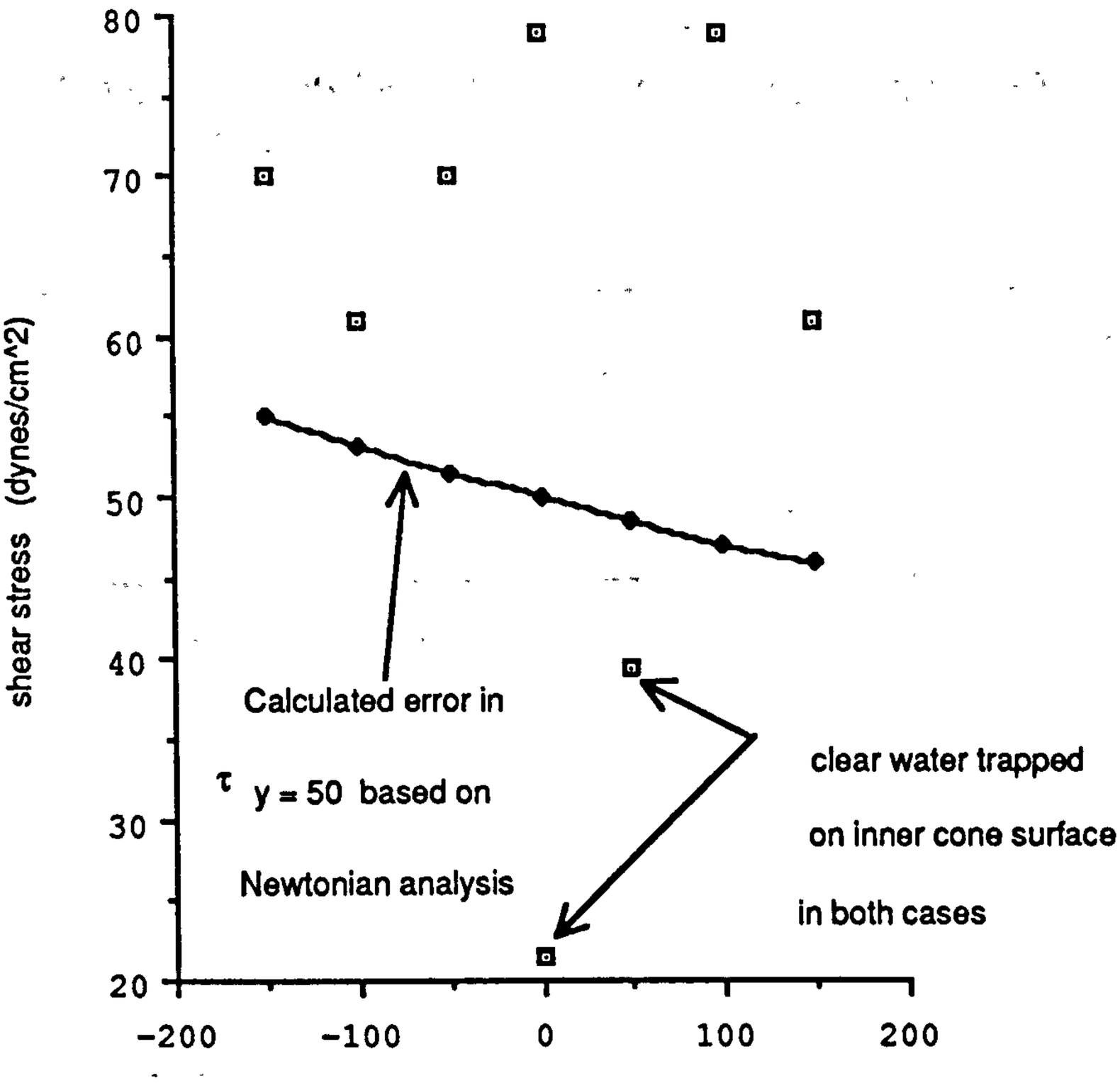

Fig. 4.14 Effect of Vertical Gap Setting Error on Measured Cement Slurry Yield Stress using AP&C

TABLE 4.4.

Variation in Sample Weights for Different Gap Setting Errors when Measuring the Yield Stress of Cement Slurry Using the APC

Gap error (μm)	-150	-100	-50	0	+50	+100	+150
Sample weight							
Calc. wt. (g)	14.96	15.23	15.50	15.77	16.04	16.31	16.58
actual wt. (g)	15.07	15.57	15.91	15.92	16.45	16.41	16.72

Table 4.2 where 80% of sample weights were within 0.2g the actual sample weights were less accurate, as shown in Table 4.4.

The stress factor, F_τ, could not be calculated directly for vertical displacement errors when measuring cement slurry (see Chapter 3). Hence, the stress factor used to compute stresses at various gap settings is the zero gap error stress factor. The results seen in Fig. 4.14 show how difficult it is to find a trend in yield value measurements of cement slurry when such small ajustments are made to a small sample and only a few runs are made. The two low values of yield stress in Fig. 4.14 occurred with samples, which on dismantling the cone, were found to have a very thin layer of clear water on the smooth cone surface inside the engraved annulus. Cement slurry covered the whole of the cone surface on dismantling with the other runs in this series. The reason for this water separation in some cases and not others is not clear.

4.5 Conclusion

Blender or propeller in a beaker type of mixing gives questionable homogeneity of sample shear history for studying the effects of mixing energy input to cement slurry systems. The size of sample can have significant effect on the precise measurement of yield stress of small cement slurry samples tested on the rheometer using the parallel plate and the annular plate and cone. The variation in sample size should therefore be taken into account in the mixing energy studies.

End and edge effects occur with all the measuring systems and are magnified when testing a high viscosity calibration oil. The end effects of the vane in cup were found to give significant contribution to the measurement of yield stress of the cement slurry,

probably due to the large aspect ratio of the vane, which can only be accommodated on the Carri-Med rheometer. End and edge effects are not so significant with the annular plate and cone when measuring cement slurry, although care is required with sample size and gap setting.

The different surface treatments did show variation in the yield stress measurement of cement slurry but this was for low unstable yield stress of an SSMP mixed cement slurry tested at 3 minutes since adding water. The reason for using these surface treatments was primarily to overcome slippage and discussion of this aspect and the results of yield stress measurement of a cement slurry at different rates of applied stress, using these systems, follows in Chapter 5.

CHAPTER 5

Yield Stress Results using Different Measuring Systems

This chapter presents and examines the results of flow run tests performed on the controlled stress rheometer to measure the yield stress of a cement slurry using the three measuring systems, detailed in previous chapters. The yield stress results, using the measuring systems with various surface treatment ,where applicable, are also discussed here, as are the effects of slippage and rate of applied stress. Another phenomenon highlighted by the results is the effect of the removal of the bleedwater from the sample prior to testing, which is briefly discussed.

5.1 Slippage

When measuring the flow properties of concentrated suspensions it is known that slippage occurs at large smooth boundary surfaces, such as the walls of a tube viscometer. The vane in cup is not subject to slippage since it measures the yield stress on a shear plane within the sample. Slippage is a result of shearing across a thin film of the suspending medium, which lies in close contact with the smooth boundary surface of the measuring system. This film must be of lower concentration than the main body of the suspension by virtue of the boundary surface. With concentric cylinders Dimond (1975) and Banfill (1981) used serrated surfaces to overcome slippage. The effect of slippage is magnified when reducing the gap between the cylinders. Using a concentric cylinder with constant shear rate apparatus, Mannheimer (1983) found that neglecting slip velocity leads to serious underestimates of apparent viscosity when testing oil well cement slurry in the vicinity of its yield stress. Although slippage occurred at stresses below the yield value, Mannheimer found it was undetectable at shear rates above 50 sec^{-1}.

5.1.1 Parallel Plates

To investigate slip using parallel plates grit paper was stuck, using a contact adhesive, to the measuring surfaces. This adhesive was found not to yield on applying the maximum torque possible with the Carr-Med over longer durations than the proposed flow runs. With a gap of 1.0 mm and using a SSMP on a w/c = 0.485 cement slurry, a peak torque of 10,000 dyne cm. was insufficient to yield the sample in an ascent time of 1 minute. When the peak torque was doubled to 20,000 dyne cm flow curves were obtained for grit surface plates enabling comparison to be made with smooth stainless steel plates. The flow curves obtained can be seen in Fig. 5.1 and

Fig. 5.2. The analysis of these curves using the Bingham model is given in Table 5.1. If the curves of Fig. 5.1 are considered as two straight lines the junction occurs at around 50 sec^{-1} with the smooth plates, thereby supporting Mannheimer's findings. The plastic viscosity of the cement slurry as a result of the slip film on the smooth plates would appear to be much greater than the initial plastic viscosity of the slurry, measured using the grit surface plates, as shown in Table 5.1. This is because of the relative thickness of the slip film to the gap between the plates. The upper straight line plastic viscosity in both cases reflects that the cement slurry, under each test, is similar. Slippage is shown to have a dramatic effect on the yield values, calculated from flow tests using a Bingham model, which are shown in Table 5.1 Using the X-axis expansion facility with the Carri-Med software, as done in Fig. 5.3 and Fig. 5.4 on these flow curves, shows the difficulty in linear analysis of the flow curve. The software requires a minimum of 10 points to calculate a Bingham model. Consequently, in many cases the straight line below a shear rate of about 50 sec^{-1} will not be analysed correctly. Also, if two straight lines exist then the slippage may not be overcome. A re-arrangement of particles undergoing shear could account for the changes in the slope of the flow curve, which are shown more clearly in Fig. 5.3.

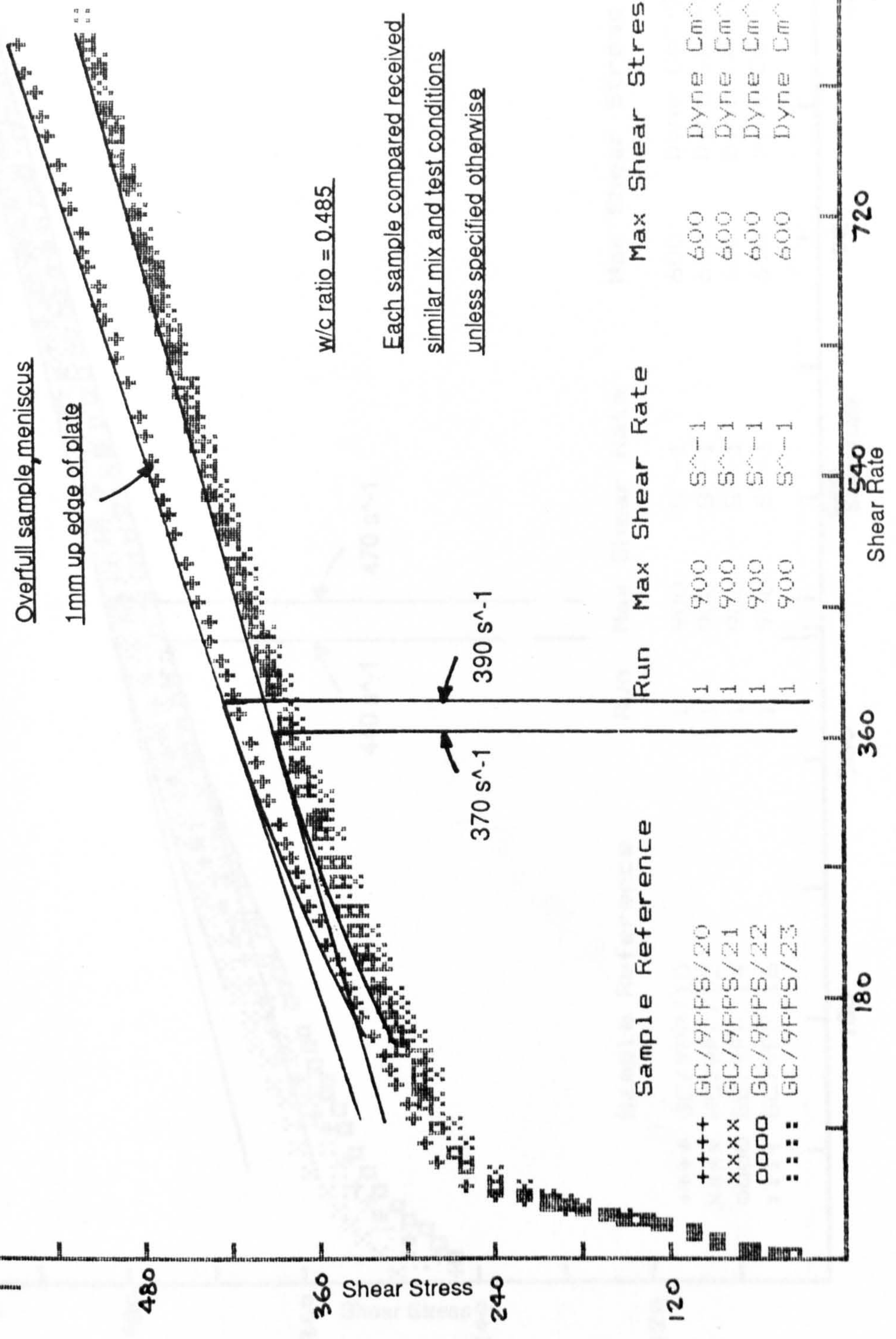

Fig. 5.1 Flow Curve - Class G Cement using Smooth s.s. Parallel Plates

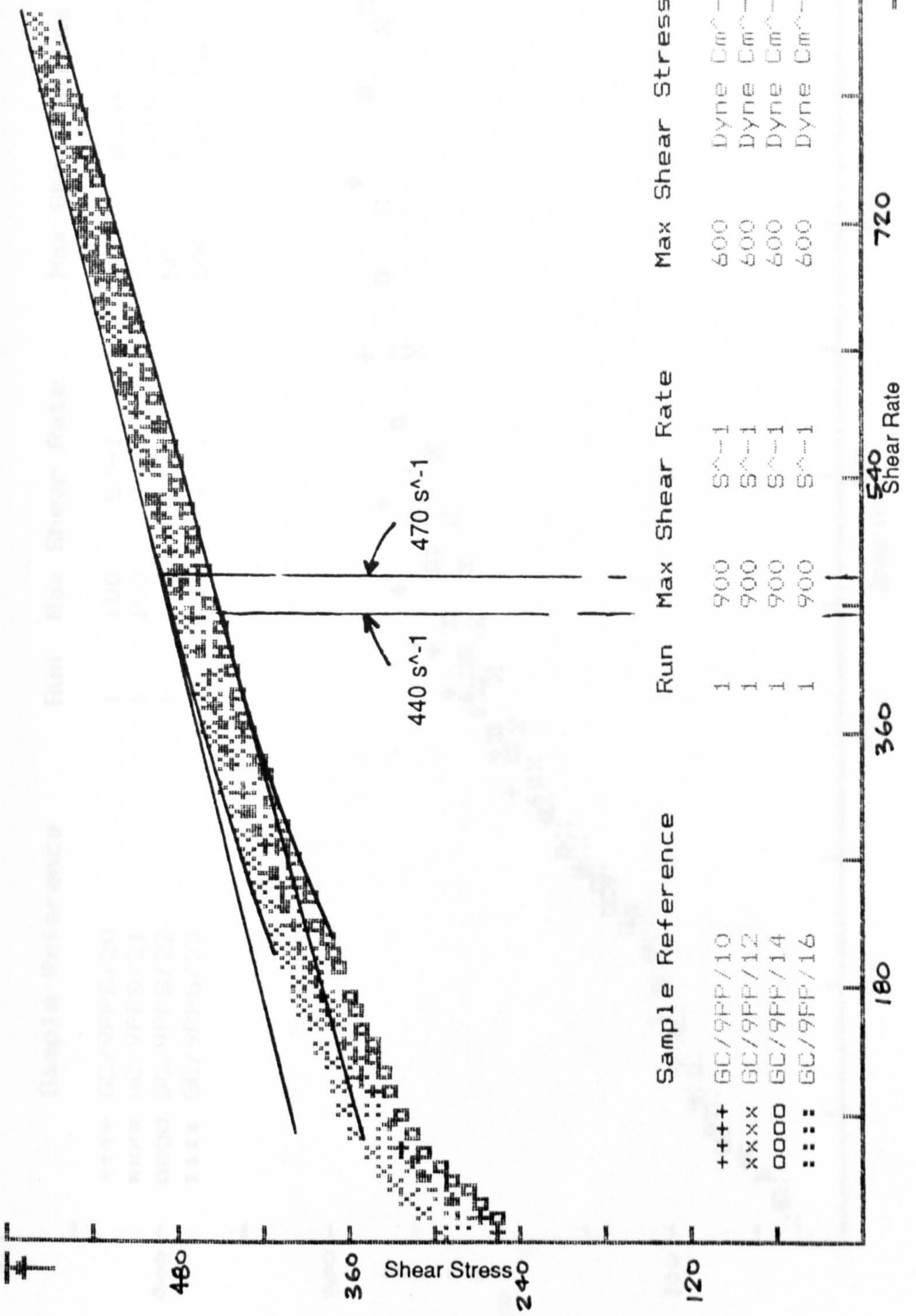

Fig. 5.2 Flow Curve - Class G Cement using Grit Surfaced Parallel Plates

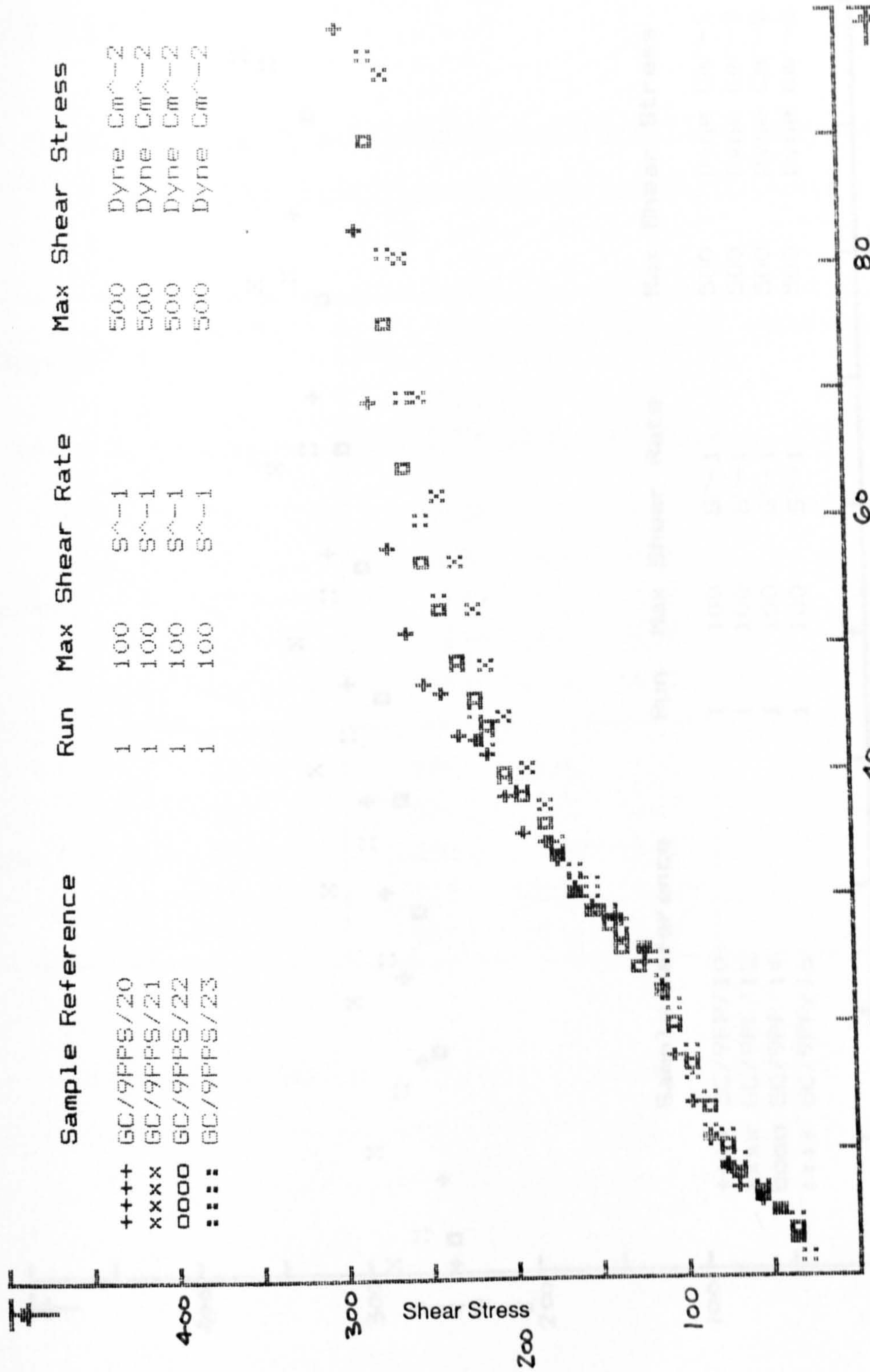

Fig. 5.3 Expansion of Cement Paste Flow Curve using Smooth s.s. Parallel Plates (see Fig. 5.1)

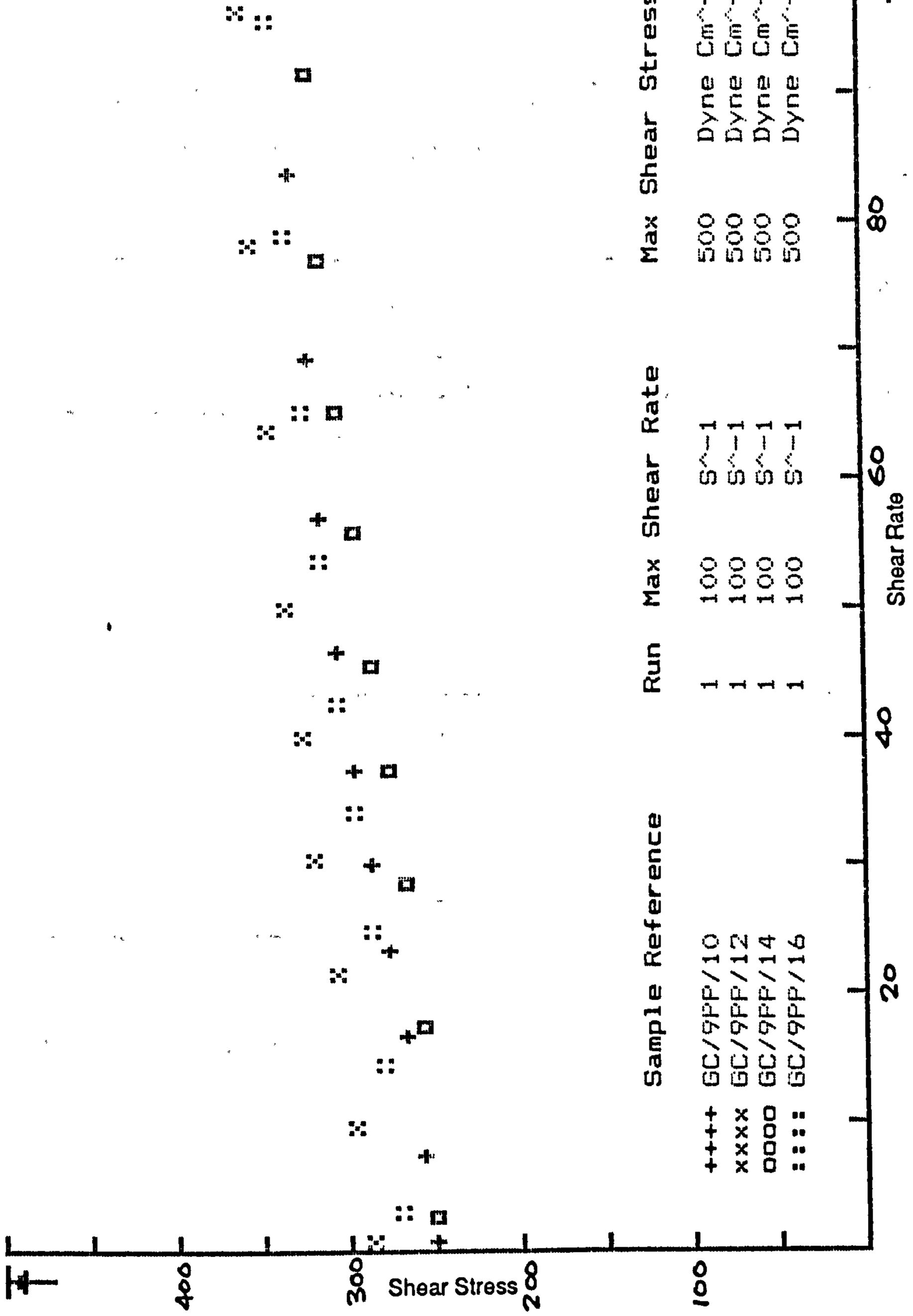

Fig. 5.4 Expansion of Cement Paste Flow Curve using Grit Coated Parallel Plates (see Fig. 5.2)

TABLE 5.1

Comparison of Rough and Smooth Surfaced Parallel Plates Measuring Cement Slurry Yield Properties Class G cement w/c = 0.485

Surface Treatment	Run No.	Lower straight line			Upper straight line
		τ_y (dynes/cm^2)	error of fit* (s^{-1})	μ_p (poise)	μ_p (poise)
smooth	21	35.29	13.13	3.79	0.318
	22	28.24	9.02	4.25	0.299
	23	22.10	12.37	4.37	0.300
	24	18.70	13.98	4.87	0.297
	25	20.54	13.01	4.51	0.310
grit	10	240.4	22.03	1.39	0.291
	13	279.2	27.79	0.82	0.276
	14	250.7	9.50	0.77	0.296
	15	217.1	26.22	1.47	0.295
	16	257.1	18.76	1.11	0.282

(* See page 76)

5.1.2 Annular Plate and Cone

To overcome slippage the measuring surfaces of the APC were initially coated with sand which was applied by spraying the surface with a thin coat of varnish then pressing the plate, or cone, into a dish of sand. The sand was sieved and various single size applications were tested, which are listed in the results of Table 4.2 in the previous chapter.

As a result of earlier cement slurry test runs, the bottom plate of the A P C had a brass plate fixed to the central hole to enable transferring the sample after weighing and the plate was clamped to the rheometer's cover plate on the ram, using 3 small brass G-clamps. The torque was limited to 100000 dyne cm as a result of the extent to which the measuring systems could produce straight line Newtonian flow curves when measuring calibration oil. There was no significant increase in angular velocity when the equilibration time was increased from 30 seconds to 1 minute whilst measuring calibration oil viscosity at low values of around 1.0 radian/second. With cement slurry the equilibration time needed to be as low as practically possible, hence 30 seconds was retained.

It was known that w/c ratio, time of hydration, amount of mixing energy and type of cement all influence the yield stress, so for comparative purposes these factors were held constant. Initially, the rate of applied stress was not held constant. The peak torque was chosen to adequately exceed the yield for a particular measuring system then simply programming a 1 minute ascent time. This was subsequently corrected and test runs were performed at similar rates of applied stress. The results of test runs on a w/c = 0.485 cement slurry mixed to SSMP and tested 6 minutes after adding water at a plate temperature of 25°C are shown in Table 5.2 .

The early test runs on the APC were carried out at rates of applied stress other than 610 dyne/cm^2/minute and as can be seen from Table 5.2 the yield values obtained were much less than the 610 dyne/cm^2/min rates. This difference, regardless of the type of surface, is most likely due to the slow manual gap setting procedure. This uses the micrometer manually, as opposed to ramming up pneumatically, to set the required gap. It was also found that small deformation differences prior to testing can be detected in the yield value, as shown in Fig. 5.5, where spoon loading as opposed to pouring the mixed sample into the testing cup, accounts for the stress difference.

In order to discover if slip was overcome by the sand or grit coatings comparison was made with the vane in cup measuring system and these results are included in Table 5.2

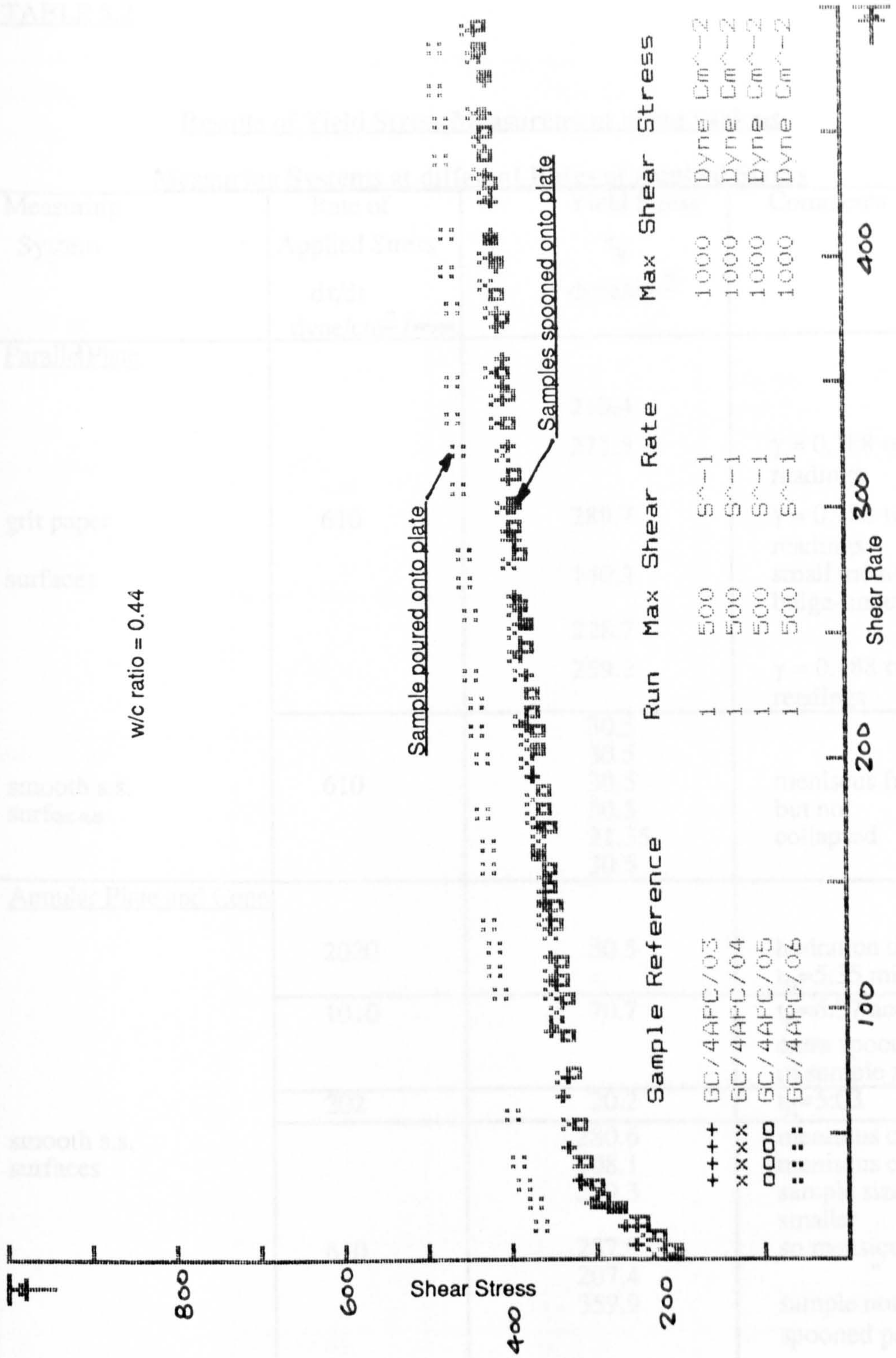

Fig. 5.5 Yield Stress of Class G Cement Slurry using Smooth AP&C

TABLE 5.2

Results of Yield Stress Measurement using various Measuring Systems at different Rates of Applied Stress

Measuring System	Rate of Applied Stress $d\tau/dt$ dyne/cm^2/min.	Yield Stress τ_y dyne/cm^2	Comments
Parallel Plate			
grit paper surfaces	610	210.4	
		271.5	$\gamma = 0.188$ two readings
		289.7	$\gamma = 0.188$ two readings
		140.3	small meniscus bulge-undercut
		228.7	
		259.2	$\gamma = 0.188$ two readings
smooth s.s. surfaces	610	30.5	
		30.5	
		30.5	meniscus full but not collapsed
		30.5	
		21.35	
		30.5	
Annular Plate and Cone			
smooth s.s. surfaces	2020	30.5	hydration time t_n=5:35 min:sec.
	1010	70.7	t_n=6:37 and extra spoonful of sample added
	202	20.2	t_n=5:03
	610	280.6	meniscus collapse
		308.1	meniscus collapse
		259.3	sample size smaller
		237.9	so mensicus held
		207.4	"
		359.9	sample not spooned poured from beaker.

Table 5.2 (continued)

Measuring System	Rate of Applied Stress $d\tau/dt$ dyne/cm^2/min.	Yield Stress τ_y dyne/cm^2	Comments
Annular Plate and cone sand coated surfaces	610	359.9 539.9 439.2 518.5 549.0	eccentric loading maybe undercut meniscus collapse mixer position altered to prevent spatter. t_n = 5:10 min:sec.
	202	141.4 202.0 707.0 151.5	sample too small stop added more. meniscus collapses maybe undercut
Vane in Cup	610	387.5 427.2 335.7 357.0 308.2	slightly bigger sample t_n=5:03 min:sec. bias overide
	850	641.7 514.2 599.2 501.5	γ = 0.024 5 or 6 readings big sample 0.23 mm up 9ϕ shaft. bias overide bias overide sample too big spooned some out
	170	986.0 833.0 977.5	bias dropout bias dropout
	4250	212.5	

NOTES Class G cement slurry w/c = 0.485. mixed using SSMP. tested 5 minutes after adding water. temperature = 25°C.

5.1.3 The Vane in Cup

For the vane system the cement slurry was weighed into the cup so as to determine the depth to just cover the vane. This was calculated using the vane and cup geometry and a cement density = 3.15 g/cm^3. Observation of the cement imprint on the vane after testing confirmed the depth of immersion. Before the vane could be fitted to the drive rod the cup with the weighed slurry had to be placed in the water jacket, which was fixed concentrically to the lower plate of the Carri-Med. The procedure meant that care had to be taken in fitting the vane so that the automatic correction of the biasing system was achieved prior to the start of the run. The jacket provided a constant temperature which was set to 25^{o}C.

From previous test runs, using the parallel plate on a class G w/c = 0.485 cement slurry and with grit coated plates to overcome slippage, a yield stress of between 200-300 dynes/cm^2 was achieved. Therefore, initially the vane, with a stress factor = 0.17 was used to test a similarly mixed slurry at a peak torque of 5000 dyne cm in an ascent time of 1 minute which gave a rate of applied stress of 850 dynes/cm^2/minute. The results of 4 test runs shown in Table 5.2 gave the yield stress between 500 and 642 dynes/cm^2.

The yield value of the slurry using the vane in cup was obtained scrutinising the flow curve for the first point at the start of continuous flow from the initial data points. This first point defines the yield stress in terms of shear rate, since the yield stress at

zero shear rate is an unknown quantity. In some cases, particularly with the vane, the data showed a minimum shear rate reading with a corresponding stress and then the shear rate returned to zero. This can happen, with the vane, 5 or 6 times before continuous flow occurs, which suggests a rearrangement and strengthening of particle structure.

5.2 Comparison of Measuring Systems

The results for both types of surface with the parallel plate were obtained prior to manually, and slowly, squeezing the plates together to the final gap setting, which avoids the sudden deformation of the sample on ram up. The action of the ram is an in-built feature of this Carri-Med model, which could not be easily altered. The slow squeezing procedure was adopted with the annular plate and cone but obviously not with the vane, since this would require manually winding the micrometer in excess of 24 complete turns prior to each test. The parallel plate results are likely to reflect lower yield values, as a result of this ram up deformation just prior to testing, which is the case. The deformation on ram up with the vane is not likely to cause as much effect on the yield value as with the parallel plate. Although, according to Haimoni (1985), Donald et al (1977) found small vanes might give a higher yield value if the ratio of the cross sectional area of the blades to that of the cup was greater than between 10 and 15%. This increase in yield value however, was probably due to the compaction effect of the vane when used in soils testing. The area ratio of our vane and cup is 20% but the disturbance effect is likely to reduce the yield value with cement slurry, regardless of vane size.

Initially the vane was immersed to its full depth with one end only immersed and the results shown in Table 5.2 are for this condition. It was thought that the yield

under this condition may not develop fully at the top of the vane and a few subsequent tests were made with the sample size increased to 12 mm above the vane. (i.e. Z_1/D = 1.0 as recommended by Haimoni (1985)). However, because of the vane geometry, the shear factors had to be revised and slippage around the shaft would have to be considered. Without taking the slippage around the shaft into account, the yield values found were 418.0, 357.0, and 427.2 dynes cm^2 with a shear stess factor of 0.1126 and a rate of applied stress of 610 dynes/cm^2/minute. At the 99% confidence level we can't be sure of a significant difference in these recorded mean yield values, although we can at the 95% level. The shear stress factor is considerably altered by the shaft immersion, hence the Z_1/D factors cannot be adequately assessed for this geometry, when measuring the yield values of cement slurry. Also the rate of applied stress, which is dependent on the shear stress factor, affects the yield value.

5.3 Effect of Rate of Applied Stress on Yield Stress

Preliminary flow runs with smooth parallel plates measuring a w/c = 0.44 class G cement slurry indicated that applied torque rate, hence rate of applied stress, had some influence on the measured rheological properties. As a result, using the parallel plate, the range of torque rates were increased from 5000 dyne cm/minute to 90,000 dyne cm/minute. It was hoped to do this by reducing the ascent time whilst keeping the peak torque at 15,000 dyne cm., thereby obtaining higher resolution, but the software would not accept times less than 1 minute. Hence to, overcome the abort test condition experienced with a 25000 dyne cm/minute applied stress rate, the programme was terminated prior to 45 rad./s, which is the cut off shear rate. This enabled sufficient points to be obtained for a partial curve analysis and use of the expansion of the X-axis facility.

The effect of torque application rate was obscured by the time elapsed since mixing, although the curves indicated good reproducibility for similar times up to 40 minutes with torque rates between 5000 and 20,000 dyne cm/min. The initial yield stress appeared to increase with torque rate, whereas the plastic viscosity decreased with torque rate for shear rates up to 30 sec^{-1}, which occurred within a few seconds of testing.

To distinguish between hydration time and torque rates flow curve tests on the parallel plate were run at 10 minute intervals from 4 to 64 minutes using the same torque rate. This set of tests was repeated, using a fresh batch of cement for each set, with the same w/c ratio and mixing procedure for the following torque rates:- 10^4, 2 x 10^4, 4 x 10^4, 6 x 10^4, 8 x 10^4 and 10^5 dyne cm/minute. Comparison of flow curve analysis was made for the various torque rates, at the same time of hydration. The change in the flow curves, both in the early stages of test and the complete up curves with time of hydration were studied using the compare facility in the Carri-Med software, as well as the X-axis expansion facility, described in Chapter 3.

The maximum shear rates varied from 25 sec^{-1} at 10,000 dyne cm/min to 895 sec^{-1} at 60,000 dyne cm/min so that analysis, using the simple Bingham partial up curve on the first 10 points, was fraught with the problem of resolution mentioned earlier and the need to operate on different lengths at the start of the flow curve to extrapolate rheological properties. It is difficult to obtain acccurate values of the initial yield stress by this means, but the results given in Table 5.3 show that the initial yield stress of a standing slurry increases with time, as is known, unless the structure of the slurry is disturbed.

The results of Table 5.3 appeared to indicate that the rate of applied stress had

nearly as much influence on the value of yield stress as did the difference in hydration time over the ranges tested. It was for this reason that future testing considered rate of applied stress as an important variable. Most of the X-axis expansions displayed sudden stress decrease, close to the point of intercept with the Y-axis, as shown in Fig. 5.6, which highlights the initial yield stress error with Bingham analysis.

The comparison of the complete up curves, shown in Fig. 5.7, shows a continuous raising of the stress level with hydration time, but at each particular time the torque rate order would differ. The stress level at the higher torque rates is just falling back at 64 minutes from the 54 minute level. The form of the curve remains reasonably constant with the curve taking longer to reach a straight line with increased hydration time. Generally, the initial slope and final slope were similar, indicating that a fully broken down paste probably has the same plastic viscosity regardless of the early hydration time or applied torque rate.

5.4 Effect of Bleedwater Removal

A notable feature of the results in Table 5.3 is the reduction in yield stress when the bleedwater is removed from the mixed slurry prior to testing a sample. When this removal was carried out,at each time a sample was tested from the same mixed slurry, which was left standing in the blender, the yield stress measurement was found to reduce progressively, as shown in tests performed at 60,000 dyne cm/min. in Table 5.3. A sample was taken from the blender by spoon at just below the surface to avoid laitance and bleedwater. As the bleedwater sometimes ran into the trough where the sample was being taken, the blender was tilted and the bleedwater scooped away by spoon.

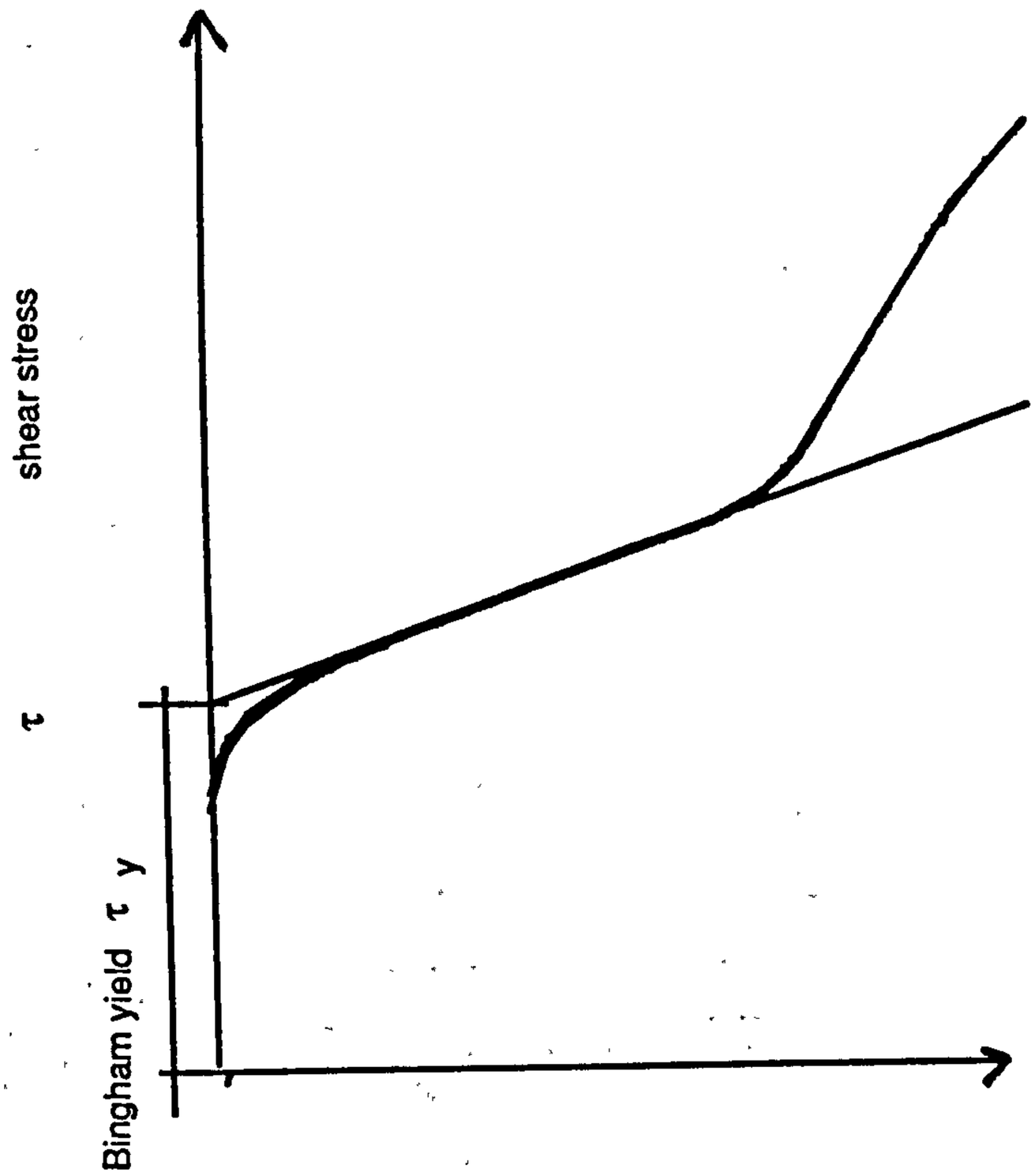

Fig. 5.6 X-axis Expansion of Flow Curve

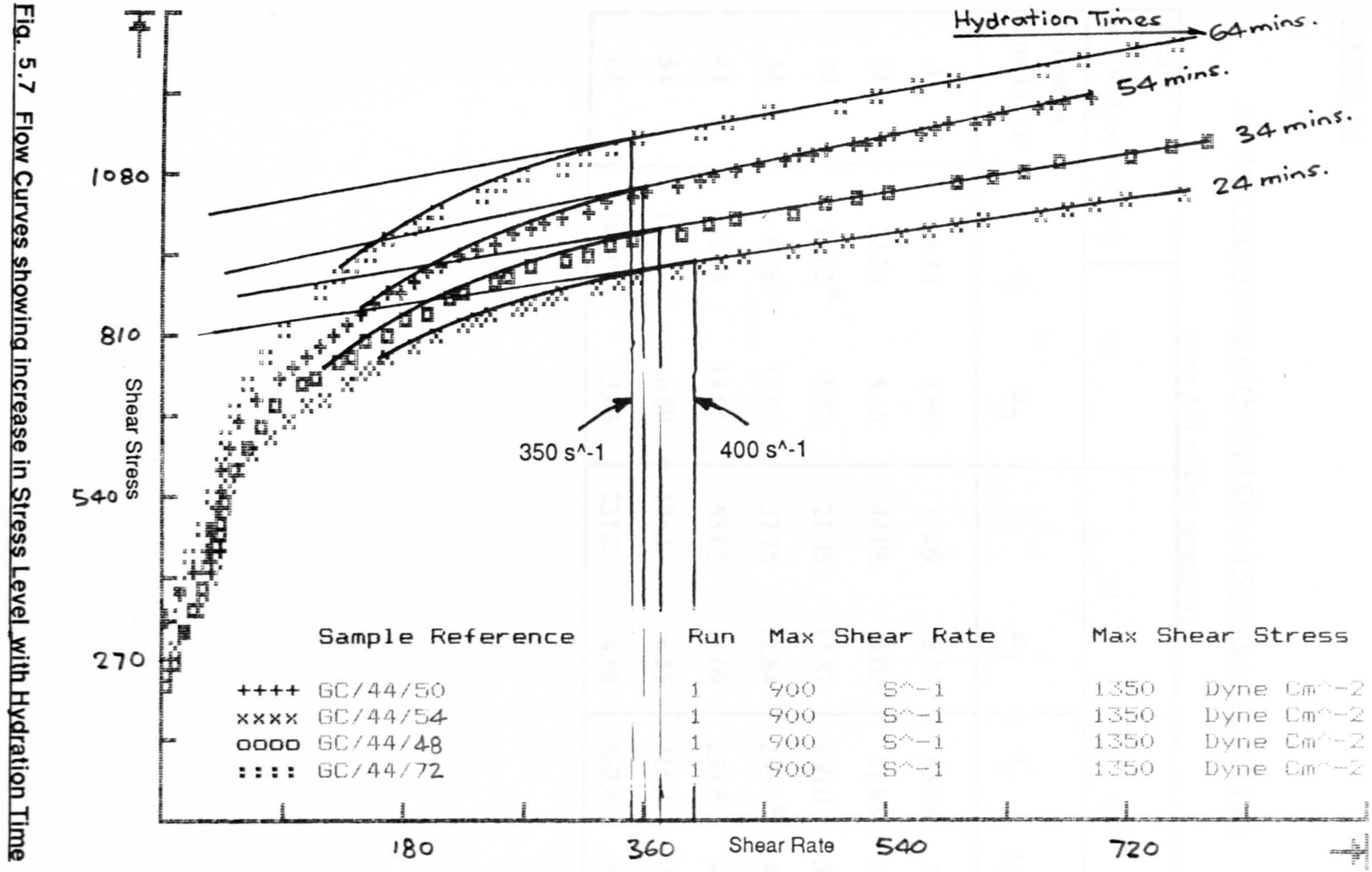

Fig. 5.7 Flow Curves showing increase in Stress Level with Hydration Time

TABLE 5.3

Results of Flow Curves of Oil Well Cement Slurry from Parallel Plate using API mixing procedure

Torque Rate (x 10^3 dyne cm/min.)	10		20		40	
Hydration Time (mins)	τ_y	μ_p	τ_y	μ_p	τ_y	μ_p
4	8.86	7.69	17.09	8.24	65.56	5.99
14	12.38	8.15	44.06	8.02	71.83	6.80
24	16.02*	8.77	21.05	13.87	130.0	5.86
34	8.98	11.02	37.75	12.84	263.5*	4.46
44	61.99	14.05	63.05	11.09	239.6	4.69
54	127.1	6.69	104.1	6.55	316.3	4.20
64	186.9	3.63	221.2	4.68	362.4	3.99

Torque Rate (x 10^3 dyne cm/min)	60		80		100	
Hydration Time (mins)	τ_y	μ_p	τ_y	μ_p	τ_y	μ_p
4	72.55	7.05	90.19	5.76	129.3	4.00
14	no data		113.6	6.35	87.67	6.99
24	216.8*	6.28	134.5	6.94	128.6	6.86
34	200.9*	5.80	143.8	6.66	143.7	6.68
44	198.9*	5.42	214.3	6.09	110.9	7.52
54	191.4*	6.06	152.0	7.82	292.8	6.83
64	91.51*	7.28	297.2	5.76	300.8	7.14

Notes

1. τ_y is in dynes/cm^2 and μ_p is in poise
2. * indicates that bleedwater was removed from the blender prior to testing the sample.
3. Slurry is Class G cement w/c = 0.44

There were some cases where yield stress shows reduction, as at 14 and 44 minutes hydration time in the 100,000 dyne cm/min. test series, and the bleedwater was not removed. It is not possible to explain the reason for this happening, although some disturbance on sampling is thought to be the cause.

Removal of the bleedwater is thought to cause disturbance of the early microstructure by removing very fine particles and also by the removal of the pore water pressure support, thereby causing microstructural collapse and rearrangement of particle structure.

5.5 Conclusion

The Waring blender not only gives homegeneity difficulties but, because of cement bleeding and sample disturbance, testing of a cement slurry with different mixing and standing times requires another method of mixing. The technique devised for mixing the cement slurry to study these aspects is outlined in the next chapter.

Confirmation of the yield stress measurement of cement slurry by comparing the results from different measuring systems was not possible. The yield stress could not be measured with smooth surfaces, either on the parallel plate or the APC. Slippage was overcome with rough surfaces but to what extent is not exactly clear, although yield stress measurement by the sand-coated APC compared well with the vane in cup. The vane, although not subject to slippage, does cause disturbance of the gel structure, when inserted into the sample. The vane during testing and just prior to yield appears to re-arrange the particle structure. For these reasons, and that the vane is not suitable for mixing the slurry, no further use was made of the vane. Further work in this thesis was carried out using the APC measuring system, with particular attention being given to rate of applied stress.

CHAPTER 6

Adaptation of C.S. Rheometer to Perform Mixing Standing and Testing of a Cement Slurry

To study the effects of shear history on the development of gel strength of an oil well cement slurry, a mixing technique which provides a well defined mixing energy input is required. The API Waring blender was shown in Chapter 4 to give an ill-defined shear history. Its ability, with suspect homogeneity,by varying either speed of impeller or mixing time, to reliably cover a simulated field mixing range is doubtful. The Waring blender, though of domestic quality, is standard throughout the oil industry. Perhaps better speed control could have been obtained by incorporating a larger powered induction motor, with gearing for high speed and by using an electronic control loop to maintain constant speed. However, improved input measurement of the blender would not effect its homogeneity.

The problems of sample selection and transfer to the Carri-Med would still remain. It was also rather wasteful to mix 600 ml and then test only 9 ml. The SSMP offered no better solution. Measurement of mixing energy requires the measurement of both torque and rotational speed of the mixing tool. On realising that the Carri-Med measured these two parameters very accurately my idea of using the controlled stress rheometer to perform the mixing of the sample was devised. This procedure obviated the problem of transferring the sample from the mixing apparatus to the measuring system. Even less disturbance of the sample is possible if the mixing tool was also the measuring tool. This is because removing a tool from the Carri-Med drive rod, and replacing another one, entails considerable deformation of the sample. The APC and vane in cup were considered, since these measuring systems were most suitable

for yield measurement. However, both of these systems require the initial mixing of the cement and water by hand. The vane in cup is unsuitable to impart a known shear or mixing energy, because

of the varying shear rate occuring radially across the sample. The annular plate and cone was chosen because the shear rate across the sample to be measured is constant and not dependent on the rheological properties of the material being measured. It would have been useful for comparison to measure the yield using the vane having mixed the cement slurry with the APC. This procedure was not possible because of the sample disturbance mentioned earlier and, with the particular apparatus, the smaller sample size of the APC.

The small sample size of the APC made it possible to cover the range of mixing energy from that used in the field to that in the API laboratory test procedures. The latter is where 600 ml of cement slurry is mixed at 12,000 r.p.m for 35 seconds. Orban et al. (1986) described various field mixing methods and estimated the mixing energy input by them. They then compared the cement slurry properties produced by the field mixers with the laboratory mixer. They found that a conventional jet mixer produces a mixing energy of around 0.5kJ/kg, whereas, the API laboratory mixing procedure produces a mixing energy of 5.5kJ/kg.

6.1 Calculation of Mixing Energy Input

Orban et al (1986) present the equation for mechanical work done by a mixer on a unit mass of slurry, as

$$E_T/M = \frac{T\omega t}{\rho V} \qquad 6.1$$

where E_T is the total energy input. As an example, for a peak hold flow curve test run on a S.G. = 1.9 cement slurry, over a 1 minute peak hold time, at a peak torque T = 25,000 dyne cm. and a sample testing volume V = 3.65 cm^3, the average angular velocity throughout the run was approximately 21 radians/sec, which gives $E_T/M = 0.45$ kJ/kg.

Now according to Van Wazer et al (1965) p.83 the rate of energy dissipation by viscous flow is the product of the shear stress times the strain rate. This gives $E = \sigma \dot{\gamma}$ and the total energy per unit mass as

$$E_T/M = \frac{E.t.V}{\rho V} = \frac{\sigma.\dot{\gamma}.t}{\rho} \qquad 6.2$$

where σ is the shear stress and $\dot{\gamma}$ the shear rate. Examining the same flow curve as used previously, knowing that $\sigma = F_\tau T$, where $F\tau = 0.0202$ is the stress factor for the APC and T is the torque, the following figures were found. The shear rate, $\dot{\gamma} = 300\ sec^{-1}$

which is obtained from $\dot{\gamma} = F_{\dot{\gamma}}\,\omega$ with the shear factor, $F_{\dot{\gamma}} = 14.3$ and using the above equation the $E_T/M = 0.48$ kJ/kg, showing that both approaches give similar results.

Equating the total energy in both approaches we find that

$\sigma\,\dot{\gamma}\,V = T\omega$ and since $\sigma = F_{\tau}.\,T$ and $\dot{\gamma} = F_{\gamma}.\,\omega$ we get, $F_{\tau} \times F_{\dot{\gamma}} \times V = 1$ 6.3

which is correct for $V = 3.46\ cm^3$. The $V = 3.66\ cm^3$ used previously in the energy calculation included the estimated volume of indentations covering the measuring surfaces. Since it was assumed that this additional volume is not being sheared the correct volume to use in the energy calculation is the volume between the smooth annular plate and the cone. This gives $E_T/M = 0.48$ kJ/kg., which is the same result as the σ - $\dot{\gamma}$ analysis. To test a range of mixing energies by varying the duration of hold of the peak torque in a flow curve run the mixing times for the following S.M.E.'s were calculated (1 SME = 5.5 kJ/kg as defined by Orban et al (1986)) by proportion as in Table 6.1. As $\dot{\gamma}\,x\,t$ is unknown until the area under the flow curve is determined, the calculated mixing times will be used in the test runs and the actual S.M.E's which are in the range 0.1 to 1.0, were evaluated after the run.

The basis for assuming that the rheometer could simulate the Waring blender mixing a slurry to the API test specification was the crude assumption that the proportionality constant in the relation of torque to rotational speed for the blender would be similar to that for the annular plate and cone. This assumption is given credence as the work provided by the blender is assumed by Orban et al (1986) to be entirely spent in shearing the slurry. This gives

$\frac{\omega^2 t}{V}$ to be constant for the same mixing energy.

Hence $\frac{(1200)^2 \text{x } 35}{600}$ for the waring blender is equal to

$$\frac{(\omega^2) \text{ x } 60}{3.46}$$

giving $\omega = 696$ r.p.m or 73 radians/sec. By increasing the run time, since the maximum rotational speed of the Carri-Med rheometer is 48 radians/sec, the API mixing energy can be simulated, as well as the other lower mixing energies.

To obtain a simulated mixing energy input to a cement slurry sample in the Carri-Med, the shear stress is held constant over a period of time and the shear rate recorded. The mixing energy per unit mass is obtained from

$$E_{T/M} = F_\tau \frac{T_{peak}}{\rho} \int_0^t \dot{\gamma}\, dt \qquad 6.4$$

where $\int_0^t \dot{\gamma}\, dt$ is the area under the peak hold flow curve.

6.2 Modifications to the Carri-Med Flow Run Programme

When performing a flow run using the Carri-Med 3.5 software, provided the peak

torque and the times for the various phases are entered in the initialising procedure, the rheometer will increase from zero to the peak torque in the ascent time, hold the peak torque for the peak hold time and decrease to zero torque in the descent time, as shown diagrammatically in Fig. 6.1. It can ignore any one, or two, of these phases but it must perform them in sequence. In order to perform a mixing shear on a cement slurry sample and then examine its yield stress, this sequence needed to be changed. Initially, the approach was to programme the peak hold phase to run first and on completion return to the ascent phase. The applied torque had to be turned off at the end of the peak hold phase and the data storage was in the wrong sequence for analysis. The placing of the two sets of phase data on two separate runs was considered but rejected because of the lengthy initialising time and the inconvenience whilst analysing. Instead by making the input descent time equate to the equilibration time between runs in the programme and cancelling the descent phase, the input descent time became the standing time between peak hold phase and ascent phase. Then, by putting the testing torque in the ascent phase equal to four times the peak torque = 25000 dyne cm. for the mixing or peak hold place, the mixing, standing and testing of the sample could be carried out with one run. Although peak hold and up curve data storage was achieved, the analysis and graph plotting was problematic. Consequently, following a disc inaccessible crash even though a copy was available ,a more simple approach was adopted. This consisted of turning the descent phase into an ascent phase with a pause between the peak hold and this new ascent phase, so that existing data storage and analysis was unaffected.

Before the simple approach was adopted a few problems had to be overcome. The first of these was access to the Carri-Med software. This was achieved by a disc supplied by Carri-Med which contained a remed version (remarks included) of the flow run, a & COMPRESS function to derem the programme currently loaded in the computer and a programme called SAMPLELOAD, which demonstrated how to load a previously saved results file. Some tips were given by Carri-Med which also proved

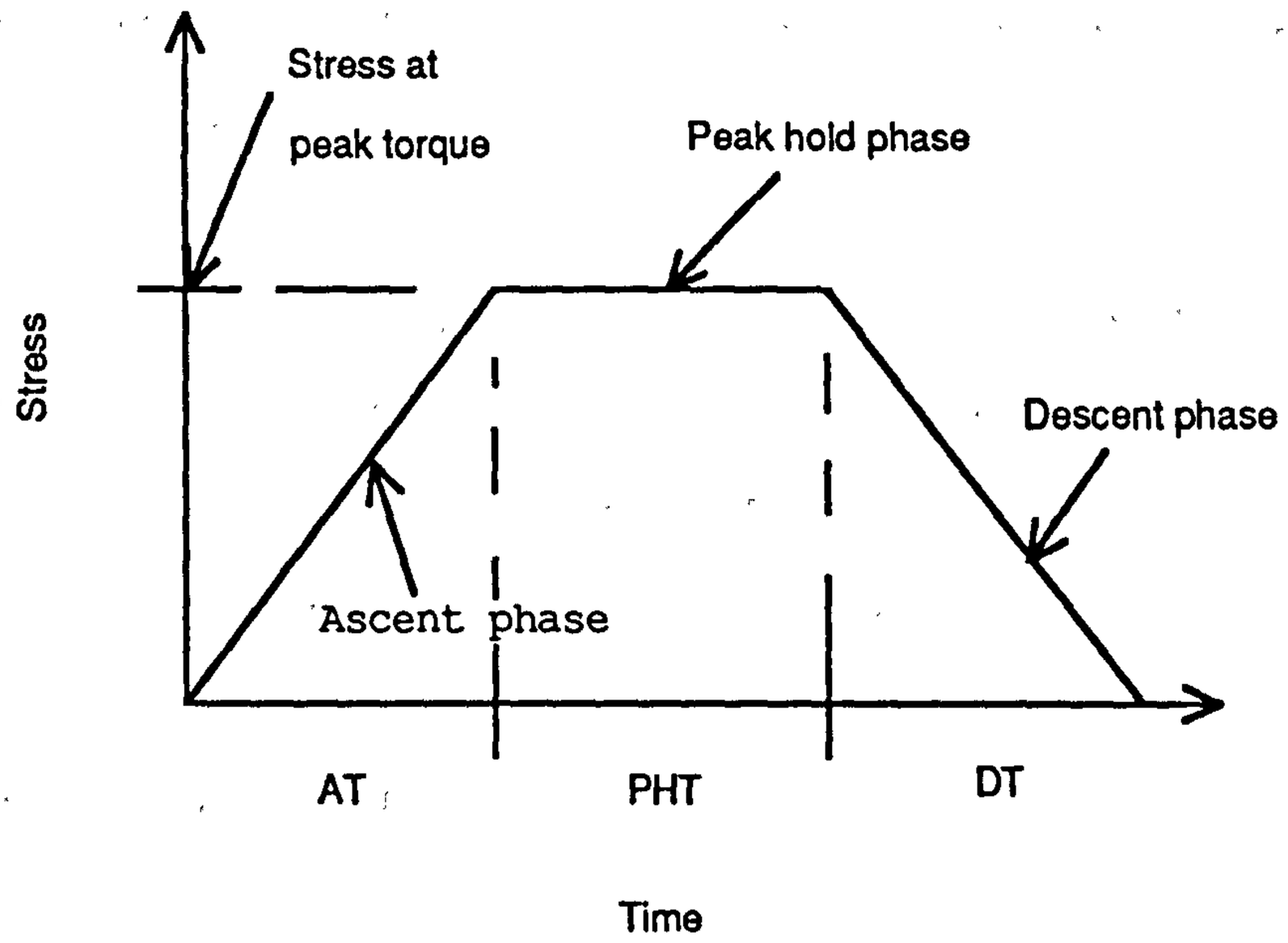

Fig. 6.1 CarriMed Flow Run Procedure

very useful.

1. The flow package disc has little free space so if you make the programme larger some other file on the disc will require deleting
2. Derem the programme before running as there may be insufficient memory space and execution will be slower.
3. The run programme may be modified to calculate the area under the peak hold curve but it would be easier to write a separate programme and use previously stored results files.

It was found that the flowrun programme could be loaded from the SAMPLELOAD disc, amendments made to the flow run programme, use & COMPRESS then save the amended programme on a copy disc of the Carri-Med Flow Release 3.5 package under AFRUN 3.5,hence modifying it. Subsequently, it was easier to

1. Boot FlowRun/Sample Loader disc.
2. Remove disc replace FLOW Release 3.5 disc
3. LOAD AFRUN 3.5,LIST and alter as required
4. SAVE AFRUN 3.5

Another problem was how to overcome the close packing phenomenon on start up of the mixing phase with the rheometer. This problem is closely followed by the problem of controlling the shear rate over the mixing time so that the sample is not thrown out of the APC nor exceeds the maximum angular velocity of the instrument of 48 radians/second, at which the rheometer cuts out.

To overcome the close packing behaviour the stress was applied to the sample instantaneously at a value above the initial static yield of the cement slurry rather than applied by incremental build up as in the flow run ascent phase. This applied stress value

was determined, by trial and error, to be 25000 dyne cm. for the particular w/c ratio and measuring system. At this applied stress the shear rate reached the cut out level in approximately 25 seconds. A simple means of control, by reducing the applied stress to 80% of the initial applied stress, was tried and found to be effective. This control was placed inside the FOR/NEXT loop of the peak hold phase with a GOSUB on the 5th loop of the 100 loop cycle. With a 1 minute mixing time this meant the control was effected at 3 seconds but in later tests mixing times of around 10 minutes rendered this control ineffective. This control had to be placed on real time rather than loop number, so after applying the torque for 3 seconds, using the descent phase changed to ascent phase simple approach programme, the torque was reduced by 20% and re-applied prior to going into the peak hold phase loops.

6.2.1 Corrections to Computer Timings

In the early stages of modifying the flowrun programme the peak hold phase was found to last 1:10 (min:sec) when 1 minute was programmed. This time discrepancy also occurred with the standing time but in this case there was an additional time lapse between the completion of the standing time digital countdown and the start of the ascent phase. The time lapse of approximately 6 seconds was due to the setting up of the graphic display and the programme routine, which monitored the initial state of the variables. The time discrepancies mentioned earlier occurred because the original programme is based not on real time but on the time to perform a computerised operation, plus a pause time, which makes up a period of real time. Unfortunately this gives a different clock for each operation and different minimum overall times for each operation, since the number of loops multiplied by the computerised operation time gives the minimum overall time with zero pause.

One minute is the minimum time, other than zero,that can be input to the programme

for ascent, descent and peak hold time. To obtain a 1 minute standing time whilst allowing for time lost in presenting the display and to correct for computer time over run which is a total of 14 seconds, the programme was modified with the line AS = AS - 60, where AS is not the ascent time in seconds, but the standing time. The input ascent time given as 1:46 (min:sec), for example, produced a standing time of 58 seconds using the equilibration routine to perform standing.

As modifications were continually being made to the programme, and that extended standing and mixing times would be required, a check on their correctness was kept using a laboratory clock. Although programmed timings were eventually got to within a second, the timing of the actual yield of the slurry could not be programmed, since this depended on the mixing and standing times as well as the testing time, which determined the rate of applied stress. The time of yield was noted on every test run from observation of the laboratory clock.

Now with the modification of the simple approach, referred to earlier, most of the time difficulties disappeared apart from the standing time which on putting ET = AS, as before, and using the equilibration routine was found to give actual times of 0:58 and 11:43 (min:sec) for input values of 1:46 and 10:46, respectively. Placing the input values in our AS = AS-60 modification we get,

AS = 646-60 = 586 and $586 \times t_e$ gave 703 seconds.

AS = 106-60 = 46 and $46 \times t_e$ gave 58 seconds.

Therefore, t_e is the time correction for the equilibration loop. The more accurate t_e is equal to 1.2, over the longer period. As the equilibration routine is used successfully in other parts of the programme and provides displays of time and temperature, it was

Table 6.1 Mixing Times needed to give a Range of Specific Mixing Energies (S.M.E.'s)

SME	1.0	0.75	0.5	0.25	0.1
Mixing time (min:Sec)	11.31	8:38	5:46	2:53	1:09

Table 6.2 Values of Ascent Time Input to obtain Required Standing Time.

Input value (min:sec) as ascent Time	5:10	9:20	13:30	17:40	26:00
Required Standing Time (min:sec)	5:00	10:00	15:00	20:00	30:00

thought prudent not to disturb it. Hence, to reduce the actual standing times obtained to those required, the input values, given in Table 6.2, were calculated as shown in the following example:-

$$\frac{11:43}{1.2} = 9:46 \text{ add } 1:00 \longrightarrow 10:46 \quad \text{(min:sec)}$$

The actual standing times measured by visual observation of the laboratory clock during the trial runs was found to be within ± 2 seconds for all such runs.

6.3 Programme to Perform Mixing Shear History

The final computer programme used to provide a mixing shear, a standing time and a flow curve test on a cement slurry in this work was a modification of the Carri-Med Flow Run Issue 3.5 programme run in Applesoft Basic. This programme is covered by copyrights. In order to demonstrate the 'simple approach' modifications, a listing is given in Appendix 1 of the modified and additional lines. There follows a brief explanation of these lines, together with the line numbers of those deleted.

Line 1035 allows a 1 minute standing time

Line 1170 set standing time flag

Line 2900 if standing time complete then go to testing routine

Line 3090 skip ascending stress routine, go to peak hold phase

Line 3140 deleted-enables programme to run with zero standing time

Line 3520 puts ascent data file to nil

Line 3630 sets starter torque flag

Lines 3643, 3645, 3646

applies starter torque then into loops applying peak hold torque

Line 3940 switches torque off

Line 3950 deleted - graphics in wrong place

Line 3960 evaluates testing peak torque, go to standing time routine

Line 4000 plot axes

Line 4050 puts start torque equal to zero

Line 4060 evaluates torque increments from peak torque

Line 4230 turns down curve into up curve plot

Line 4250 reset flag, zero standing time

Line 4940 to line 5050

deleted - up curve plotting routine

Line 5070 print data stored in down curve file as up curve.

6.4 Evaluation of Energy from Peak Hold v. Time Curve

The area under the peak hold shear rate against time curve enables the mixing energy per unit mass to be calculated, as shown in Section 6.1 equation no. 6.4. The computer programme written to obtain this mixing energy from test run data stored on the initialised storage disc is listed in Appendix 2.

The area under the curve is calculated using Simpson's Rule;

$$A = \frac{h}{3} [y_1 + y_n + 4 (y_{even}) + 2 (y_{odd})] \qquad 6.5$$

where y_n is an odd ordinate. From the raw data print of the peak hold data it is found that 100 data pairs of time and shear rate are stored, which does not include y_0 nor the data for the starter torque applied for the first 3 seconds. The start-up area of the curve is small as shown in Fig. 6.2 and especially so for the longer mixing times. y_0 is the shear rate at zero time, which can be estimated by extrapolation giving $y_0 = 2y_1 - y_2$, with the condition that if $y_0 < 0$ then $y_0 = 0$ and hence A1, the start up area also equals zero. Otherwise $A1 = 3y_1 - 1.5y_2$, assuming a triangular start up area. Applying Simpson's Rule to the rest of the curve

$$AR = \frac{t_m}{300} [y_0 + y_{100} + 4(y_{odd}) + 2 (y_{even})] \qquad 6.6$$

AREA UNDER MIXING CURVE

Sample Ref. No. BCG/9EAPC/26 Run No. 1

Mixing Time = 11: 22 (min: sec)

Standing Time = 11: 45 (min: sec)

Start up area is 288.3

Mixing curve area is 221393.5

ENERGY / UNIT MASS IS 4.7084 kJ / kg

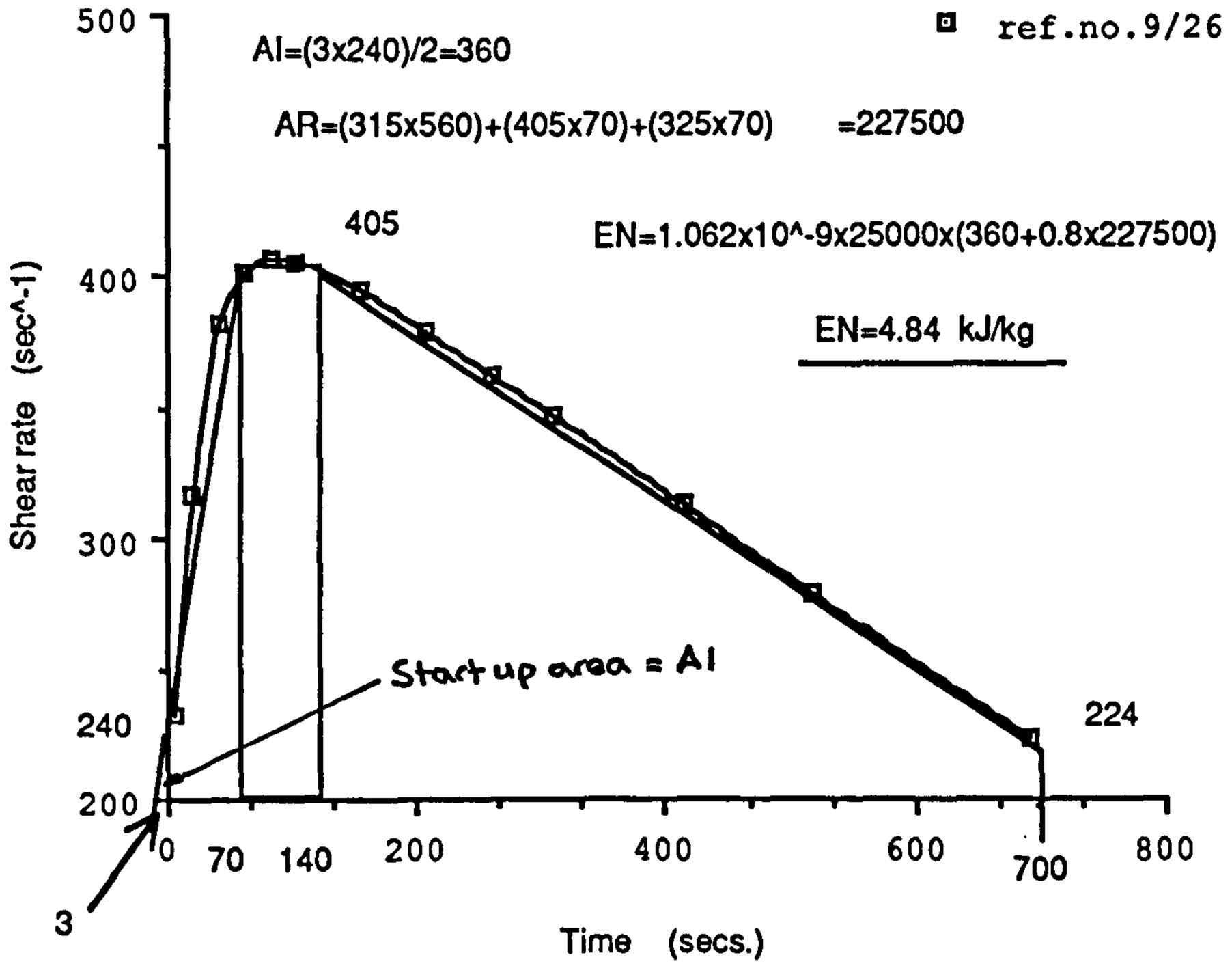

Fig. 6.2 Area under typical peak hold curve

AREA UNDER MIXING CURVE

Sample Ref.No. BCG/10EAPC/07
Run No. 1

Mixing Time = 2:53 (min:sec)
Standing Time = 30:0 (min:sec)

Start up area is 0
Mixing curve area is 81717.5365

ENERGY/UNIT MASS IS 1.7350794 kJ/kg

UP CURVE FLOW DATA

Point No.	Shear Rate	Shear Stress
1	.143	848.4
2	.143	1080.7
3	17.446	1121.1
4	91.52	1141.3
5	222.93	1151.4

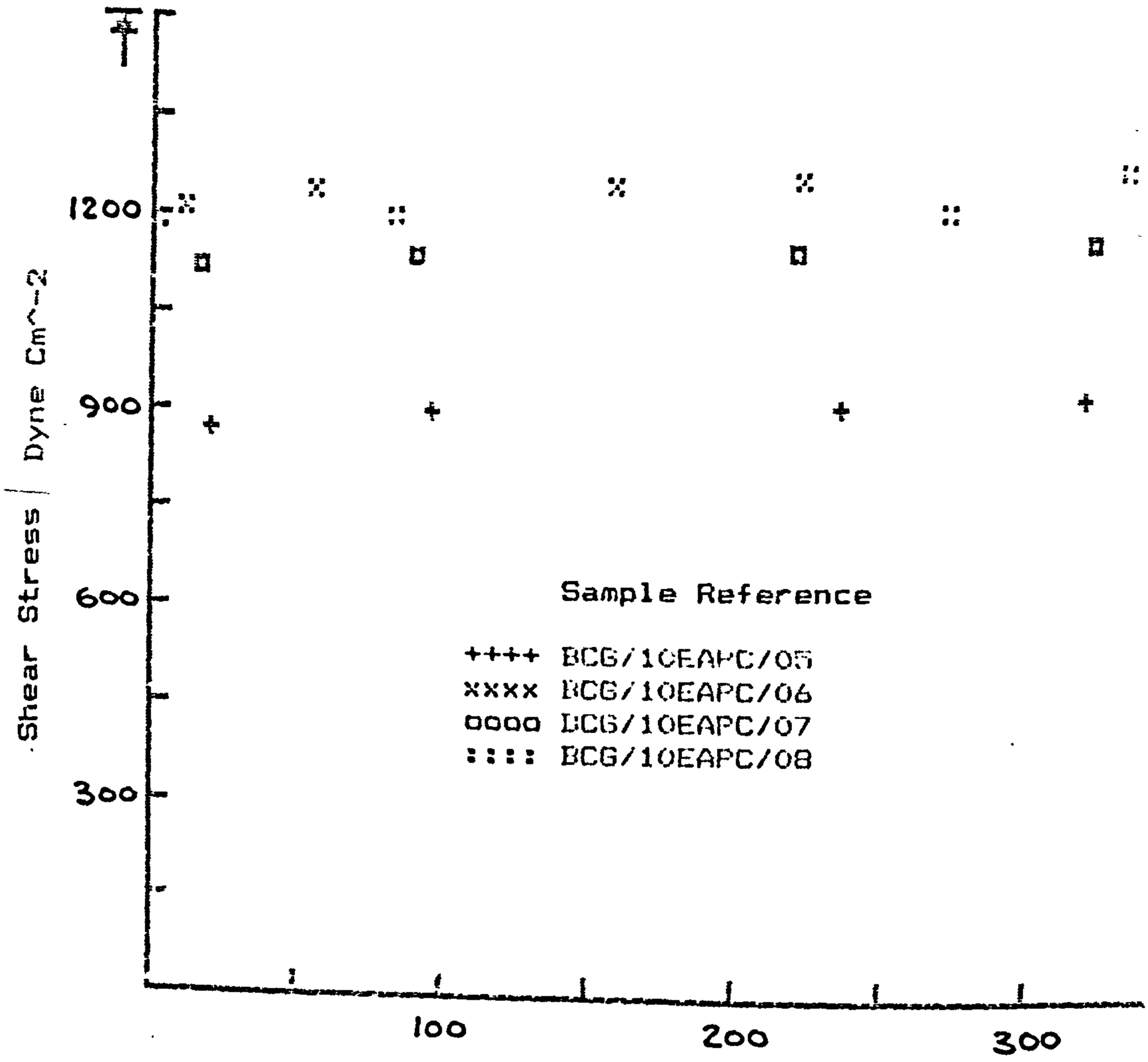

Fig. 6.3 Computer Print Out of Test Run

where t_m is the overall mixing time and the odd and even suffixes refer to the data point numbers rather than ordinates.

Having calculated the area under the curve this is converted into energy per unit mass by multiplying by the applied stress, which is equal to the applied peak torque times the stress factor for the particular measuring system, and dividing by the cement slurry density, calculated from the w/c ratio and the specific gravity of the cement. A rough check on the area under the curve, by estimating the area as 2 parallelograms and 1 rectangle, gave, on one selected run, the total area to within 3% of the computed value. It showed the start-up area to be about 0.15% of the total area with a mixing time of 682 seconds. This indicated that this area could be ignored even with mixing times as low as 1 minute. The print out showing a typical peak hold flow curve and the computer calculated area under the curve together with its energy conversion is given in Fig. 6.2. Also shown on the computer print out are the first five data point sets for the test flow curve. From this data the yield stress, being the first point of continuous flow, is readily obtained, as shown in Fig. 6.3

6.5 Procedure for Mixing Standing and Testing Slurry

The procedure finally adopted for the mixing, standing and yield stress testing of an oil well cement slurry, on the Carri-Med controlled stress rheometer, whilst using the annular plate and cone, was as follows. Assuming that the water and air supply to the rheometer was correct, the air bearing and gap setting on the installed APC measuring system were set and checked as described in the calibration section of Chapter 3, and the Carri-Med modified flow run programme was booted in the Apple 11e, with a data storage disc in drive 2. The following sequence was carried out:-

1. Press I key to initialise procedure, then input reference number, data, peak torque, standing time, peak hold time and ascent time. (other factors are held constant for this series of tests)

2. Enter return key to give one run, no key for immediate analysis and return key, again, to give the maximum shear rate for plotting purposes.

3. Weigh the cement and water in separate 150 ml glass beakers, place the annular plate on the balance and obtain the net tare, start the clock and blend the cement into the water by hand, using a small stainless steel spatula, until 1:00 (min:sec).

4. Pour approximately 16g cement slurry into centre of annular plate, transfer annular plate to ram of rheometer and clamp plate and ram together using 3 G-clamps by 1:35 (min:sec).

5. At 2:06 (min:sec), with bias and temperature indicator lights on, hit space bar to commence run. Ram rises to 1 mm from required setting. Turn micrometer thumbwheel a full turn to squeeze the sample to the correct gap by 2:20 (min:sec).

6. The rheometer automatically starts the mixing phase at 3:00 (min:sec), stops mixing, waits for standing time to elapse and starts applying stress in accordance with programmed times.

7. Using the ESC facility, terminate the testing phase when the digital reading of angular velocity is approx. 25 rad/sec. The computer then calculates the statistics of variation in temperature, re-plots graphs to suitable scales and requests

storage of data. Data is stored and on pressing the no key to a request for a repeat run the ram is lowered.

8. The annular plate and the cone are dismantled from the drive rod of the rheometer for cleaning, together with the beaker and the spatula. Cleaning was done with a toothbrush and running water after removing the bulk of the paste with the spatula. After drying the cone was re-assembled on the rheometer drive rod and allowed to bias so that the procedure could be repeated.

This procedure was followed for all the runs whose results are given and discussed in Chapter 7.

CHAPTER 7

Results of Yield Stress Testing of Oil Well Cement Slurry using APC Mix Procedure

Using the procedure, for mixing, standing and testing a cement slurry, described in detail in the previous chapter test runs were made on w/c = 0.44 oil well cement slurry without additives. This chapter describes the extent of the testing programme and the various factors which affect a successful mixing test, together with how these factors were put to good use, or overcome. The results of the series of test runs, which varied the mixing time, standing time and rate of applied stress during testing, are given and commented upon. These results are analysed in detail and a model is produced showing the relationship between yield stress, mixing energy, mixing time and standing time of a cement slurry. The results of a small range of various w/c ratio slurries, using similar cement and tested using the above procedure, are given and discussed.

Further discussion, with regard to the results and findings in analysis, is given in Chapter 8.

7.1 Scope of APC Mix Procedure Testing

The development of the procedure given in section 6.5 was hampered by electrical and mechanical difficulties with the equipment, as well as the computer programming difficulties already discussed in Chapter 6. The behaviour of the cement slurry, whilst undergoing this test procedure, such as close packing and shrinkage, also gave delaying problems, and will be discussed further shortly. For these reasons the experimental programme using the APC mix procedure was curtailed from that originally planned. It was intended to investigate standing times from 1 to 60 minutes, with 15 minute intervals, and mixing energy input in terms of S.M.E. from 0.1 to 1.0, in 0.25 intervals (approximately). Also, to look at w/c ratio and additives, such as bentonite and superplasticisers. This programme was for a class G oil well cement slurry, tested at a temperature = 25°C, the first part of the programme was with a w/c ratio = 0.44, and the rates of applied stress which were not changed ranged from 500 to 2000 dyne/cm^2 (/min.), in steps of 500.

The standing times were restricted to 1, 11, 20 and 30 minutes, although the range of mixing energies was achieved. It was felt that standing times in excess of 30 minutes would be unlikely to succeed because of the problems experienced with bias drop out and air compressor overheating, caused by continuous running, which resulted in loss of air pressure to the air bearing. These and other causes of failure during a mixing flow run on the controlled stress rheometer are discussed more fully in the next section.

The input mixing times were those found in section 6.1 and the input standing times are those given in Table 6.2. The input times for the rates of applied stress were

calculated from the maximum stress applied being the stress factor times the peak testing torque (i.e. 2021 dyne/cm^2) and the times corresponding to the rates are 4:02, 2:01, 1:21 and 1:01 (min:sec).

7.2 Factors affecting Successful Mixing Flow Runs

As noted above, electrical and mechanical problems hindered the programme, so study was made of the reasons for the failure of a mixing flow run on the Carri-Med C.S. rheometer. This study included the trial runs made during the development of the mixing programme. The results of the study are shown in Table 7.1.

The main reason for failure was bias drop-out. The term bias drop-out means that during any of the phases (mixing, standing or testing) the green bias light goes out on the rheometer and the ram is automatically lowered, ruining the experiment. Although this type of failure occurred in earlier runs, as they were of short duration usually 1 minute, the chance of failure was much lower than with the longer mixing and standing times. It was also thought that the cutting in, or out, of the compressor motors was solely to blame. However when a laboratory lamp was stood on the rheometer to highlight the sample its switch was also found to fail the rheometer. To check that the bias drop-out was an electrical phenomenon the drive rod with the measuring system attached was subjected to spin, lift and lateral movements, when the ram was in both raised and lowered position. The bias indicator light only extinguished when the ram was down and subjected to spin and lateral movement, showing that movement, in various directions, of the system in the ram up position did not cause bias drop-out. Though fewer than bias drop-out, the temperature control on occasions did go awry and it is concluded that both these failure mechanisms are caused by electrical disturbances which are either mains voltage surges or radio

Table 7.1

Test Run Success Record

Failure mode	Development stage	Experimental Stage		Total %
		Prior to L1829 installation	After L1829	
Bias drop-out	10	25	6	18.0
Erratic temp. conrol	5	2	-	3.0
Sample flung out	5	-	2	3.0
Sample remains rigid	-	7	13	8.8
Programme error/ modification	17	-	-	7.5
Compressor overheating	-	3	-	1.3
Operator error	1	1	-	0.9
Total Failure	38	38	21	42.5
Total runs	69	100	59	100
Success rate %	45	62	64	57.5

frequency interference (r.f.i.). These affect the rheometer's built in microprocessor, possibly by interfering with the signal in the IEEE cable, thereby initialising one of the numerous ESC routines. The name given to these failure mechanisms is therefore a misnomer and merely reflects the point in the computer routine at which the failure occurred. It was not possible to override bias drop-out by re-programming, since this invoked error traps.

Initially to overcome the interference caused by the voltage surges of the compressor motor a plug and socket mains filter type RS-238-700 was fitted to the rheometer mains supply lead. With the longer mixing times, a FR114 Schaffner with EMI filter was borrowed from the Dept. of Electrical Engineering and Electronics of Liverpool University. The equipment to monitor the transients or assess the protection required was not available in the University and would be a very complex and time consuming pursuit. The difficulty of assessing the attenuation of a transient in a buildings electrical network, together with the attenuation roll-off with increase in frequency of the protection device,made the selection of a suitable protection device a process of trial and error. The mains supply to the compressor was placed remote from the rheometers plug socket. Then the relief valve on the air receiver was cracked so that the compressor motors' cut out pressure of 100 p.s.i. was never reached and since this caused over-heating of the motors, a reduced continuous running pressure of 75 p.s.i. was used. However the FR114 Schaffner was discarded within 2 weeks, since suitable protection was not obtained. Recourse was made to confining testing to certain times of the day and switching off as many ovens and refrigerators as possible to ensure a successful run. Finally, a Belling Lee type L1829 r.f.i. filter was permanently wired in to a distribution board located on the wall just 1 metre above the rheometer. The filter was directly connected very close to the rheometer. The Apple 11e was initially connected to a RS-238-700 plug in filter then subsequently directly

wired to the L1829. The ancillary equipment cables and interface connections were, as had always been the practice, laid parallel with no undue crossing or loops. Bias drop out still occurred but the combined mixing, standing and testing time was now of the order of 45 minutes and with all the ruses the likelihood of a successful run seemed better. The failures attributable to electrical interference prior to the installation of L1829 were 25% of the total previous runs, this figure was reduced to 10% of the total subsequent runs after installation. The percentage of successful runs increased from 45% of the total runs during the development stage to 63% during the experimental stage.

The other major cause of failure of a mixing flow run was the close packing phenomenon. From Table 7.1 this accounts for 8.8% of the total runs and 20.6% of the failed runs. For no obvious reason, this failure mode occurred towards the end of the 30 minute standing time runs, when the mixing time was 8.38 (min:sec). It appeared as a slow start to the mixing phase, as if a thicker paste was being mixed, but the cement came from the same drum, where the cement was kept in a tightly sealed polythene bag to exclude air. The only obvious environmental change, during that period, was the University heating system switch on which raised the room temperature in the vicinity of the rheometer from approx. 17°C to approx. 21°C. However, the continuous running of the compressor caused the motors to overheat which meant that by the end of a 1 1/2 hour session the local vicinity room temperature had risen from 17°C to 20°C. This had occurred during previous sessions, however, without causing the sample stiffening phenomenon. The Peltier temperature system kept the plate measuring system at 25°C (to within ± 0.02°C, normally), so the difference in room temperature only affected the cement slurry for approx. 2 minutes prior to being loaded onto the rheometer. Although the cement and deionised water was kept in sufficient quantity in 500 ml glass vessels near the rheometer and would

have adjusted to the changes in room temperature.

Cleaning the pores of the engraved surface of the APC with dilute HCL, changing the drum of cement, from which a sample was taken, for another in the same consignment and using a much earlier copied disc in case of corruption, did not solve the puzzle. The radiators were turned off in the laboratory. A run was subsequently made at 25°C which displayed similar high speed mixing to the earlier runs - with the same mixing time. Fig. 7.1 shows the decline in shear rates caused by the apparently stiffer slurries. The run, reference number 10.18, became too stiff on mixing and did not produce a yield on testing. This was also the case with run ref. 10/26, which was also mixed for 11:31 (min:sec) and failed to produce a yield. The other 6 runs that suffered failure by remaining rigid during this period and before the phenomenon was overcome failed to start mixing. These runs were eventually re-run successfully, although the rigid sample failed runs were run at room temperature between 20°C and 22°C. Cool mixing water at 12°C was tried but mixing shear rates only managed 240 sec^{-1} compared to previous shear rate maximums in excess of 500 sec^{-1}, so this cause was discounted. It was thought that water was leaking from the annular centre plate but this was disproved. Another consideration was that stray electrical currents were orientating particles to form a more rigid structure. To test this idea a 0-24μA microammeter (Cambridge Instrument Unipivot) was used and 12-16μA was recorded just prior to the mixing phase, by placing the positive probe on the cone and the negative probe on the annular plate. 20-24μA was recorded during the mixing and standing phases. The standing phase usually displayed 1 or 2μA higher than the mixing phase, but this may have been due to the difficulty in maintaining contact with the probes whilst mixing. With the plates empty but in contact a zero μA reading

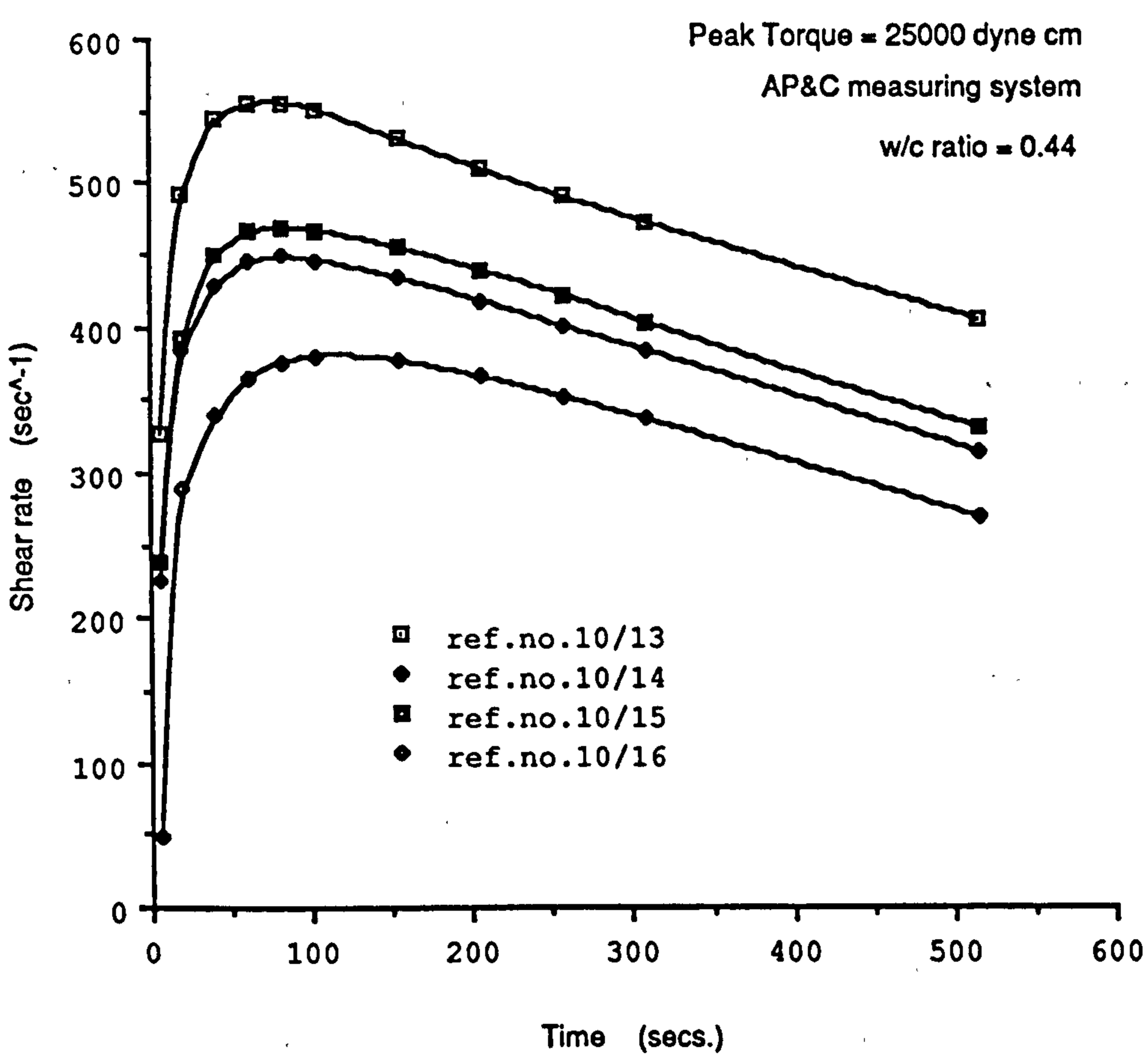

Fig. 7.1 Peak Hold Mixing Curves showing decline in shear rate

occurred, whereas with de-ionised water a reversed electrical current of 2-4μA was measured. The close packing phenomenon was not related to this electrical phenomena since rigidity occurred without affecting the electrical current values just mentioned.

Run 10/24 was obtained, though sluggish during mixing, at a temperature of 21.5°C, whereas run 11/01, which was carried out at 17.5°C, refused to mix and had to be re-run. Hence, high temperature though it may have some effect was not the sole cause of sample rigidity. Run 10/20 and 10/23 had 5 and 6 reruns, respectively, before being successfully completed, though the majority of failures were bias drop-outs. Run 11.01 above differed from the other runs by being slow in pouring the sample into the annulus and slow in squeezing the sample on ram up. The re-run on being quick in these actions and quick in blending the cement and water, though not vigorous so as to cause air entrapment, did achieve a sluggish run at 18.5°C. Run 11/03 with a normal blend and quick squeeze time of 1:20 (min:Sec) produced a 448 sec^{-1} maximum shear rate compared to 260 sec^{-1} with the 11/01 re-run. The 11/03 run was at 19.5°C indicating that the cause of the apparent stiffening of the sample was more related to slurry preparation and loading than temperature. A slow blend, with a quick pour of the sample into the centre annulus and on early squeeze gave rise to the best mixing shear rates. Probably, this was because the longer time that the sample stood, between squeeze and mixing, produced more bleedwater making start up easier. Whereas, a too fast squeeze destroys structure in the slurry, which then has to reform causing bleedwater to occur at a later time. Initial blending of the cement and water can have a dramatic effect. With run 11/12 the radiators were back on and room temperature was 20°C. The sample remained rigid, although loading procedure was in accordance with optimum pouring, clamping and squeezing times. Re-run of 11/12 gave too gentle a blend and a somewhat lumpy slurry was observed together

with a 312 sec^{-1} maximum shear rate and a longer build up to that maximum. The next re-run of 11/12 produced another rigid sample and the following re-run threw the sample every where due to poor blending.

In conclusion, a consistent normal blending is essential, as interference with the initial blending technique plays havoc with the mixing phase. Pouring and squeezing of the sample, has to be precisely timed for consistent results and higher room temperatures cause sluggish mixing shear rates. The close packing phenomenon is highly sensitive to sample preparation and the causes of the phenomenon remain baffling. The subsequent sample rigidity phenomenon experienced when examining a variation in w/c ratio was the result of insufficient torque rather than the close packing phenomenon just discussed.

7.3 Use of the APC Mix Procedure

The APC Mix Procedure, as has been shown, required considerable fine tuning to perform consistently the scope of testing outlined in section 7.1. In order to use the procedure, as itemised in section 6.5, the following checks and monitoring functions were incorporated.

Dust covers were removed daily from the rheometer and computer. The glass bowls of the compressed air filter system were dried of condensation after each session. The air bearing was checked occasionally as described in Chapter 3. The zero gap setting, also described in Chapter 3, was checked before commencing a run session, by averaging 4 readings. The fluctuation in these readings is shown in Fig.7.2

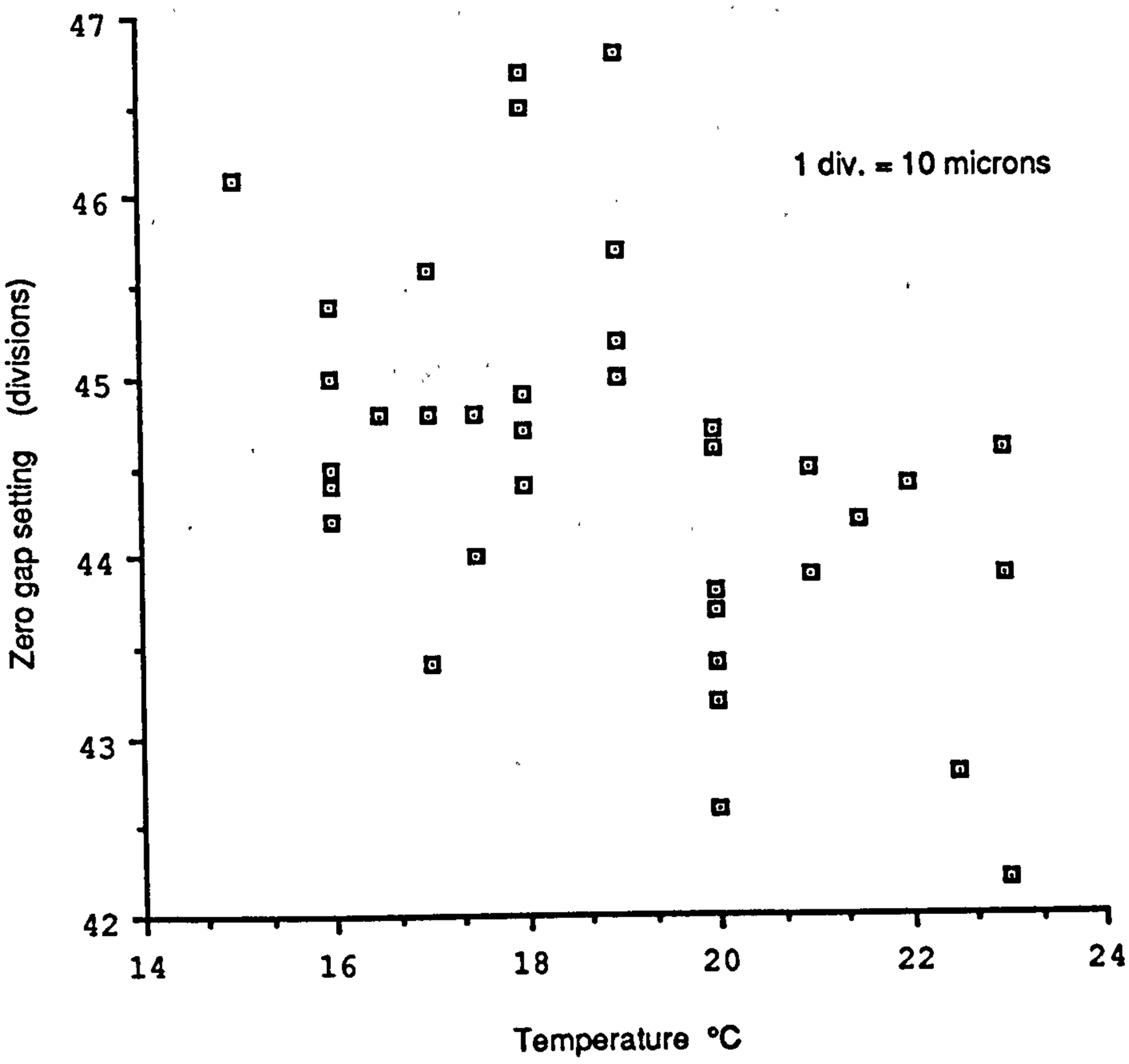

Fig. 7.2 Plot of Gap Setting against Room Temperature

The reading is in divisions into which the micrometer thumbwheel is divided and reflects the division at which the zero gap occurred. Consistently lower readings would indicate wear and higher readings an increase due to thermal expansion. The readings show very little wear has taken place, the sample standard deviation being less than 10μm. The temperature effect, according to Carri-Med, is approximately 0.5μm of gap reduction per ^{o}C increase in temperature. The temperatures given in Fig. 7.2 are those of room air temperature within a distance of 0.5m of the rheometer measuring system and taken at the time of zero gap setting. Room air temperatures did vary by up to 4^{o}C due to over-heating of the compressor motors and laboratory ovens. Cooling by the draught from the air bearing air outlets is not reflected by these values. However room temperature increases were recorded during the course of a testing session, since these affected sample preparation prior to loading into the rheometer.

A laboratory clock was used to record the following times for each run.

1. start of mixing
2. stop mixing
3. completion of standing time
4. start of applied stress
5. start of shear rate

These times were identified by changes in the angular velocity digital display in the case of items 1, 2 and 3 and by computer display with items 4 and 5. To assess the time that mixing stopped, the additional time to account for inertia was also recorded, which was when the measuring system finally came to rest. This additional time was

in most cases matched by the time between completion of standing time and start of applied stress, a period of approximately 3 seconds. In the early tests with short standing times the times for items 4 and 5 were identical. Table 7.2 shows the additional time of standing between the specified standing time and the time at which the sample yielded for each run concerned. The rates of applied stress, in code form, are also given for each run in Table 7.2. The lower additional times should relate to the higher rates of applied stress since the yield stress should be reached sooner. Generally, this is the case with a few exceptions which indicate the delicate nature of the strength of the cement slurry in that it could survive the test or fail unexpectedly.

The weights of water, cement and slurry sample were measured and recorded to 2 decimal places of a gram for each run. The water and cement was always to within ± 0.02 g of that required. The weight of the sample was generally between 16.0 and 18.0 g. As the sample was poured from the beaker into the annulus, control over the weight was not possible. Any excess slurry was squeezed out of the measuring annulus by the cone. The excess slurry formed a bund around the annulus which was found not to take part in the mixing phase of the sample between the measuring plates. The shape of the meniscus bulge did change with varying size of sample. Notes on this experimental observation were made as well as when overspill of the sample occurred. Estimates were also made of the reduction in sample size, as a result of shrinkage at the completion of a run. During mixing the meniscus bulge changed to a concave profile on being sheared and on standing the profile was noted as having moved inward towards the centre, between the plates.

These estimates together with sample weights for the runs concerned are given in Table 7.3. Fig. 7.3 shows some typical overspills and final meniscus shapes in cross-section.

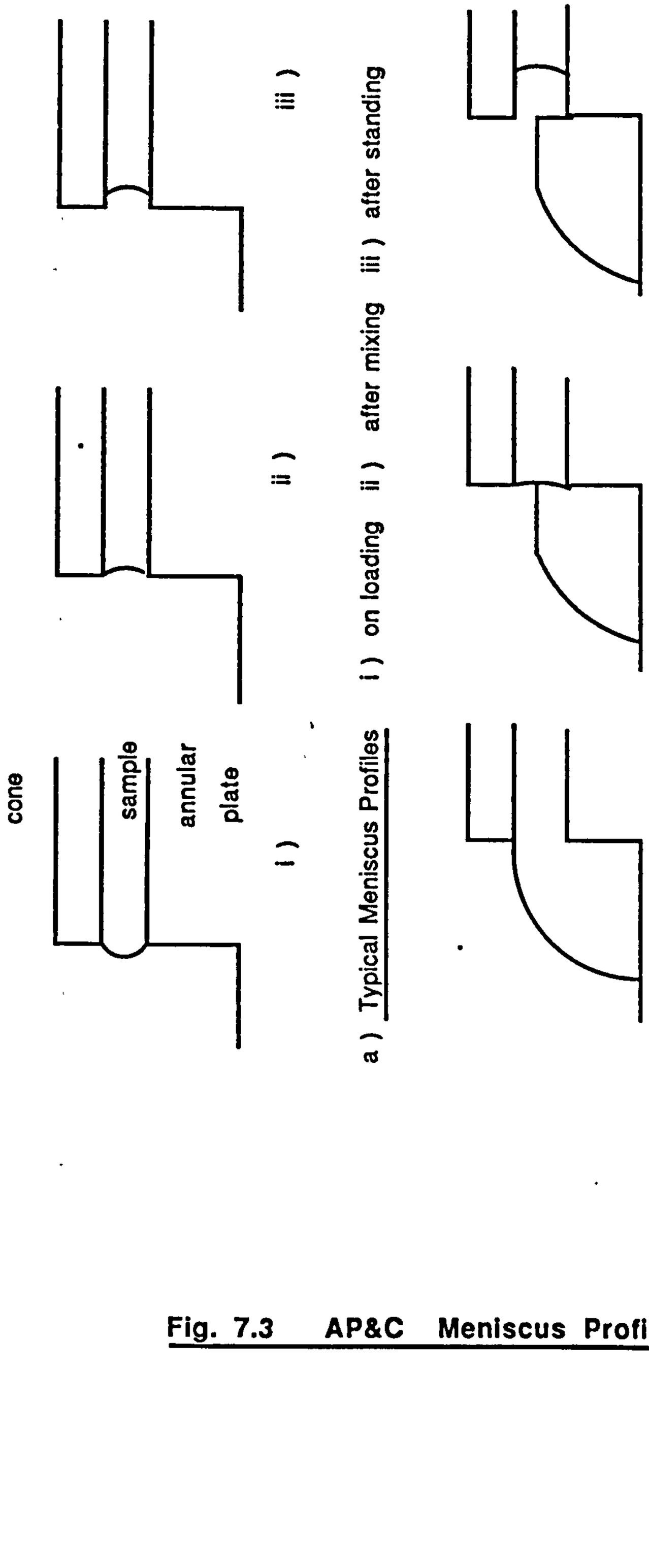

Fig. 7.3 AP&C Meniscus Profiles

Table 7.2

Run ref. No.	Standing Time (min:sec)	Rates of Applied Stress (see code below)	Additional time to yield (min:sec)
9/34	11:43	2	0:09
9/35	"	3	0:13
9/36	"	4	0:17
9/37	"	4	0:28
9/38	"	3	0.13
9/39	"	2	0:11
9/40	"	1	0:09
9/41	"	1	0:30
9/42	"	2	0:30
9/43	"	3	0:30
9/33	"	4	0:32
10.01	30:00	4	2:52
10/02	"	3	1:27
10/03	"	2	0:48
10/04	"	1	0:52
10/05	"	1	0:33
10/06	"	2	050
10/07	"	3	0:11
10/08	"	4	2:23
10/09	"	4	1:37
10/10	"	3	0:37
10/11	"	2	0:38
10/12	"	1	0:34
10/13	"	1	0:28
10/14	"	2	0:37
10/15	"	3	0:49
10/16	"	4	1:33
10/17	"	4	1:53

10/21	20:00	3	0:25
10/22	"	3	0:23
10/23	"	3	0:35
10/24	"	3	0:30
10/25	"	3	0:31
10/26	"	4	no yield
11/01	"	4	2:27
11/02	"	4	3:59
11/03	"	4	0:43
11/04	"	4	0:56
11/06	"	4	2:04
11/07	"	1	0:34
11/08	"	1	0:24
11/09	"	1	0:21
11/10	"	1	0:48
11/11	"	1	0:25
11/12	11/43	7	1:59
11/13	"	6	1:04
11/14	"	5	0:40
11/35	"	3	0:52
11/36	"	3	0:17
11/37	"	3	0:40
11/38	"	3	0:07
11/39	"	3	0:10
11/40	"	3	0:45
11/41	"	3	0:25
11/42	"	3	0:07

Rates of applied	code	1	2	3	4	5	6	7
stress	dyne/cm^2/min	2000	1500	1000	500	400	200	100

With the larger samples overspill occurred prior to mixing. The spillage occurred over one section of the periphery and during the build up to maximum angular velocity, in the mixing phase, the length of spillage increased around the circumference. The collapse of the meniscus and over-spill appeared to be dragged slowly around the circumference with angular velocities up to 28 radians/sec. but no further progression of the spillage occurred at 32 radians/sec. With lower maximum angular velocities of up to 20 radians/sec., during the mixing phase, the meniscus bulge collapsed but seeping and oozing, around the periphery, was not observed. Invariable eccentricity of the sample occurred, even to a very small degree, however carefully the sample was loaded. This eccentricity was confirmed by the difference in meniscus bulge around the periphery on loading.

7.4 Graphs of Yield Stress against Mixing Energy

The graphs of yield stress against mixing energy for a 0.44 w/c ratio class G cement slurry having undergone various standing times since completion of the mixing phase, are shown in Fig. 7.4. The yield stress used here is the earliest stress monitored that produces continuous flow, which is as previously defined. The energy per unit mass is that obtained from the area under the peak hold shear rate against mixing time using the programme in Appendix 2. Table 7.4 shows the values of τ_y and E_T/M abstracted from the computer data and the results of a linear regression on the original results. Two sources of error were identified, the observed undercut of the sample prior to testing and the variation in sample weights. A correction to the data was required to account for these errors. The correction factor to be muliplied by the original data is also given in Table 7.4. The way these factors are determined will now

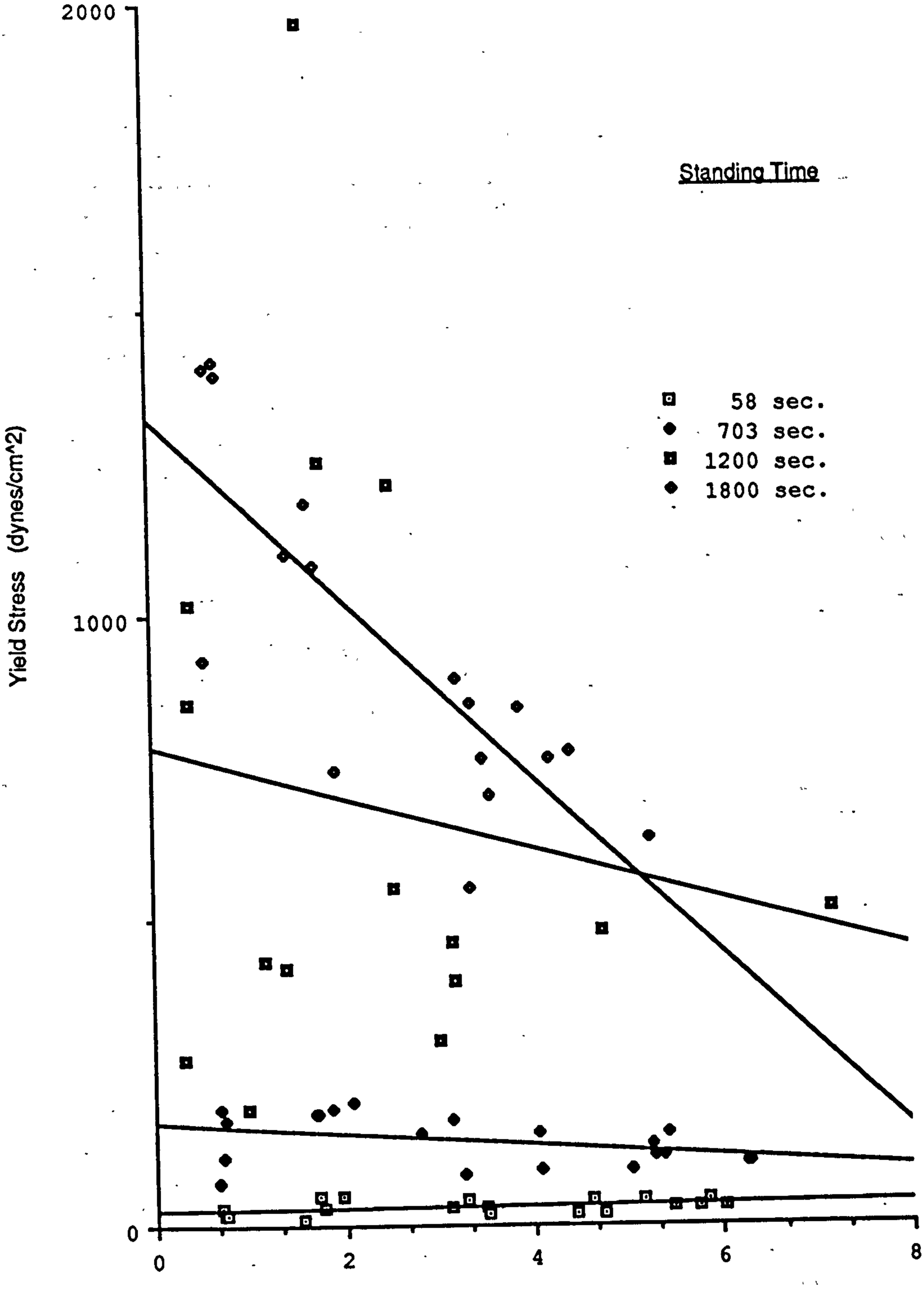

Fig. 7.4 **Graph of Yield Stress against Mixing Energy**

Table 7.3

Run Ref. No.	Sample wt. (g)	Estimated undercut after standing (mm)	Comments
9/05	16.02		
06	16.06		
07	16.03		
08	16.29		
09	16.34		small over-squeeze
10	16.06		
11	16.61		bleedwater on cone surface after test.
12	16.38		
13	16.14		
14	17.32		
15	17.68		
16	16.11		
17	17.26		
18	16.06		
19	16.38		
20	16.08		bleedwater on cone surface after test.
21	16.38		
22	16.58		
23	16.48		
24	16.61		
25	16.16		
26	16.51		
27	17.85	1.0	bleedwater on cone after test
28	18.52	1.0	
29	16.35	1.0	
30	17.15	0.5	
31	17.29	0.5	3mm eccentric undercut after test
32	16.44	0.5	
33	18.15	0.5	
34	17.77	1.0	
9/35	16.47	0.5	1.5mm eccentric undercut after test
36	16.08	1.0	

Table 7.3 (cont'd)

Run Ref. No.	Sample wt. (g)	Estimated undercut after standing (mm).	Comments
37	18.31	1.0	1.5mm eccentric undercut after test
38	16.24	1.0	
39	16.24	0.5	
40	16.76	1.0	
41	16.15	0.5	
42	16.11	1.0	
43	16.24	1.0	
44	17.94	0.5	
10/01	17.74	1.0	
02	17.22	1.0	
03	17.22	1.0	
04	16.34	1.0	
05	16.30	1.0	
06	17.67	1.0	
07	16.22	1.0	
08	16.67	1.0	
09	16.52	2.0	gap set + 50µm.
10	16.45	2.0	
11	16.07	2.0	
12	17.36	2.0	
13	16.62	2.0	
14	16.71	2.0	
15	16.07	2.0	~ 3.0 undercut after test
16	15.93	3.0	
17	16.69	2.0	~ 4.0 undercut after test
10/21	16.81	1.0	
22	17.63	2.0	
23	16.66	1.0	peak torque = 27500 dyne cm
24	16.91	1.0	
25	16.48	2.0	
26	23.00	2.0	
11/01	16.38	1.5	
02	16.34	1.5	
03	16.27	1.0	

Table 7.3 (cont'd.

Run Ref. No.	Sample wt. (g)	Estimated undercut after stadnding (mm.)	Comments
04	16.68	1.5	electrical probe moved cone prior to mixing
06	17.25	1.5	
07	17.50	1.5	
08	16.31	1.0	electrical probe moved cone prior to mixing
09	16.54	1.5	
10	16.49	2.0	slurry appeared lumpy on pouring
11	16.96	1.5	
12	17.75	2.0	
13	16.25	1.5	
14	16.79	1.5	

Table 7.4

Correction Factor for Energy/Unit mass	Run Ref No.	Energy/ Unit Mass kJ/kg	Yield stress dyne/cm^2	Standing Time sec.	Corr. Factor for τ_y	Regression Analysis on original τ_y and E_T/M
0.968	9/05	0.725	20.02	58		y = Bx + A
0.962	06	0.694	30.03			A = 26.37
0.966	07	0.711	20.2			B = 1.204
0.931	08	0.747	20.2			x=0 y =26.37
						x=5 y=32.39
0.924	09	1.725	50.5			corr.coeff =
0.962	10	1.953	50.5			0.212
0.917	11	1.767	30.3			
0.919	12	1.554	10.1			
0.951	13	3.514	20.2			
0.917	14	3.478	30.3			
0.917	15	3.126	30.3			
0.955	16	3.289	40.4			
0.917	17	4.610	40.4			
0.962	18	5.165	40.4			
0.919	19	4.740	20.2			
0.959	20	4.432	20.2			
0.919	21	5.742	30.3			
0.917	22	5.845	40.4			
0.917	23	5.480	30.3			
0.917	24	6.014	30.3			
0.948	25	6.292	101	703	1.060	
0.917	26	4.072	90.9		1.060	
0.917	27	6.266	101		1.124	y=B x + A
0.917	28	5.365	111.1		1.124	A=168.97
0.923	29	5.026	90.9		1.124	B=-9.522
0.917	30	5.412	151.5		1.060	x= 0 y=168.97
0.917	31	5.242	131.3		1.060	x=5 y=121.36
0.917	32	5.280	111.1		1.060	corr.coeff =
0.917	33	3.140	171.7		1.060	-0.446
0.917	34	2.794	151.5		1.124	
0.917	35	4.048	151.5		1.060	
0.959	36	3.274	80.8		1.124	
0.917	37	1.693	181.8		1.124	
0.937	38	1.853	191.9		1.124	
0.937	39	2.097	202		1.060	

0.917	40	1.729	181.8		1.124	
0.950	41	0.697	191.9		1.060	
0.955	42	0.727	171.7		1.124	
0.937	43	0.719	111.1		1.124	
0.917	44	0.665	70.7		1.060	
0.917	10/01	0.620	1403.9	1800	1.124	
0.917	02	0.721	1414		1.124	
0.917	03	0.556	929.2		1.124	
0.924	04	0.725	1393.8		1.124	y = Bx +A
0.929	05	1.931	747.4		1.124	A = 1322.35
0.917	06	1.445	1100.9		1.124	B = -144.66
0.940	07	1.735	1080.7		1.124	x= 0 y=1322.4
0.917	08	1.677	1181.7		1.124	x=5 y=599.0
0.917	09	3.503	767.6		1.272	corr. coeff
0.917	10	3.362	555.5		1.272	= -0.806
0.961	11	3.386	858.5		1.272	
0.917	12	3.894	848.4		1.272	
0.917	13	5.268	636.3		1.272	
0.917	14	4.232	767.6		1.272	
0.961	15	4.442	777.7		1.272	
0.981	16	3.587	707		1.449	
0.917	17	3.231	898.9		1.272	
0.917	21	0.310	272.7	1200	1.124	
0.917	22	0.988	191.9		1.272	
0.917	23	2.541	555.5		1.124	
0.917	24	3.192	400.0		1.124	y = B x + A
0.917	25	7.185	522.2		1.272	A = 786.58
0.919	11/01	2.550	1212		1.195	B = -41.38
0.924	02	1.671	1969.5		1.195	x = 0 y =786.6
0.933	03	3.023	303		1.124	x = 5 y =579.7
0.917	04	1.188	434.3		1.195	corr coeff = 0.157

0.917	06	0.413	1020.1		1.195
0.917	07	0.398	858.5		1.195
0.928	08	1.410	424.2		1.124
0.917	09	3.173	464.6		1.195
0.917	10	1.828	1252.4		1.272
0.917	11	4.760	484.8		1.195
0.917	12	0.901	181.8	705	1.272
0.936	13	0.868	191.9	705	1.195
0.917	14	0.710	212.1	705	1.195

be explained.

The yield stress is obtained from $\tau_y = F_\tau . T$, where T is the torque measured on the rheometer. Stress correction due to undercut, or reduced value of R_1, is achieved by using the correction factor equal to

$$\frac{(R_{1corr}^3 - R_2^3)}{(R_1^3 - R_2^3)}$$

R_{1corr}. is an observed estimate of the reduced radius of the sample at the completion of the standing time.

The sample weight of 15.6g was found to produce undercut, whereas 16.0g gave a good bulge to the meniscus. The ideal meniscus profile is a spherical shape with its centre at the centre of the annular plate, which gives an imperceptible bulge of 0.02mm and an undercut on the cone surface of 0.07 mm. Because of slight eccentricity, when loading the sample, and variation in sample spread, when squeezing to the correct gap setting, samples larger than 16.0g were used. The meniscus bulge or surface tension was destroyed on shearing the sample and excess sample was spilled. The excess sample did not then receive shearing energy. The maximum amount of sample to receive energy is estimated at 16.4 g and the minimum to ideally fill the meniscus is estimated at 15.8g. The correction to the energy per unit mass or E_T/M is proportioned over this range by,

$$E_{T/}M = \frac{\sigma\dot{\gamma}t}{\rho} = F_{\gamma}F_{\tau}\frac{T\omega\tau}{\rho} = \frac{T\omega t}{V\rho} \qquad 7.1$$

$$E_T/M_{corr.} = \frac{V}{V+V_{add}}\ E_T/M = \frac{1}{1+\frac{Wadd}{6.588}}\ E_T/M \qquad 7.2$$

where 6.588g is the weight of the sample under test between the cone and the annular plate, which is bounded by the radii, $\dot{R}_1$ and R_2. $W_{add.}$ being any additional weight

of sample over 15.8g but not exceeding 16.4g. The corrected τ_y and E_T/M are given in Table 7.5, together with the rates of applied stress during the testing phase. The linear regression analysis was made for the corrected data and for the data split into groups of rates of applied stress, shown in Table 7.6. The correlation coefficients for the corrected data did not show any improvement on the original data, and even with

the data split as above there was no linear relationship between τ_y and E_T/M .

However the yield stress increased with increase in standing time and decreased with increase in mixing energy per unit mass. Although very little change in yield stress was found with increase in mixing energy at the short standing time of 58 seconds. To see if the additional standing time shown in Table 7.2, which comes from the time it takes during the testing phase to reach yield stress, had any effect on the results, the hydration time was plotted against $\tau_y/\rho E_{T/M}$ for each variation in standing time. These graphs are shown in Figs. 7.5 to 7.8, which show the four standing times and expand the trends which are hidden by the scale of Fig. 7.4.A similar exponential curve emerges in each case, but the points in the 1200 second standing time curve, which do not fit ,were all found to be of much lower shear rates during the mixing

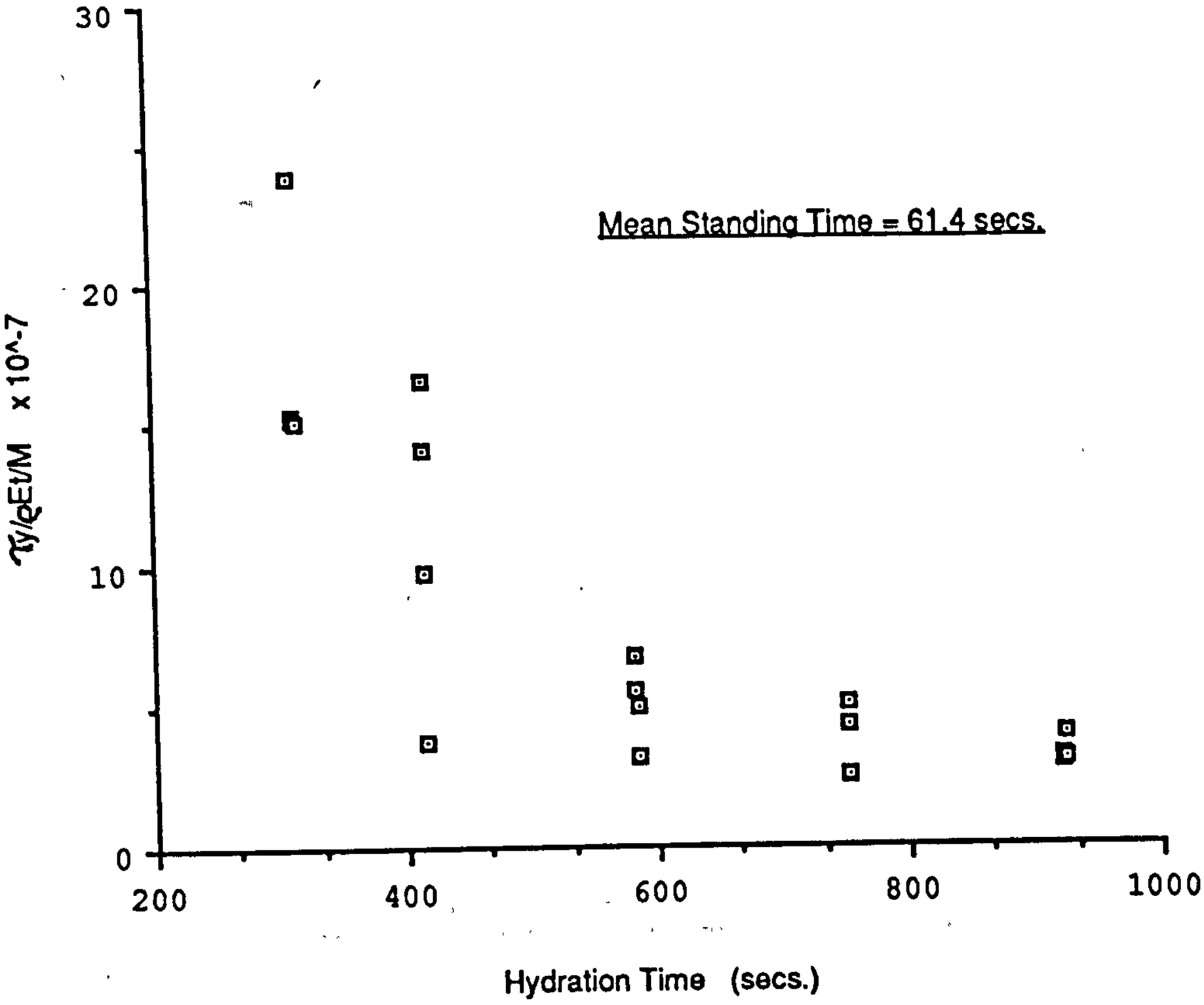

Fig. 7.5 Graph of τy/ρEt/M against Hydration Time

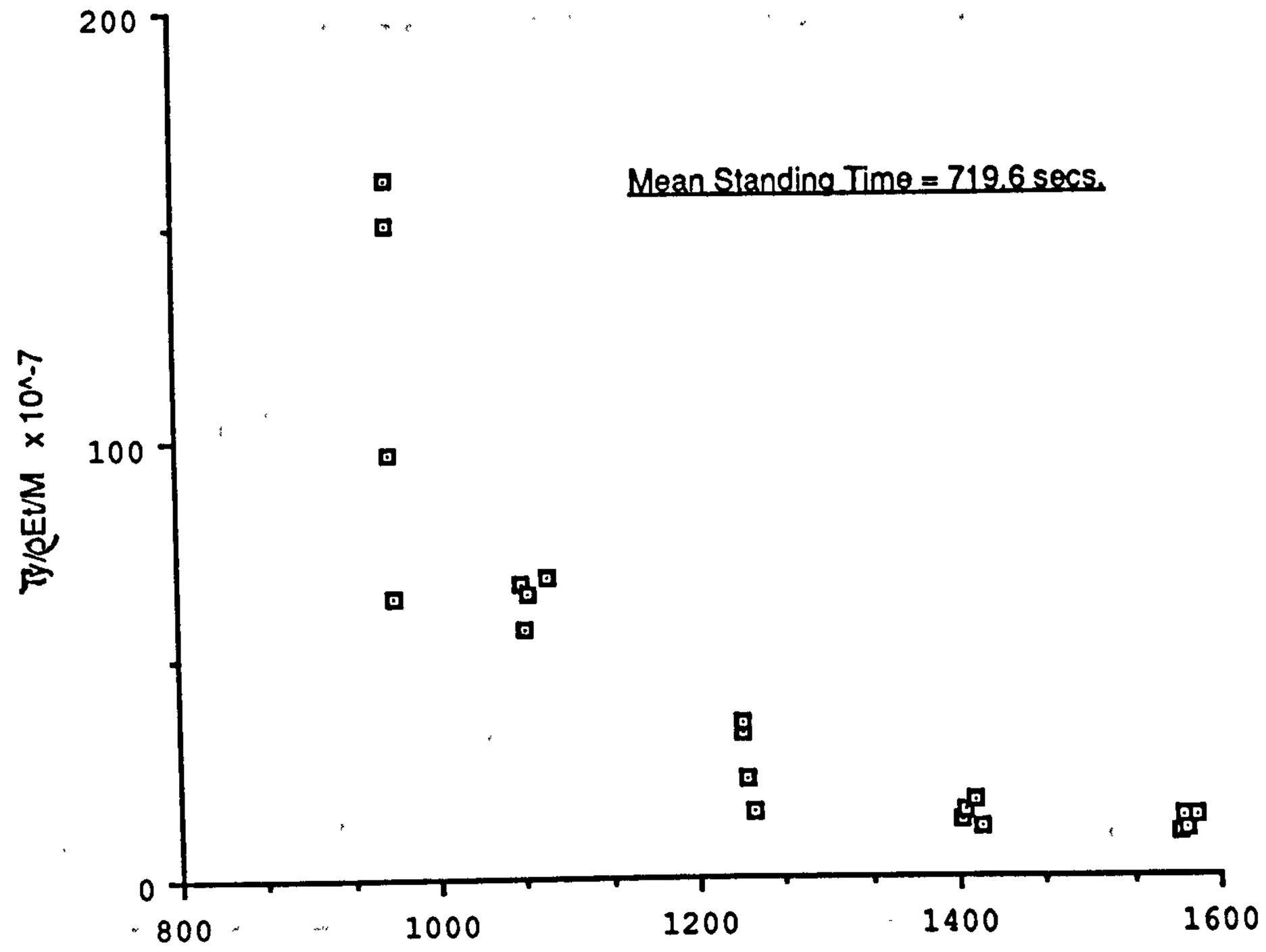

Fig. 7.6 Graph of τy/ρEt/M against Hydration Time

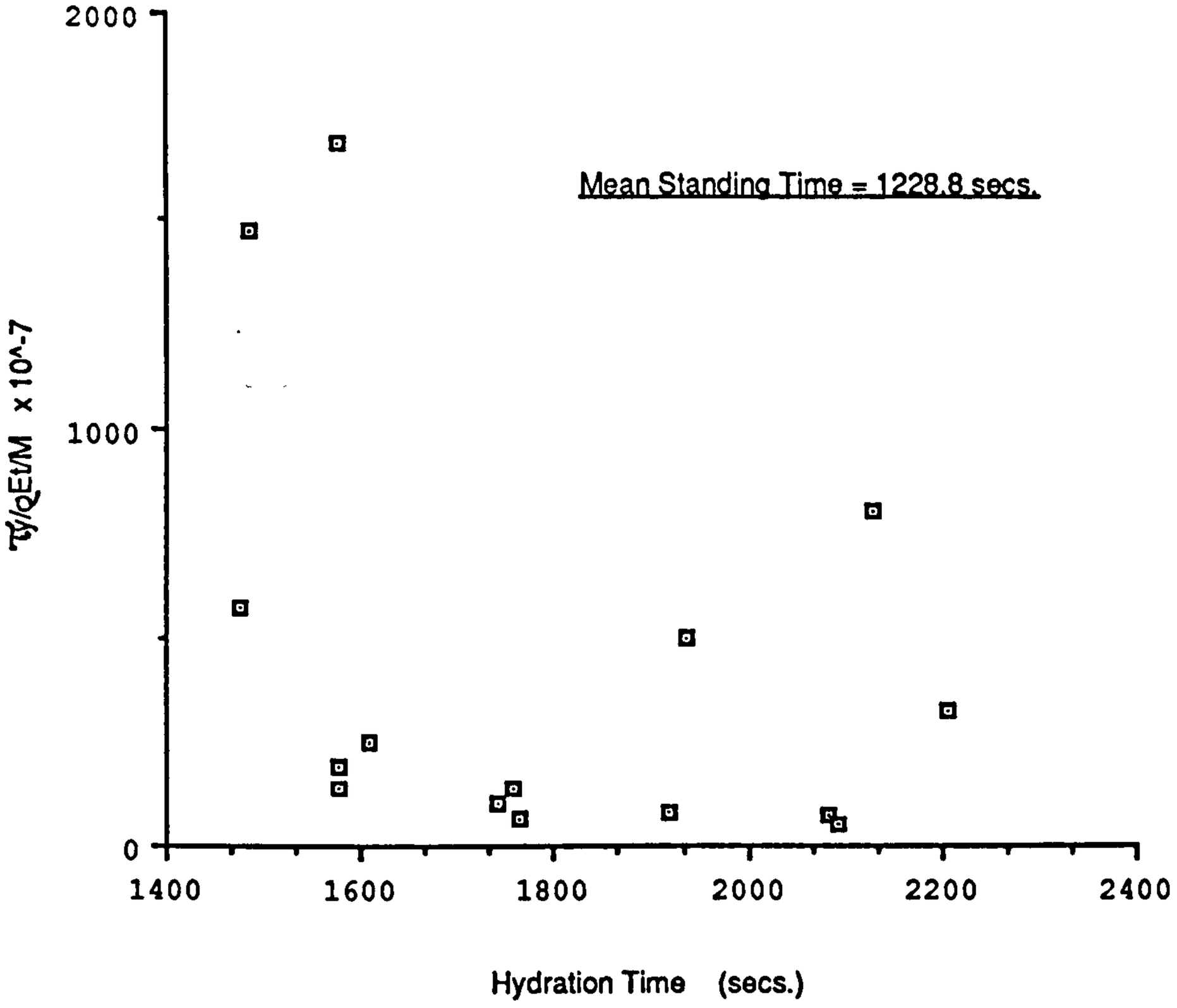

Fig. 7.7: Graph of τy/ρEt/M against Hydration Time

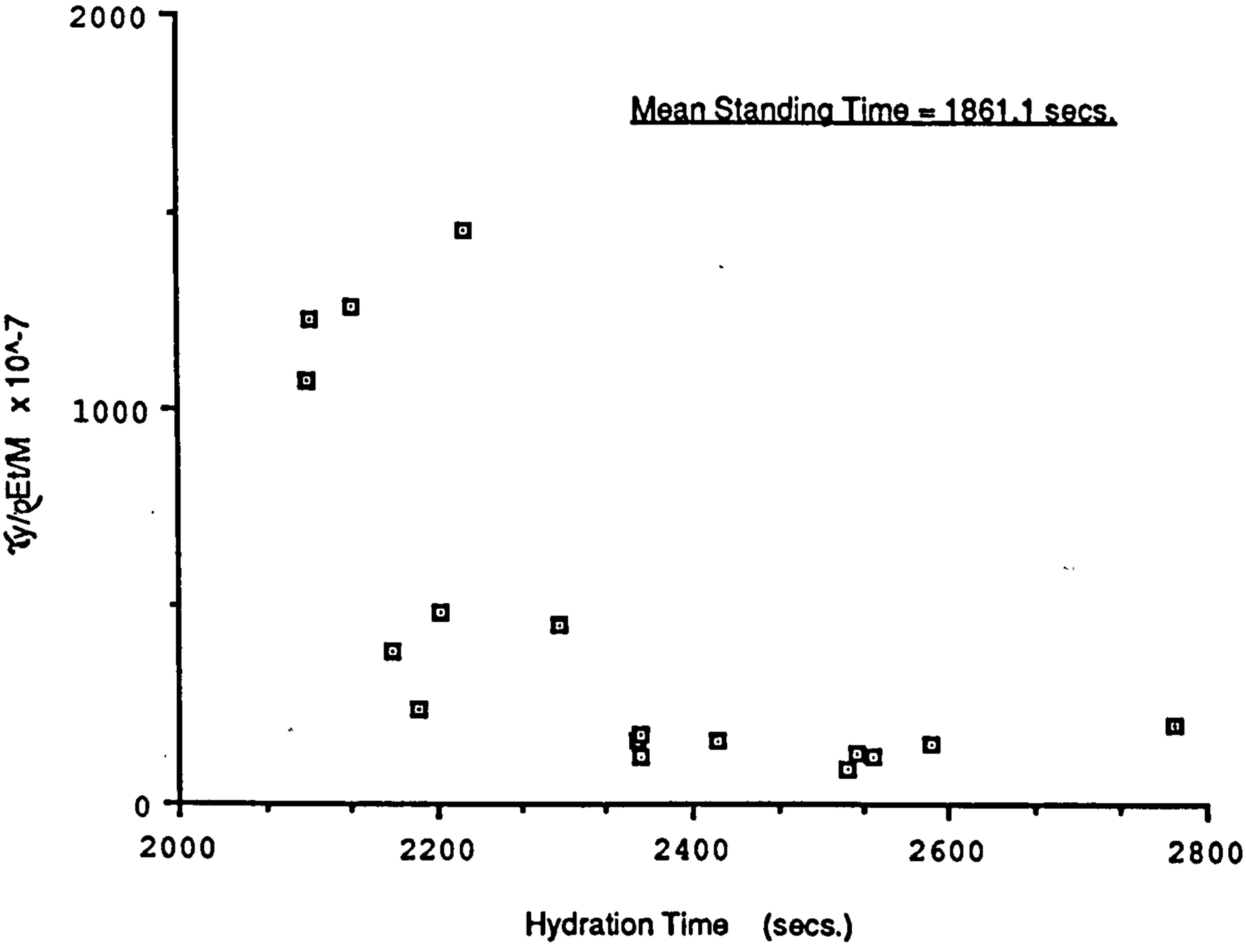

Fig. 7.8 Graph of τy/ρEt/M against Hydration Time

Table 7.5

Run Ref No.	Corrected Energy/ Unit Mass	Corrected Yield Stress	Rate of Applied Stress (see code) (Table 7.2)
9/05	0.702	20.2	4
/06	0.668	30.3	3
/07	0.687	20.2	2
/08	0.695	20.2	1
/09	1.594	50.5	1
/10	1.879	50.5	2
/11	1.620	30.3	3
/12	1.428	10.1	4
/13	3.342	20.2	4
/14	3.189	30.3	3
/15	2.867	30.3	2
/16	3.141	40.4	1
/17	4.227	40.4	1
/18	4.969	40.4	2
/19	4.359	20.2	3
/20	4.250	20.2	4
/21	5.277	30.3	4
/22	5.360	40.4	3
/23	5.025	30.3	2
/24	5.515	30.3	1
/25	5.965	107.1	1
/26	3.734	96.0	2
/27	5.746	113.5	3
/28	4.920	124.9	4
/29	4.639	102.2	4
/30	4.963	160.6	3
/31	4.807	139.2	2
/32	4.842	117.8	1
/33	2.879	182.0	1
/34	2.562	170.3	2
/35	3.712	160.6	3
/36	3.140	90.8	4
/37	1.552	204.3	4
/38	1.736	215.7	3
/39	1.965	214.1	2
/40	1.585	204.3	1
/41	0.662	203.4	1
/42	0.694	193.0	2
/43	0.674	124.9	3
/44	0.610	74.9	4

Run Ref. No	Corrected Energy/ Unit Mass	Corrected yield Stress	Rate of Applied Stress
10/01	0.569	1578.0	4
/02	0.661	1589.3	3
/03	0.510	1044.4	2
/04	0.670	1566.6	1
/05	1.794	840.1	1
/06	1.325	1237.4	2
/07	1.631	1214.7	3
/08	1.538	1328.2	4
/09	3.212	976.4	4
/10	3.083	706.6	3
/11	3.254	1092.0	2
/12	3.571	1079.2	1
/13	4.831	809.4	1
/14	3.881	976.4	2
/15	4.269	989.2	3
/16	3.519	1024.4	4
/17	2.963	1143.4	4
/21	0.284	306.5	3
/22	0.906	244.1	3
/23	2.330	624.4	3
/24	2.927	449.6	3
/25	6.589	664.2	3
11/01	2.343	1448.3	4
/02	1.544	2353.6	4
/03	2.820	340.6	4
/04	1.089	519.0	4
/05	0.379	1219.0	4
/07	0.365	1025.9	1
/08	1.308	476.8	1
/09	2.910	555.2	1
/10	1.676	1593.1	1
/11	4.365	579.3	1
/12	0.826	231.2	7
/13	0.812	229.3	6
/14	0.651	253.5	5

Table 7.6

Linear Regression of Corrected τ_y and E_T/M; $y = Bx + A$

Run Ref. Nos.	A	B	Corr. Coeff. r	y at x = 5
9/05 to 9/24	26.72	1.08	0.163	32.11
9/25 to 9/44	186.78	-11.99	-0.472	126.8
10/01 to 10/17	1451.73	-132.84	-0.713	787.5
10/21 to 11/11	934.31	-50.73	-0.145	680.6

Correlation Coefficients with Data split into Groups of Rate of Applied Stress

Run Ref. No.	Rate of Applied Stress (dynes/cm^2/min.)	Correlation coefficient
9/05 to 9/24	2000	0.085
	1500	0.215
	1000	0.185
	500	0.712
9/25 to 9/44	2000	-0.972
	1500	-0.740
	1000	-0.310
	500	-0.100
10/01 to 10.17	2000	-0.695
	1500	-0.457
	1000	-0.797
	500	-0.977
10/21 to 11/11	2000	-0.404
	1500	-
	1000	-0.809
	500	-0.191

phase. In order to account for the variation in shear rate and to assess the exponential fit the ln $\tau y/\rho E_T/M$ was plotted against $\dot{\gamma}_{max}$ x t_{hyd}. The $\tau_y/E_T/M$ was chosen because it is non-dimensional, as is $\dot{\gamma}_{max}$ x t_{hyd}. The time of hydration is the time from adding the water to the time at which yield stress is measured. The plot is shown in Fig. 7.9 giving no correlation between

$$\ln \frac{\tau_y}{\rho E_T/M}$$

and $\dot{\gamma}_{max}$ x t_{hyd} but indicating significant differences between mixing times and standing times. A plot of ln K, where

$$K = \frac{\tau_y}{\rho E_T/M}$$

the Kitching number, was made against the modified standing times as shown in Fig. 7.10 and ignoring the low mixing shear rate points mentioned earlier gave high correlation coefficients. Fig. 7.11 shows the plot when ln (K x $\dot{\gamma}_{max}$ x t_{mix}) was tried to overcome low shear rates by characterising the energy input but this was not successful, since long mixing times accentuate the low shear rates rather than bring them into line. ln K was plotted against mixing times and produced shallow exponential curves so the ln K was re-plotted against ln t_{mix}, these curves are shown in Fig. 7.12 and Fig. 7.13. Since these plots also show the discrepancies caused by

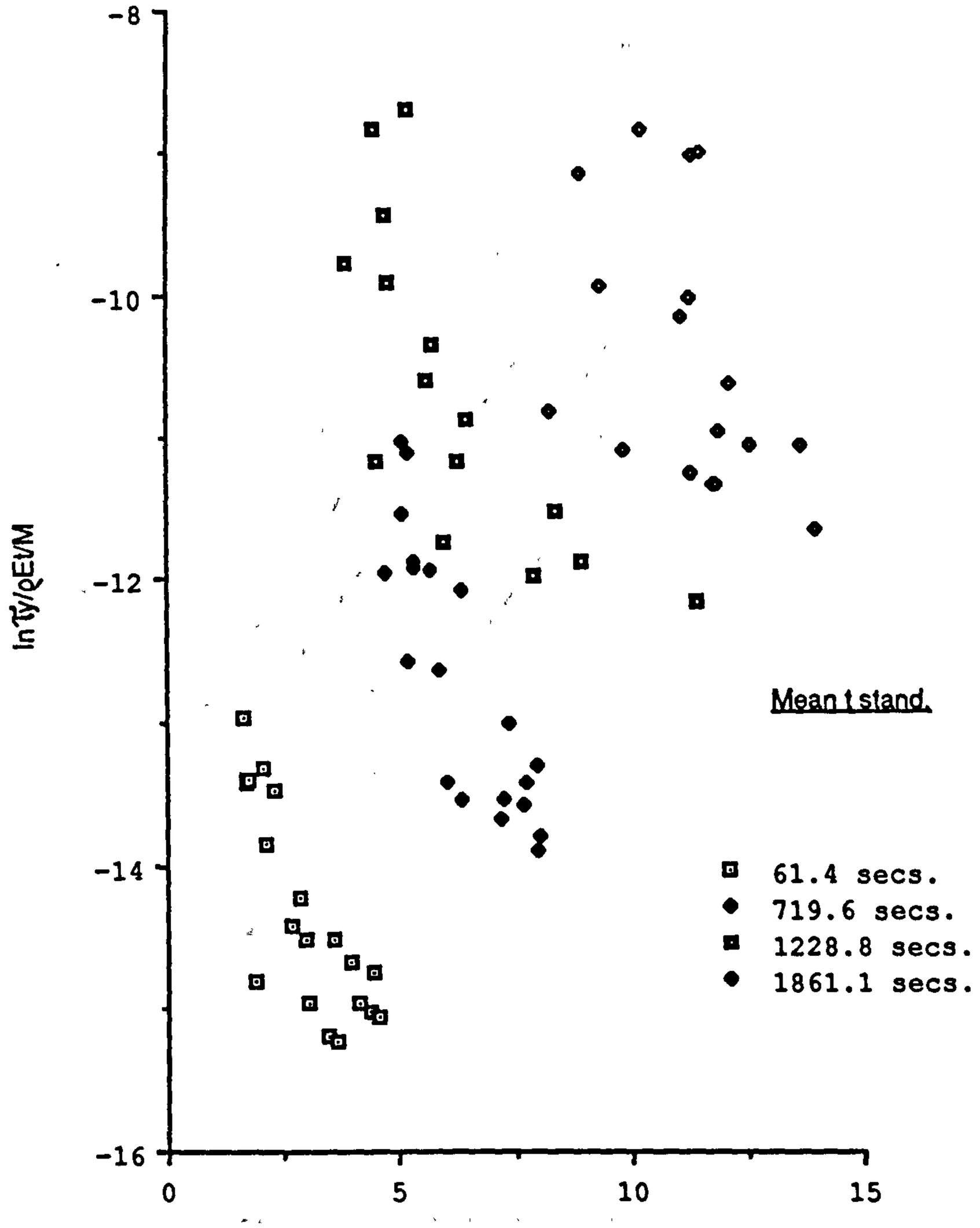

Fig. 7.9 Plot of ln Ty/QE'M against γ̇max. x t hyd.

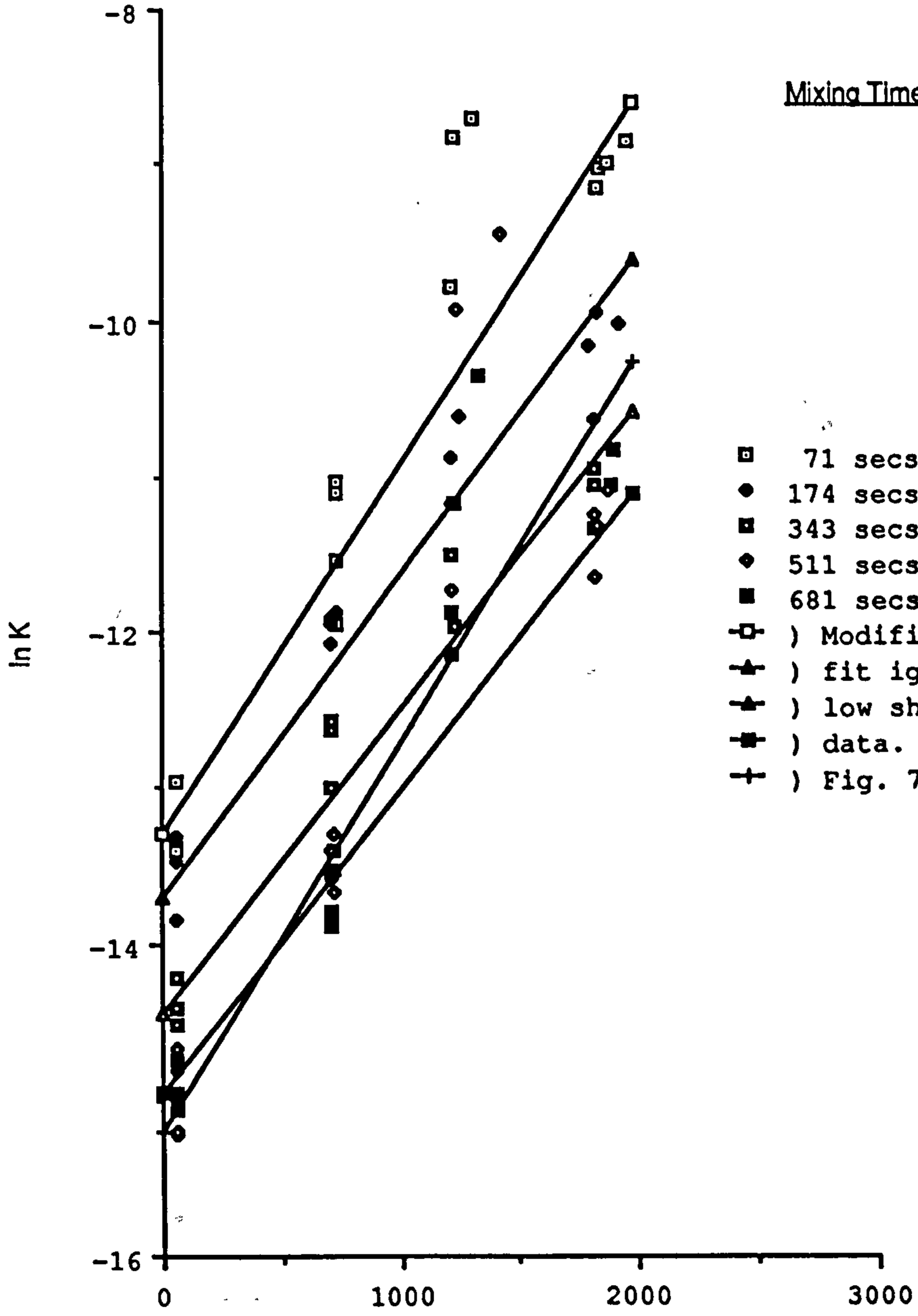

Fig. 7.10 Graphs of ln K against Standing Time

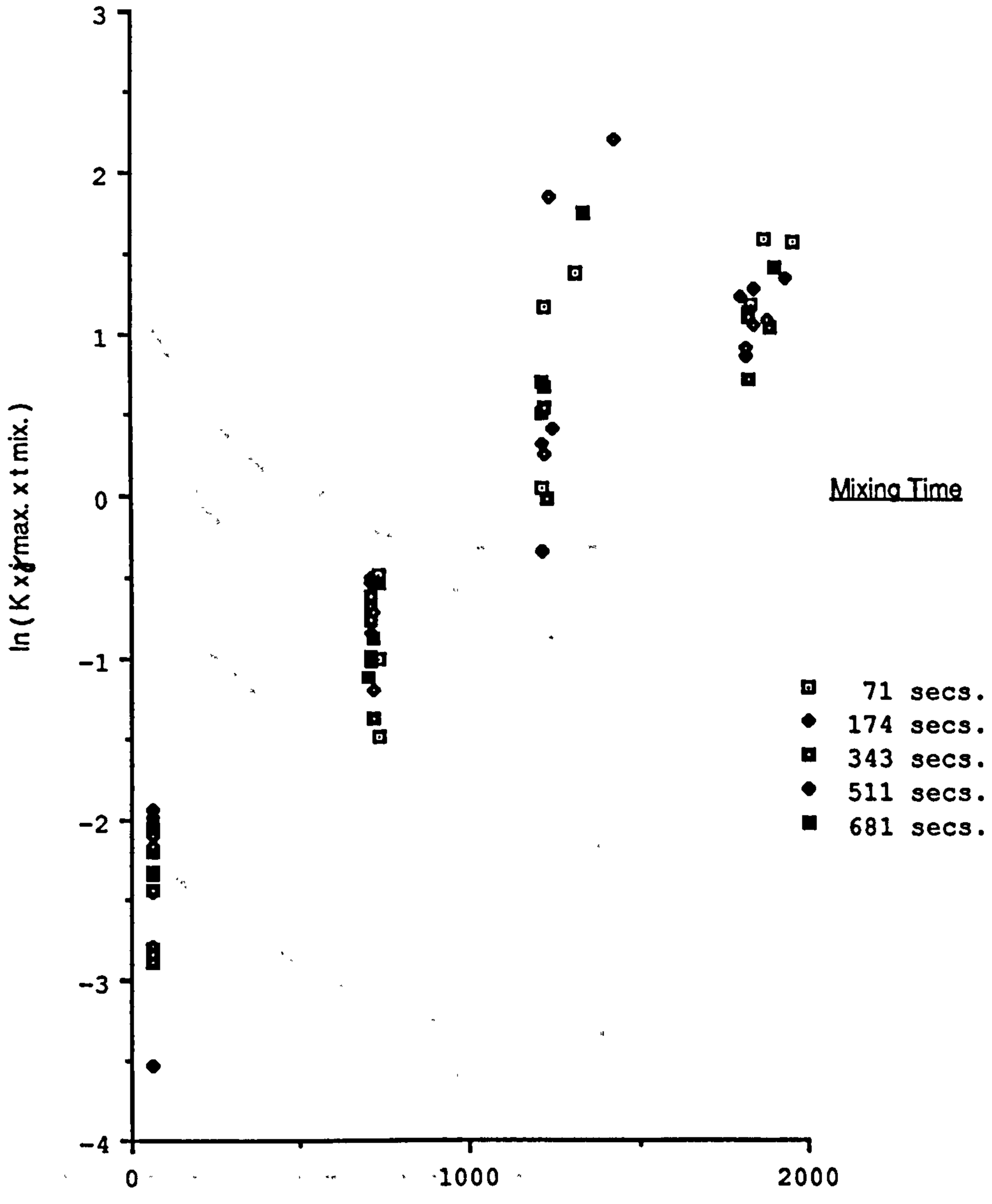

Fig. 7.11 Plot of ln (K x γmax. x t mix.) against t stand.

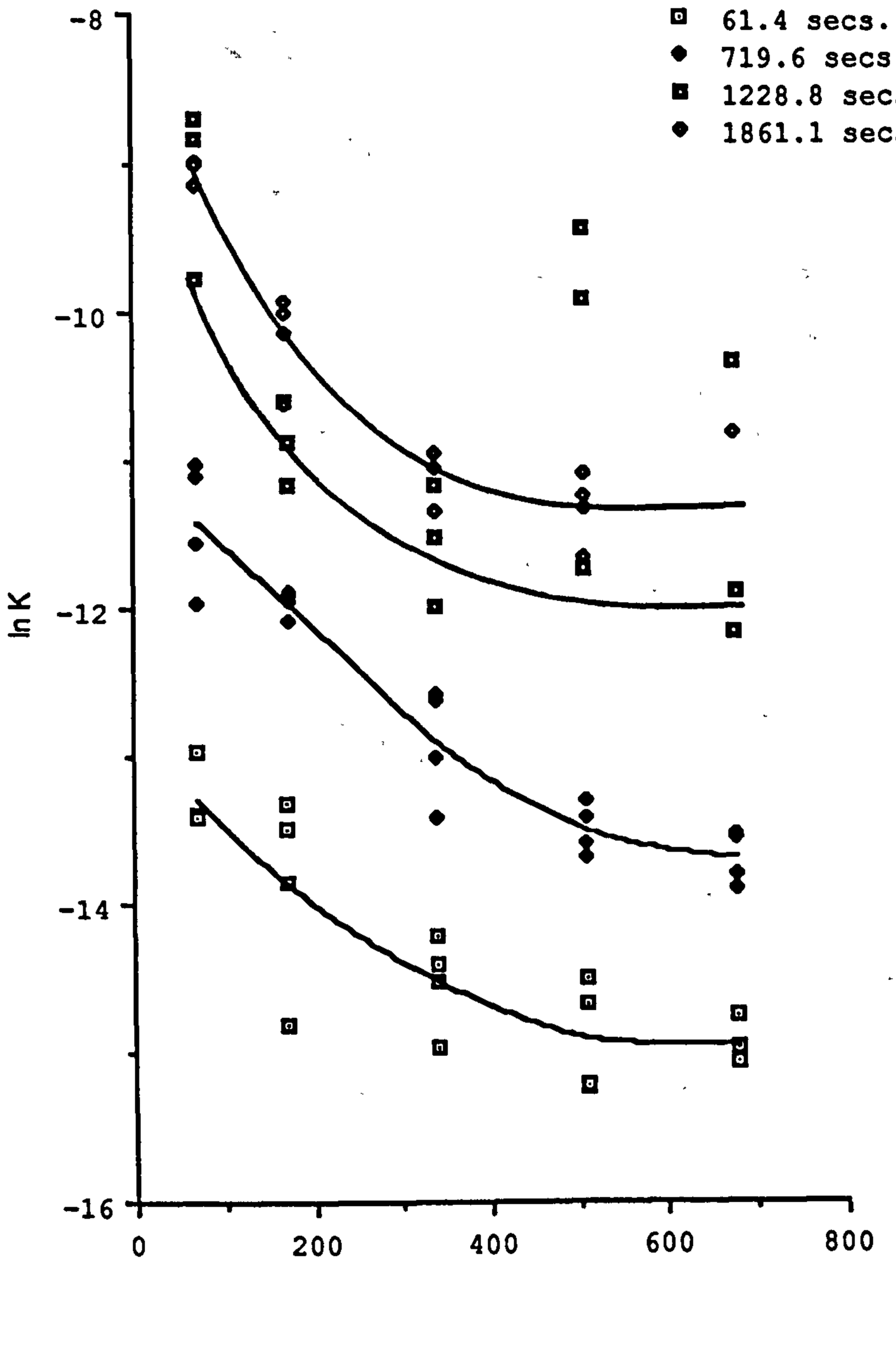

Fig. 7.12 Graphs of ln K against Mixing Time

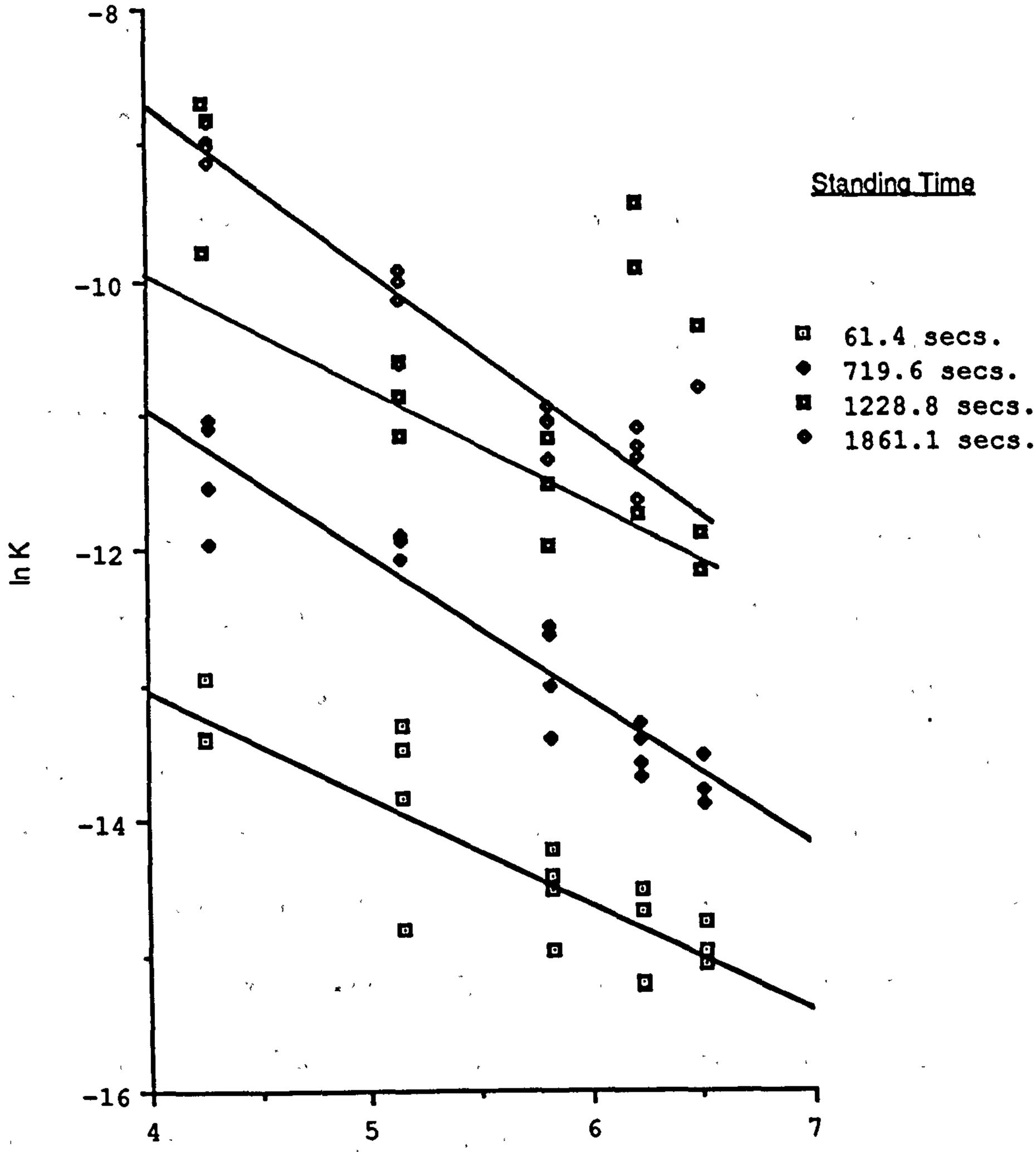

Fig. 7.13 Graphs of ln K against ln (t mix.)

the low shear rate data a plot was made of the maximum angular velocity measured during the mixing phase with ln K shown in Fig. 7.14. This shows no correlation between these parameters but there appears to be a boundary between two groups of results at about 28 rad/sec (400 sec.$^{-1}$). If Ω max exceeds 28 rad/sec then points covering the full range of ln Kare observed. If Ω max. is below 28 then only a restricted range is covered. This implies that unless the energy input reaches a threshold equivalent to a shear rate of approximately, 400 sec^{-1} the energy input cannot be compared using a proportional time basis, and it was arbitrarily decided to exclude the low shear rate points from the subsequent analysis. Sheets 1 and 2 in Appendix 4 show the data from the experiments from which the graphs were drawn. Good correlation coefficients for the linear regression of both ln K v ln t_{mix} and ln K v t_{stand} . were obtained as shown in Table 7.7. However these analyses were based on the mean value of ln K for the four rates of applied stress. Since ln (mean N) is not the same as the mean of ln N the results were re-analysed by taking the mean of K then obtaining ln K_{mean} as shown in Table 7.8. Fig.7.15 shows the relationship of ln K to ln t_{mix} on this basis. Fig. 7.16 and Fig. 7.17 show a slightly closer relationship between ln K and $(t_{stand})^{1/2}$ which is confirmed by the correlation coefficients of Table 7.8. The problem of the poor results of t_{stand} = 1200 sec. is shown on Fig. 7.16 as is the invalid relationship of ln t_{stand} to ln K.

The relationships obtained ignoring the poor t_{stand} = 1200 sec results and the t_{mix} = 681 sec. results, since by ignoring the t = 1200 sec. result there are then insufficient results for analysis at the 681 sec. mixing time, have the following forms

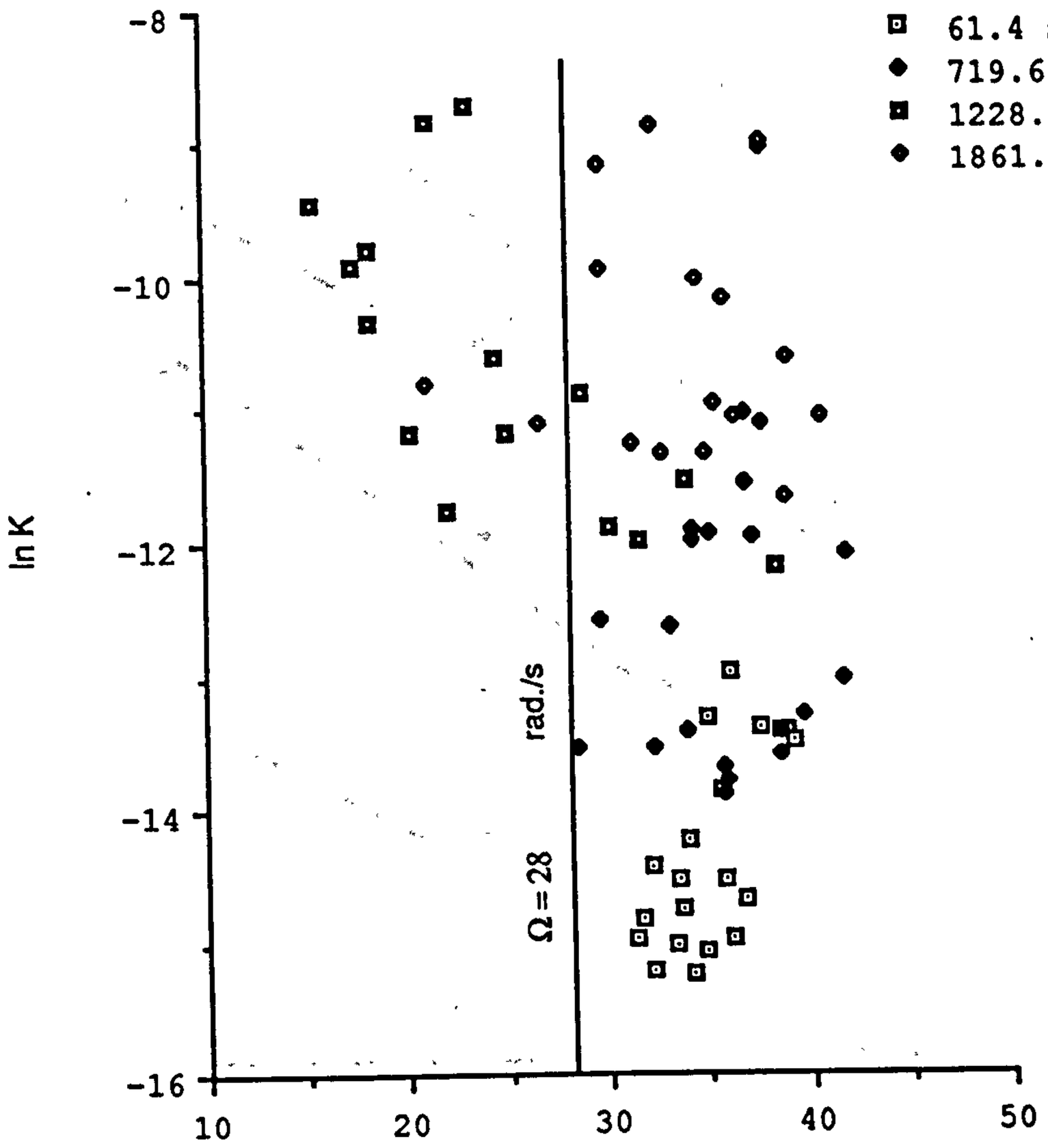

Fig. 7.14 Plot of ln K against Angular Velocity

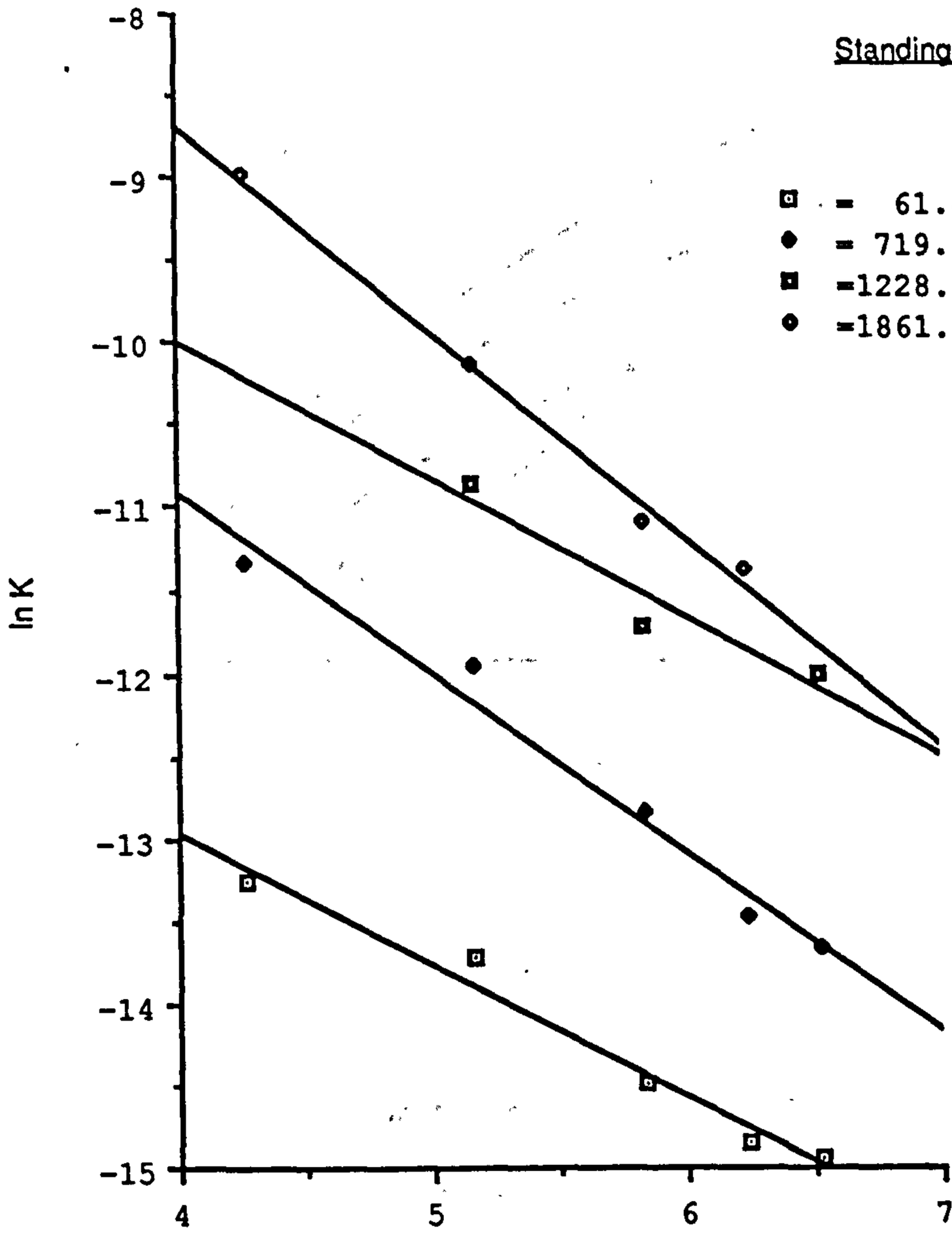

Fig. 7.15 Graph of ln K against ln t mix.

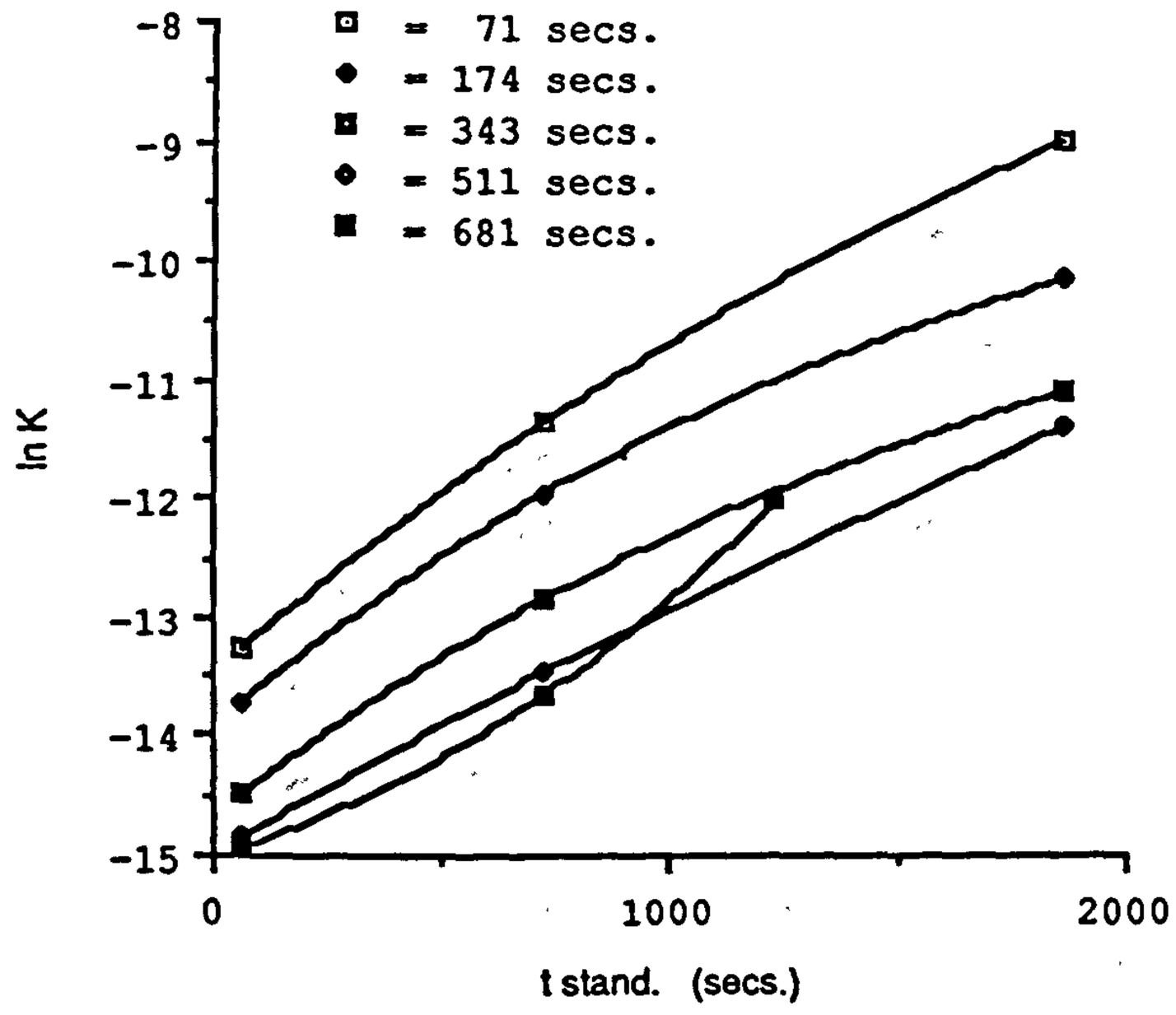

Fig. 7.16 Graphs of ln K against t stand. and ln(t stand)

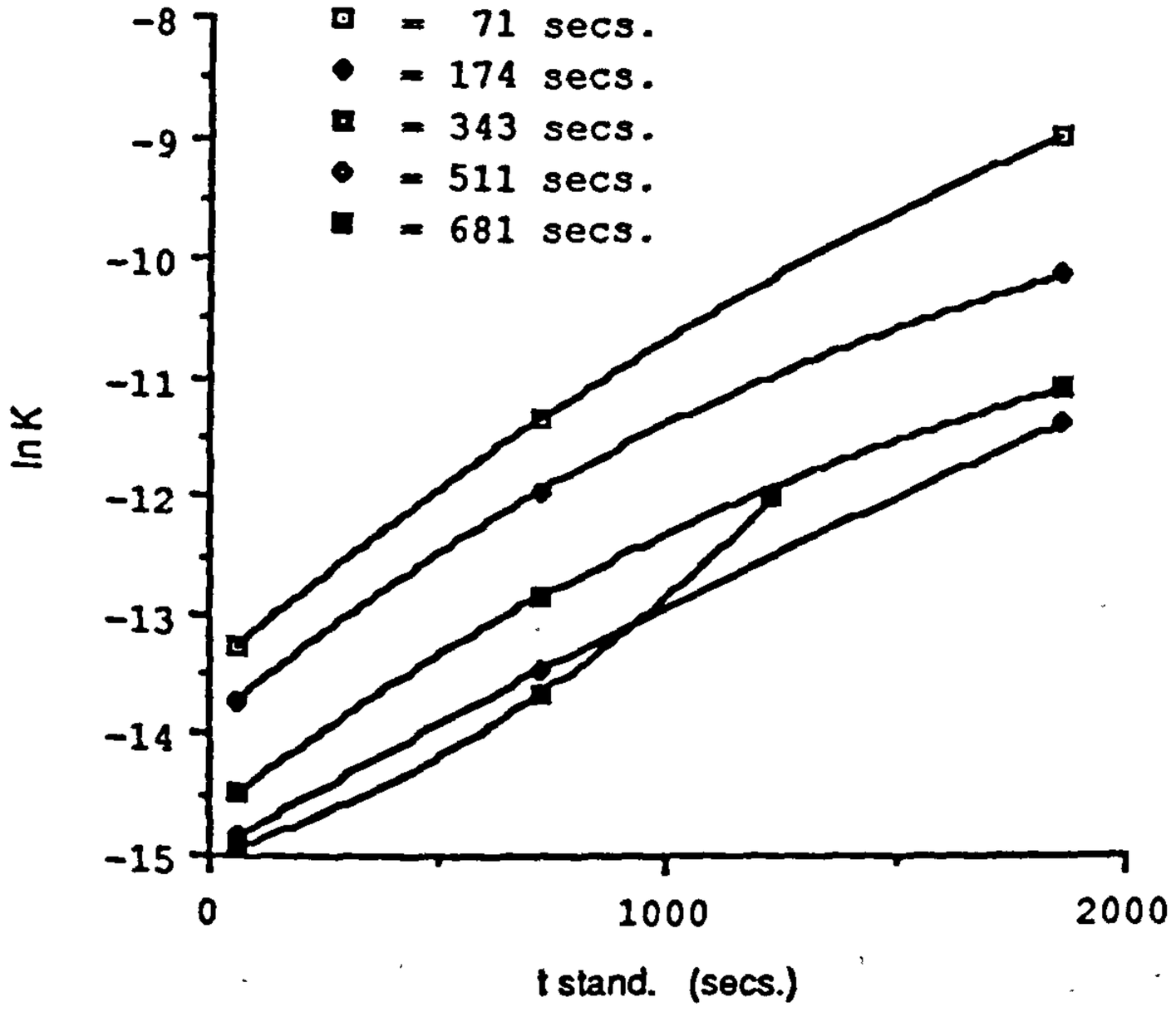

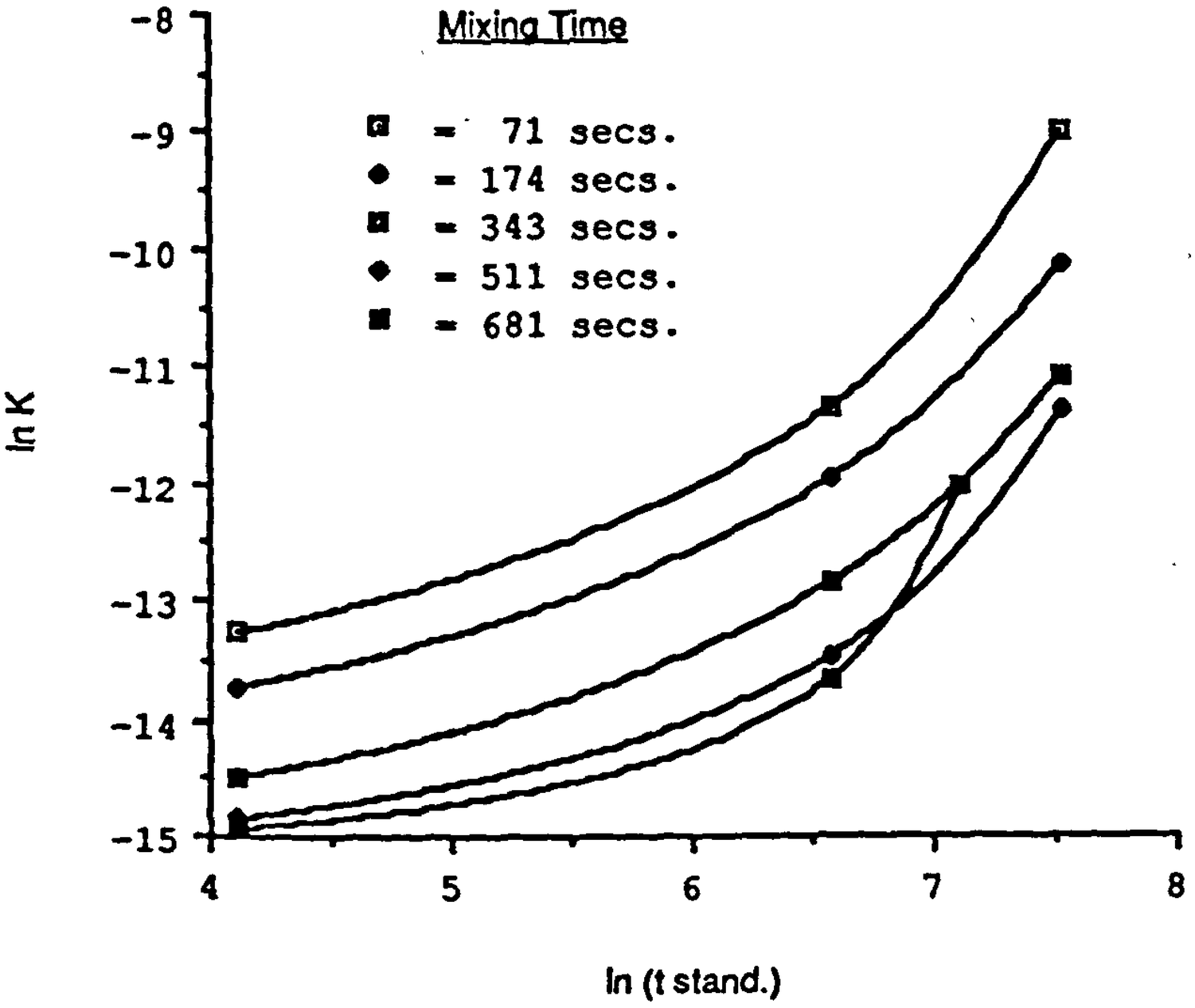

Fig. 7.16 Graphs of ln K against t stand. and ln(t stand)

Mixing Time

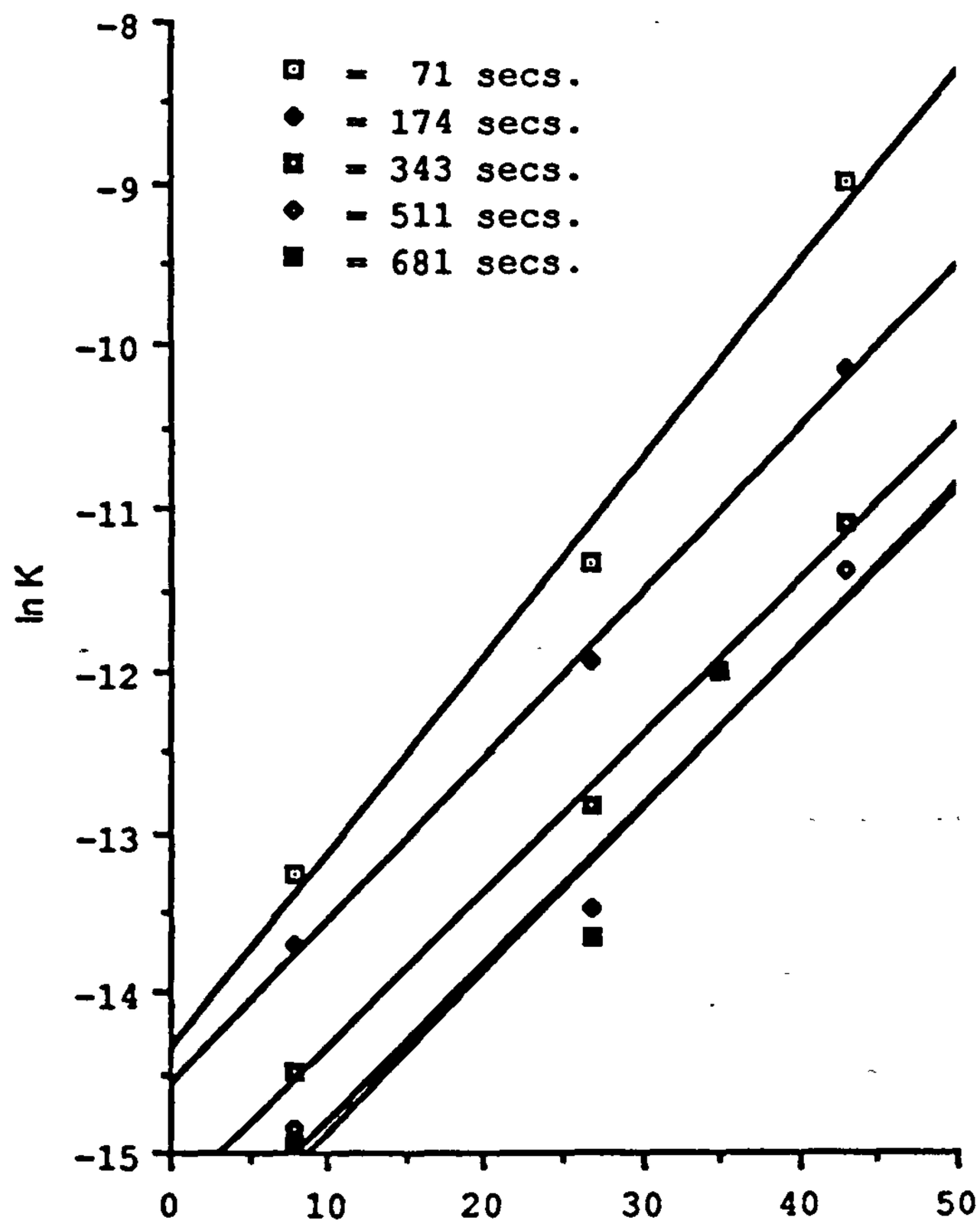

Fig. 7.17 Graph of ln K against (t stand.)^0.5

Table 7.7

Mean Values of ln K

Mean Standing Time (secs.)	Mixing Time (secs.)				
	71	174	343	511	681
61.4	-13.281	-13.855	-14.521	-14.900	-14.944
719.6	-11.407	-11.949	-12.893	-13.480	-13.674
1228.8	-	-10.863	-11.739	-	-12.012
1861.1	-8.989	-10.171	-11.093	-11.397	-

Linear Regression of ln K v ln t_{mix}

$y = Bx + A$

Standing Time (secs.)	61.4	719.6	1228.8	1861.1
A	-9.901	-6.727	-6.626	-3.697
B	-0.785	-1.062	-0.841	-1.250
Corr.coeff.r	-0.993	-0.986	-0.956	-0.997

Linear Regression of ln K v t_{stand}

$y = Bx + A$

Mixing Time (secs.)	71	174	343	511	681
A	-13.300	-13.701	-14.434	-14.961	-15.207
B	0.00236	0.00206	0.00194	0.00193	0.00248
corr. coeff. r	0.997	0.978	0.983	0.999	0.989

Table 7.8

Mean Values of K then take ln

Mean Standing Time (secs.)	Mixing Time (secs.)				
	71	174	343	511	681
61.4	-13.261	-13.714	-14.385	-14.849	-
719.6	-11.343	-11.946	-12.841	-13.469	-
1228.8	-	-	-	-	-
1861.1	-8.983	-10.138	-11.083	-11.382	-

Linear Regression of ln K v ln t_{mix}

$y = Bx + A$

Standing Time (secs.)	61.4	719.6	1861.1
A	-9.780	-6.602	-3.690
B	-0.798	-1.080	-1.248
Corr.coeff.r	-0.988	-0.988	-0.997

Linear Regression of ln K v $(t_{stand})^{1/2}$

$y = Bx + A$

Mixing Time (secs.)	71	174	343	511
A	-14.324	-14.554	-15.295	-15.762
B	0.1206	0.1011	0.0961	0.0975
corr. coeff. r	0.995	0.999	0.998	0.987

$$\ln \tau_y/\rho\, E_T/M = B_2 (t_{stand})^{\frac{1}{2}} + A_2 \qquad 7.3$$

$$\ln \tau_y/\rho\, E_T/M = B_1 (\ln t_{mix}) + A_1 \qquad 7.4$$

where A_1 and A_2 are non-dimensional intercepts and $B_2 = f(t_{mix})$ and $B_1 = f(t_{stand})$. By plotting B_2 v $(t_{mix})^{1/2}$, B_1 v $(\ln t_{stand})$, A_2 v $(\ln t_{mix})$ and A_1 v $(t_{stand})^{1/2}$ linear relationships were obtained and the better fit lines of B_1 v $\ln (t_{stand})$ and A_1 v $(t_{stand})^{1/2}$, shown in Table 7.9 were used to obtain the following formula. This formula is for the development of yield stress of an oil well cement slurry of w/c = 0.44 at 25°C having attained a maximum shear rate 400 sec^{-1} during mixing and after undergoing a known shear mixing energy per unit mass, for a known mixing time, followed by standing still for t_{stand} seconds.

$$\tau_y = \rho \frac{E_T}{M} e^{(0.1724(t_{stand})^{\frac{1}{2}} - 11.1607)} t_{mix}^{(-0.2619 - 0.1284 \ln t_{stand})} \qquad 7.5$$

This formula has proved reasonably accurate over the range t_{mix} = 60 to 700 seconds and t_{stand} = 60 to 1900 seconds, for E_T/M from 0.5 to 6.0 kJ/kg., as shown by Table 7.10 by predicting results with a mean error of 13.8% and 9.8% with standard deviations of 13.4 and 7.5, respectively, if the poor results of t_{stand} = 1228.8 sec and t_{mix} = 681 sec. are ignored. Fig. 7.18 shows the graphs obtained using the formula in predicting K.

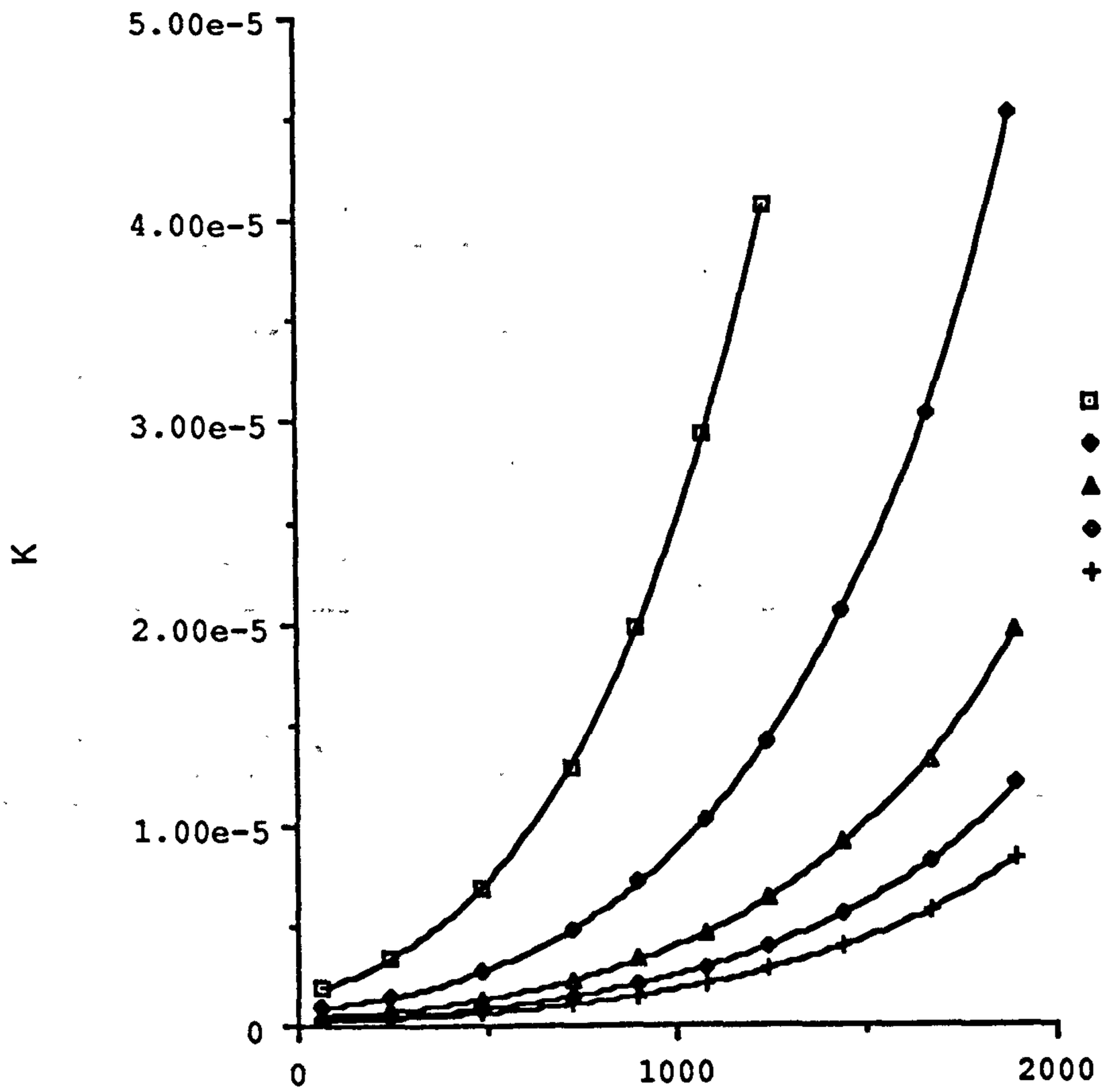

Fig. 7.18 Predicted K values for various Mixing and Standing Times

Table 7.9

Plot B_2 v $(t_{min})^{1/2}$ and B_1 v $(\ln t_{stand})$

$(t_{min})^{1/2}$	8.426	13.191	18.520	22.605
B_2	0.002343	0.001942	0.001851	0.001916
linear regression	$A_3 = 0.002470$	$B_3 = -2.916 \times 10^{-5}$	$r = -0.808$	

$\ln(t_{stand})$	4.117	6.579	7.529
B_1	- 0.798	- 1.080	-1.248
linear regression	$A_4 = -0.2629$	$B_4 = -0.1284$	$r = 0.994$

plot A_2 v $(\ln t_{mix})$ and A_1 v $(t_{stand})^{1/2}$

$\ln(t_{mix})$	4.263	5.1591	5.838	6.236
A_2	-13.259	-13.643	-14.474	-14.920
linear regression	$A_5 = -9.5168$	$B_5 = -.08461$	$r = -0.972$	

$(t_{stand})^{1/2}$	7.836	26.825	43.140
A_1	-9.780	-6.602	-3.69
Linear regression	$A_6 = -11.1607$	$B_6 = 0.1724$	$r = 1.000$

giving ,

$$A_1 = 0.1724\ (t_{stand})^{1/2} - 11.1607$$

$$B_1 = -0.1284 \ln(t_{stand}) - 0.2619$$

Table7.10

Comparison of actual and predicted K results using equation 7.5

T_{mix} (secs.)	T_{stand} (secs.)	actual $Kx10^{-6}$	predicted $Kx10^{-6}$	error %	comments
343	1228.8	8.178	6.281	-23.2*	
174	61.4	1.107	0.929	-7.1	
681	61.4	0.326	0.316	-3.0*	ignoring poor
174	719.6	6.485	4.810	-25.8	results
681	719.6	1.166	1.062	-8.9*	$t_{mix} = 681$
174	1228.8	19.154	13.950	-27.2*	$t_{stand} = 1228.8$
174	1861.1	39.548	42.713	8.0	marked *
343	1861.1	15.371	18.551	20.7	s.d. = 7.5
681	1228.8	6.132	2.806	-54.3*	mean error =
71	61.4	1.741	1.888	8.4	
71	719.6	11.852	12.969	9.4	9.8% otherwise
71	1861.1	125.526	128.446	2.3	all results
343	61.4	0.512	0.544	6.2	s.d. = 13.4
343	719.6	2.650	2.269	-14.4	mean
511	61.4	0.356	0.397	11.5	error = 13.8%
511	719.6	1.414	1.460	3.3	
511	1861.1	11.399	11.365	-0.3	

Experiments using low rates of applied stress were carried out but, as can be seen from the results in Data Sheet 1 in Appendix 4 run Ref. No. 11/12, 11/13 and 11/14, the maximum angular velocity recorded was 19.0 rad/sec., which rendered them inapplicable to the above formula and as with similar results the predicted ln K by the formula is too small.

7.5 Determination of Mixing Peak Torque for Various w/c Ratios

It was initially proposed to vary the w/c ratio from 0.36 to 0.52 thereby covering the range of w/c ratio of oil well cements, which can be considered for field use, and those which have been investigated by other researches in the past. (Tattersall and Banfill 1983, Dowell Schlumberger 1984) However the 0.36 w/c ratio proved too rigid to mix, only just managing to flow whilst using a peak torque of 500,000 dyne cm, the maximum for the Carri-Med. The 0.52 w/c ratio on the other hand exceeded the maximum angular velocity of the rheometer and had to be terminated, the particular mixing control sequence being ineffective. It was decided to concentrate on the w/c ratios from 0.40 to 0.48 in steps of 0.02. To assess the peak torque to be used for each w/c ratio the yield stress was studied over a maximum peak torque of 500,000 dyne cm. during a minimum ascent time of 1 minute, using the APC measuring system. This gave increments of 2500 dyne cm. and 50.5 dyne/cm^2 for torque and stress, respectively, ensuring the shortest test time to yield . This is important since during the mixing phase, of the mixing/standing/testing (MST) programme, the instantaneous peak torque is applied 3:0 (min:sec) after adding water, so yield is required at that time. In practice yield occurred within 15 seconds after 3:0 (min:sec), using this test procedure. The sample preparation was identical to the previous MST flow runs. Fig. 7.19 shows a number of trial runs determining the torque at yield and

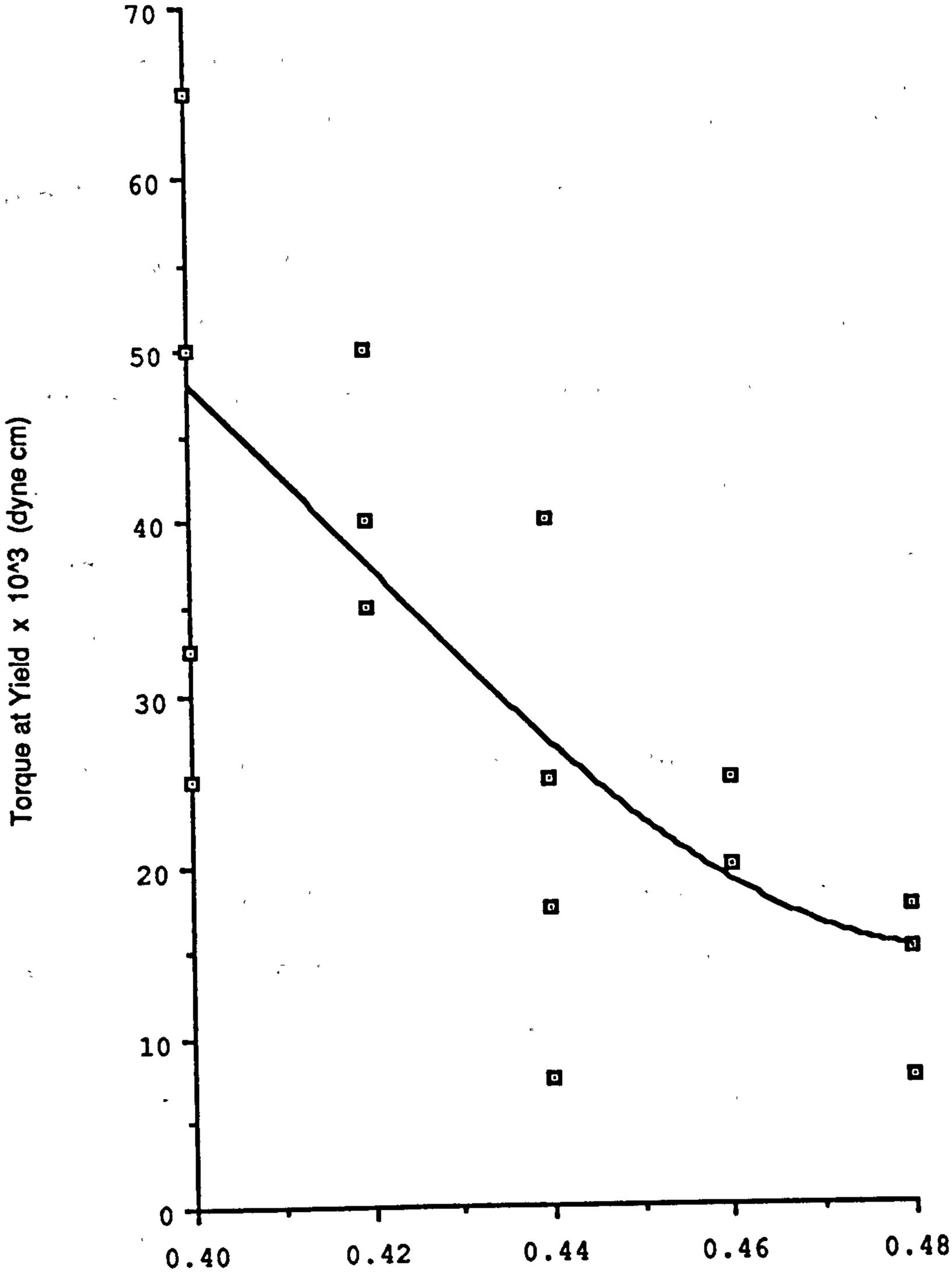

Peak Torque	50	35	25	20	15

(x 10^3 dyne cm)

Fig. 7.19 Selection of Peak Torque at various w/c ratios

the selected values of peak torque to be used in the MST runs for each value of w/c ratio. These values were chosen so that when the selected peak torque value was reduced to control the mixing phase, during an MST run, the mixing speed was contained. This required a delicate choice of peak torque whereas, the trial runs show the yield torque to be widely variable. It was found that should the sample remain rigid on applying the peak torque during the MST run the draw rod could be given a quick manual tweak, which would not unduly affect the area under the γ-t curve, because of the very short time duration, but would ensure a run. The runs where this procedure was adopted are denoted by * in Table 7.11.

7.6 Effect of w/c on Yield Stress with same Mixing Energy

Table 7.11 shows the results of MST flow runs programmed to run using approximately the same mixing energy whilst varying the w/c ratio on yield stress. The similar mixing energy, was determined by proportioning the peak hold time of the required energy to the ratio of the required peak torque to the selected peak torque, for that particular w/c ratio. The required energy time is 2:53 (min:sec) and peak torque is 25000 dyne cm. Hence, for w/c = 0.42 and selected peak torque = 35000 dyne cm.

$$PT = 2{:}53 \times \frac{25}{35} = 2{:}04$$

The standing time for these runs was 703 seconds and the rate of applied stress was kept at 1000 dyne/cm^2/min. making DT = 2:01 (min:sec). These values were chosen because previous results showed better repeatability at similar values and they are in the middle of the range of the present study. The weight of water in the sample is calculated from

Table 7.11

Ref No.	w/c ratio	wt. sample prior to test	undercut to τ_y	corr. factor
*11/35	0.42	17.89	0.5	1.060
36	0.46	17.26	0.5	1.060
* 37	0.40	19.19	1.0	1.124
38	0.48	18.16	1.0	1.124
* 39	0.46	16.86	2.0	1.272
* 40	0.40	21.28	1.0	1.124
* 41	0.42	17.21	1.0	1.124
42	0.48	16.66	1.0	1.124

	Energy Unit (kJ/kg)	Yield Stress (dyne/cm^2)	Corr. E_T/M (kJ/kg)	Corr.τ_y (dyne/cm^2)
11/35	0.786	757.5	0.721	803.0
36	0.753	232.3	0.691	246.2
37	0.945	575.7	0.867	647.1
38	0.590	70.7	0.541	79.5
39	0.584	70.7	0.536	89.9
40	0.994	656.5	0.911	737.9
41	0.904	383.8	0.829	431.4
42	0.570	70.7	0.523	79.5

Ref No.	t_{mix} (sec.)	t_{stand} (sec.)	t_{hyd} (sec.)	max γ (sec^{-1})	max Ω (rad/s)
11/35	126	752	1060	254.5	17.8
36	215	717	1115	225.4	15.8
37	87	743	1014	340.2	23.8
38	287	711	1177	201.2	14.1
39	211	712	1110	188.0	13.1
40	86	746	1018	360.4	25.2
41	123	725	1034	305.3	21.3
42	286	707	1175	193.8	13.6

	ρ	K ($x10^{-7}$)	ln K	ln K lnt_{mix} $(t_{stand})^{1/2}$
11/35	1.928	577.7	-9.759	-1.721
36	1.880	189.5	-10.874	-2.181
37	1.954	382.0	-10.173	-1.667
38	1.858	79.1	-11.747	-2.493
39	1.880	89.2	-11.627	-2.332
40	1.954	414.5	-10.091	-1.646
41	1.928	269.9	-10.520	-1.880
42	1.858	81.8	-11.714	-2.492
9/38	1.904	65.3	-11.940	-2.302
11/12	1.904	147.0	-11.128	-2.002
11/13	1.904	148.3	-11.119	-2.071
11/14	1.904	204.5	-10.797	-2.044

$$w_w = \frac{w/c \times 50 \times 3.16}{(1 + w/c \times 3.16)} \quad g$$

and the weight of cement from $w_c = 3.16\ (50 - w_w)$ g. The actual weights of water and cement varied by no more than ± 0.01 g from those calculated. The energy per unit mass, given in Table 7.11, before the corrected E_T/Mwhich is the correction due to an oversize sample, was also corrected in the computer software to account for the variation in slurry density. This was done by amending the weights of water and cement to suit the w/c ratio, in line 690 of the programme in Appendix 2. Since all the sample weights were in excess of 16.4 g the maximum correction factor of 0.917 was applied to all test runs to obtain the corr . E_T/M. The variation in actual t_{mix} values from those calculated for peak torque by proportion, mentioned at the beginning of this section, were due to the few seconds waiting for mixing to start before applying the tweak. The maximum Ω rad/s, achieved in all MST runs concerning w/c ratio, was below the 400 sec^{-1} shear rate required to apply the formula obtained in section 7.4.

As before, the E_T/M is in kJ/kg, which is $10^7 cm^2/S$, and with ρ in $g.cm^{-3}$, $\tau y/\rho E_T/M$ needs to be muliplied by 10^{-7} to work in the correct c.g.s. units.

The plot of K v w/c ratio is shown in Fig. 7.20. Ignoring point (3) which came from the previous higher shear rate data and taking the mean of the same w/c ratio data to perform a linear regression,gives a rather poor fit with correlation coefficient = -0.921. There is a tendency for the $\tau y/\rho E_T/M$ to decrease with increasing w/c ratio, which was to be expected. To see if the discrepancy in the linear regression was due

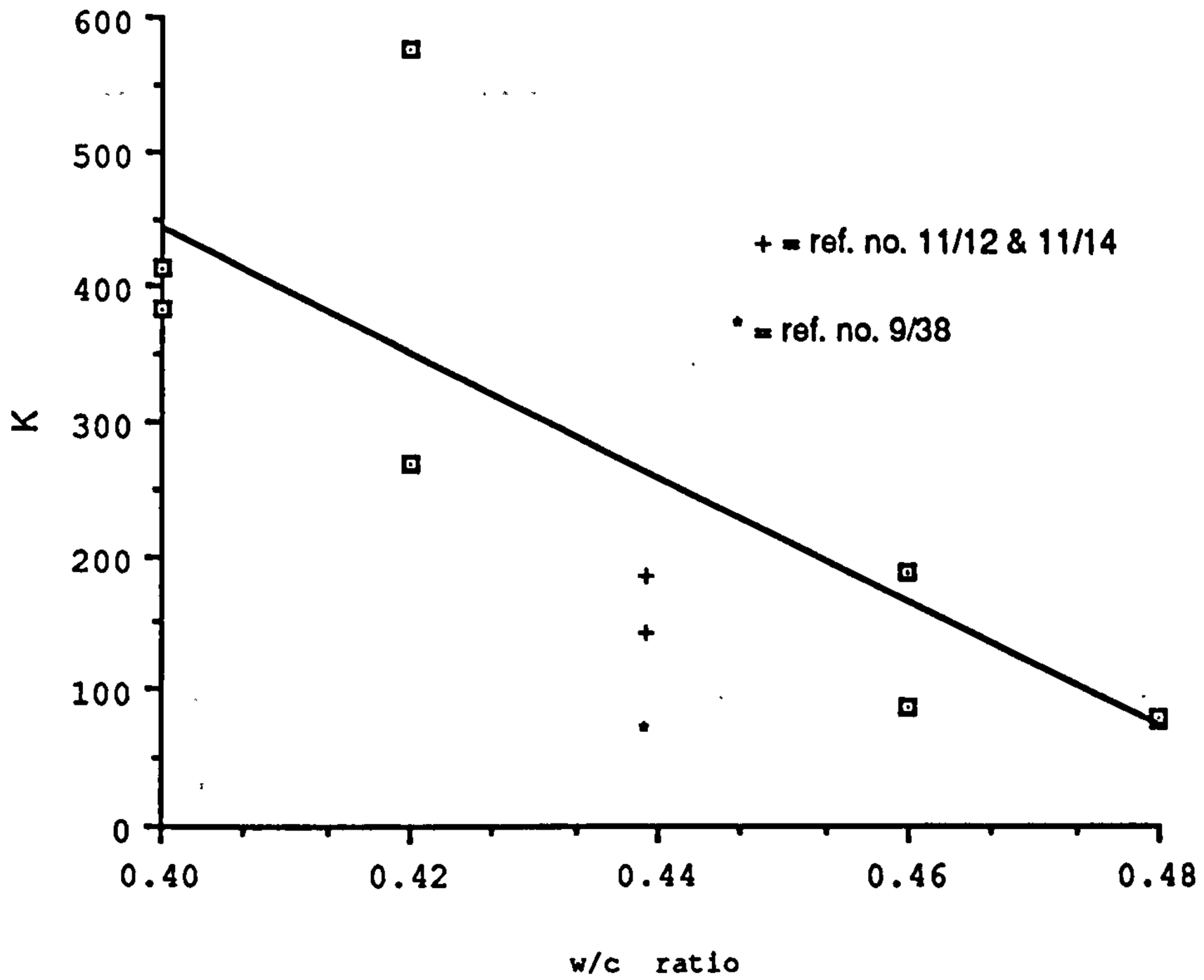

Fig. 7.20 Graph of K against w/c ratio

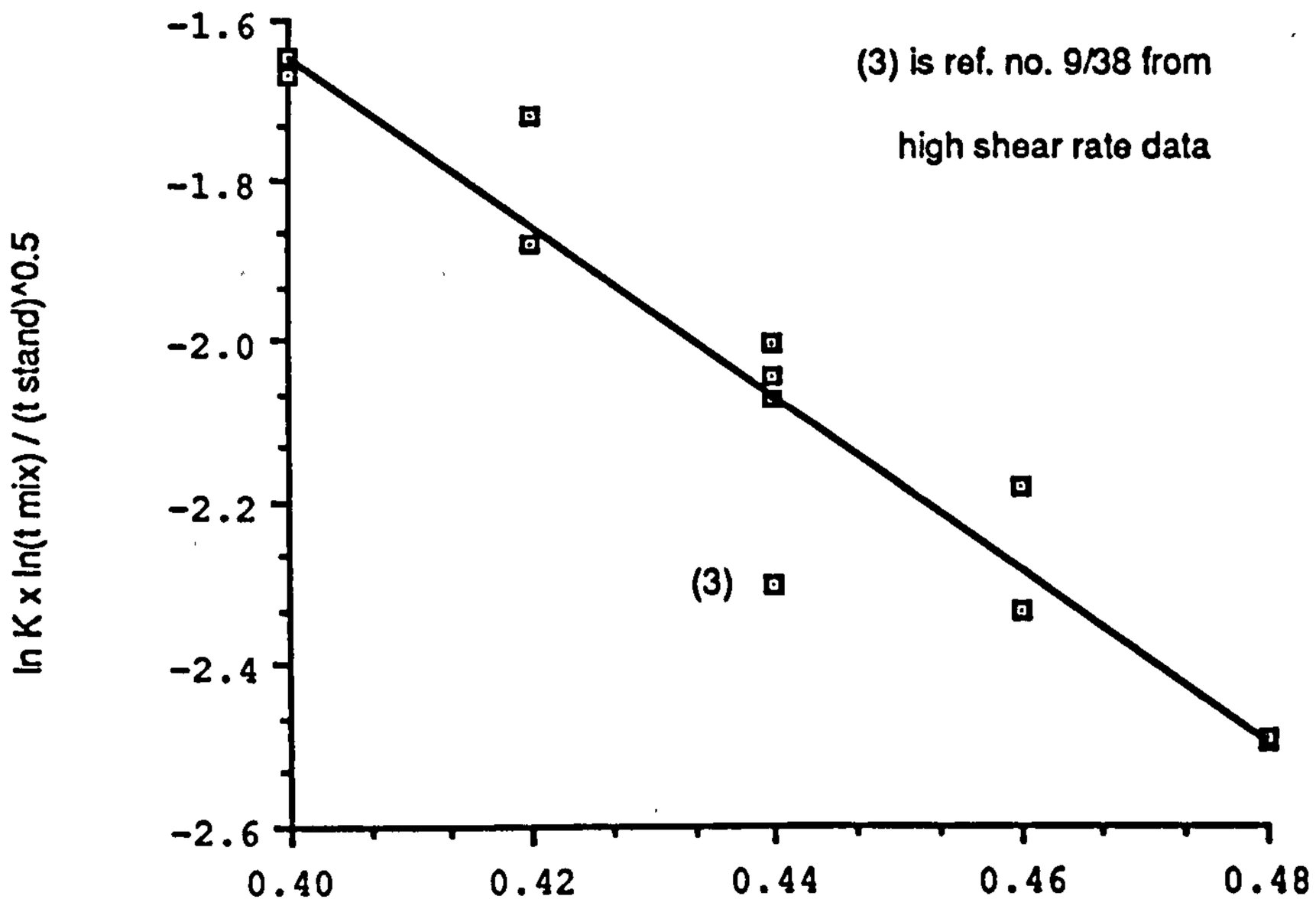

Fig. 7.21 Graph of K function against w/c ratio

Table 7.12

Ref.No.	t_{mix}	t_{stand}	ln K
35	126	752	-11.812
36	215	717	-12.485
37	87	743	-11.421
38	287	711	-12.818
39	211	712	-12.475
40	86	746	-11.402
41	123	725	-11.849
42	286	707	-12.823

w/c ratio	K x 10^{-7}	y = Bx + A linear regression
0.4	398.3	A = 2265.7
0.42	423.8	B = -4600
0.44	166.6	r = - 0.921
0.46	139.4	x = 0.4
0.48	80.5	y = 425.7 x = 0.48 y = 57.7

w/c ratio	ln K ln t_{mix} $(t_{stand})^{1/2}$	y = Bx + A linear regression
0.40	-1.657	
0.42	-1.801	A = 2.626 B = -10.625
0.44	-2.039	r = -0.997 x = 0.40
0.46	-2.256	y = - 1.624 x = 0.48
0.48	-2.492	y = -2.474

to the variation in t_{mix} and t_{stand} and to reduce the effect of these parameters ln K is multiplied by ln t_{mix} and divided by $(t_{stand})^{1/2}$ then plotted against w/c ratio, as shown in Fig. 7.21. The linear regression of the mean value of this new factor is -0.997, as shown in Table 7.12. It does ignore the high shear rate data for w/c = 0.44 but gives very good correlation with w/c ratio.

7.7 Conclusion

The results of yield stress testing of an oil well cement slurry show that τ_y increases with increase in standing time and decreases with an increase in mixing time, as might be expected, but a poor correlation was found between τ_y and E_T/M. However, good correlations were found betwen ln K and ln t_{mix} and also between ln K and $(t_{stand})^{1/2}$, where

$$K = \frac{\tau_y}{\rho E_T/M}$$

is the non-dimensional Kitching number. An expression relating K to the mixing time and standing time was obtained. Some points, which are the results of low shear rate mixing, do not fit this relationship. As a result of low shear rate mixing correlation of K with varying w/c ratio was not good but good correlation of the same results was achieved with

$$\ln \frac{K.\ln t_{mix}}{(t_{stand})^{1/2}}$$ to w/c ratio.

Further discussion and explanation of these results follows in Chapter 8.

CHAPTER 8

Further Discussion of Experimental Results and Phenomena

During the series of test runs using the MST technique on the controlled stress rheometer with the APC measuring system to measure the yield stress of an oil well cement slurry the results obtained and phenomena observed required explanation. This chapter examines in more detail the experimental results together with the findings of other researchers and provides better understanding of the effects of shear rate during mixing, interparticle interaction during early hydration, bleeding during testing and the rigid close packing phenomena, when applied to the testing of a cement slurry. Comparison of the yield stress model with the models of other researchers is made, as is the comparison of the measurement of yield stress of a cement slurry after standing for a short time.

8.1 Effect of Shear Rate during Mixing Phase

The results of the MST runs show that shear energy input alone is insufficient to determine the breakdown aspect of the yield stress during the mixing phase and that the level of that energy input, defined by the maximum shear rate achieved during mixing, is important. Since correlations to eliminate the effects of this shear rate, or to achieve a continuous relation with the other parameters, proved ineffective, the need to achieve a certain level of shear rate to obtain a particular stage of breakdown, or destruction of a particular interparticle force, appears to be supported. Further, the value of mixing shear rate, 400 sec^{-1}, chosen to enable the data to be compared is found to be in the most suitable region, without evaluating any interparticle forces. This is done by considering the remark of Tadros (1986), that the shear rate above which the flow curve of a concentrated flocculated suspension becomes linear is the value above which viscous stresses rupture all flocs formed. If Figs. 5.1, 5.2 and 5.7 are examined, primarily because the shear rates of these curves are sufficiently in excess of 400 s^{-1} (being approx. 900 sec^{-1}) to allow a reasonable straight line to be fitted on the portion of curve between these values. The departure of the curve from the straight line is in the region of 350 to 470 sec^{-1} for these graphs, which are w/c = 0.485 and w/c = 0.44 class G cement slurries. They were mixed using the APC procedure with the Waring blender and tested with the parallel plate measuring system. Early flow curve tests on hand mixed only samples, using the APC, were to obtain a peak torque to commence the mixing phase of a MST run, so only a few data points are recorded, which are insufficient for the above examination. Hand mixed

only samples are difficult to control during a flow run on the rheometer and tend to close pack, or, on yield, rapidly increase the shear rate with increasing shear stress. Then the flow run has to be terminated at approx. 40rad/sec. to protect the rheometer. This meant that the maximum shear rate was about 570 sec^{-1} with the APC and 100 sec^{-1} with the vane in cup measuring systems, again, making the above examination impossible.

Other explanations of deviation from the straight line such as slippage, or anomalous plug flow, can be discounted. This is because slippage is eliminated at shear rates in excess of 50 sec^{-1} (Mannheimer, 1983) and anomalous plug flow showed no discontinuity to the flow curve with serrated concentric cylinders; whereas smooth cylinders showed deviation to the flow curve until the plug broke up and shear flow occurred across the whole gap (Tattersall and Banfill 1983). In Figs. 5.1 and 5.2 both smooth and grit-surfaced parallel plates show deviation to the flow curve at similar shear rates.

However,the deviation from the straight line of the parallel plate flow curves occurred with slurries which had been mixed at high shear rates in the Waring blender. The homogeneity of this mixer has already been questioned in section 4.1.1. As the parallel plate shear rate is calculated at the rim and varies across the radius, a slightly higher shear rate for deviation would be expected. This is found for rough surfaces (Fig. 5.2), but not for smooth (Fig. 5.1). The relationship between shear rate and mixing energy to determine the manner and level of structural breakdown requires further investigation.

8.2 Interparticle Interactions during Mixing

During the mixing of a cement paste shear forces breakdown the interparticle bonds, disrupt flocs and also cause aggregation by colliding particles. The nature of this breakdown and buildup depends not only on the amount of shear history, or mixing energy input, but also the maximum shear rate which is attained. The particular interparticle forces involved are a) hard sphere, b) electrostatic, c) steric and d) Van der Waals, and their evaluation, with respect to colloidal suspensions, is excellently reviewed by Tadros (1986). However application to cement paste is by no means straightforward especially when considering aspects such as polydispersity, chemical reaction and the effects whilst undergoing shear. Quantitative evaluation of the interparticle forces at any point in time in cement paste undergoing mixing shear, is impossible to date and would only serve to say which particular size particle bonds, or flocs, had been broken. The problems of cement particle anisotropy and orientation, floc growth, electro-chemical interaction, hydrodynamics and inhomogenity of yield surface, which interfere with interparticle interaction during structural breakdown is a vast subject beyond the scope of this thesis. To give some perspective a brief description of the development of particle interaction during the early stages of cement hydration follows.

When water is added to cement the cement particles are to some extent dispersed, not entirely, since some dry flocs remain and, according to Hansen (1952), some hydration reactions are thought to take place without the cement

compounds going into solution (Dimond, 1975). The water coating the cement particle surface immediately forms a supersaturated sulphate ion solution, with C_3A hydration, which forms a microcrystalline film of ettringite or a colloidal suphoaluminate gel. C_3S hydration occurs at the same time, although inhibited by the calcium sulphate. The calcium and hydroxyl ions form the saturated solution and a calcium silicate hydrate membrane is formed, delaying C_3S hydration. Membrane formation can be a mixed sulpho-aluminate-silicate gel since both silicate and aluminate are mutually exchangeable. This membrane is semi-permeable and takes place until the internal pressure causes the membrane to rupture and hydration products grow out into the solution (Tattersall and Banfill, 1983). They also describe the disruption of the membrane which can form bridges between particles by initial shear action during mixing. On hydration the bridging membrane surrounds the dry flocs held together by weak surface forces. The membrane reforms around the broken flocs which are still capable of flocculation due to the charge on the particles. The differing strengths of the links account for the apparent irreversibility of breakdown.

Particles obtain charge as a result of both the imperfections in crystal structure surface and by preferential adsorption of specific ions on the surface, resulting in the electrical double layer to preserve neutrality. The double layer comprises the particle charge and the diffuse layer of counter ions, which surround it. The condenser capacity thickness of this layer is measured in tens of nanometers and depends on the electrolyte concentration of the continuous phase. As Tattersall and Banfill (1983) point out the forces of these

interparticle interactions resulting from particle charges are comparable to gravity for colloidal size particles (approx 0.1μm), but are less important with cement grains of size 1-100μm, which is a typical range. However the membrane gel layer particles are of colloidal size and Van der Waals attraction forces decrease with inverse proportion to the square of the interparticle distance. As Haimoni (1987) points out this decrease is less rapid than for a pair of atoms, since the interparticle attraction force is the sum of all the interatom attraction forces. The repulsive forces, due to interference of the electrical double layer as particles approach each other, decrease approximately exponentially with distance. To determine interparticle distance stability for monodisperse colloidal particles in a suspension the resultant potential energies for these forces are summed and may be represented for three electrolyte concentrations, as shown in Fig. 8.1. The ionic strength of the cement suspensions continuous phase is low. Hence, the energy barrier to be overcome for aggregation of the approaching particles into the primary minimum energy well is high resulting in a stable suspension. The suspension can be flocculated by increasing the ion concentration, such as by adding an inert salt. The secondary minimum occurs with relatively coarse suspensions , so that particle flocs, trapped in this energy well, are able to be discrupted on application of shear; whereas, those trapped in the deep primary well by Van der Waals attraction, without repulsion and when left standing cannot be disrupted by normal shear fields (Tadros 1986). Cement grains are anisotropic and the ion distribution on their surface is irregular hence on deformation and particle orientation the interparticle forces change which subsequently results in structural breakdown and yield. Tattersall and Banfill (1983) suggest the

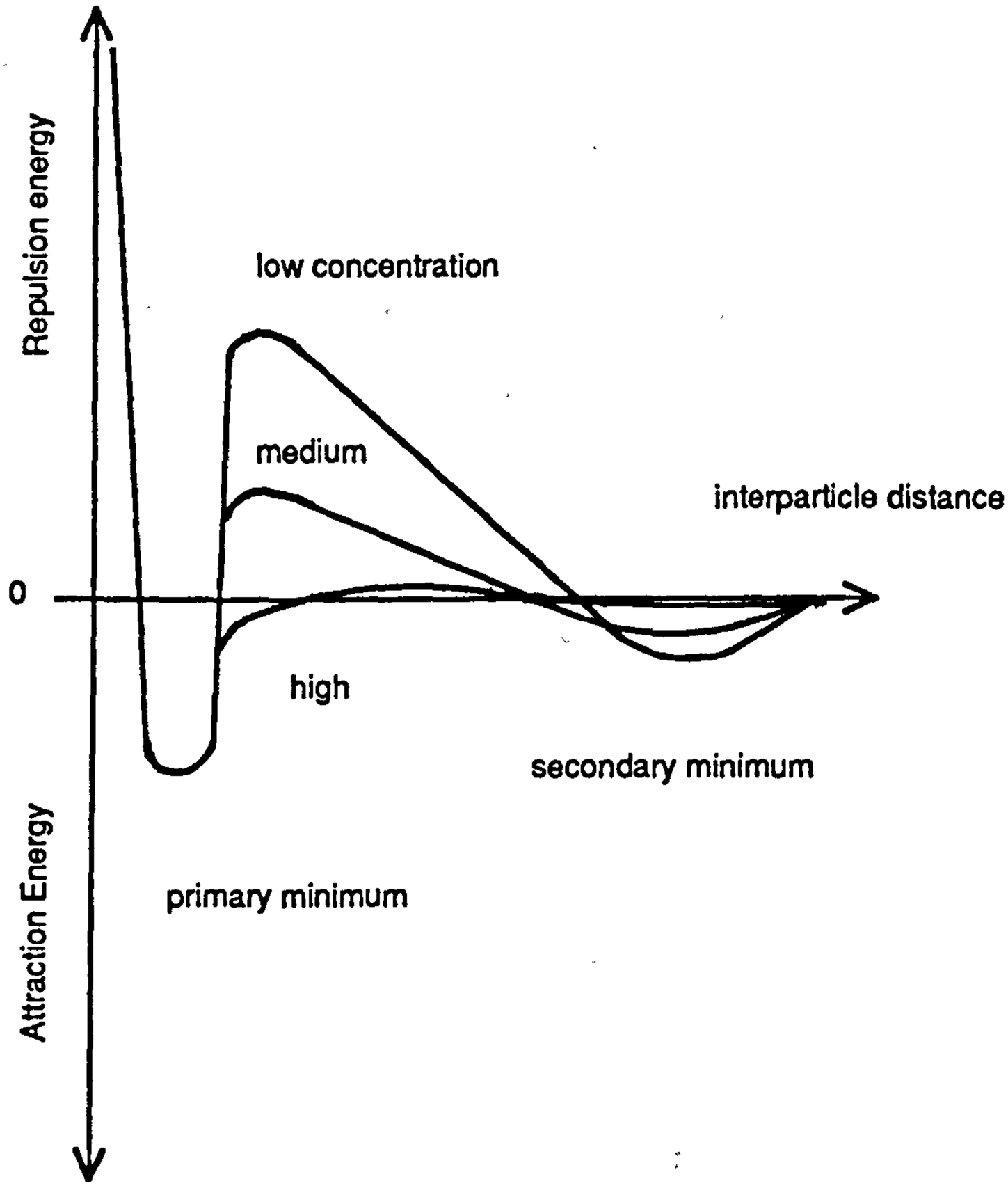

Fig. 8.1 Resultant potential energy curves at various concentrations

irreversible structural breakdown of a cement paste, that is not fully broken down by shear, supports the membrane model, since attraction and repulsion forces are not sufficiently irreversible when shearing stops. Also, that there is an order of magnitude between the membrane strength and the flocculated linkage, which corresponds to the difference between initial yield and the fully broken down yield. Haimoni (1987) describes the formation of clusters of cement particles by attraction forces. These clusters trap the continuous phase which increase the effective volume fraction of solids and could form a continuous network throughout the suspension, under certain conditions, thereby accounting for the close packing phenomena frequently observed in the experimental work described in this thesis.

A further complication in the evaluation of the maximum shear rate required to shear certain flocculated networks is that there is no homogeneity of mineral phases throughout the particle size distribution, because of various grindabilities. There is a higher proportion of gypsum below 3µm in OPC (Dimond 1975). This particle size non-homogeneity of the mineral phases causes a more variable matrix of flocculated particles, which may well be subject to local yield stresses. These in turn influence the shear rate at which certain networks are broken.

8.3 Rigid Close Packing

To obtain consistent shear rates whilst mixing using the MST technique on the Carri-Med is a difficult problem. A computerised controlled shear rate programme for a Carri-Med developed by the manufacturers is no longer

available because of problems with hunting as the rheometer learns the material characteristics. As described in section 7.2, the shear rate during the mixing phase of a cement slurry is highly dependent on the initial blending of the cement and water. To obtain consistent shear rates during mixing, further attention must be given to the selection and placing of the sample in the measuring system and, also to the room temperature at which blending and placing is carried out. However, rigid close packing phenomena may still occur which, providing sufficient torque is applied, can only be attributed to the arrangement of particles in the cement slurry sample.

Cross (1986) whilst working on glass fibre slurries having single and bimodal sized cylindrical shaped particles, using a controlled shear rate rheometer with cone and plate measuring system, found examples of the rigid close packing phenomena. Using particles of 12 and 17μm dia with varying length up to 3mm, the maximum volume concentration, ϕ_0, was found to reduce as the aspect ratio increased, when ϕ_0 was measured by sedimentation under gravity. During shear with a low ratio of gap to particle size (gap approx. 1100μm) a sharp rise in shear stress, terminating in sample fracture, was observed. Localised close packing of particles occurred as liquid drained away on rapid shearing leaving rigid close packed zones. Rheological dilatancy is associated with high concentration as $\phi \rightarrow \phi_0$ but experiments by Cross showed this in slurries at relatively low concentration, but high particle aspect ratio. Under shear homogeneous slurries would form discrete clumps

and move radially outwards from the measuring system. Cross also found that although the viscosity tended to fall as shear rate increased, with increase in the duration of shear the viscosity increased. This phenomenon was attributed to particle collisions, doublet formation and transfer of particles from one shear plane to another.

Wildemuth and Williams (1984) demonstrated the shear dependence of the maximum packing fraction, ϕ_m, by analysing a wide range of data on spherical particles of neoprene, polymers, bitumen and glass in various continuous phases such as water, oil, glycerol and lithene, ranging in size from 0.05 to 65μm. The data was plotted as relative viscosity, η_r, against reduced volume fraction $\phi/\phi_M(\tau)$ where $\phi_M(\tau)$ was obtained from the generalised Eilers model,

$$\eta_r = \left[1 + \frac{0.5[\eta]\phi}{1 - \phi/\phi_M} \right]^{[\eta]\phi_M} \qquad 8.1$$

where $[\eta]$ is the intrinsic viscosity, which is, for spheres, independent of τ and equal to Einstein's k in $\eta = 1 + k\phi$. ϕ_M thus incorporates all shear dependence as the data was measured over τ values from 0 to 50 Pa and showed excellent

correlation to the equation when the power $[\eta]\phi_M = 2$. When the data was fitted to different constant values of shear stress, $\eta_r \rightarrow \infty$, as $\tau \rightarrow \tau_y$, when $\phi \rightarrow \phi_M$, but this occurred at different values of ϕ_M as τ varied as shown in Fig.8.2. Hence, provided $\phi_{M0} < \phi < \phi_{M\infty}$, a yield stress was shown, by Wildemuth and Williams, to be derived from the intermediate microstructure, ϕ_M, which is described by two phases, a loose flocculated phase and a dense disperse phase. The volume of these phases and the volume of the particles in them are V_F, V_D, V_{PF} and V_{PD}, respectively. This gives $\phi_{M0} = V_{PF}/V_F$ and $\phi_{M\infty} = V_{PD}/V_D$ from which they obtained

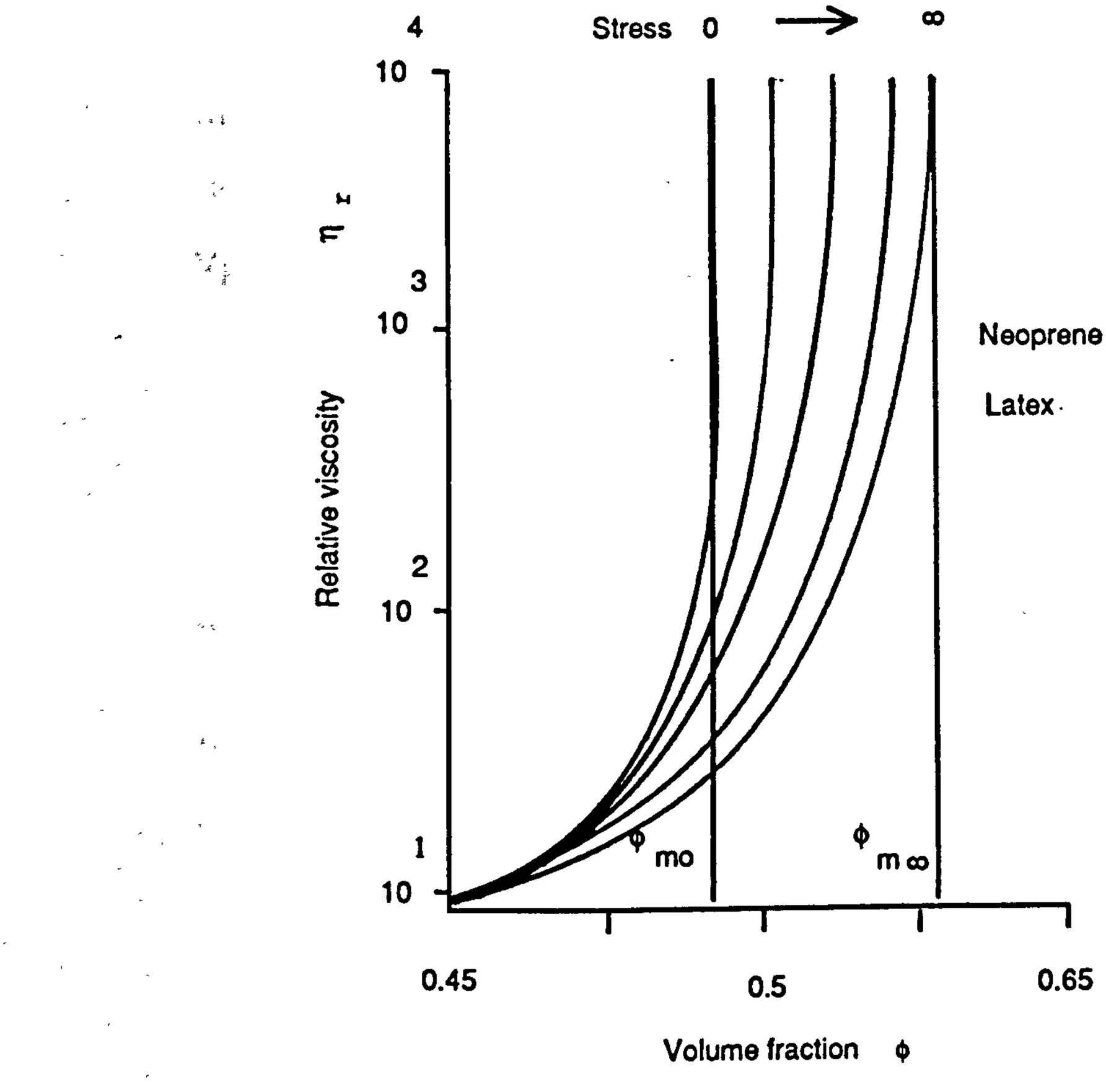

Fig. 8.2 Viscosity prediction at different levels of shear stress

(Wildemuth and Williams, 1984)

$$\frac{1}{\phi_M} = \frac{1}{\phi_{M0}} - \left(\frac{1}{\phi_{M0}} - \frac{1}{\phi_{M\infty}}\right) f \qquad 8.2$$

where f is the fraction of total particles that exist in the disperse phase. Using an exchange rate equation, analogous to chemical reaction, on the change from V_{PF} to V_{PD} at a steady state gave,

$$f = \frac{1}{1 + k_F/k_D} \qquad 8.3$$

where k_F is a rate constant for floc recovery and k_D for destruction.

Assuming $k_D \propto \tau^m$ since the mechanism and, hence, dependence on τ is not known, f becomes

$$\frac{1}{1 + A\tau^{-M}} \qquad 8.4$$

Hence, by inversion of equation 8.2 and using equation 8.4 the yield stress was predicted as

$$\tau_y(\phi) = \left[A \frac{\phi_{M\infty}}{\phi_{M0}} \left(\frac{\phi - \phi_{M0}}{\phi_{M\infty} - \phi}\right) \right]^{1/M} \qquad 8.5$$

since the τ at which the ϕ becomes ϕ_M is the yield stress, as no flow occurs.

No restrictions are made concerning shape and polydispersity, which are accommodated by ϕ_M, as are electroviscous effects, surface chemistry and differences in thermal expansion between the particles and the continuous phase, as these factors are reflected in the state of aggregation. The equation for yield stress requires experimental derivation of the factors A and M, which come from the simplest form of rate equation. It assumes that the only mechanism, by which no flow occurs, is when $\phi > \phi_{M0}$ and that there is a continuous rising transition from the loose floc to the dense dispersed phase so that a rigid structural network giving $\tau_y \rightarrow \infty$, is not possible at ϕ lower than $\phi_{M\infty}$.

Schreuder et al (1985) investigated spherical glass particles, size 45-65μm, in a glycerol plus water mixture, a polar system, and dioctylphthalate (DOP), a non-polar medium. A solid volume fraction of 0.63 was used throughout and oscillatory shear was investigated after squeezing the sample between two coaxial cylinders. Whether or not the glass beads were silanised, no difference in rheological behaviour was found in DOP and the relative viscosities were the same as for the unsilanised beads in glycerol. Hence coagulation was found to

be independent of structures formed by shear, in concentrated suspensions. During oscillatory shear at large deformation a virtually underformable structure formed. The deformation leads to accumulation of the suspended particles, which prevent further deformation resulting in rigid close packing. At small deformation, linear viscoelastic behaviour was observed with sheet formation, or ordered layers, at low frequencies, becoming less developed at higher frequencies showing a transition between the viscoelastic and underformable states. The large deformation, leading to rigid close packing, was experienced if squeezing the paste too fast was performed.

The previous researchers found that under shear the particles in a concentrated suspension reform and can display a rigid structure. The important point to note is that rigid close packing is the result of an initial shear application which occurs when placing and squeezing the sample to the required measuring configuration. It can occur after mixing and prior to testing, but was not found during the mixing phase. The cement slurry did build up structure during prolonged mixing. This infers that the rigid structure is a particular arrangement of particles which can be disrupted by movement, whereas the build up of structure is a separate phenomena. It is likely that the rigid structure occurs only with laboratory measuring systems, since the

phenomenon is not reported in field work and organisation of a particle network structure across field pipe diameters is most improbable.

8.4 Shrinkage and Surface Settlement

When a cement slurry sample was placed on the bottom plate of the rheometer, a thin film of water was seen to form on the top surface of the blob. As the sample was squeezed to the required gap, any excess bleedwater would be expected to be displaced, such that the rough measuring surfaces would be in contact with the slurry matrix. The amount of bleedwater can be estimated using Doran's work (1984). Surface settlement prior to testing or mixing in the MST technique (see section 6.5) would take place for approx. 40 sec. and may be estimated to total < 2μm at the APC periphery, where the thickness is 2098μm. After mixing with the MST procedure, the sample in the experiment was allowed to stand for a time, up to 30 minutes. Assuming that during mixing the sample is re-homogenised, the total estimate of surface settlement is still only 10.5μm, which is well within the height of the engravings. Doran (1984) employed soil mechanics test apparatus such as the oedometer cell (BS 1377, 1975) to show that bleeding is a self-weight consolidation phenomenon, involving the dissipation of excess pore-water pressure. The previous sedimentation theory for bleeding was not realistic being based on Stokes law, which was made inapplicable by hindered particles. Bleeding is influenced by surface area, particle shape, flocculation and chemical reaction and although its

rate was found by Doran (1984) to be constant throughout the dormant period a relationship between cement composition and bleeding was not obtained. Lee (1979) found that an unusual feature of self-weight consolidation was that it started from a region near the undrained base, so to accommodate continuous outward flow of water during consolidation, the excess pore water pressure in this region must be dissipated first.

Doran (1984) found that, provided the w/c ratio was not high enough to cause channelled bleeding (this is the result of breakdowns in floc structure, exhibited by high shear mixes at the higher w/c ratios than the low shear mixes), the surface settlement was of the form shown in Fig. 8.3. Although temperature varied continuously during bleeding, bleed rate was not affected by the variation in temperature, but a reduction in average temperature reduced the maximum settlements due to the reduction in setting time. High shear rates during mixing would also reduce both maximum settlement and time to reach maximum settlement. Two mechanisms stop the bleeding process, one is setting, the other is the complete dissipation of pore water pressure. The latter is unlikely to occur,except with short drainage paths, before setting begins. The free water determination with the particular class G cement used in the MST runs is 3.0 ml. according to the manufacturers. This is determined in a 250ml graduated glass cylinder over a period of 120 minutes. (section 6 API Spec. 10, 1986). Assuming that setting has not occurred, although thickening by this time has exceeded 100Bc, from the curve in Appendix 3, which indicates a cement slurry too thick to pump at downhole temperatures and pressures, then, if settlement is about to stop, the $\sqrt{120}$ minutes is on the up curve and by proportioning the settlement to the square root of time, the

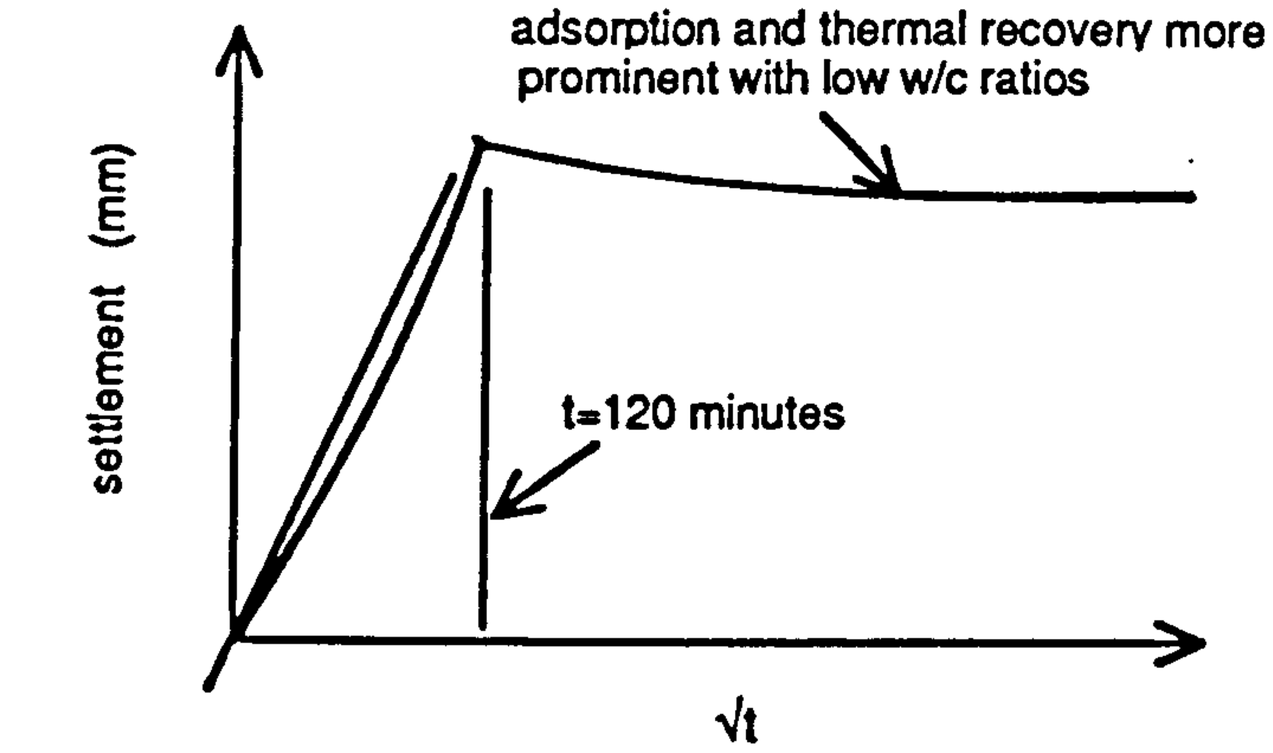

Fig. 8.3 Typical surface settlement of cement paste

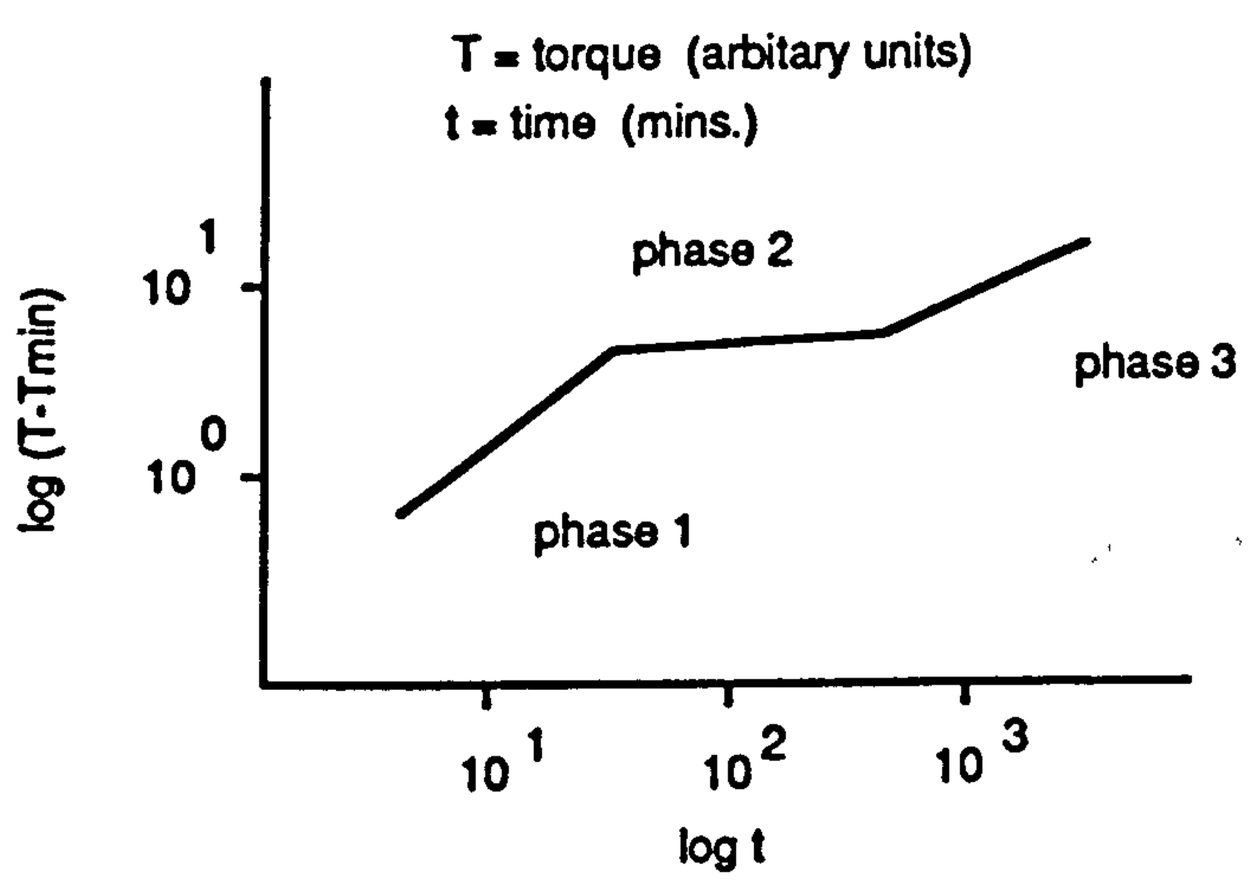

Fig. 8.4 Stiffening phases during hydration

estimates of settlement made earlier can be determined. According to Doran (1984), it is doubtful that measurements of accumulated water give accurate estimates of surface settlement, although they will be adequate for shallow samples.

Even if, as a result of the small sample placed on the rheometer, the pore water pressure dissipation was almost immediate, the maximum settlement at the maximum gap of the APC would only be 25μm and this is insufficient to clear the indentations on the engraved surface of the cone.

In the early stages of hydration, the take up of water may exert forces on the weak cement matrix structure causing a volume reduction. The self-supporting structure begins forming at an early age, as can be seen from the thickening curve in Appendix 3, and once supporting, can cause the pore water pressure to fall below hydrostatic pressure since free water may be drawn into structure by the reduced volume of hydrating cement. The volume reduction of the sample in the APC was observed whilst in the standing phase of a test run.

8.5 Limitations of the Yield Stress Model

It must be emphasised that the yield stresses obtained using the model derived in section 7.4 can only be used over the range of shear energy per unit mass used in the experiments and the mixing times and standing times which were applicable to the test results. The model has only been tested for a class G oil well cement slurry of w/c ratio = 0.44, at a temperature of 25°C, whilst

using a particular density of engraved surface APC measuring system. It should be appreciated that the constants of the model reflect these ranges and conditions. It is only after obtaining agreement from data using different geometry of APC that confidence in the results can be achieved.

Over the range of standing time from 60 to 700 seconds the value of the exponential term in the model increases almost 25 times, whereas the t_{mix} term decreases approx 4 times at $t_{mix} = 60$ seconds, and 8 times at $t_{mix} = 700$ seconds. This shows that the model displays greater sensitivity to standing time than to mixing time. Since ideally, E_T/M has a direct linear relationship with t_{mix}, the effect of increasing the t_{mix} from 60 to 700 seconds at a t_{stand} = 60 secs. is to increase the τ_y some 1.7 times, whereas, the same increase in t_{mix} at $t_{stand} = 700$ secs. results in a decrease in τ_y, of 0.78 times. From the model for

$$t_{stand} = 60, \quad K = e^{-9.83}\ t_{mix}^{-0.79} \qquad 8.6$$

$$t_{stand} = 700, \quad K = e^{-6.60}\ t_{mix}^{-1.10} \qquad 8.7$$

$$E_T/M = \frac{\sigma\dot{\gamma}\, t_{mix}}{\rho}$$, if ideally, t and $\dot{\gamma}$ are constant during the mixing, then,

$$\text{since } K = \tau_y/\rho E_T/M, \text{ at } t_{stand} = 60, \frac{\tau_y}{\sigma\dot{\gamma}} = e^{-9.83}\ t_{mix}^{+0.21} \qquad 8.8$$

and

$$t_{stand} = 700, \frac{\tau_y}{\sigma\dot{\gamma}} = e^{-6.60}\ t_{mix}^{-0.10} \qquad 8.9$$

Hence, the effect of the mixing time on the yield stress must take into account the mixing time component in E_T/M. Unfortunately, because the shear rate varies during mixing, the t_{mix} term cannot be taken out of E_T/M as simply as above. The model has no theoretical basis it, merely, provides the closest values. The fact that $\tau_y = 0$ when $t_{mix} = 0$ is of no justification for expanding the model since the value of τ_y when $t_{stand} = 0$ is indeterminate. However with normal values of t_{mix} and increasing values of t_{stand} the value of τ_y tends to infinity, as expected. The model can be compared with those of Tattersall (1955), Banfill (1980) and Domone and Thurairatnam (1988).

Tattersall (1955) assumed zero build up during shear and a linear relation between excess torque (i.e. $> T_e$, where T_e is the torque causing viscous flow) and the number of linkages left in structural breakdown to derive

$$T - T_e = k(\omega - \omega_1)\exp^{-Bt} \qquad 8.10$$

(see page 58)

where ω_1 is the intersection of T_0 v ω and T_e v ω. k is the slope of a plot of $(T_0 - T_e)$ v $(\omega - \omega_1)$, ω is the angular velocity of the measuring system and B is the slope of a plot of ln $(T - T_e)$ v t. Both plots were found to be linear for cement pastes with w/c ratios from 0.28 to 0.32.

$$B = \frac{2\pi k}{n_0 \psi}\,\omega(\omega - \omega_1)$$ in the derivation, where n_0 =

original number of linkages and ψ = work done to break a linkage.

The paste was mixed vigorously by hand for approximately 1/2 to 3/4 minutes loaded at 40 r.p.m. (29 sec^{-1}) into a coaxial cylinder viscometer then, after standing for 1 minute, the run was started.

Since T_e accounts for viscous flow $(T - T_e)$must be a function of breakdown stress, which could be considered as the yield stress of the remaining structure at any point in time and as

$$k(\omega - \omega_1) = \frac{Bn_0\psi}{2\pi\omega}$$

this must be a function of mixing shear energy, or E_T/M. The exponential power , -Bt, because of the test procedure outlined above, must include the effects of standing and mixing times, although based on the testing times alone. The plots of B v $\omega(\omega-\omega_1)$ give an unexplained intercept, which may, possibly, be accounted for by considering a build up with the breakdown of structure, such that the exponential power is two terms, similar to the yield stress model in this thesis. Another interesting comparison is the dependence on the inverse of shear rate on the

$$\frac{Bn_0\psi}{2\pi\omega}$$

term, which aligns with the mixing shear energy in the τ_y model.

Unfortunately, to account simply for shear rate dependence of the mixing shear energy term in this way was shown to be invalid in the yield stress model, as can be seen from the graphs in Figs. 7.11 and 7.14.

Banfill (1980) provided the model

$$T - T_{min.} = At^b \qquad 8.11$$

to account for the increase in torque with time, subsequent to the cement paste reaching equilibrium (i.e. equal breakdown and build up), or complete breakdown; after which, depending on various additives, the cement paste would in time thicken until setting occurred. Bhatty and Banfill (1984)

monitored this effect on cement paste with retarders, using a Gallenkamp propeller turbine mixer rotating at 2500 r.p.m. for between 4-6 minutes to ensure homogeneity and a fully broken down cement paste of w/c = 0.35. They tested immediately on loading, at 20°C, using a helical impeller in a serrated cylinder, to overcome both settlement and slippage, with the Haake RV2 viscometer. During the test the impeller was rotated at a speed of 512 r.p.m, which was estimated to be an average shear rate of 213 sec^{-1}. A plot of log $(T - T_{min})$ v logt, such as shown in Fig. 8.4, found the relationship of equation 8.11 to be correct, but comprising three phases. Phase 1 was found to be independent of admixture type and concentration. Since chemical reactions occur in the first few minutes, this phase was considered to be reaggregation or flocculation, possibly aided by the removal of water from the paste, during early hydration, and the changing morphology of the particle structure. Phase 2 represents the dormant period, which is lengthened and the slope of the curve flattened by retarder, and phase 3, also affected by retarder, represents the more rapid hydration leading to initial setting. The constant A is interpreted as a process rate parameter and constant b as a mechanism type parameter.

During the mixing phase of the MST technique, when oil well cement slurry was mixed at constant torque the speed of rotation of the cone decreased during prolonged mixing periods as shown in Fig. 8.5. The form of this relationship is similar to the behaviour reported by Banfill (1980) and Bhatty and Banfill (1984) for cement pastes subject to continuous steady shear. However, the times are substantially different. The time at which the shear rate peaked during the mixing time is given in Table 8.1 and is found to be

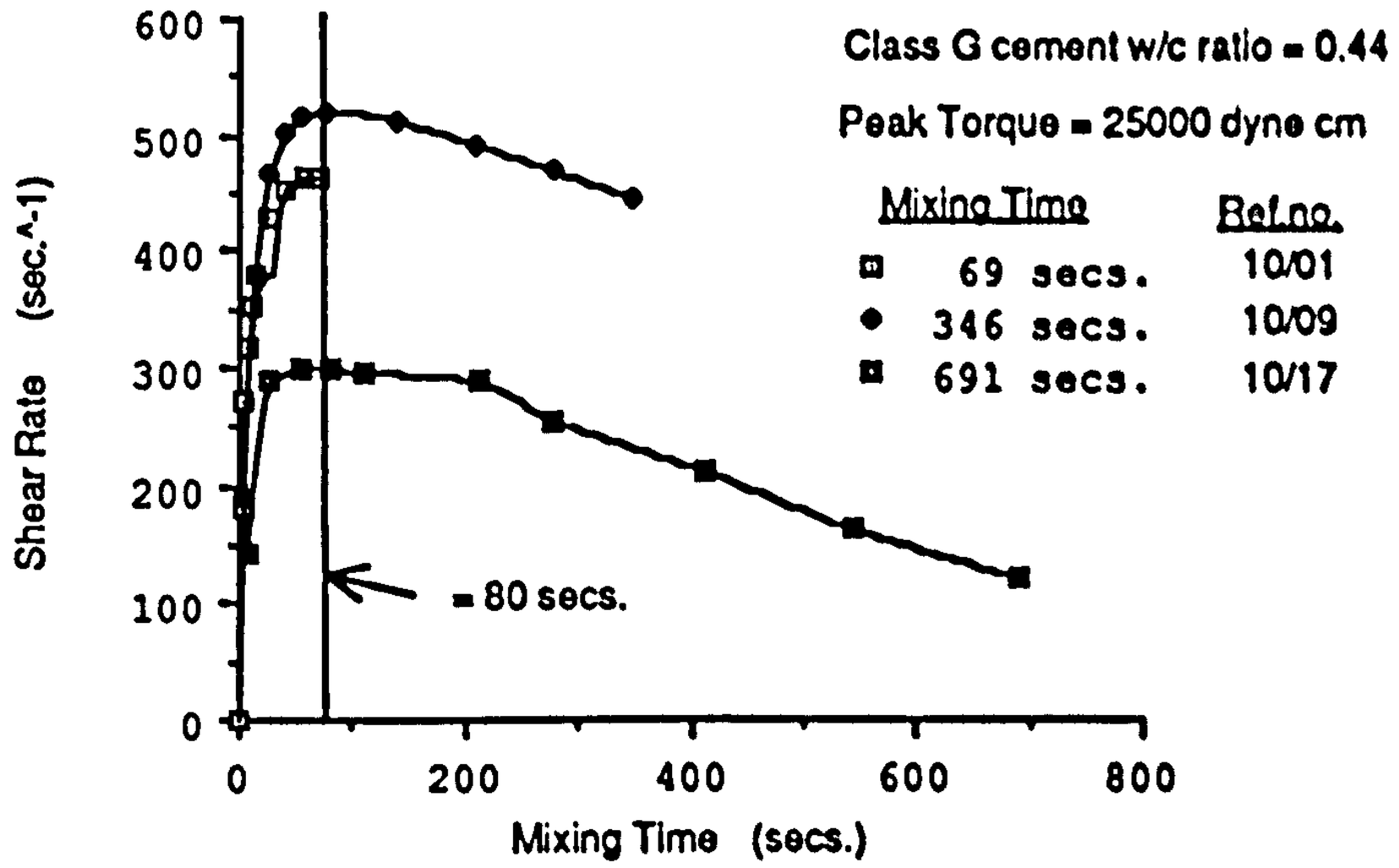

Fig. 8.5 Thickening of Cement Slurry during Prolonged Mixing

TABLE 8.1

Run Ref. No.	t_{peak} (secs.)	Max.Shear $\dot{\gamma}$ (sec^{-1})	Max.t_{mix} (secs.)	w/c ratio
10/16	73	381.8	518	0.44
/17	83	299.6	691	0.44
/22	87	288.7	173	0.44
/23	90	359.4	346	0.44
/24	70	315.3	518	0.44
/25	90	549.0	691	0.44
11/01	70	261.1	691	0.44
/02	67	222.1	518	0.44
/03	59	451.7	346	0.44
/04	80	351.1	173	0.44
/06	no peak		71	0.44
/07	no peak		72	0.44
/08	69	412.7	173	0.44
/09	80	484.9	346	0.44
/10	57	248.8	518	0.44
/11	86	430.1	691	0.44
/12	68	271.3	173	0.44
/13	57	259.5	173	0.44
/14	82	221.4	173	0.44
11/37	no peak		87	0.40
/38	50	201.2	288	0.48
/39	75	188.0	216	0.46
/40	no peak		87	0.40
/41	93	305.3	124	0.42
/42	49	193.8	288	0.48
9/37	78	490.1	173	0.44
/38	77	534.1	173	0.44
/39	77	598.9	173	0.44
/40	79	502.3	173	0.44
/41	no peak		69	0.44
/09	88	499.1	173	0.44
/10	87	562.4	173	0.44
/11	85	509.2	173	0.44
/12	81	451.7	173	0.44
/13	104	515.8	346	0.44
/14	83	511.6	346	0.44
/15	114	459.3	346	0.44
/16	95	484.9	346	0.44
/17	98	478.3	518	0.44
/18	109	525.8	518	0.44
/19	93	488.2	518	0.44

/20	96	459.3	518	0.44
9/21	90	476.8	691	0.44
/22	97	480.0	691	0.44
/23	104	449.2	691	0.44
/24	93	498.3	691	0.44
/25	93	511.6	619	0.44
/26	93	407.5	691	0.44
/27	86	514.1	691	0.44
/28	79	461.7	691	0.44
/29	104	511.6	518	0.44
/30	85	569.0	518	0.44
/31	85	552.3	518	0.44
/32	80	552.3	518	0.44
/33	76	475.0	346	0.44
/34	80	423.4	346	0.44
/35	76	598.0	346	0.44
/36	93	486.6	346	0.44
10\01	no peak		69	0.44
/05	80	559.1	173	0.44
/06	78	427.7	173	0.44
/07	88	514.1	173	0.44
/08	80	494.2	173	0.44
/09	87	521.5	346	0.44
/10	87	499.9	346	0.44
/11	83	506.5	346	0.44
/12	78	581.4	346	0.44

independent of the mixing time. It is also independent of the maximum shear rate which was achieved during mixing time, and appears to be dependent on the composition of the mix, as well as the variation in temperature. However, verification of such dependence requires investigation. The mean t_{peak} = 84.1 seconds with s.d. =11.89 from 56 entries, at the w/c ratio = 0.44. The t_{peak} time pinpoints either the complete breakdown of the cement slurry, or the equilibrium of breakdown and build up of structure. From the t_{peak} time, the Phase 1 of the build up, as referred to by Bhatty and Banfill (1984), begins. However, it seems incongruous that the low maximum shear rate data (< 400 sec^{-1}), which does not conform to the yield model and has t_{peak} at or below 84 seconds, still reach completion, or equilibrium of breakdown, having received less than half the mixing shear energy. This suggests that the beginning of Phase 1 is chemical reaction, rather than deflocculation or rearrangement of particles, but this suggestion also requires verification. Although structure begins to build up after t_{peak}, the effect of prolonged mixing is to reduce the yield stress. This can be seen in Fig. 7.4.

It is to be expected that this build up of structure is reflected in the power of the t_{mix} term, just as it is in the Banfill (1980) model, since the exponential term mainly accounts for standing time effects. If the t_{mix} term is considered for, say, t_{mix} = 10 seconds and t_{mix} = 100 seconds, keeping the standing time constant, to see the effect of t_{mix} on yield stress, but using both the yield model power of t_{mix} and the power with the ideal t_{mix} component of E_T/M, mentioned earlier. These figures are given in Table 8.2 and show that mixing

Table 8.2

The Effect of Including the t_{mix} component from E_T/M in the t_{mix} term of the Yield Stress model for long and short values of t_{mix} and t_{stand}

t_{stand} (secs.)	t_{mix} (secs.)	$f(t_{mix})$ in model (from eq. 8.6 and 8.7)	incl. t_{mix} in E_T/M (from eq. 8.8 and 8.9)
		$t_{mix}^{-0.79}$	$t_{mix}^{+0.21}$
10	10	0.16	1.62
	100	0.03	2.63
		$t_{mix}^{-1.10}$	$t_{mix}^{-0.10}$
700	10	0.08	0.79
	100	0.01	0.63

reduces the yield, especially with prolonged mixing. However, at low standing times, when taking the t_{mix} component of E_T/M into account, the yield stress can increase with time. This effect can just be seen in Fig. 7.4 on the low standing time curve.

The other model, recently obtained by Domone and Thurairatnam (1988), to express the yield stress of various types of cement, with and without additives, used in the offshore industry is

$$\tau_y = a.e^{b/w} \qquad 8.12$$

where a and b are constants, which have not been fully investigated, although dependent on the type of cement. w is the water cement ratio. Using a high shear rate Silverson mixer for 5 minutes total mixing time, including adding components, the testing was made using a Contraves Rheomat 115 concentric cylinder viscometer. The Bingham yield stess was obtained from the flow curves to give the general relation between yield stress and water cement ratio, of equation 8.12. This is compatible with the yield model of this thesis, where the water cement ratio was constant, hence making the power of the exponential a constant. Again further investigation is required to relate the dependency of the constants. However,the model of Domone and Thurairatnam (1988) does explain why the results from various w/c ratios did not fit the yield model in this thesis, since account of w/c ratio is required in the power of the exponential and not just in the slurry density in the K number.

8.6 Yield Results of other Researchers

Mannheimer (1983), working on an Oklahoma class H cement slurry w/c ratio = 0.38, prepared in accordance with API RP 10B (Section 4) specification, at a room temperature of 24 ± 2°C. and using a Weissenberg rheogoniometer found the yield stress value to be 110 dynes/cm^2, by extrapolation of the no-slip date (i.e. data above $\gamma = 50$ sec^{-1}).

Orbán et al (1986) investigated various mixing energies from a laboratory API Spec. 10 blender to jet mixers used in the field. They used a class G oil well cement mixed with tap water, according to section 5 and tested in accordance with Appendix H of API Spec. 10. at 20°C, or 85°C, depending on the series of experiments, using a rotational viscometer and applying the Bingham model to obtain the yield value. In the laboratory mixing of a 1.9 S.G. slurry the yield was 23.5 lbf/100 ft^2 (113 dynes/cm^2). On reducing the energy to that employed in the field, which is approx., one tenth of the energy of the laboratory blender, the yield stress rose to 30lbf/100ft^2 (144 dynes/cm^2) and by increasing the energy to, approx., 4 times the laboratory blender, a yield stress of 51 lbf/100ft^2 (250 dynes/cm^2) could be obtained. The standing time is virtually zero ,since the sample in the constant shear rate viscometer was continually rotated, on transfer from the consistometer, whilst the dial readings at various descending speeds were made.

Haimoni (1987) used a specific mix comprising, in % by weight of class G cement, of 65% distilled water, 10% gypsum and 2% calcium chloride.

Mixing was carried out as specified in API Spec. 10 (1986) and stirred in an atmospheric consistometer at 20°C, the controlled room temperature 20°C was used to perform the tests. The vane was used, in conjunction with three instruments, the Rheomat 15, the Fann viscometer and the Weissenberg rheogoniometer, which gave widely varying mean gel strenths of 58.5 Pa, 87.2 Pa and 111.05 Pa ± 10 Pa, respectively, for the above mix, after standing for 10 minutes. The reason given for the variation was the rotation speed of 6 r.p.m., which, due to the measuring system stiffness, gave varying times to failure; hence, widely varying rates of strain. Using a rotation speed of 0.6 r.p.m., where the measured gel strength was fairly constant, the Fann viscometer was used to measure the yield stress of the above mix with the vane giving the following mean values of gel strength for various standing times:-

Standing Time (mins.)	14	40	70
Gel Strength (Pa)	215	1136	2777
s.d.	4	166	435

(1 Pa = 10 dyne/cm^2)

For comparison with the yield stress data of the Carri-Med, BP (Kellingray, 1989, personal communication) provided the following data on a neat class G cement at w/c ratio = 0.44, which was tested on a Fann viscometer using procedures laid down in the API Spec 10 (1986) for measuring gel strengths.

Cement sample	A	B	C	D
10 sec. Gel strength (lbf/100ft^2)	15(72)	16(77)	14(67)	14(67)
10 min Gel strength (lbf/100ft^2)	19(91)	18(86)	18(86)	16(77)

(The figures in brackets are in dynes/cm^2)

The foregoing results of other researchers indicate the difficulty of comparison. First because of differences in material and its preparation and second because of different instruments and the techniques in their use. Generally, the yield stress of a cement slurry of w/c = 0.44, increases with less mixing energy input than the API specification and increases dramatically with longer standing times. The 10 minute gel strengths with the Fann viscometer are low, possibly, due to the 3 r.p.m speed of rotation during the test, as referred to in the Haimoni results. Haimoni's mix contained $CaCl_2$, which is at 2% an effective accelerator, and gypsum, at 10% ,to control flash setting of the C_3A. This mix would be expected to show higher yield stress values at the standing times tested than the neat class G cement slurry.

Unfortunately, there are too few results from other researchers with regard to yield stress, after periods of standing time, to enable comparison of the constants in the model. There are too many variations of a four constant model to fit the available data and substantial data would be required for such an exercise.

8.7 Conclusion

The effects of the varying shear rate during mixing, the reasons behind the rigid close packing phenomena and the surface settlements during testing have been further

discussed. Further data is required to verify the yield stress model and support the explanation given for some of the phenomena. The future research work is outlined in the next chapter.

CHAPTER 9

Future Research Work

The original objective of this work was to use the controlled stress rheometer to probe the rheology and stability of oil well cement slurries under realistic conditions. The work described in this thesis has shown that yield stress behaviour is an enormous subject fraught with difficulties, both experimental and theoretical. The computer based controlled stress rheometer is suitable for this work, provided the various operational difficulties are overcome. There remain, however, many aspects, some that have been exposed by this thesis, that require further research work. This chapter considers the future research work on this subject to be the refinement of the experimental technique, the extension of the research from this thesis and the development of, as yet, untried, though related, areas.

9.1 Further Refinements of Experimental Technique

Prior to making test runs with improved experimental technique modifications to the ancillary equipment should be undertaken first.

These include:-

a) continuous air supply to the air bearing of the rheometer without overheating compressors or condensation in the air filters.

b) adequate electrical surge protection for both rheometer and computer

The APC measuring system requires reproducibility, since the surface treatment is a cause of variation in yield stress measurement. Comparison with a smooth stainless steel APC having grooves cut radially around the annulus of both plate and cone, should suffice and if electro-rheological effects are to be ignored, use of a non-polar material should also be considered. A change in size and geometry would, as suggested by Harris (1977), overcome the departure from the theoretical ideal free surface at the rim of the APC, found when testing cement slurries. The problem of the minimum gap to prevent jamming of particles, and the maximum cone angle of 4^{o} - 5^{o} to comply with the theoretical assumptions, must be borne in mind.

Corrections which had to be applied, due to shrinkage and variation in weight of the sample, require to be overcome,or better accounted for, as does the eccentricity on loading the sample. Rectification of these faults can be improved upon.

9.2 Further Research Arising from this Thesis

The yield stress model of this thesis has four constants and from the discussion in Chapter 8 it is likely that the w/c ratio has a dependency on one or more of them. In the limited work with w/c ratio a correlation was found between $[\ln K.\ln(t_{mix}) / (t_{stand})^{1/2}]$ and w/c ratio which supports such a dependency. Hence further work on w/c ratio would obtain this dependency. The work of Domone and Thurairatnan (1988) may be useful in this regard. To further develop the dependency of the constants, work with additives such as that of Bhatty and Banfill (1984), would also be very helpful. This would automatically lead to yield stress prediction equations with a time dependence for the numerous admixtures in cement slurry systems found in the oil industry.

The effect shear rate has on the mixing shear energy per unit mass, E_T/M, needs to be assessed. This is because the low shear rate, during the mixing phase of the test runs, did not fit the yield stress model and, although various parameters were used, such as $\dot{\gamma}_{max}{}^{x}\, t_{hyd.}$ and $\dot{\gamma}_{max} \times t_{mix}$, to eliminate the effects of low $\dot{\gamma}_{max}$ during the mixing phase, none were successful.

Another aspect of the mixing phase which needs investigation is why, under constant stress, is the $\dot{\gamma}_{max}$ reached at approximately the same time from the start of mixing, regardless of the $\dot{\gamma}_{max}$ level attained. Even if the sample receives half the mixing energy per unit mass, it will begin to thicken at the same time from the start of mixing.

It is thought that use of the time to reach $\dot{\gamma}_{max}$, say t_{peak}, and the value of $\dot{\gamma}_{max}$ achieved could be used as a quality control, for ensuring successful two phase mixing of concentrated suspensions.

The reduction in yield stress as a result of removing the bleedwater which was observed in the results in section 5.4, requires explanation. This is contrary to expectation since a lower w/c ratio cement slurry would show increased yield stress. If, however, some disruption of the fragile structure, prevention of gel formation, or removal of fines can be shown to occur, then an explanation may be achieved.

Rigid close packing can be accounted for by too small a gap, or insufficient torque, but when these are sufficiently large the prediction of the occurrence of the phenomena is most difficult. Sample preparation when blending which results in non-homeogeneity and local high particle density prior to the mixing phase of the MST; the orientation of particles when squeezing the sample on loading; the reorganised particles consolidate on completion of the mixing phase; these are all means by which the rigid close packing phenomena can occur. Considering that there are of the order of 10^8 particles of average size 30μm in the measuring space of the APC and that between 50 and 100 are required to form a rigid lattice member at, say 45°, the probability of sufficient bracing structure occurring across the gap becomes more likely. Further investigation of this phenomena is required to determine if just increasing the sample size overcomes the problem.

9.3 Other Further Related Research Work

The following areas of research would develop the yield stress model to a useful form in the oil well cementing industry and lay the foundation for closing the gap between the theoretical models and the empirical ones.

a) variation of yield stress with temperature and pressure
b) theoretical development of the structural kinetics model to account for both build up and break down of structure
c) investigation of the electroviscous effect of hydrating oil well cement slurries,their significance and if electrorheological effects can be used in oil well cementing to advantge.

The temperature and pressure investigation was started by Keating and Hannant (1989) using a sealed vane in a cylinder and measuring the yield stress, using extrapolation of the flow curve, of an oil well cement slurry having developed 52°C temperature and 35.6 MPa pressure at 40 minutes. Gel strength increased with time and was reduced when the pressure was removed.

Theoretical development of a yield stress model should take note of the Tattersall (1955) linkage derivation and include for a build up term, which was assumed negligible (i.e. little or no tendency for a re-building of structure to take place). This we now know to be invalid since re-building occurs with the oil well cement slurry, approximately 1 minute after commencing the mixing phase. Another direction, that might prove beneficial, although time dependency is the difficulty,is the approach of Wildermuth and Williams (1984), who working with a shear dependent maximum packing fraction, ϕM,

on concentrated suspensions of rigid spherical particles have shown the concentration, ϕ, can describe yield stress and non-Newtonian effects and they suggest application to anisotropic and polydisperse suspensions.

The chance observation of an electric current between the cone and plate suggest that electrorheological effects might be significant. A survey by Deinega and Vinogradov (1984) indicates that the formation of hydrate layers on the particles creates the possibility of polarization of the disperse phase. With greases strong orientation effects contribute to frozen flow patterns stopping flow. This is considered as a formation of chain structures in the direction of lines of force of the electric field, which is normal to the direction of flow. It might be possible to produce enhanced flow rates by applying an electric field to cement slurry. This could have profound implications for cementing practice.

Finally, it should be possible to use the yield stress to predict slurry stability, and settling rates, in an oil well annulus, and one extension of this work should involve comparison with performance of the slurry in the field.

CHAPTER 10

Conclusion

While the experimental determination of the yield value of oil well cement slurries is not without its problems, the results of this investigation show that controlled stress rheometry can be used successfully.

10.1 Yield Stress in terms of Mixing Shear Energy

There is a relationship between the yield stress of an oil well cement slurry and the total mixing shear energy per unit volume in terms of the time of mixing and the time of standing. This reflects the development of yield stress of an oil well cement slurry with time.

An increase in mixing shear energy can increase the yield stress provided the cement slurry is not allowed to stand, since standing develops yield stress very rapidly and masks the effect of mixing.

The development of yield stress of the cement slurry as a result of standing can be significantly reduced by increasing the time of mixing, hence the increase in total mixing shear energy, without affecting the total amount of standing time. There was no significant effect of hydration time on yield stress.

An empirical model to predict the yield stress of an oil well cement slurry may

be expressed in the form.

$$\tau_y = \rho \frac{E_T}{M} e^{(a(t_{stand})^{\frac{1}{2}} - b)} t_{mix}^{(-c-d\ln(t_{stand}))} \qquad 12.1$$

where a, b, c and d are constants, which depend on the constituents of the mix and the conditions of mixing. These constants can be determined by experiment. ρ is the density of the slurry, E_T/M is the total energy dissipated during mixing per unit mass. t_{stand} and t_{mix} are the standing and mixing times, respectively. This model has been found applicable over the range of variables tested.

All these findings were at normal temperature and pressure. They appear to be relevant and applicable to plug flow in pipelines.

10.2 Measurement of Yield Stress using a C.S. Rheometer

The controlled stress rheometer when interfaced with a computer to programme and monitor test runs is suitable to measure the yield stress of an oil well cement slurry. This is especially true when measuring the effects on yield stress due to various mixing shear histories, which can be done on the slurry while in-situ.

The use of the annular plate and cone (APC) to perform the mixing shear history and be the measuring system to evaluate yield stress without the need to transfer the sample is a significant novel development not used before. The

stainless steel APC may be engraved to overcome slipppage.

Different measuring systems - parallel plate, vane in cup and APC using different surface treatments gave significantly different measured yield stresses for similar materials. The vane in cup which is designed to measure yield directly with no solid surface shear stress transfer interface indicated lower yield values than the APC. This could not be fully explained, but may be due to the non-ideal dimensions of the vane necessary to fit in the space available in the rheometer.

All measuring systems indicated that the yield stress of an oil well cement slurry tested, as soon as possible after mixing, depends on the rate of applied stress. The manner in which the sample was loaded into the measuring system and the time at which the rate of applied stress reached the developed yield stress, accounted to some extent for these differences in the very early age yield stress. However, the rate of applied stress had no significant effect on the measurement of yield stress of an oil well cement slurry, provided that during the time to reach that yield stress the yield stress had not changed significantly, which was the case with prolonged standing times.

During a programmed mixing phase using its facility for holding a peak torque while plotting shear rate against time, the CS rheometer can monitor the maximum shear rate and the time at which that maximum occurs to ensure that the shear history can be accurately determined.

It is hoped that the work in this thesis will have broader application than just oil well cements. In fact the experimental approach should be applicable to any

particulate suspension which undergoes a mixing process and where chemical reaction occurs.

References

API Specification 10 (Spec 10) 3rd Ed. July (1986) Specification for Materials and Testing for Well Cements, American Petroleum Institute, Dallas, Texas.

Banfill P.F.G., (1980) Rheology of setting of P.C. pastes 7th inter. cong. on Chem of Cem. Paris ed. Septima IV, 324-328

Banfill P.F.G., (1981) A viscometric study of cement pastes containing superplasticizers with a note on experimental technqiue.Mag. Conc. Res. vol 33 No. 114 Mar., 37-47

Banfill P.F.G., (1987) Present Experimental Problems with the Rheology of Cement Pastes, paper at meeting Brit. Soc. Rheo/Coll. Interface Sci. Faraday Div. Roy. Soc., Chem., University of Bath, 9-10 April.

Banfill P.F.G., Saunders D.C., (1981) On the Viscometric examination of Cement Pastes. Cem and Conc. Res. 11, 363-370.

Bhatty J.I., Banfill P.F.G., (1984) A Viscometric Method of Monitoring the effect of cement pastes. Cem. and Conc. Res. Vol. 14, 64-72.

Bhatty J.I., Banfill P.F.G., (1982) Sedimentation behaviour of cement pastes subject to continuous shear in rotational viscometers. Cem. and Conc. Res. 13. 69-78.

Bird R.B., (1979) Use of Simple Molecular Models in the Study of the Mechanical Behaviour of Solutions of Flexible Macromolecules. J. of Non-Newtonian Fluid Mechanics. 5, 1-12.

Bird R.B., Armstrong R.C., Hassager O., (1973) Dynamics of Polymetric Liquids. Vol. 1, Fluid Mechanics. John Wiley.

Bird R.B., Turian R.M., (1962) Viscous heating effects in a Cone and Plate viscometer, Chem. Eng. Sci, 17, 331-334.

Bye G.C., (1983) Portland Cement Composition, Production and Properties. Pergamon.

Carri-Med (1986) Instruction Manual for Controlled Stress Rheometer, Dorking, England.

Chaffey C.E., (1976) Particle linking and Viscosity in Structural Theories of Pseudoplastic Flow. J. Coll Interface Sci., Vol. 56, No. 3. Sept.

Cheng D. C-H., (1985) Yield Stress -A Time Dependent Property and How to measure it. Warren Spring Laboratory, Dept. of Industry.

Cheng D. C-H., (1987) Thixotropy: Description and Measurement, course entitled Applied Rheology 14-18 Sept. Royal Society of Chemistry, Univ. Bristol.

Donald I.B., et.al.(1977). The Vane Test - A Critical Appraisal. Proc. 9th Int. Conf. Soil Mech. Found. Eng. Onkyo. Vol.1 p. 81-88 ——→

Dowell Schlumberger (1984), Cement Technology, London. ——→

Jones T.E.R., Davies J.M., Thomas A., (1987). Rheol. Acta. 26. p 14-19 ——

Cross M.M., (1965), Rheology of non-Newtonian Fluids - A new flow equation for Pseudo Plastic systems. J. Colliod Sci., 20, 417-437.

Cross M.M., (1986) Rheological behaviour of glass fibre/polyol suspensions of Reinforced Reaction Injection Moulding process. Ph.D., Dept. Polymer Science and Tech. UMIST.

Cross M.M., Kaye A., (1986) Techniques for the viscometry of Suspensions, Polymer Eng. Sci. Vol. 26 No. 2 Jan. 121-126.

Cross M.M., Kaye A., (1987) Simple procedures for obtaining viscosity/shear rate data from a parallel disc viscometer, Polymer Vol. 28, March p. 435-440.

~~Cement Technology. (1984) Dowell Schlumberger, London.~~

Deinega Yu. F., Vinogradov G.V. (1984) Electric Fields in the Rheology of Disperse Systems. Rheologica Acta Vol., 23 636-651.

Dimond C.R. (1975) The Rheology of Cement Pastes Ph.D. thesis Univ. Sheffield.

Domone P.L., Thurairatnam H., (1988) The effect of water/cement ratio, plasticizers and temperature on the rheology of cement grouts. Advaces in Cem. Res. Vol. 1 No. 4 Oct. 195-206.

Doran S.M., (1984) Surface Settlement and Bleeding in Fresh Cement Grouts. Ph.D., Dept. Civil Engng. Kings Coll., London Univ.

Haimoni A., (1985) Developments in the Shear Vane Test to Measure Gel Strength of Oil Well Cement Slurry. Report No. 4 October unpublished.

Haimoni A., (1987) Rheology of a Specific Oil Well Cement. Ph.D. Dept. Civ. Engng. Univ. Surrey.

Harris J., (1967) A continuum theory of time-dependent elastic flow. Rheol. Acta 6, 6-12.

Harris J., (1977) Rheology and non-Newtonian Flow. Uni. Micro. Intern.

Ish Shalom M & Greenberg S.A., (1960) The rheology of fresh P.C. pastes Proc. 4th Internat. Symp. on Chem. of Cem. Oct. Monograph 43 Vol. 2 Washington Nat. Bur. Stan. 1962., 731-748.

Jones T.E.R., (1987) Controlled Stress Rheometry, course Applied Rheology 14-18th Dept., Royal Society of Chemistry, Univ. Bristol.

Jones T.E.R., Taylor S., (1977) A mathematical model relating the flow curve of a cement paste to its water cement ratio. Mag. Conc. Res. Vol. 29 No. 101 Dec. 207-212.

Kaye A., (1987) Private Communication 4th June.

Keating J., Hannant D.J. (1989) Shear Vane Tests on Oil Well Cements at High Temperature and Pressure. Concrete Soc. Materials Res. Seminar. Uni. Surrey July.

Keentok M., Milthorpe J.F., O'Donovan E., (1985) On the shearing zone around Rotating Vanes in Plastic Liquids: Theory and Experiment J. Non-Newtonian Fluids Mechanics, 17, 23-35.

Keentok M., Tanner R.I., (1982) Cone and plate and parallel plate rheometry. of some polymer solutions J. Rheology. Vol. 26.

Krieger I.M., Elrod H., (1953) Direct determination of the Flow Curves of Non-Newtonian Fluids II. Shearing Rate in Concentric Cylinder Viscometer. J. App., Physics Vol. 24 No. 2 Feb., 134-136.

Krieger I.M., Maron S.H., (1952) Direct determination of the flow curves of non-Newtonian fluids. J. Applied Physics Vol. 23 No. 1 Jan., 147-149.

Krieger I.M., Woods M.E., (1966) Direct Determination of the Flow Curves of non-Newtonian Fluids IV. Parallel Plane Rotational Viscometer. J. of Applied Physics. Vol. 37, No. 13 Dec. 4703-4

Lapasin R., Longo V., Rajgel S., (1980) A thixotropic model for cement powder pastes Proc. 8th Inter. Cong. on Rheology, Naples Vol. 3, New York,Plenum 659-664.

Lee K., (1979) An Analytical and Experimental Study of Large Strain Soil Consolidation. D. Phil. Univ. Oxford (1979).

Legrand C., (1981) The flocculent state of cement paste and its consequences for rheological behaviour. Cahiers de la Group, Francais de Rheologie Oct., 129-136.

Mannheimer R.J., (1983) Effect of slip on flow properties of cement slurries can flaw resistance calculations. Oil & Gas J. Dec. 5, 144-147.

Merrifield E.M., (1980) Factors affecting the interpretation of in-situ shear vane test Ph.D thesis Univ. Surrey.

Mewis J., (1979) Thixotropy - A General Review. J. of non-Newtonian Fluids 6, 1-20.

Nguyen Q.D., (1983) Rheology of Concentrated Bauxite Residue Suspensions Ph.D thesis, Monash Univ., Australia.

Nguyen Q.D., Boger D.Y., (1985) Direct Yield Stress Measurement with the Vane Method. J. Rheol. 29 (3), 335-347.

Oldroyd J.G., (1947) A Rational Formulation of the Equations of Plastic Flow for a Bingham Solid, Proc. Cambridge Philos. Soc. Vol 43, 100-105.

Oldroyd J.G. (1956) Non-Newtonian Flow of Liquids and Solids Ch. 16 Rheology, Theory and Applications Vol. 1 ed. Eirich Academic, New York.

Orban J.A., Parcevaux P.A., Guillot D.J., (1986) Specific Mixing energy: A key factor for cement slurry quality, SPE. 15578, 61st Annual Conf., Soc. Pet. Eng., New Orleans, 1-5.

Richards J.W., (1967) Interpretation of Technical Data. Iliffe. London.

Robertson R.E., Stiff H.A.JR., (1976) An improved mathematical model for relating shear stress to shear rate in drilling fluids and cement slurries. J. Soc. Petroleum Engrs. Vol. 16 part 1, Feb.

Roy D.M., (1979) Rheological properties of cement mixes 111. The effects of mixing procedures on viscometric properties of mixes containing superplasticizers. Cem. and Conc. Res. Vol. 9. No. 6., 731-739.

Roy D.M., Asaga K., (1980)) Rheological properties of cement mixes: v The effects of time on viscometric props. of mixes containing Superplasticizers: conclusions Cem. and Conc. Res. 10, 387-394.

Sabins F.L., Sutton D.L., (1986) The relationship of thickening time gel strength and compressive strength of oil well cements SPE Prod. Eng., Mar., 143-152.

Schreuder F.W.A.M., Van Diemen A.J.G., Stein H.N., (1986) Viscoelastic Properties of Concentrated Suspensions. J. Colloid and Interface Sci. 111 (1), 35-43.

Tadros Th.F., (1986) Control of the properties of suspensions. Colloids and Surfaces, Vol. 18, 137-173.

Tattersall G.H., (1955) Structural breakdown of cement paste at constant rate of shear, Nature 175 (4447), 166.

Tattersall G.H., Banfill P.F.G., (1983) The Rheology of Fresh Concrete, Pitman.

Tattersall G.H., Dimond C.R. (1976) Hydraulic Cement Pastes: Their Structure and Properties. Proc. Conf. Univ. Sheffield Publ. 15,121, Slough, Cem. and Conc. Assoc.

Van Wazer J.R., Lyons J.W., Kim K.Y., Colwell, R.E., (1963) Viscosity and Flow Measurement, Interscience. New York.

Walters K., (1975) Rheometry. Chapman and Hall. London.

Walters K., Barnes H.A., (1985) The Yield Stress Myth, Rheo. Acta, 24, 323-326.

Wildemuth C.R., Williams, M.C., (1984) Viscosity of Suspensions modelled with a shear dependent maximum packing fraction. Rheol. Acta 23, 627-635.

Worrall W.E., Tuliani S., (1964) Viscosity changes during the ageing of clay-water suspensions. Trans. Brit. Ceramic Soc. 63, (4), 167-185.

APPENDIX 1

MODIFICATIONS TO CARRI-MED FLOW RUN RELEASE 3.5

```
1035 AS = AS - 60
1170 DK = 1
2900 IF DK = 2 THEN 4000
3090 GOTO 3520
3520 IF AS > 0 THEN FOR N = 1 TO
        200: GD(N) = 0: TP(N / 10) = TS NEXT N
3630 QK = 1
3643 IF QK = 2 THEN 3660
3645 PA% = 30: CALL PA
3646 TA = 0.8* TA:QK = QK + 1: GOTO 3640
3940 DD$  = "00000":SA% = 1: GOSUB 11500
3960 TQ =  4 * TQ:  ET = AS: DK = DK + 1: GOTO 2710
4000 IF DS> 0 THEN GOSUB 12050
4050 TA = 0
4060 TI = TQ / 200:SX = (DS / 200) * 1000-355:IF SX < = 0 THEN SX = 1
4230 HPLOT XP, YP:TA = TA + TI: NEXT N
4250 DK = 1:AS = 0
5070 HOME : VTAB42: PRINT T$(24 );
```

The following lines were deleted

```
3140
3950
4940-5050
```

APPENDIX 2

PROGRAMME TO CALCULATE E_T/M FROM PEAK HOLD DATA

```
20    REM
30    REM    AP'CARE.A
70    REM
80    FRE 0
100   REM  PRINT BANNER
105   HOME : VTAB 2: PRINT  SPC( 8
      ):"AREA UNDER MIXING CURVE":
       POKE 34,3
106   PRINT
110   PRINT "  This programme calc
      ulates the area"
120   PRINT "under the peak hold s
      hear rate v time"
130   PRINT "curve for the AP&C ge
      ometry undergoing"
133   PRINT "mixing shear."
135   PRINT "  The area is convert
      ed into energy"
140   PRINT "/unit mass (kJ/kg) fo
      r a cement slurry"
145   PRINT "S.G.=1.9 ."
150   PRINT "  Should this or the
      geometry"
160   PRINT "in current use change
       the programme"
170   PRINT "would require modific
      ation to suit."
180   PRINT "   The following info
      rmation is required"
185   PRINT
190   INPUT "          Sample Ref. N
      o. ";SR$
200   INPUT "                Run  N
      o. ";RN
205   PRINT
210   INPUT "          Standing Time
       (seconds)   ";TS
215   PRINT
220   INPUT "            Mixing Time (
      seconds)     ";TM
230   PRINT
235   INPUT "            Peak Torque (
      dyne cm.) ";TA
240   REM  READ DATA FROM DISC IN
      D2
```

APPENDIX 2

```
250   REM
255   REM   DIMENSION ARRAYS
260   REM
265   DIM PARAM$(21)
290   DIM B(200,1),R(200,1)
300   DIM RP(100)
310   REM   OPEN FILE ON DISC
320   FILE$ = LEFT$ (CR$ + "
                  ",19) +  STR$ (R
      N)
330   PRINT  CHR$ (13); CHR$ (4);"
      OPEN";FILE$;",D2"
340   PRINT  CHR$ (4);"READ";FILE$

350   REM  READ PARAMETERS
360   FOR LP = 0 TO 21
370   INPUT PARAM$(LP)
380   NEXT
390   IF  LEFT$ (PARAM$(21),1) <>
      "F" THEN  PRINT : PRINT "THI
      S IS NOT A FLOW RESULT FILE"
      : PRINT : STOP
400   REM  READ PEAK HOLD DATA
410   IF  VAL (PARAM$(19)) = 0 THEN
      470
420   FOR LP = 1 TO  VAL (PARAM$(1
      9))
430   INPUT RP(LP)
440   NEXT
450   REM
460   REM  READ UP CURVE DATA
470   IF  VAL (PARAM$(20)) = 0 THEN
      510
480   FOR LP = 1 TO  VAL (PARAM$(2
      0))
490   INPUT R(LP,1),ST(LP,1)
500   NEXT
510   PRINT  CHR$ (4);"CLOSE"
520   REM  CALCULATE AREA
530   REM
540 HY = 2 * RP(1) - RP(2)
550 AI = 1.5 * HY
555  IF AI < 0 THEN AI = 0
560 HE = RP(100) + HY
570  FOR LP = 1 TO 99
580  IF LP / 2 =  INT (LP / 2) THEN
      610
590 HE = HE + 4 * RP(LP)
600  GOTO 620
610 HE = HE + 2 * RP(LP)
620  NEXT
630  REM
640 AR = TM * HE / 300
```

APPENDIX 2

```
650  REM
660  REM  CONVERT AREA TO ENERGY
670  REM
680  REM  SE OF CEMENT SLURRY
690 WW = 29.08:WC = 66.1:SG = 3.1
     6
700 SL = (WW + WC) / (WW + (WC /
     SG))
710 R1 = 3.0:R2 = 1.5
715 PI = 3.141592654
720 FS = 1.5 / PI / (R1 ^ 3 - R2 ^
     3)
730 NU = FS / SL / 10 ^ 7
740 EN = NU * TA * (AI + 0.8 * AR
     )
750  REM
760  REM  PRINT RESULTS
770  REM
775  HOME : PR# 1: VTAB 2: PRINT
      SPC( 8);"AREA UNDER MIXING
     CURVE"
778  PRINT : PRINT  CHR$ (27);"-"
     ; CHR$ (1);
780  HTAB 3: VTAB 7: PRINT "Sampl
     e Ret.No. ";SR$
790  PRINT  CHR$ (27);"-"; CHR$ (
     0);
800  PRINT "          Run  No. ";R
     N
905  PRINT
910 MI =  INT (TM / 60):SE = TM -
     MI * 60
820  PRINT "  Mixing Time   = ";M
     I;":";SE;" (min:sec)"
830 MI =  INT (TS / 60):SE = TS -
     MI * 60
840  PRINT "  Standing Time = ";M
     I;":";SE;" (min:sec)"
850  PRINT
855  PRINT "  Start up area is
          ";AI
856  PRINT "  Mixing curve area i
     s ";AR
857  PRINT
860  PRINT "ENERGY/UNIT MASS IS "
     ;EN;" kJ/kg"
```

APPENDIX 2

```
865   PRINT : PRINT
870   PRE 0: HTAB 3: VTAB 24
880   INPUT "Press <RETURN> for Up
       Curve Data":KE$
890   REM  DISPLAY UP CURVE DATA
900   HOME : VTAB 2: PRE 1: PRINT
       SPC( 11);"UP CURVE FLOW DAT
      A  ": PUKE 34,3
903   PRINT
905   HTAB 3: VTAB 5
910   PRINT "Point No."; SPC( 3);"
      Shear Rate"; SPC( 3);"Shear
      Stress": PRINT
920   FOR LP = 1 TO 5
930   PRINT  SPC( 6);LP; SPC( 9);R
      T(LP,1); SPC( 10);ST(LP,1)
950   NEXT
955   PRINT : PRINT "       ********
      **********************      ":
       PRINT : PRINT
960   END
```

APPENDIX 3

CHEMICAL AND MINERAL PHASE ANALYSIS

	Oil Well Class G %	Typical cement values of OPC %	Sulphate resisting %
SiO_2	21.78	20	24
Al_2O_3	3.78	6	2
Fe_2O_3	4.99	3	3
CaO	64.32	63	62
MgO	0.74	1.5	2.3
SO_3	2.34	2.3	2.3
K_2O	0.38	0.9	0.7
Na_2O	0.09	0.4	0.4
Loss	1.01	—	—
I.R.	0.16	—	—
C_3S	57.6	54	44
C_2S	19.0	17	35
C_4AF	15.2	9	9
C_3A	1.39	11	0.2
$\overline{CS}$	3.98	3.9	3.9

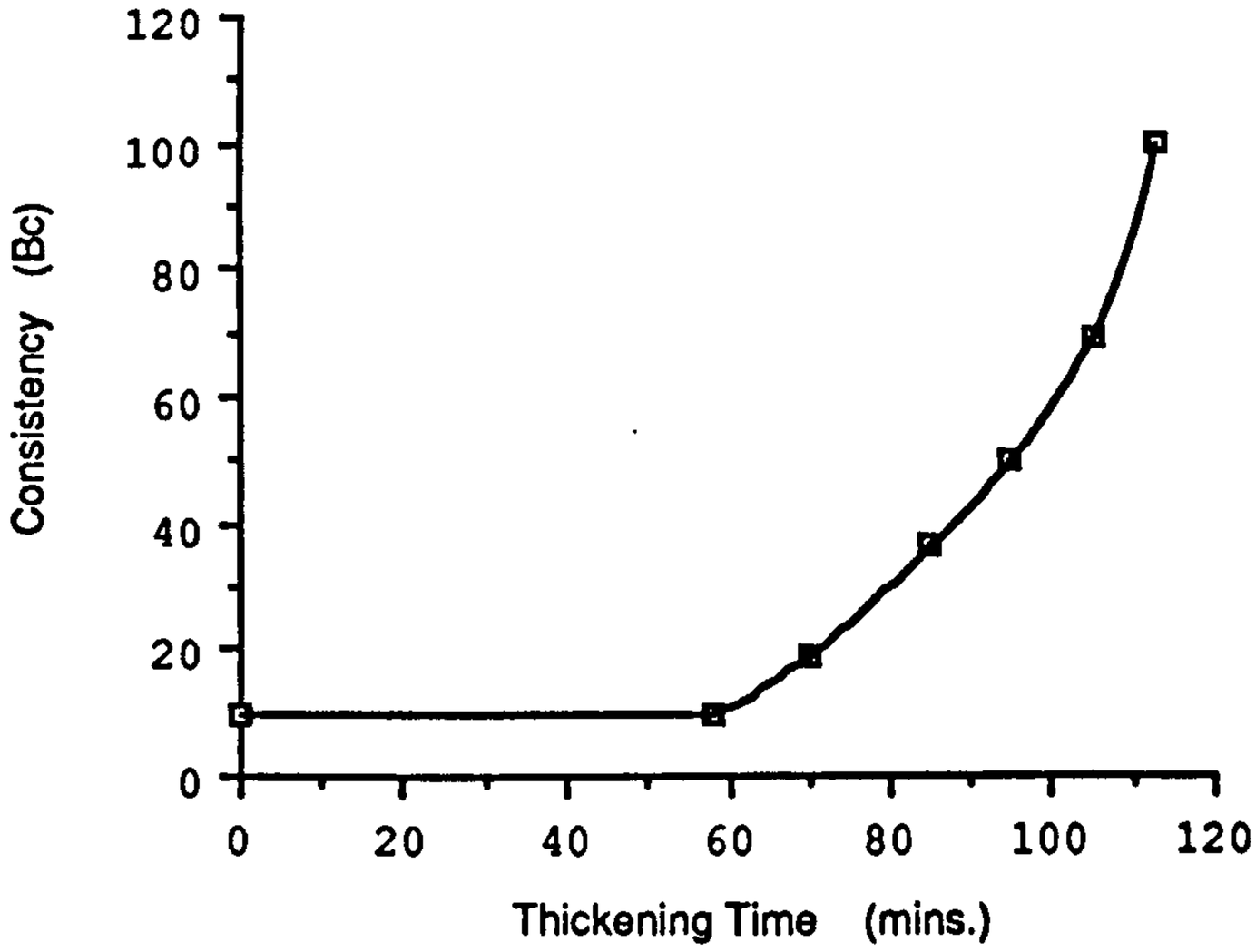

Viscosity curve API schedule 5

(supplied with cement by Blue Circle Industries PLC, May,1988)

APPENDIX 3

TYPICAL PARTICULATE PROPERTIES OF CLASS G OIL WELL CEMENT

Apparent particle density = 3180 kg./m^3

Surface area = 310 m^2/kg.

Particle Grading

Size (micron)	% finer than
1000	100
500	99.99
250	99.98
125	99.3
90	97.2
63	90.2
45	80.6
40	74
25	60
20	52
15	42
10	32
5	18
2	0

from Haimoni (1987)

APPENDIX 4

DATA SHEET NUMER 1

Max Ω (rad/sec.)	Run Ref. No	$\tau_y/\rho E_T/M$ x 10-7	X = hydration time	$\dot{\gamma}$ x X x 10^5	Modified standing time
38.6	9/05	15.11	313	1.728	62
36.1	06	23.82	312	1.611	61
37.6	07	15.44	311	1.672	60
39.0	08	15.27	311	1.734	60
34.9	09	16.64	415	2.071	62
39.3	10	14.12	415	2.332	62
35.6	11	9.82	416	2.118	63
31.6	12	3.71	414	1.871	61
36.1	13	3.17	585	3.020	62
35.8	14	4.99	584	2.990	61
32.1	15	5.55	582	2.672	59
33.9	16	6.76	583	2.826	60
33.4	17	5.02	752	3.592	61
36.8	18	4.27	753	3.963	62
34.1	19	2.44	752	3.667	61
32.1	20	2.50	753	3.456	62
33.3	21	3.02	924	4.400	64
33.6	22	3.96	923	4.435	63
31.4	23	3.17	921	4.135	61
34.8	24	2.89	921	4.583	61
35.8	25	9.43	1569	8.032	709
28.5	26	13.50	1571	6.403	711
36.0	27	10.37	1574	8.103	714
32.3	28	13.33	1583	7.312	723
35.8	29	11.57	1417	7.254	722
39.8	30	17.00	1413	8.042	722
38.6	31	15.21	1404	7.750	713
38.6	32	12.78	1402	7.739	711
33.2	33	33.20	1235	5.863	712
29.6	34	34.91	1235	5.228	712
41.8	35	22.72	1239	7.406	716
34.0	36	15.19	1243	6.043	720
34.3	37	69.14	1085	5.322	731
37.3	38	65.26	1070	5.707	716
41.9	39	57.23	1068	6.399	714
35.1	40	67.70	1066	5.351	712
37.0	41	161.37	965	5.106	733
37.7	42	150.79	964	5.197	733
36.9	43	97.33	965	5.092	733
34.3	44	64.49	967	4.743	735
32.5	10/01	1456.56	2224	10.336	1972
38.0	02	1262.81	2137	11.611	1887

APPENDIX 4 DATA SHEET NUMBER 1 (cont'd)

29.9	03	1075.55	2100	8.978	1848
37.9	04	1228.05	2104	11.403	1852
39.1	05	245.95	2187	12.228	1833
29.9	06	490.49	2204	9.424	1850
36.0	07	391.15	2165	11.149	1811
34.6	08	453.57	2297	11.369	1943
36.5	09	159.66	2420	12.631	1897
35.0	10	120.37	2360	11.812	1837
35.4	11	176.25	2361	11.952	1838
40.7	12	158.72	2357	13.718	1834
38.9	13	88.00	2520	14.018	1828
31.4	14	132.13	2529	11.356	1837
32.8	15	121.70	2541	11.918	1849
26.7	16	152.89	2585	9.870	1893
21.0	17	202.67	2775	8.333	1913
18.3	21	566.82	1475	3.860	1225
20.2	22	141.51	1576	4.552	1223
25.1	23	140.75	1757	6.306	1235
22.0	24	80.67	1920	6.040	1230
38.4	25	52.94	2092	11.488	1231
18.3	11/01	324.65	2207	5.775	1347
15.5	02	800.61	2130	4.721	1439
31.6	03	63.43	1765	7.976	1243
24.6	04	250.31	1609	5.660	1256
23.3	06	1689.26	1576	5.251	1324
21.3	07	1476.20	1485	4.523	1234
28.9	08	191.45	1578	6.521	1224
33.9	09	100.20	1743	8.450	1221
17.4	10	499.23	1939	4.825	1248
30.1	11	69.70	2085	8.975	1225
19.0	12	147.01	1177	3.198	822
18.1	13	148.31	1135	2.938	767
15.5	14	204.52	1097	2.432	743

APPENDIX 4

DATA SHEET NUMBER 2

Run Ref. No	t_{mix}	$y = \frac{\tau_y \dot{\gamma}_{max} t_{mix}}{\rho E_T/M}$	Run Ref. No.	t_{mix}	y
9/05	71	.0592	10/01	72	4.8736
06	71	.0873	02	72	4.9401
07	71	.0589	03	72	3.3116
08	71	.0604	04	72	4.7919
09	173	.1436	05	173	2.3791
10	173	.1373	06	173	3.6282
11	173	.0865	07	173	3.4836
12	173	.0290	08	173	3.8826
13	343	.0561	09	343	2.8584
14	343	.0878	10	343	2.0664
15	343	.0874	11	343	3.0602
16	343	.1124	12	343	3.1685
17	512	.1228	13	512	2.5063
18	512	.1150	14	512	3.0377
19	512	.0609	15	512	2.9226
20	512	.0588	16	512	2.9888
21	681	.0979	17	681	4.1446
22	681	.1296	21	71	1.0532
23	681	.0969	22	174	0.7112
24	681	.0976	23	343	1.7328
25	681	.3288	24	510	1.2944
26	681	.3747	25	681	1.9797
27	681	.3636	11/01	681	5.7856
28	681	.4193	02	511	9.0677
29	511	.3027	03	343	0.9831
30	511	.4944	04	173	1.5234
31	511	.4290	06	71	3.9968
32	511	.3605	07	72	3.2373
33	343	.5406	08	174	1.3767
34	343	.5069	09	343	1.6661
35	343	.4658	10	512	6.3602
36	343	.2533	11	682	2.0460
37	174	.5901	12	174	0.6951
38	174	.6057	13	174	0.6680
39	174	.5967	14	174	0.7888
40	174	.5913			
41	72	.6148			
42	72	.5854			
43	72	.3698			
44	72	.2278			